1-1-2018

Maximum Recovery Of Mechanical Energy Through Work Integration: A Work Exchange Network Synthesis Approach

Aida Amini Rankouhi
Wayne State University,

MAXIMUM RECOVERY OF MECHANICAL ENERGY THROUGH WORK INTEGRATION: A WORK EXCHANGE NETWORK SYNTHESIS APPROACH

by

AIDA AMINI RANKOUHI

DISSERTATION

Submitted to the Graduate School

of Wayne State University,

Detroit, Michigan

in partial fulfillment of the requirements

for the degree of

DOCTOR OF PHILOSOPHY

2018

MAJOR: CHEMICAL ENGINEERING

Approved by:

_____

Advisor Date

_____

_____

_____

_____

DEDICATION

To Homeira, Masoud,

Anoosheh, and Pedram

ACKNOWLEDGEMENTS

I would like to express my sincere appreciation to my advisor, Dr. Yinlun Huang, for his continuous support and mentorship throughout my Ph.D. study at Wayne State University. His guidance, encouragement, patience, and criticism helped me in growing as a researcher and engineer. I could not have imagined having a better advisor and I believe the lessons I learned from him would be the invaluable assets for my future career.

I am profoundly grateful to the members of my dissertation committee, Drs. Charles Manke, Cristina Piluso, Evrim Dalkiran, and Helen E Durand for their insightful comments, support, and encouragement. Additionally, I am very grateful for the support and friendship I was offered by past and current lab members: Hao Song, Shaoqing Bai, Navdeep Bhadbhade, Majid Moradi-Aliabadi, Raha Gerami, and Seyedparham Pourmirjafari-Firouzabadi.

I gratefully acknowledge the funding sources from National Science Foundation and Graduate School of Wayne State University that made my Ph.D. work possible.

A special thanks to Dr. Guangzhao Mao, Dr. Korosh Torabi, Dr. Steven Salley, Angela Childrey, Tracy Castle, my friends at ChE/MSE Graduate Students Organization, and Chloe Luyet. I am extremely thankful to my industrial mentor, Dr. Sam Kharchenko, for his valuable guidance and advice. Additionally, I greatly appreciate all the staff at Wayne State University who made the school feels like home.

Finally, and most importantly, I would like to express gratitude to my parents, Homeira Jamali and Masoud Amini-Rankouhi, for their endless love, support, sacrifices, and teaching me to be independent, to work hard, to care for people and to live with honesty, my sister, Anoosheh Amini-Rankouhi, for her selfless love and care, my husband, Pedram Jahanian, for his unfailing love, encouragement, and understating during my pursuit of Ph.D. degree, and my best friends, Neshat Basiri and Mohammad Soroush Barhaghi, for being there for me through the life's thick

and thin. I would also like to thank my aunt, Mehrshid, my uncle, Ali, my cousins, Babak and Arezou, my friends back home, Shirin, Maryam, Matin, Sara, and Sepideh, and my dear friends in Michigan, for the wonderful companionship during the past six years.

TABLE OF CONTENTS

DEDICATION ii

ACKNOWLEDGEMENTS iii

LIST OF TABLES viii

LIST OF FIGURES x

CHAPTER 1 INTRODUCTION 1

1.1 Main Goals and Scientific Contributions 1

1.2 Organization of Dissertation 3

CHAPTER 2 MECHANICAL ENERGY RECOVERY THROUGH WORK EXCHANGER NETWORK INTEGRATION: CHALLENGES AND OPPORTUNITIES 6

2.1 Mechanical Energy Recovery Fundamentals 7

2.2 WEN Synthesis-Progress Overview 15

2.3 Challenges and Opportunities 18

CHAPTER 3 PREDICTION OF MAXIMUM RECOVERABLE MECHANICAL ENERGY VIA WORK INTEGRATION: A THERMODYNAMIC MODELING AND ANALYSIS APPROACH 22

3.1 Mathematical Framework for Energy Recovery Targeting 22

3.2 Case Studies 32

3.2.1 Case 1- Prediction of the Maximum Recoverable Mechanical Energy of a System Operated under Isothermal Conditions 32

3.2.2 Case 2 – Prediction of the Maximum Recoverable Mechanical Energy of a System Operated under Adiabatic Conditions 41

3.3.3 Discussion 48

3.4 Summary 48

CHAPTER 4 SYNTHESIS OF COST EFFECTIVE HEAT INTEGRATED WORK EXCHANGE NETWORK 50

4.1 Work Exchanger Network Synthesis Methodology 50

4.2 Heat Integrated Work Exchange Network Design 57

4.2.1 WEN Design Modification using Heat Integration 63
4.3 Basic Cost Analysis 64
4.4 Case Studies 66
4.5 Summary 95
CHAPTER 5 MODELING AND SIMULATION OF A PISTON-TYPE WORK EXCHANGER FOR MECHANICAL ENERGY RECOVERY 97
5.1 Objectives and Significance 97
5.2 Modeling and Simulation of Work Exchanger Systems Using Aspen Plus 100
5.2.1 Construction of work exchanger module with Aspen Plus 101
5.2.2 Simulation Procedures 103
5.2.3 Simulation Results 105
5.3 CFD-based Modeling and Simulation of Piston-type Direct Work Exchanger 109
5.3.1 Challenges and Opportunities 110
5.3.2 Piston-Type Work Exchanger Configuration 113
5.3.3 Modeling Piston Dynamics 114
5.3.4 Simulation System Setup 116
5.3.5 Analysis of Direct Piston-type Work Exchanger Full Cycle 120
5.4 Summary 131
CHAPTER 6 DATA-DRIVEN MODELING AND ANALYSIS OF ENERGY EFFICIENCY OF GEOGRAPHICALLY DISTRIBUTED MANUFACTURING 133
6.1 Data-driven Energy Analysis Methodology 135
6.2 Case Study 144
6.3 Summary 162
CHAPTER 7 CONCLUSIONS AND FUTURE WORK 164
7.1 Conclusions 164
7.2 Future Work 167

APPENDICES 172
Appendix A 172
Appendix B 177
Appendix C 180
REFERENCES 189
ABSTRACT 197
AUTOBIOGRAPHICAL STATEMENT 199

LIST OF TABLES

Table 2.1. Evaluation of mechanical energy exchanged by process streams under different operating conditions 11

Table 3.1. Process stream data for Case 1 34

Table 3.2. Energy recovery analysis for Case 1 40

Table 3.3. Performance comparison of WENs by different methods for Case 1 41

Table 3.4. Process stream data for Case 2 43

Table 3.5. Energy recovery analysis for Case 2 45

Table 3.6. Performance comparison of WENs by different methods for Case 2 46

Table 4.1. Directory of formulas to be used in prediction and synthesis stages for HEN located before/after WEN design 62

Table 4.2. Process stream data for Case 1 67

Table 4.3. Energy recovery and operation cost comparison based on HEN location for Case 1 71

Table 4.4. Energy recovery analysis for Case 1 79

Table 4.5. Process stream data for Case 2 80

Table 4.6. Energy recovery and operation cost comparison based on HEN location for Case 2 83

Table 4.7. CAPEX and OPEX of units in Case 2 93

Table 4.8. Performance comparison of HIWENs by different methods for Case 2 94

Table 6.1. Manufacturing-sector-based energy consumption percentage in the U.S. in 2012 .. 148

Table 6.2. Manufacturing-sector-based energy loss percentage in the U.S. in 2012 149

Table 6.3. Manufacturing-sector-based energy consumption and total value of shipment in the U.S. and State of MI in 2012 153

Table 6.4. Manufacturing-sector-based energy consumption in State of MI in 2012 154

Table 6.5. Manufacturing-sector-based energy loss percentage in MI in 2012 156

Table 6.6. Manufacturing-sector-based energy loss in MI in 2012 157

Table 6.7. Total value of shipment for manufacturing sectors in three energy intensive counties in MI 160

Table 6.8. Manufacturing-sector-based energy consumption and direct loss in three energy intensive counties in MI 161

Table 6.9. Carbon dioxide emission of MI and three counties with respect to manufacturing sectors 161

LIST OF FIGURES

Figure 2.1. Sketch of work transfer units: (a) a (flow) WE and (b) an SSTC. 8

Figure 2.2. Valve position in each operational step of a work exchanger: (I) depressurization step; (II) low-pressure displacement step; (III) pressurization step; (IV) high-pressure displacement step. 9

Figure 2.3. P-V diagram for a flow work exchanger. 12

Figure 2.4. P-V-W diagram for work exchanger. 13

Figure 2.5. P-W diagram for the work exchanger. 14

Figure 2.6. Comparison of (a) heat transfer in a HE and (b) work transfer in a WE. 19

Figure 3.1. Flowchart for derivation of matrix $\bar{\boldsymbol{\Gamma}}$ 25

Figure 3.2. Flowchart for evaluation of maximum recoverable mechanical energy. 33

Figure 3.3. Work exchange networks designed by different methods for Case 1: (a) the solution by the proposed model-based method to achieve the maximum energy recovery, and (b) the solution derived by Liu *et al.* (2014). 42

Figure 3.4. Flowsheet of heat-integrated work exchange network for Case 2: (a) work exchanger network, and (b) heat exchanger network. 47

Figure 4.1. Generation of $\boldsymbol{W}_{W}$ and $\bar{\boldsymbol{P}}_{\boldsymbol{M}}$ 56

Figure 4.2. Generation of $\boldsymbol{W}_{C_1}$, $\boldsymbol{W}_{C_2}$, and $\boldsymbol{W}_{\boldsymbol{E}}$ 57

Figure 4.3. Flowchart for HEN location decision making. 59

Figure 4.4. (a) HEN located before WEN design, and (b) HEN located after WEN design. 60

Figure 4.5. Cost estimation for one work exchanger unit. 65

Figure 4.6. (a) HEN located before WEN design for Case 1, and (b) HEN located after WEN design for Case 1. 70

Figure 4.7. Flowsheet of heat-integrated work exchange network for Case 1 :(a) work exchanger network, (b) heat exchanger network. 78

Figure 4.8. Flowsheet of modified heat-integrated work exchange network for Case 1. 79

Figure 4.9. (a) HEN located before WEN design for Case 2, and (b) HEN located after WEN design for Case 2. 84

Figure 4.10. Flowsheet of heat-integrated work exchange network for Case 2: (a) work exchanger network, and (b) heat exchanger network. 92

Figure 5.1. Schematic illustration of a piston-type work exchanger (Cheng and Fan, 1968). ... 99

Figure 5.2. Schematic representation of a work exchanger module. 101

Figure 5.3. Summary of the Excel model set up. 105

Figure 5.4. Work exchanger unit in the Aspen Plus environment. 106

Figure 5.5. Inlet data required to run the simulation. 107

Figure 5.6. Final streams and unit capacity results for Case 1. 108

Figure 5.7. Simulated work exchanger network in Aspen Plus for Case 2. 109

Figure 5.8. Single piston hydraulic free-piston engine (Mikalsen and Roskilly, 2009)..... 111

Figure 5.9. Piston-type work exchanger geometry model..... 114

Figure 5.10. The balance of forces on the piston. 115

Figure 5.11. An inlet check valve with one DOF translation (Ansys Inc. Fluent Theory Guide, 2017). 120

Figure 5.12. Contours of pressure variation during stages I-II. 123

Figure 5.13. Contours of pressure variation during stages III-IV. 124

Figure 5.14. Pressure change profile for HP and LP streams in full cycle (Stages I-IV). 125

Figure 5.15. Piston position in a full cycle (Stages I-IV). 125

Figure 5.16. Valve no. 1 (inlet low-pressure stream) position during the full cycle (Stages I-IV). 126

Figure 5.17. Valve no. 2 (outlet low-pressure stream) position during the full cycle (Stages I-IV). 126

Figure 5.18. Valve no. 3 (inlet high-pressure stream) position during the full cycle (Stages I-IV). 127

Figure 5.19. Valve no. 4 (outlet high-pressure stream) position during the full cycle (stages I-IV). 127

Figure 5.20. Piston position vs. time under different operating pressures. 129

Figure 5.21. Piston position vs. time under different operating temperatures. 130

Figure 5.22. The compression ratio of the low-pressure stream for a maximum displacement of the piston. 131

Figure 6.1. Chemical sector manufacturing energy and carbon footprint (U.S. DOE, 2012).. 146

Figure 6.2. Manufacturing energy consumption map. 152

Figure 6.3. Manufacturing carbon dioxide emission map. 158

Figure 6.4. Manufacturing energy consumption in counties of Michigan. 160

Figure 6.5. Energy consumption, energy loss, and carbon dioxide emission of three energy intensive counties in MI. 162

CHAPTER 1 INTRODUCTION

Improvement of energy efficiency and development of low-carbon technologies are two key solution approaches to ensuring future energy security and improving environmental cleanness, according to the International Energy Agency (IEA, 2017). In 2016, the primary energy consumption in the U.S. was 97.583 Quadrillion Btu (QBtu), out of which 22 % were consumed by industries; the energy generated in that year, however, was about 83.412 QBtu. This difference was the amount of net import. For instance, the average petroleum import in 2016 reached 10.06 million barrels per day (U.S. EIA, 2018). The continuous fluctuation of crude oil price also affects the nation's energy security. It is known that the average crude oil price of the OECD countries was increased from $8.74 per MBtu in 2005 to $18.25 per MBtu in 2012 and then decreased to $7.04 per MBtu in 2016 (BP, 2018). From the environmental sustainability point of view, the U.S. industries are responsible for about one-third of the overall GHG emission (U.S. EIA, 2018).

In the U.S., the chemical process industry accounts for about 40% of the total primary energy consumption among all the manufacturing sectors (Energetics Inc., 2014). Needless to say, how to further improve energy conservation in chemical plants is of significant importance.

1.1 Main Goals and Scientific Contributions

Process sustainability has become a main concern in industries, for which energy efficiency is a key indicator. Over the past decades, the chemical process industry has shown a great success in energy recovery in process systems through applying heat integration technologies. In chemical plants, thermal and mechanical energy are two common forms of energy. While the former can be effectively recovered by heat exchanger networks (HEN's), the recovery of the latter, however, has not drawn sufficient attention. Note that process work is more expensive than process heat, but recovery of mechanical energy is much more challenging.

From the thermodynamics point of view, heat flow where temperature is the state variable can be systematically managed to improve thermal energy efficiency, while work flow where pressure is the state variable must be carefully characterized so that opportunities for recovering mechanical energy can be identified. It is known that a large number of chemical plants have process streams to be pressurized, which require work for compression, or depressurized, which can produce work through expansion. Naturally, work exchange among process streams through synthesizing work exchanger networks (WENs) should be a feasible approach for mechanical energy recovery.

Due to the lack of fundamental understanding, the known methods for WEN system analysis and design are only very basic, where a few critical assumptions were inappropriately made in order to make the design problems solvable. Thus, significant research efforts are needed. The ultimate research goal is to introduce a type of process integration for effective work integration. To achieve this goal, a comprehensive thermodynamic analysis of work exchange in the unit operation as well as work integration at a system level is required. This will help us to have better insight towards the development of a work exchange network synthesis. Also, a methodological approach for energy target setting, process flowsheet, and combined heat and work integrated system is studied. This requires an investigation of the available devices for mechanical energy recovery, economic analysis of the devices, and a comprehensive discussion on energy recovery using the device of interest to identify required modifications of units to be used commercially in chemical plants.

The successful accomplishment of these objectives leads us to introduce a novel, rigorous, and general thermodynamic modeling and analysis approach for target setting of mechanical energy recovery prior to WEN synthesis. A process synthesis methodology for designing a heat-

integrated work exchange network is proposed, where both mechanical and thermal energy efficiencies as well as economic feasibility are considered. For investigating an energy recovery device that can be operated for mechanical energy recovery involving gas streams, a CFD-based model has been developed and various simulations to study the design of such a device, and its operational behavior under different operating conditions are conducted. In addition, to show the requirement of energy efficiency improvement in manufacturing sectors, a general data-driven method has been developed for analysis of energy efficiency of manufacturing sectors in different geographical zones. Industries consume about one-third of the total energy in the U.S. In manufacturing sectors around the country, significant energy loss occurs in various types of process systems and energy generation, conversion, and distribution steps. There exists a variety of information about national-level manufacturing and energy use. Integrated use of the accessible data could generate valuable information about energy efficiency and environmental impact in different manufacturing regions in the U.S.

1.2 Organization of Dissertation

Since the energy efficiency improvement in chemical processes covers a broad spectrum, the dissertation body is composed of two sections. The first section focuses on the new type of process integration called work exchange network design using a mechanical energy recovery device known as a direct work exchanger. For a bigger picture of the possible energy efficiency improvement in manufacturing sectors including the chemical and petrochemical sectors, a data-driven study is conducted to analyze the manufacturing sectors' performance in terms of energy efficiency and environmental impact in different geographical scales. This investigation will be helpful towards a possible collaboration with industries in the region for thermal and mechanical energy efficiency improvement in process systems

In Chapter 2, the concept of work integration and its fundamentals are discussed. This will be followed by a general review of the frontier research on work exchanger network (WEN) synthesis, which is a system approach to implementing work integration. Challenges in WEN synthesis, such as energy targeting, equipment innovation and costing, and system configuration when heat integration is incorporated, are discussed. Future research opportunities in WEN design and deployment are also considered. In Chapter 3, a thermodynamic modeling and analysis method to identify accurately the maximum amount of recoverable mechanical energy of any process system of interest, is introduced. It is greatly beneficial if the maximum amount of mechanical energy recoverable by a WEN can be determined prior to network design.

In Chapter 4, the focus will be on the next step towards completion of WEN synthesis, which is introducing a thermodynamic model-based synthesis approach to develop a cost effective heat-integrated work exchanger network (HIWEN), in which direct work exchangers may work under different operating conditions. Case studies will demonstrate that the resulting HIWENs can recover the maximum amount of mechanical and thermal energy at the lowest cost.

In Chapter 5, the investigation of the feasibility and design of a piston-type work exchanger (WE) that works for processing gas-phase process streams, is presented. The main approach is to use Aspen Plus and Computational Fluid Dynamic (CFD) simulation techniques to construct a WE model. In simulation, different unit configurations are compared, and different operational characteristics, cycle time, and dynamic behavior of the work exchanger, which are critical in the improvement of energy recovery efficiency are studied.

In Chapter 6 that includes the second part of the dissertation, a general data-driven modeling and analysis method to study energy consumption, energy loss, and CO_2 emissions in the manufacturing sectors at the state or county level, is introduced. The state of Michigan is

selected to illustrate methodological applicability. Finally, concluding remarks and future directions are sketched in Chapter 7.

CHAPTER 2 MECHANICAL ENERGY RECOVERY THROUGH WORK EXCHANGER NETWORK INTEGRATION: CHALLENGES AND OPPORTUNITIES

The chemical and petrochemical sector consumes almost 40% of the total primary energy use of all the manufacturing industries, but the energy loss is about 52% and the combustion emission reaches 46% of the total emission in manufacturing sectors (Annual Energy Outlook, 2015, Energetics Inc., 2014). Therefore, a significant improvement of energy efficiency in chemical and petrochemical plants is of great importance. Over the past three decades, heat integration technologies have been widely and successfully used to recover thermal energy, mainly through the integration of cost-effective heat exchanger networks (HENs) in process systems (Linnhoff and Flower, 1978, Floudas *et al.*, 1986, Yee and Grossmann, 1990, Shenoy, 1995).

In chemical and petrochemical plants, mechanical energy is another form of energy. It is known that about 30% of mechanical energy is lost in production (Energetics Inc., 2014), but how to recover mechanical energy effectively has not been fully explored. From the thermodynamics point of view, heat flow where temperature is the state variable is directly related to thermal energy efficiency, while work flow that occurs when a pressure difference exists between process streams should be characterized to evaluate mechanical energy efficiency. In plants, pressurization of process streams requires work for compression, while stream depressurization produces work through expansion. Ammonia manufacturing is among well-known examples. In production, natural gas is pressurized before entering a primary reformer, and air is pressurized before entering a secondary reformer. Ammonia synthesis occurs at a very high pressure, and thus a syngas mixture entering the reactor needs to be pressurized first. After the product stream containing mostly ammonia leaves the reactor, it should be depressurized (Strelzoff, 1978). Another example is offshore LNG production in the gas processing industry, where high-pressure natural gas streams need to be cooled by liquid CO_2 and then expanded to lower pressures to exchange heat

with liquid N_2. It should be further depressurized in a turbine to reach its storage pressure (Simonds and Williams, 1968, Aspelund, 2006, Aspelund *et al.*, 2007, Razib *et al.*, 2012). Apparently, if the available mechanical energy in the high-pressure streams is sufficiently utilized to pressurize the lower pressure streams through work exchange, the energy cost in operation could be considerably reduced; this energy efficiency improvement should also contribute to the reduction of CO_2 emission.

2.1 Mechanical Energy Recovery Fundamentals

It is recognized that the utilization of the mechanical energy available in a set of high-pressure streams for pressurizing a set of lower pressure streams in a process system may greatly reduce energy cost for compression operation. The pressure driven mechanical energy can be recovered using two types of work transfer units (WTUs), the direct or indirect recovery devices. The former is called work exchanger (WE), which was first introduced for seawater reverse osmosis desalination systems (to replace energy-intensive pumps and turbines) by Cheng *et al.* (1967). The device was built using two displacement vessels configured in parallel that could simultaneously pressurize one fluid stream in one vessel and depressurize an equivalent volume of another stream in the other vessel in each operational cycle. Figure 2.1(a) is a sketch of one vessel, where the stream flows are controlled by four valves (Cheng *et al.*, 1967, Cheng and Cheng, 1970). As a comparison, an indirect WTU, namely single-shaft-turbine-compressor (SSTC), is sketched in Fig. 2.1(b). This type of unit exchanges work in two steps: the pressure energy of a high-pressure stream is first converted to mechanical energy using an expander (turbine), and then to a compressor to pressurize a low-pressure stream (Chen and Wang, 2012). This type of device, however, has a low operational efficiency.

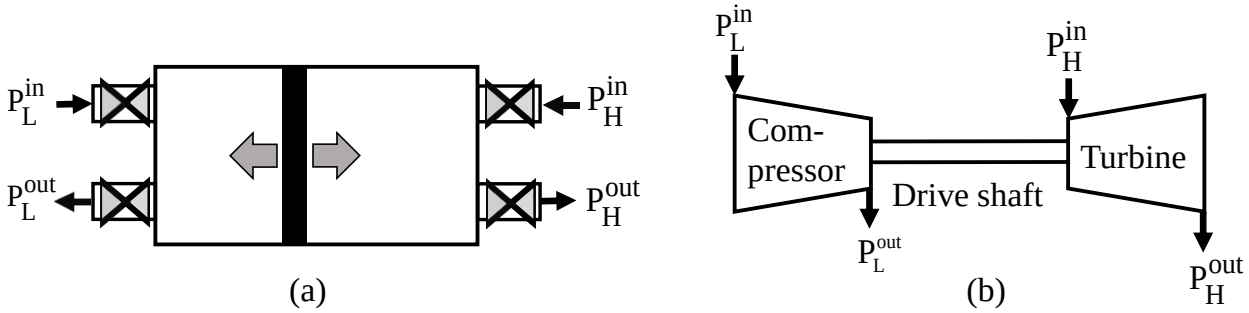

Figure 2.1. Sketch of work transfer units: (a) a (flow) WE and (b) an SSTC.

The work exchanger designed by Cheng *et al*. (1967) is sketched in Fig. 2.1(a). The process unit has two compartments divided by a piston; the movement of the piston is determined by the pressure difference between the two sides of it. In the sketch, the high-pressure stream in the right compartment can be depressurized from its input pressure P_H^{in} to output pressure P_H^{out}, and the low-pressure stream in the left compartment can be pressurized from its input pressure P_L^{in} to output pressure P_L^{out}. According to Cheng *et al*. (1967) the work exchange operation, through controlling the opening of the four valves shown in Fig. 2.2, occurs in the following four consecutive steps:

I) Depressurization step. After the displacement vessel is filled with high-pressure stream at P_H^{in}, valve v_3 is closed and valve v_4 is opened. This makes the high-pressure stream in the right compartment of the vessel flows out and the content in it is depressurized. This step takes a very short time. Valves v_1 and v_2 are closed in this step.

II) Low-pressure displacement step. When the pressure in the right compartment of the vessel drops to a pressure below P_L^{in}, valve v_1 opens. This makes the low-pressure stream flows into the left compartment of the vessel, and the depressurized high-pressure stream in the right

compartment continues to flow out through valve v_4. The piston moves to the right-hand end. Valves v_2 and v_3 are closed. At the end of the step, the vessel is filled with the low-pressure feed.

III) Pressurization step. After the displacement vessel is filled with the low-pressure stream at P_L^{in}, valve v_4 is closed, valve v_3 is opened, and some high-pressure stream flows into the right compartment of the vessel at P_H^{in} to pressurize the content in the left compartment. Similar to step (I), this step takes a very short time. Valves v_1 and v_2 are closed in this step.

IV) High-pressure displacement step. When the pressure in the left compartment of the vessel exceeds P_L^{out}, valve v_2 opens, and the pressurized low-pressure stream flows out through valve v_2. The high-pressure stream flows in continuously through valve v_3. The piston moves from the right-hand end to the left-hand end. Valves v_1 and v_4 are closed. At the end of this step, the vessel is filled with high-pressure stream at P_H^{in}.

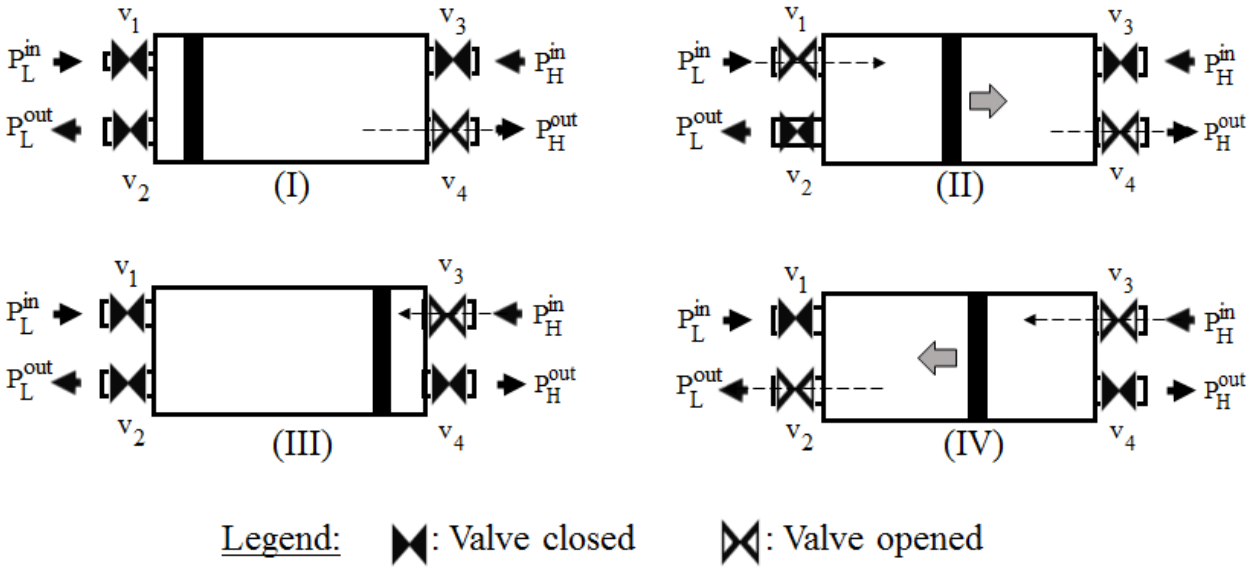

Figure 2.2. Valve position in each operational step of a work exchanger: (I) depressurization step; (II) low-pressure displacement step; (III) pressurization step; (IV) high-pressure displacement step.

The above steps repeat in operation. Note that steps (II) and (IV) take most of the time in each operational cycle, as compared with steps (I) and (III). Thus, it has been suggested to use two displacement vessels for the unit to be operated with appropriate timing, where fluid flows through the system continuously except for the short periods during steps (I) and (III). Also based on the four consecutive steps, the inlet pressure of the low-pressure stream should be higher than the outlet pressure of the high-pressure stream, and the inlet pressure of the high-pressure stream should be higher than the outlet pressure of the low-pressure stream for a continuous operation. The reversible shaft work (*W*) of each stream is expressed below (Kyle, 2003), in mathematical manipulation, the theorem of integration by parts is applied.

$$W_H = \int_{P_H^{in}}^{P_H^{out}} VdP = PV\Big|_{P_H^{in},V_H^{in}}^{P_H^{out},V_H^{out}} - \int_{V_H^{in}}^{V_H^{out}} PdV\,, \tag{2.1}$$

$$W_L = \int_{P_L^{in}}^{P_L^{out}} VdP = PV\Big|_{P_L^{in},V_L^{in}}^{P_L^{out},V_L^{out}} - \int_{V_L^{in}}^{V_L^{out}} PdV\,, \tag{2.2}$$

where *V* is the volumetric flow rate of a stream. In each of the above two equations, the first term on the right is the difference of the flow work between the high and low pressures, and the second term is the shaft work for the non-flow process.

Note that if the process streams are in gas phase, the operation can be under different conditions, such as isothermal, isentropic, or polytropic. Using an equation of state (*PV*=*znRT*) and thermodynamic laws, we can derive formulas for calculating the mechanical energy that should be removed from a given high-pressure stream or be received by a given low-pressure stream to meet their depressurization or pressurization needs, respectively. These formulas are summarized in Table 2.1. Note that in the table, there are two parameters, *k* [i.e., k_H in (T2.1-3) and k_L in (T2.1-4)] and *m* [i.e., m_H in (T2.1-5) and m_L in (T2.1-6)]. Parameter *k* is the ratio of

the heat capacities at the constant pressure and volume (i.e., $k = c_p / c_v$), and parameter *m* is related to parameter *k* (i.e., $m = k\eta_p / \left[1 - k\left(1 - \eta_p\right)\right]$), where η_p is the polytropic efficiency. If η_p reaches 100% (i.e., no friction), then parameters *k* and *m* are equal. For more detailed information about formula derivation, see Walas (1990), and Liu *et al.* (2014). Deng *et al.* (2010) studied the operation under the polytropic condition, and reported that the work recovery efficiency of a gas-gas work exchanger is lower than that of a liquid-liquid work exchanger. They indicated that the operational efficiency is decreased if the compression ratio is large; in that case, a multi-stage work transfer unit should be considered.

Table 2.1. Evaluation of mechanical energy exchanged by process streams under different operating conditions

Operating condition	W_H	W_L
Isothermal	$zRT_H \left(\frac{V_{H_i}\rho_{H_i}}{M_{w_{H_i}}}\right) ln\left(\frac{P_H^{in}}{P_H^{out}}\right)$ (T2.1-1)	$zRT_L \left(\frac{V_{L_j}\rho_{L_j}}{M_{w_{L_j}}}\right) ln\left(\frac{P_L^{out}}{P_L^{in}}\right)$ (T2.1-2)
Isentropic (adiabatic, frictionless)	$\frac{k_H}{k_H - 1} zRT_H^{out} \left(\frac{V_{H_i}\rho_{H_i}}{M_{w_{H_i}}}\right)\left(\left(\frac{P_H^{in}}{P_H^{out}}\right)^{\frac{k_H - 1}{k_H}} - 1\right)$ (T2.1-3)	$\frac{k_L}{k_L - 1} zRT_L^{in} \left(\frac{V_{L_j}\rho_{L_j}}{M_{w_{L_j}}}\right)\left(\left(\frac{P_L^{out}}{P_L^{in}}\right)^{\frac{k_L - 1}{k_L}} - 1\right)$ (T2.1-4)
Polytropic (adiabatic, frictional)	$\frac{m_H}{m_H - 1} zRT_H^{out} \left(\frac{V_{H_i}\rho_{H_i}}{M_{w_{H_i}}}\right)\left(\left(\frac{P_H^{in}}{P_H^{out}}\right)^{\frac{m_H - 1}{m_H}} - 1\right)$ (T2.1-5)	$\frac{m_L}{m_L - 1} zRT_L^{in} \left(\frac{V_{L_j}\rho_{L_j}}{M_{w_{L_j}}}\right)\left(\left(\frac{P_L^{out}}{P_L^{in}}\right)^{\frac{m_L - 1}{m_L}} - 1\right)$ (T2.1-6)

The work exchange between high-pressure and low-pressure streams during the four steps is also illustrated in a pressure-volume (P-V) diagram as shown in Figure 2.3 (Cheng *et al.*, 1967). In this figure, lines 2-3, 7-8-9 represent depressurization step, lines 3-4 and 9-10, low-pressure displacement, lines 4-1 and 10-6-6′, pressurization step; and lines 1-2 and 6-7, high-pressure displacement.

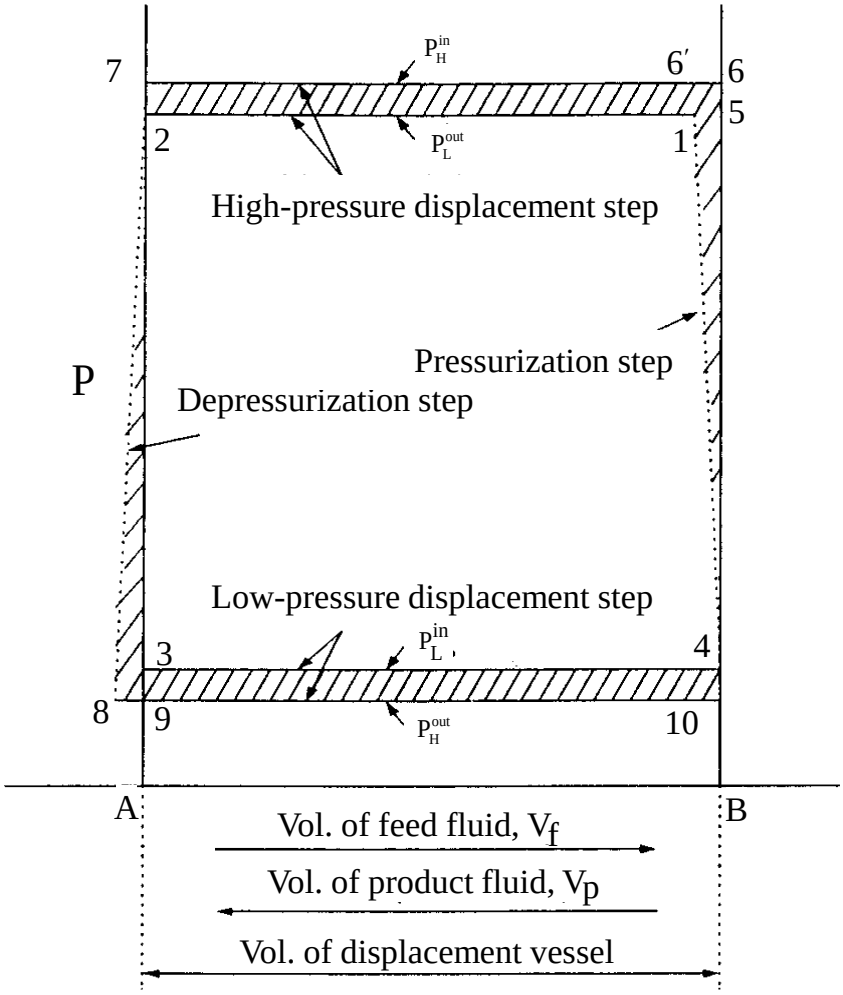

Figure 2.3. P-V diagram for a flow work exchanger.

Huang and Fan (1996), added one dimension to P-V (i.e., Pressure-Volumetric flowrate) diagram to visualize the energy exchanges among streams. The result is a three-dimensional diagram called P-V-W (i.e., Pressure-Volumetric flowrate-Work) diagram as shown in Figure 2.4.

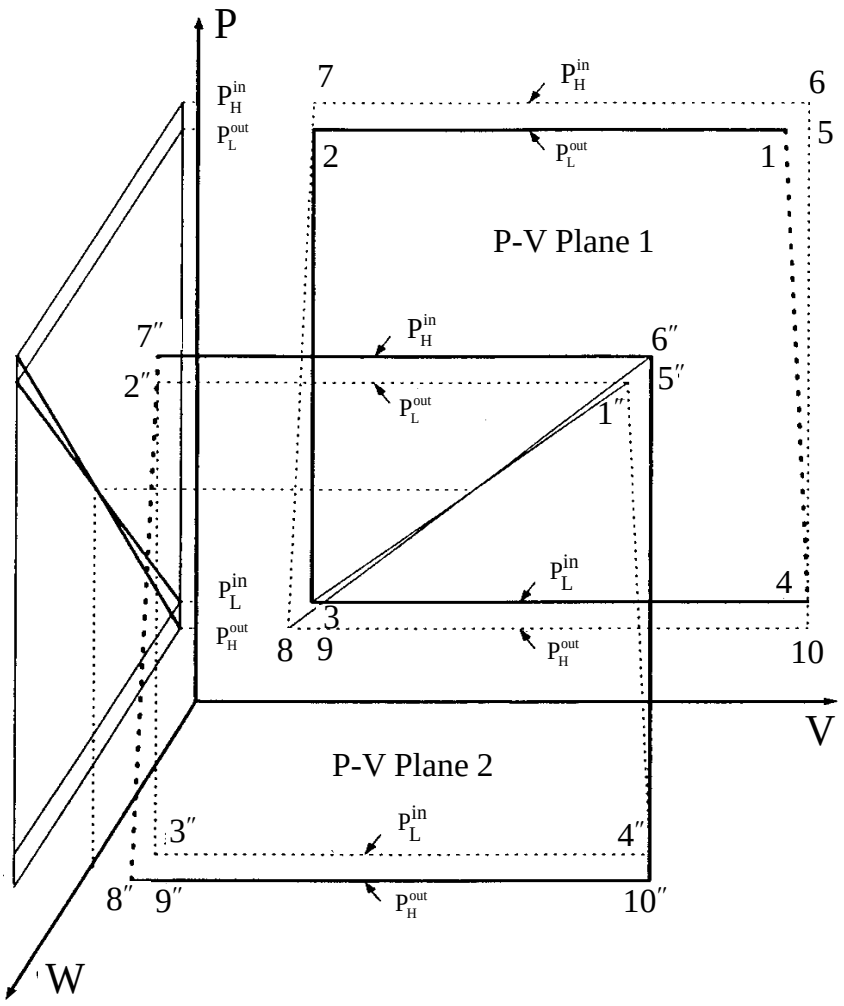

Figure 2.4. P-V-W diagram for work exchanger.

P-W (i.e., Pressure-Work) diagram is generated from the P-V-W diagram and as shown in Fig. 2.5 contains two operating lines to describe work exchange between a high-pressure stream and a low-pressure stream, assuming no energy loss in operation. This diagram demonstrates a distinctive feature, i.e., the two operating lines cross each other. This is due to the following necessary condition for feasbile work exchange:

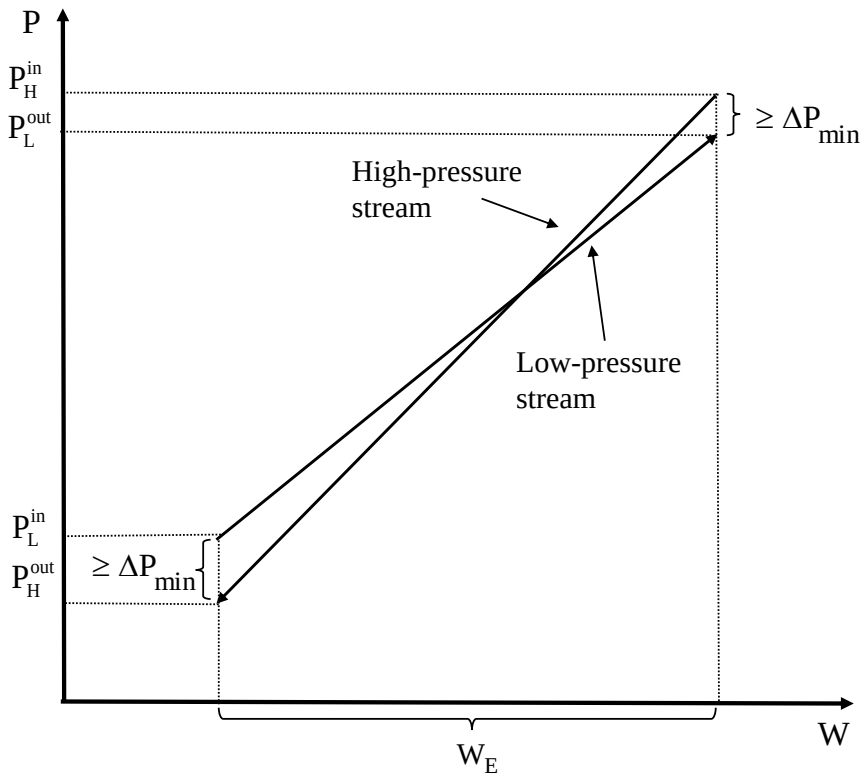

Figure 2.5. P-W diagram for the work exchanger.

(i) Work energy should not be exchanged between any pair of low-pressure streams or pair of high-pressure streams.

$$\left.\begin{array}{ll} P_H^{in} > P_H^{out} & \text{for HP stream} \\ P_L^{in} < P_L^{out} & \text{for LP stream} \end{array}\right\} \tag{2.3}$$

(ii) Also note that in Fig. 2.5, the slope of the operating line for the high-pressure stream must be greater than that for the low-pressure stream. Since the slope is the reciprocal of the volumetric flow rate of a process stream, the following inequality holds:

$$V_H < V_L. \tag{2.4}$$

(iii) The source pressure of high-pressure stream should be higher than the target pressure of the low-pressure stream at least in the amount of the minimum pressure difference (ΔP_{min}); the

source pressure of the low-pressure stream should be higher at least in the amount of ΔP_{min} than the target pressure of the high-pressure stream.

$$\left.\begin{aligned} P_H^{in} - P_L^{out} &\geq \Delta P_{\min} \\ P_L^{in} - P_H^{out} &\geq \Delta P_{\min} \end{aligned}\right\} \tag{2.5}$$

Determination of ΔP_{min} affects the efficiency of the work exchangers. Cheng *et al.* (1967) reported that the optimized value is between 35 to 70 kPa. The process streams through a work exchanger can be in either liquid or gas phase. For the streams in the gas phase, the work exchanger may be operated under isothermal, isentropic, or polytropic condition.

2.2 WEN Synthesis-Progress Overview

Inspired by the notion of heat integration through HEN synthesis, Huang and Fan in 1996 introduced the notion of work integration, and defined a new type of process synthesis called work exchanger network (WEN) synthesis (Huang and Fan, 1996). In a WEN, mechanical energy is transferred between process streams using flow work exchangers that were constructed by Cheng *et al.* (1967), which are now widely used in the desalination industry (Flowserve, 2017, Pique, 2003). In this work, this type of unit is called direct work exchanger, or simply work exchanger. The *P*-*W* diagram introduced by Huang and Fan (1996) was used to characterize work exchange of any pair of high-pressure stream and low-pressure stream. It was then employed to investigate various stream matching conditions and basic rules for synthesizing a thermodynamically feasible and cost effective WEN.

The WEN synthesis problem did not catch sufficient attention until recent years. Deng *et al*. (2010) conducted a basic thermodynamic analysis on a gas-gas work exchanger. Chen and Feng (2012) used the *P*-*W* diagram technique to study a WEN problem with an ammonia synthesis example. Liu *et al*. (2014) developed a graphical method using an improved P-W diagram. By

their method, a thermodynamically feasible WEN was developed, where work exchangers, compressors and expanders were used. Their methodology, however, is incapable of predicting the maximum amount of recoverable mechanical energy prior to synthesis, and thus the efficiency of energy recovery by a resulting WEN is low. Besides, their work did not consider the capital cost issue, even in terms of the number of work transfer units used in network design as an approximation.

Zhuang *et al.* (2017) have presented a transshipment model for adiabatic processes and formulated an NLP model. The work exchange network is designed to calculate the minimum utility consumption for the condition that all streams satisfy the constraints of pressures and temperatures. Then, heat integration is introduced by adding heaters and coolers for the step-wise design of both work and heat integration to minimize TAC. The direct work exchanger is used as the energy recovery device. Note that in the economic analysis of the direct work exchangers, one-fifth of the total cost of one compressor and one expander (turbine) is considered. In another study, Zhuang *et al.* (2017) have worked on the transshipment model for an isothermal process for minimizing the utility consumption. They developed the work exchange network using a set of matching rules. In a recent study by Zhuang *et al.* (2017), an upgraded graphical method is presented to conduct a work exchange network synthesis using direct work exchangers. They have work on the similar type of composite curves for high-pressure and low-pressure matching studied by Liu *et al.* (2014). However, they have introduced a pressure index (μ) to modify the P-W composite curves for linear μ-W plots.

Using single-shaft-turbine-compressor (SSTC) units, which can be called indirect work exchangers, Razib *et al*. (2012) proposed a WEN design method, and a process configuration was identified by a superstructure-based MINLP algorithm in their case study. Huang and Karimi

(2016) presented an MINLP formulation to synthesize work-heat exchange network at the lowest total annualized cost. In each stage of the presented superstructure, streams will pass through a heat exchanger network first and then work exchanger network and will go through additional heaters or coolers to reach the target temperatures. Considering the fact that energy provided through expansion increases with inlet temperature and required through compression decreases by inlet temperature, they have assumed high-pressure streams as cold streams and low-pressure streams as hot streams in heat exchanger network. Recently, Nair *et al.* (2018) have studied a new MINLP model for total annualized cost minimization work-heat exchange network synthesis without pre-assuming the hot or cold streams for high-pressure and low-pressure streams. Then, the streams will go through stages of a heat exchanger network first and then a work exchanger and additional heat exchanger network to reach the target temperatures. In this work, they have also considered stream property correlations and the phase change possible.

Onishi *et al*. (2014) introduced a new MINLP optimization model for the synthesis of a WEN using SSTC units, with hypothetical heat integration for optimal pressure recovery from process gas streams. Onishi *et al.* (2017) also worked on multi-objective modeling (moMINLP) for the synthesis of work and heat exchange network to simultaneously minimize total annualized cost and overall environmental impact. In both studies, streams will go through a heat exchanger network first and then a work exchanger network. Similar to Huang and Karimi (2016), high-pressure streams are considered as cold streams and low-pressure streams as hot streams but to reach the target temperature after the final stage of work exchanger network, high-pressure streams will be heated and low-pressure streams will be cooled.

Cui *et al.* (2017) developed a process superstructure for a 4-column methanol distillation system to improve energy efficiency through heat and work exchanger networks to reduce steam

and electricity consumption. In WEN design, they have considered using the shaft work of expanders as power for running the pumps.

Despite the studies on the application of direct or indirect work exchangers, as an early investigation heat and work integration was studied through the placement of heat engines and heat pumps (Townsend and Linnhoff, 1983). Fu and Gundersen (2015, 2016) also investigated the relevance of heat and work integration. In their study, a graphical design procedure was presented for integrating compressors and expanders into HEN. The placement of each pressurization/depressurization unit and its influence on the pinch point temperature and exergy consumption were also analyzed.

2.3 Challenges and Opportunities

The known studies have shown that WEN synthesis is a new type of process integration technology, and WEN can be integrated into process systems to recover mechanical energy that is consumed by compressors, pumps, turbines, and other types of pressure vessels in the process industries.

There are various similarities between HEN and WEN syntheses, as fundamentally in each type of network, a set of high-potential streams (hot streams in HEN or high-pressure streams in WEN) transfer energy to a set of low-potential streams (cold or low-pressure streams) due to the existence of a driving force (ΔT in HEN and ΔP in WEN). In HEN, heat transfer units are easy to operate. By contrast, the compressors and expanders in WEN may operate in multiple stages, which could be under isothermal or non-isothermal condition. Thus, the shaft work either demanded for compression or provided by a work force may be significantly different. In addition, required compression and provided expansion energy is operating temperature dependent.

Methodologically, the Pinch Analysis technique successfully used in HEN synthesis cannot be directly used for WEN synthesis, because the basic notion of pinch point for heat exchange is not applicable for work exchange. As shown in the T-H diagram in Fig. 2.6(a), the temperature of the hot stream must be higher than that of the cold stream in the entire temperature range involved. However, this is not the case for work exchange between a high-pressure stream and a low-pressure stream as shown in the P-W diagram in Fig. 2.6(b). Therefore, the method for determining the maximum energy recovery by a HEN cannot be applied to a WEN problem. Besides, the basic formula for estimating the minimum number of heat transfer units in a HEN cannot be simply applied to the estimation of the minimum number of work transfer units in a WEN.

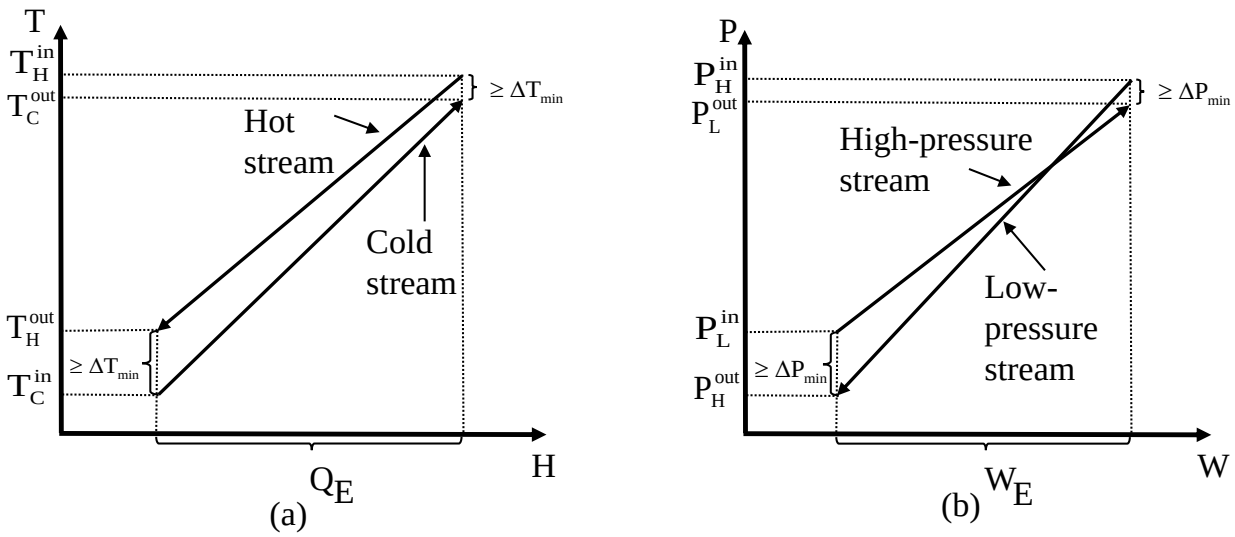

Figure 2.6. Comparison of (a) heat transfer in a HE and (b) work transfer in a WE.

It is noticed that WE, either direct or indirect, has only limited industrial applications. There is a serious lack of technological innovation in equipment design, especially for gas-gas or gas-liquid direct WE. This requires a more fundamental study on the designed operational behaviour of such a type of device. Also note that if a WE involves a gas stream's pressurization

or depressurization, the stream temperature can be changed considerably in operation. Therefore, such a WEN should be designed with heat integration technology incorporated; thereby leading to a hybrid exchange network.

WEN synthesis problems could be mathematically formulated and solved by MINLP techniques. Other types of synthesis methods could be also attractive, especially if a WEN design problem involves not too many high/low pressure streams, which is common. In such a case, heuristic based methods may demonstrate advantages, as a derived solution structure becomes explainable, which allows engineers to address some practical design issues that could be difficult to formulate mathematically. Note that since heat-incorporated WEN system is structurally highly interacted, its operation could be sophisticated in terms of system dynamics, control, and process safety.

The essential purpose of WEN synthesis is to improve process sustainability. This is the reason in addition to energy; economic conservation plays a key role in development of any new technology. However, cost estimation of the direct work exchangers has not been studied for different capacities and sizes similar to other unit operations such as compressors and heat exchangers. The limited application of these devices in desalination processes could be defined as the main reason. A pilot study of flow work exchangers for desalination processes by Cheng and Fan (1968) is the only available source which discussed the cost of the unit for a specific capacity. Thus, to investigate the economic feasibility of using direct work exchangers in chemical processes, the development of a unique formula for cost estimation of the unit would be of great importance.

Among different types of WEs, the Dual Work Exchange Energy Recovery Device (DWEER) has been widely used for seawater reverse osmosis (RO) desalination, which is one of

the most efficient energy recovery systems developed to date (by Flowserve Corporation). This type of device (dealing with liquid streams) has been reported to have low mixing and leakage losses, low maintenance cost, and self-adjustment capability to different flow rates and pressures. Despite that, WEs dealing with gas phase streams will demonstrate different operational characteristics. Note that operational safety related to leakage and mixing losses should be considered, especially when processing gas streams.

Another important concern is the operational performance of WEs, as the units may have a longer cycle time, depending on the operational mode, in comparison to compressors and expanders. Therefore, WEN dynamic control could be a challenge, as an effective operational coordination strategy is needed for operating different types of units working in continuous or batch-like operational modes. This requires a more comprehensive study on system control design.

CHAPTER 3 PREDICTION OF MAXIMUM RECOVERABLE MECHANICAL ENERGY VIA WORK INTEGRATION: A THERMODYNAMIC MODELING AND ANALYSIS APPROACH

The known studies have clearly shown that WEN, either using direct or indirect work exchangers, is a new type of process network system for recovering mechanical energy that is consumed or provided by compressors, pumps, turbines, and other types of pressure vessels. However, there is still no known method that can be used to predict the maximum amount of mechanical energy recoverable by work exchangers prior to process synthesis. As the pinch concept is not valid in work exchange analysis, the traditional pinch analysis method is in general not applicable for WEN synthesis. Thus, a new type of synthesis methodology should be developed. As the first step, prediction of maximum recoverable mechanical energy prior to network synthesis should be of great significance, as this could help determine if a WEN is economically attractive for energy recovery, and if so, the predicted energy recovery can be set as a target to achieve in the process synthesis phase.

In this chapter, we focus on introducing a mathematical modeling and analysis method which aims at predicting the maximum amount of mechanical energy that can be feasibly recovered using work exchangers. The modeling and analysis method can be applied to the design of a work exchange system operated under isothermal or adiabatic conditions. To illustrate methodological efficacy, two case study problems selected from the literature are investigated and the results are compared with those by other methods.

3.1 Mathematical Framework for Energy Recovery Targeting

A WEN synthesis problem can be stated as follows. Given a set of high-pressure streams (H_i, i = 1, 2, ⋯, N_H) and a set of low-pressure streams (L_j, j = 1, 2, ⋯, N_L), their supply and target pressures (i.e., $P^s_{H_i}$, $P^t_{H_i}$, $P^s_{L_j}$, and $P^t_{L_j}$), volumetric flowrates (i.e., V_{H_i} and V_{L_j}), and the

minimum acceptable pressure difference between any pair of high-pressure and low-pressure streams (i.e., $\Delta P_{\min}$), synthesize a WEN that can recover the maximum amount of mechanical energy at the lowest cost.

To set an energy target for this type of synthesis problem, we introduce a thermodynamic modeling and analysis method that can be used to determine precisely the maximum amount of mechanical energy recoverable by a WEN prior to flowsheet development. The modeling involves an introduction of a number of matrices and vectors, which is followed by a model-based computational procedure.

Identification of pressure intervals of low-pressure streams for pressurization by high-pressure streams. This task can be accomplished in two steps.

Step 1. Construct matrix $\bar{\boldsymbol{\Gamma}}$. For each low-pressure stream L_j (j = 1, 2, ⋯, N_L), it is required to identify the largest pressure interval, within which L_j can receive mechanical energy thermodynamically feasibly from each high-pressure stream H_i (i = 1, 2, ⋯, N_H). Thus, we introduce matrix $\bar{\boldsymbol{\Gamma}}$ to accommodate all $N_H \times N_L$ intervals in the following structure:

$$\bar{\boldsymbol{\Gamma}} = \begin{pmatrix} \overline{\Gamma}_{H_1,L_1} & \overline{\Gamma}_{H_1,L_2} & \cdots & \overline{\Gamma}_{H_1,L_{N_L}} \\ \overline{\Gamma}_{H_2,L_1} & \overline{\Gamma}_{H_2,L_2} & \cdots & \overline{\Gamma}_{H_2,L_{N_L}} \\ \vdots & \vdots & \ddots & \vdots \\ \overline{\Gamma}_{H_{N_H},L_1} & \overline{\Gamma}_{H_{N_H},L_2} & \cdots & \overline{\Gamma}_{H_{N_H},L_{N_L}} \end{pmatrix}, \tag{3.1}$$

where

$$\overline{\Gamma}_{H_i,L_j} = \left[\Gamma^a_{H_i,L_j}, \Gamma^b_{H_i,L_j} \right], \tag{3.2}$$

where $\overline{\Gamma}_{H_i,L_j}$ is the identified pressure interval between streams H_i and L_j; $\Gamma^a_{H_i,L_j}$ is the lower-bound pressure; $\Gamma^b_{H_i,L_j}$ is the upper-bound pressure. Figure 3.1 shows a flowchart that can be used to generate each pressure interval in the matrix, where the necessary condition for work transfer between a pair of *H* and *L* streams shown in Eq. 2.5 is implemented.

Step 2. Construct matrix $\overline{\boldsymbol{P}}$. Note that within any specific pressure interval of a low-pressure stream, it can accept energy from only one high-pressure stream. However, in matrix $\overline{\boldsymbol{\Gamma}}$, some identified interval(s) of an *L* stream may be associated with more than one *H* stream. If this occurs, then the overlapped pressure range between the identified interval(s) should be specified; only one such an interval can be kept, and the others should be excluded. Therefore, we introduce another matrix named $\overline{\boldsymbol{P}}$ ($N_H \times N_L$), which should be derived through manipulating element values in matrix $\overline{\boldsymbol{\Gamma}}$.

$$\overline{\boldsymbol{P}} = \begin{pmatrix} \overline{P}_{H_1,L_1} & \overline{P}_{H_1,L_2} & \cdots & \overline{P}_{H_1,L_{N_L}} \\ \overline{P}_{H_2,L_1} & \overline{P}_{H_2,L_2} & \cdots & \overline{P}_{H_2,L_{N_L}} \\ \vdots & \vdots & \ddots & \vdots \\ \overline{P}_{H_{N_H},L_1} & \overline{P}_{H_{N_H},L_2} & \cdots & \overline{P}_{H_{N_H},L_{N_L}} \end{pmatrix}, \tag{3.3}$$

where

$$\overline{P}_{H_i,L_j} = \left\lfloor P^a_{H_i,L_j}, P^b_{H_i,L_j} \right\rfloor. \tag{3.4}$$

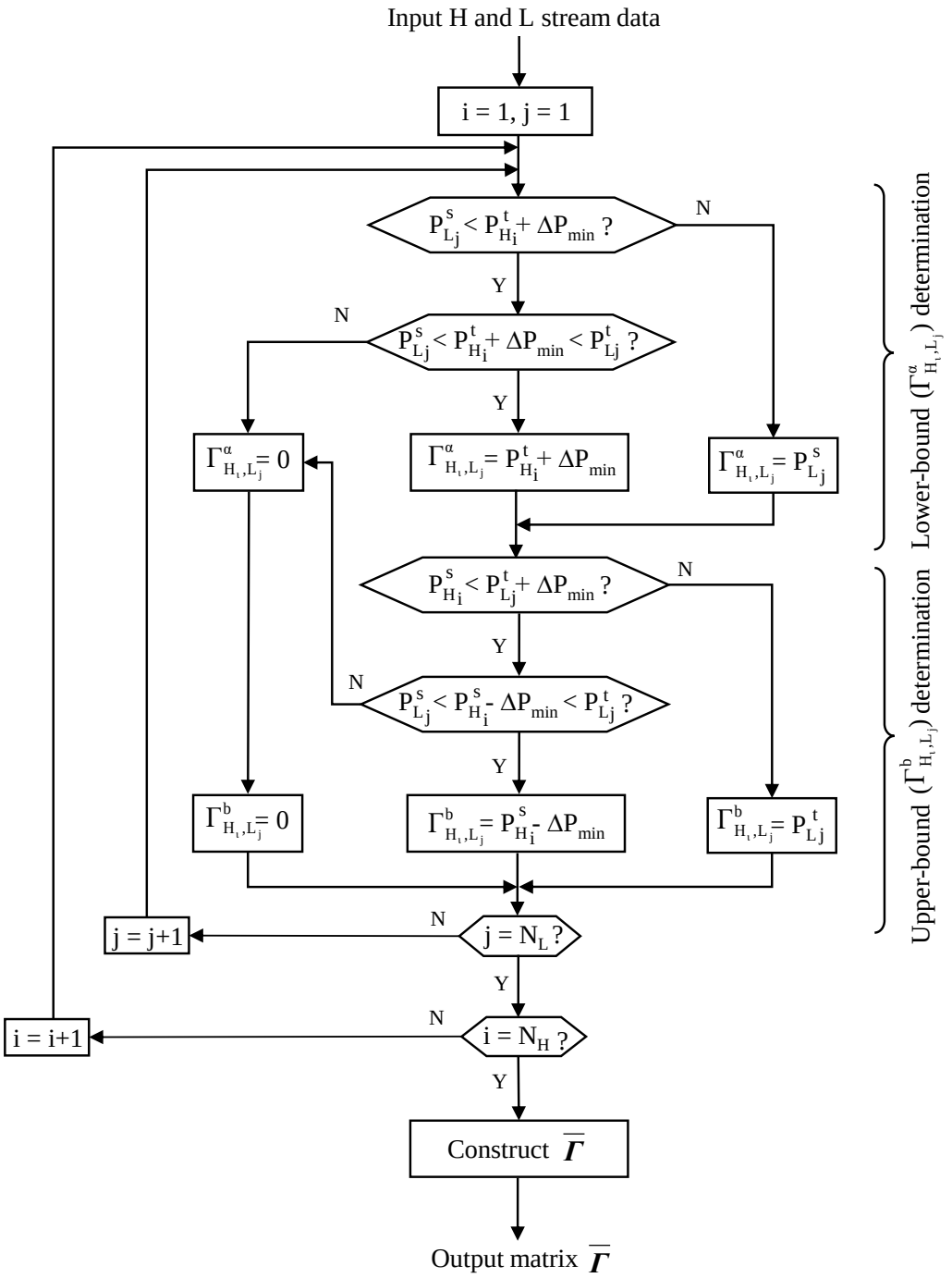

Figure 3.1. Flowchart for derivation of matrix $\overline{\Gamma}$.

The element, $\overline{P}_{H_i,L_j}$ can be determined in two sub-steps. The first sub-step is to calculate $\overline{P}^l_{H_i,L_j}$ using the following formula:

$$\overline{P}^l_{H_i,L_j} = \begin{cases} \overline{\Gamma}_{H_i,L_j}; & \text{if } V_{H_i} > V_{H_{i+l}} \\ \overline{\Gamma}_{H_i,L_j} \cap \overline{\overline{\Gamma}_{H_i,L_j} \cap \overline{R}_{(H_i,L_j)\to(H_{i+l},L_j)}}\ ; & \text{otherwise} \end{cases} \tag{3.5}$$

where *l* is an index whose value should satisfy two conditions: (1) $l \le |N_H - 1|$ but $l \ne 0$, and (2) $0 < (i+l) \le N_H$. Note that the long bar above the intersection of $\overline{\Gamma}_{H_i,L_j}$ and $\overline{R}_{(H_i,L_j)\to(H_{i+l},L_j)}$ in the above equation is an operation of complement in set theory.

The second sub-step of the evaluation is to determine $\overline{P}_{H_i,L_j}$, which is the intersection of all identified $\overline{P}^l_{H_i,L_j}$'s, i.e.,

$$\overline{P}_{H_i,L_j} = \bigcap\left(\overline{P}^l_{H_i,L_j}\right). \tag{3.6}$$

Note that $\overline{R}_{(H_i,L_j)\to(H_{i+l},L_j)}$ in Eq. 3.5 is the overlapped pressure range between the $(H_i,L_j)-$th interval and the $(H_{i+l},L_j)-$th interval in the *j*-th column of matrix $\overline{\boldsymbol{\Gamma}}$; it can be determined through performing the following operation:

$$\overline{R}_{(H_i,L_j)\to(H_{i+l},L_j)} = \left[\left(\Gamma^a_{H_i,L_j} \vee \Gamma^a_{H_{i+l},L_j}\right), \left(\Gamma^b_{H_i,L_j} \wedge \Gamma^b_{H_{i+l},L_j}\right)\right]. \tag{3.7}$$

Evaluation of mechanical energy transfer from high-pressure streams to low-pressure streams. Using the pressure interval information in matrix $\overline{\boldsymbol{P}}$, we can calculate the

mechanical energy that can be transferred from each individual high-pressure stream to each individual low-pressure stream. Matrix $\boldsymbol{W}_{\beta}$ ($N_H \times N_L$) is thus introduced to collect all energy transfer data in a structured way, i.e.,

$$\boldsymbol{W}_{\beta} = \begin{pmatrix} W_{\beta_{H_1,L_1}} & W_{\beta_{H_1,L_2}} & \cdots & W_{\beta_{H_1,L_{N_L}}} \\ W_{\beta_{H_2,L_1}} & W_{\beta_{H_2,L_2}} & \cdots & W_{\beta_{H_2,L_{N_L}}} \\ \vdots & \vdots & \ddots & \vdots \\ W_{\beta_{H_{N_H},L_1}} & W_{\beta_{H_{N_H},L_2}} & \cdots & W_{\beta_{H_{N_H},L_{N_L}}} \end{pmatrix} \tag{3.8}$$

where

$$W_{\beta_{H_i,L_j}} = \begin{cases} zRT^s_{L_j}\left(\dfrac{V_{L_j}\rho_{L_j}}{M_{w_{L_j}}}\right) ln\left(\dfrac{P^b_{H_i,L_j}}{P^a_{H_i,L_j}}\right); & \text{Isothermal condition} \\ \left(\dfrac{k_L}{k_L-1}\right) zRT^s_{L_j}\left(\dfrac{V_{L_j}\rho_{L_j}}{M_{w_{L_j}}}\right)\left(\left(\dfrac{P^b_{H_i,L_j}}{P^a_{H_i,L_j}}\right)^{\frac{k_L-1}{k_L}} - 1\right); & \text{Isentropic condition (adiabatic)} \\ \left(\dfrac{m_L}{m_L-1}\right) zRT^s_{L_j}\left(\dfrac{V_{L_j}\rho_{L_j}}{M_{w_{L_j}}}\right)\left(\left(\dfrac{P^b_{H_i,L_j}}{P^a_{H_i,L_j}}\right)^{\frac{m_L-1}{m_L}} - 1\right); & \text{Polytropic condition (adiabatic)} \end{cases} \tag{3.9}$$

Note that in the isentropic and polytropic conditions, the outlet temperature of a low-pressure stream changes after each compression step. Hence, in calculation of $W_{\beta_{H_i,L_j}}$, the inlet temperature of low-pressure stream, $T^s_{L_i}$, should be multiplied by $\left(\dfrac{P^a_{H_i,L_j}}{P^s_{L_j}}\right)^{\frac{k_L-1}{k_L}}$ or $\left(\dfrac{P^a_{H_i,L_j}}{P^s_{L_j}}\right)^{\frac{m_L-1}{m_L}}$ for the isentropic or polytropic condition, respectively, in order to eliminate calculation error.

In matrix $\boldsymbol{W}_{\beta}$, the sum of the element values in any row (e.g., the *i*-th row) is the total amount of mechanical energy from the corresponding high-pressure stream (i.e., H_i) to all N_L

low-pressure streams (i.e., $\sum_{j=1}^{N_L} W_{\beta_{H_i,L_j}}$). This amount of energy required for pressurizing all the low-pressure streams can be greater than, equal to, or less than the total amount of energy that the high-pressure stream (H_i in this case) can transfer. Understanding the value difference is important as this could affect design decision during flowsheet development. Here, a vector named W_γ ($N_H \times 1$) is defined to include this type of value information for each high-pressure stream.

$$\boldsymbol{W}_\gamma = \begin{pmatrix} W_{\gamma_1} \\ W_{\gamma_2} \\ \vdots \\ W_{\gamma_{N_H}} \end{pmatrix}, \tag{3.10}$$

where

$$W_{\gamma_i} = W_{H_i} - \sum_{j=1}^{N_L} W_{\beta_{H_i,L_j}} \quad . \tag{3.11}$$

According to Eqs. (T2.1-1), (T2.1-3), and (T2.1-5) in Table 2.1, the value of W_{H_i} can be estimated as follows:

$$W_{H_i} = \begin{cases} zRT_{H_i}\left(\dfrac{V_{H_i}\rho_{H_i}}{M_{w_{H_i}}}\right) ln\left(\dfrac{P^s_{H_i}}{P^t_{H_i}}\right); & \text{Isothermal condition} \\ \dfrac{k_H}{k_H - 1} zRT^t_{H_i}\left(\dfrac{V_{H_i}\rho_{H_i}}{M_{w_{H_i}}}\right)\left(\left(\dfrac{P^s_{H_i}}{P^t_{H_i}}\right)^{\frac{k_H-1}{k_H}} - 1\right); & \text{Isentropic condition (adiabatic)} \\ \dfrac{m_H}{m_H - 1} zRT^t_{H_i}\left(\dfrac{V_{H_i}\rho_{H_i}}{M_{w_{H_i}}}\right)\left(\left(\dfrac{P^s_{H_i}}{P^t_{H_i}}\right)^{\frac{m_H-1}{m_H}} - 1\right); & \text{Polytropic condition (adiabatic)} \end{cases} \tag{3.12}$$

Note that in the isentropic and polytropic conditions, the outlet temperature of high-pressure stream, $T_{H_i}^t$, will change after each stage of expansion, which can be evaluated as follows:

$$T_{H_i}^t = \begin{cases} T_{H_i}^s \left(\dfrac{P_{H_i}^t}{P_{H_i}^s} \right)^{\frac{k_H - 1}{k_H}}; & \text{Isentropic condition (adiabatic)} \\ \\ T_{H_i}^s \left(\dfrac{P_{H_i}^t}{P_{H_i}^s} \right)^{\frac{m_H - 1}{m_H}}; & \text{Polytropic condition (adiabatic)} \end{cases} . \tag{3.13}$$

Determination of the minimum amount of external energy requirement. The element values in vector W_γ can be positive, zero, and negative. The sum of all positive values in vector W_γ (i.e., $W_{\gamma_i} > 0$) is the total amount of mechanical energy of N_H high-pressure streams that cannot be used for pressurizing feasibly low-pressure streams. This amount of energy should be removed by expanders. We use variable W_E^U to quantify this total external power for expanders, i.e.,

$$W_E^U = \sum_{i=1}^{n_H^+} W_{\gamma_i} , \tag{3.14}$$

where W_{γ_i} included in the above equation must be of a positive value, and n_H^+ is the total number of the elements with a positive value each in vector W_γ.

On the other hand, if the *i*-th element in $\boldsymbol{W}_\gamma$ has a negative value, this means the energy transferred from high-pressure stream H_i to N_L low-pressure streams is insufficient. The sum of all the negative values in the vector W_γ is part, but not all, of the total demand of the external

compression power needed for pressurizing the low-pressure streams. This amount can be evaluated by variable $W_{C_1}^U$ that is defined below:

$$W_{C_1}^U = -\sum_{i=1}^{n_H^-} W_{\gamma_i}, \tag{3.15}$$

where W_{γ_i} included in the above equation must be of a negative value, and n_H^- is the total number of elements having a negative value each in vector $\boldsymbol{W}_\gamma$.

Note that matrix $\bar{\boldsymbol{P}}$ contains the pressure intervals of low-pressure streams for feasibly receiving mechanical energy from high-pressure streams. In general, there must be other pressure intervals of low-pressure streams, within which no energy can be received from any high-pressure stream, based on the necessary condition for feasible work exchange shown in Eq. 2.5. Thus, in order to meet the pressurization requirement for those intervals, additional external compression power will be needed. Variable $W_{C_2}^U$ is designated for this purpose; it can be calculated as follows:

$$W_{C_2}^U = W_L^{tot} - W_{H\to L}^{tot}, \tag{5.16}$$

where W_L^{tot} is the total demand of all N_L low-pressure streams for pressurization, which can be calculated as:

$$W_L^{tot} = \sum_{j=1}^{N_L} W_{L_j}, \tag{3.17}$$

and $W_{H\to L}^{tot}$ is the total amount of energy that can be obtained by all low-pressure streams from all high-pressure streams, which can be calculated as follows:

$$W_{H\to L}^{tot} = \sum_{i=1}^{N_H}\sum_{j=1}^{N_L} W_{\beta_{i,j}}. \tag{3.18}$$

Therefore, the total amount of external compression energy needed by pressuring the low-pressure streams is:

$$W_C^U = W_{C_1}^U + W_{C_2}^U . \tag{3.19}$$

Estimation of the maximum amount of recoverable mechanical energy. The maximum amount of mechanical energy that can be feasibly recovered from high-pressure streams is the difference between the amount of mechanical energy to be removed from the high-pressure streams and the minimum amount of external expansion utilities. Here we introduce variable W_R^{tot}, which can be expressed as follows:

$$W_R^{tot} = W_H^{tot} - W_E^U , \tag{3.20}$$

where W_H^{tot} is the total amount of energy of all N_H high-pressure streams for depressurization, which can be calculated as:

$$W_H^{tot} = \sum_{i=1}^{N_H} W_{H_i} . \tag{3.21}$$

On the other hand, this amount can be also expressed by evaluating the difference between the total amount of mechanical energy needed by all low-pressure steams and the minimum amount of external compression power evaluated in Eq. 3.19, i.e.,

$$W_R^{tot} = W_L^{tot} - W_C^U . \tag{3.22}$$

Calculation procedure. The models and evaluation methods described above can be organized as a procedure, which is shown in Fig. 3.2. The procedure is general for a WEN synthesis problem of any size. It can be readily coded as a computational program using Excel or so (Appendix B). Note that in above formulations, construction of matrices $\bar{\boldsymbol{\Gamma}}$ and $\bar{\boldsymbol{P}}$ requires

more calculation steps. This will be illustrated in Case 1 in the following section. Calculation of the remaining matrices and vectors using Eqs. 3.8 to 3.22 are straightforward.

3.2 Case Studies

Two case study problems selected from the open literature are investigated in this section, in order to demonstrate the significance and efficacy of the introduced methodology. As stated, the methodology is used to determine the maximum amount of mechanical energy thermodynamically feasibly recoverable by a WEN prior to synthesis.

3.2.1 Case 1- Prediction of the Maximum Recoverable Mechanical Energy of a System Operated under Isothermal Conditions

This design problem studied by Liu *et al*. (2014) involves three high-pressure streams and two low-pressure streams. The process stream data is listed in Table 3.1.

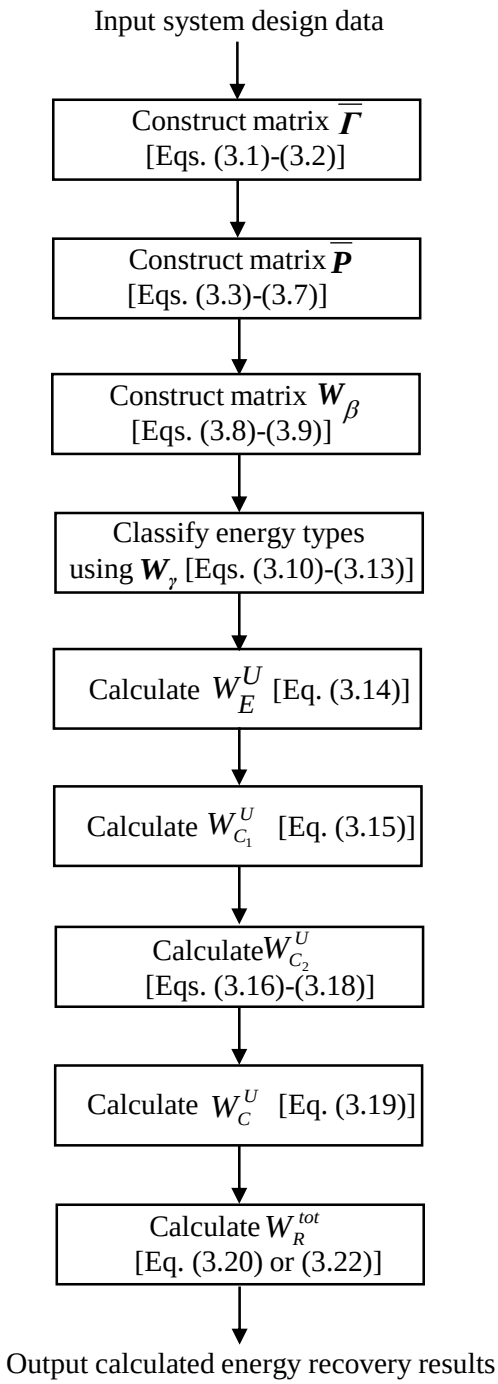

Figure 3.2. Flowchart for evaluation of maximum recoverable mechanical energy.

The minimum acceptable pressure difference between any pair of high-pressure and low-pressure streams (i.e., ΔP_{min}) is 70 kPa. It is assumed that each stream is an ideal gas, and the work transfer units are operated under isothermal condition. It is also assumed that the process operational efficiency is 100%.

Table 3.1. Process stream data for Case 1

Stream No.	Supply pressure (P^s, kPa)	Target pressure (P^t, kPa)	Volumetric flowrate (V, Nm^3/s)	Inlet temperature (T^s, K)
H_1	2,000	150	1.23	525
H_2	780	180	0.57	480
H_3	780	220	0.85	420
L_1	200	700	1.85	330
L_2	200	1,600	0.83	360

$\overline{\Gamma}$ is a 3×2 matrix as follows:

$$\overline{\boldsymbol{\Gamma}} = \begin{pmatrix} \overline{\Gamma}_{H_1,L_1} & \overline{\Gamma}_{H_1,L_2} \\ \overline{\Gamma}_{H_2,L_1} & \overline{\Gamma}_{H_2,L_2} \\ \overline{\Gamma}_{H_3,L_1} & \overline{\Gamma}_{H_3,L_2} \end{pmatrix}. \tag{3.23}$$

Among the six elements in the matrix, we show the calculation of only three elements, $\overline{\Gamma}_{H_1,L_1}$, $\overline{\Gamma}_{H_3,L_1}$, and $\overline{\Gamma}_{H_2,L_2}$, as the derivation of these element values can demonstrate different ways of calculation shown in the flowchart of Fig. 3.1.

a) Evaluation of $\overline{\Gamma}_{H_1,L_1}$. This requires calculation of the lower- and upper-bound values of the interval.

a-1) Calculation of $\Gamma^a_{H_1,L_1}$. Since $P^s_{L_1}$ (200 kPa) is less than the sum of $P^t_{H_1}$ (150 kPa) and ΔP_{min} (70 kPa), which is further less than $P^t_{L_1}$ (700 kPa), we have:

$$\Gamma^a_{H_1,L_1} = P^t_{H_1} + \Delta P_{\min} = 150 + 70 = 220 \ \text{kPa}. \tag{3.24}$$

a-2) Calculation of $\Gamma^{b}_{H_1,L_1}$. Note that $P^{s}_{H_1}$ (2,000 kPa) is greater than the sum of $P^{t}_{L_1}$ (700 kPa) and ΔP_{min} (70 kPa). Thus,

$$\Gamma^{b}_{H_1,L_1} = P^{t}_{L_1} = 700 \text{ kPa}. \tag{3.25}$$

Therefore,

$$\overline{\Gamma}_{H_1,L_1} = [220, 700]. \tag{3.26}$$

b) Evaluation of $\overline{\Gamma}_{H_3,L_1}$. This also requires calculation of the lower- and upper-bound values of the interval.

b-1) Calculation of $\Gamma^{a}_{H_3,L_1}$. As $P^{s}_{L_1}$ (200 kPa) is less than the sum of $P^{t}_{H_3}$ (220 kPa) and ΔP_{min} (70 kPa), which is further less than $P^{t}_{L_1}$ (700 kPa), we have:

$$\Gamma^{a}_{H_3,L_1} = P^{t}_{H_3} + \Delta P_{\min} = 220 + 70 = 290 \text{ kPa}. \tag{3.27}$$

b-2) Calculation of $\Gamma^{b}_{H_3,L_1}$. Note that $P^{s}_{H_3}$ (780 kPa) is greater than the sum of $P^{t}_{L_1}$ (700 kPa) and ΔP_{min} (70 kPa). Thus,

$$\Gamma^{b}_{H_3,L_1} = P^{t}_{L_j} = 700 \text{ kPa}. \tag{3.28}$$

Thus,

$$\overline{\Gamma}_{H_3,L_1} = [290, 700]. \tag{3.29}$$

c) Evaluation of $\overline{\Gamma}_{H_2,L_2}$. Again, the lower- and upper-bound values of the interval should be separately calculated.

c-1) Calculation of $\Gamma^{a}_{H_2,L_2}$. Since $P^{s}_{L_2}$ (200 kPa) is less than the sum of $P^{t}_{H_2}$ (180 kPa) and ΔP_{min} (70 kPa), which is further less than $P^{t}_{L_2}$ (1,600 kPa), we have:

$$\Gamma^{a}_{H_2,L_2} = P^{t}_{H_2} + \Delta P_{\min} = 180 + 70 = 250 \ \text{kPa}. \tag{3.30}$$

c-2) Calculation of $\Gamma^{b}_{H_2,L_2}$. Note that $P^{s}_{H_2}$ (780 kPa) is less than the sum of $P^{t}_{L_2}$ (1,600 kPa) and ΔP_{min} (70 kPa). Moreover, $P^{s}_{L_2}$ (200 kPa) is less than the difference between $P^{s}_{H_2}$ (780 kPa) and ΔP_{min} (70 kPa) and further less than $P^{t}_{L_2}$ (1,600 kPa). This gives rise to the following:

$$\Gamma^{b}_{H_2,L_2} = P^{s}_{H_2} - \Delta P_{\min} = 780 - 70 = 710 \ \text{kPa}. \tag{3.31}$$

Thus,

$$\overline{\Gamma}_{H_2,L_2} = [250,\ 710]. \tag{3.32}$$

d) Construction of a complete matrix $\overline{\boldsymbol{\Gamma}}$. By referring to the calculation examples above, three other elements in matrix $\overline{\boldsymbol{\Gamma}}$ can be readily derived. The following matrix shows a complete element calculation result:

$$\overline{\boldsymbol{\Gamma}} = \begin{pmatrix} [220,700] & [220,1,600] \\ [250,700] & [250,710] \\ [290,700] & [290,710] \end{pmatrix}. \tag{3.33}$$

Matrix $\overline{\boldsymbol{P}}$ has the same dimension as matrix $\overline{\boldsymbol{\Gamma}}$, i.e.,

$$\overline{\boldsymbol{P}} = \begin{pmatrix} \overline{P}_{H_1,L_1} & \overline{P}_{H_1,L_2} \\ \overline{P}_{H_2,L_1} & \overline{P}_{H_2,L_2} \\ \overline{P}_{H_3,L_1} & \overline{P}_{H_3,L_2} \end{pmatrix}. \tag{3.34}$$

In the following derivation, we show how to calculate two elements, $\overline{P}_{H_1,L_1}$ and $\overline{P}_{H_2,L_1}$. Calculation of other four elements can be performed in the same way.

a) Calculation of $\overline{P}_{H_1,L_1}$. This interval is derived from interval $\overline{\Gamma}_{H_1,L_1}$. According to Eq. 3.5, the value of index *l* should be determined first; it must satisfy two conditions: (1)

$l \le |N_H - 1|$ but $l \neq 0$, and (2) $0 < (i+l) \le N_H$, where $N_H = 3$. Based on the first condition, *l* can be 2, 1, -1, or -2. However, based on the second condition, *i* should be 1 (referred to H_1). Thus, *l*'s value of -1 or -2 is not valid. Therefore, we just need to evaluate $\overline{P}^1_{H_1,L_1}$ and $\overline{P}^2_{H_1,L_1}$. In this case, V_{H_1} (1.23 Nm^3/s) is greater than V_{H_2} (0.57 Nm^3/s). Thus, we have:

$$\overline{P}^1_{H_1,L_1} = \overline{\Gamma}_{H_1,L_1} = [220,\ 700]. \tag{3.35}$$

Since V_{H_1} (1.23 Nm^3/s) is greater than V_{H_3} (0.85 Nm^3/s). Thus, we also have:

$$\overline{P}^2_{H_1,L_1} = \overline{\Gamma}_{H_1,L_1} = [220,\ 700]. \tag{3.36}$$

Therefore, using Eq. 3.6 gives:

$$\overline{P}_{H_1,L_1} = \cap\left(\overline{P}^1_{H_1,L_1},\ \overline{P}^2_{H_1,L_1}\right) = [220, 700] \tag{3.37}$$

b) Calculation of $\overline{P}_{H_2,L_1}$. This interval is derived from $\overline{\Gamma}_{H_2,L_1}$. The values of index *l* should be decided, based on two conditions: (1) $l \le |N_H - 1|$ but $l \neq 0$, and (2) $0 < (i+l) \le N_H$. Again, based on the first condition, *l* can be 2, 1, -1 or -2. However, based on the second condition, *i* = 2 (referred to H_2), *l*'s value can be only -1 or 1. Therefore, we just need to evaluate $\overline{P}^{-1}_{H_2,L_1}$ and $\overline{P}^1_{H_2,L_1}$. Note that since V_{H_2} (0.57 Nm^3/s) is less than V_{H_1} (1.23 Nm^3/s), the following calculation is performed based on Eq. 3.5:

$$\begin{aligned} \overline{R}_{(H_2,L_1)\to(H_1,L_1)} &= \left[\left(\Gamma^a_{H_2,L_1} \vee \Gamma^a_{H_1,L_1}\right), \left(\Gamma^b_{H_2,L_1} \wedge \Gamma^b_{H_1,L_1}\right)\right] \\ &= [(250 \vee 220), (700 \wedge 700)] = [250,\ 700] \end{aligned} \tag{3.38}$$

Then,

$$\begin{aligned}\overline{P}^{-1}_{H_2,L_1} &= [250,700]\cap\ \overline{[250,700]\cap[250,700]} = [250,700]\cap\ \overline{[250,700]} \\ &= [250,700]\cap((-\infty,250)\cup(700,\infty)) = [0,0].\end{aligned} \tag{3.39}$$

Since V_{H_2} (0.57 Nm^3/s) is less than V_{H_3} (0.85 Nm^3/s), the following calculation should be performed based on Eq. 3.5:

$$\begin{aligned}\overline{R}_{(H_2,L_1)\to(H_3,L_1)} &= \left[\left(\Gamma^a_{H_2,L_1}\vee\Gamma^a_{H_3,L_1}\right),\left(\Gamma^b_{H_2,L_1}\wedge\Gamma^b_{H_3,L_1}\right)\right] \\ &= [(250\vee 290),(700\wedge 700)] = [290,\ 700].\end{aligned} \tag{3.40}$$

Then,

$$\begin{aligned}\overline{P}^{1}_{H_2,L_1} &= [250,700]\cap\ \overline{[250,700]\cap[290,700]} = [250,700]\cap\ \overline{[290,700]} \\ &= [250,700]\cap((-\infty,290)\cup(700,\infty)) = [250,\ 290].\end{aligned} \tag{3.41}$$

Therefore,

$$\overline{P}_{H_2,L_1} = \cap\left(\overline{P}^{-1}_{H_2,L_1},\overline{P}^{1}_{H_2,L_1}\right) = [0,\ 0]. \tag{3.42}$$

c) Construction of a complete matrix $\overline{\boldsymbol{P}}$. Using the same approach, we can calculate the values of four other elements in matrix $\overline{\boldsymbol{P}}$. All these values are assembled as follows:

$$\overline{\boldsymbol{P}} = \begin{pmatrix}[220,700] & [220,1600] \\ [0,0] & [0,0] \\ [0,0] & [0,0]\end{pmatrix}. \tag{3.43}$$

Using Eqs. 3.8 and 3.9, we can obtain matrix $\boldsymbol{W}_\beta$ (3×2) as follows:

$$\boldsymbol{W}_\beta = \begin{pmatrix}262.12 & 219.92 \\ 0 & 0 \\ 0 & 0\end{pmatrix}. \tag{3.44}$$

As shown, the mechanical energy of stream H_1 will be transferred to streams L_1 and L_2, but streams H_2 and H_3 will not transfer any. Note that for the high-pressure streams, the amounts of mechanical energy available can be calculated using Eq. 3.12 as: $W_{H_1} = 620.48$ kW, $W_{H_2} = 148.82$ kW, and $W_{H_3} = 167.61$ kW. With this information, we are able to derive the values of vector $\boldsymbol{W}_\gamma$, using Eqs. 3.10 and 3.11, i.e.,

$$\boldsymbol{W}_\gamma = \begin{pmatrix} W_{\gamma_1} \\ W_{\gamma_2} \\ W_{\gamma_3} \end{pmatrix} = \begin{pmatrix} 138.43 \\ 148.82 \\ 167.61 \end{pmatrix}. \tag{3.45}$$

In the above vector, W_{γ_1} (138.43 kW) is the remaining amount of energy of stream H_1 after transferring 262.12 kW to stream L_1 and 219.92 kW to stream L_2. The sum of the three element values in vector $\boldsymbol{W}_\gamma$ is the total amount of mechanical energy of the three high-pressure streams that cannot be used to pressurize any low-pressure stream. Thus, we can calculate the amount of external expansion energy provided by the system using Eq. 3.14, which gives:

$$W_E^U = 138.43 + 148.82 + 167.61 = 454.86 \text{ kW}. \tag{3.46}$$

Using Eqs. 3.15 to 3.19, we can obtain the following:

$$W_{C_1}^U = 0, \tag{3.50}$$

and

$$W_{C_2}^U = 514.19 - 482.04 = 32.15 \text{ kW}. \tag{3.51}$$

Therefore, the minimum amount of external compression energy needed for the system is:

$$W_C^U = W_{C_1}^U + W_{C_2}^U = 32.15 \text{ kW}. \tag{3.52}$$

Now we can calculate the maximum amount of mechanical energy that can be recovered by a WEN using Eqs. 3.20 and 3.21, i.e.,

$$W_R^{tot} = W_H^{tot} - W_E^U = (620.48 + 148.82 + 167.61) - 454.86 \;=\; 482.05 \;\text{kW}. \tag{3.53}$$

The same result can be obtained using Eq. 3.22, i.e.,

$$W_R^{tot} = W_L^{tot} - W_C^U = (283.71 + 230.49) - 32.15 \;=\; 482.05 \;\text{kW}. \tag{3.54}$$

Table 3.2 summarizes the benefit of mechanical energy recovery using a WEN. It is shown that a WEN can recover 93.75% of the energy for stream compression, and 51.45% of the energy for stream expansion.

Table 3.2. Energy recovery analysis for Case 1

External utility type	External energy requirement (kW)		Energy recovery by WEN (%)
	Without WEN	Using WEN	
Compression	514.19	32.15	93.75
Expansion	936.91	454.86	51.45

As a separate effort from this work, we have successfully synthesized a WEN for this design problem using a methodology that we developed, which is shown in Fig. 3.3(a). Since network synthesis is beyond the scope of this chapter, derivation of a process flowsheet is not discussed here. In the derived network, the maximum mechanical energy recovery predicted by the introduced methodology (482.05 kW) is indeed achieved. The network contains two work exchangers, two compressors, and three expanders. As a comparison, the solution derived by Liu *et al*. (2014) is plotted in Fig. 3.3(b). In their solution, four work exchangers are used to recover a total of 367.56 kW of mechanical energy, which is 23.75% less than the maximum recoverable mechanical energy that was predicted. In addition, the number of compressors and expanders used in their solution is larger than that in our solution. The comparison of energy recovery and process unit requirement is summarized in Table 3.3.

Table 3.3. Performance comparison of WENs by different methods for Case 1

Solution	Energy recovery efficiency (%)		Number of work exchangers	Number of utility units	
	Compression	Expansion		Compressor	Expander
Fig. 3.3(a), by this work	51.45	93.75	2	2	3
Fig. 3.3(b), by Liu *et al*. (2014)	39.23	71.48	4	3	5

3.2.2 Case 2 – Prediction of the Maximum Recoverable Mechanical Energy of a System Operated under Adiabatic Conditions

Razib *et al*. (2012) studied an interesting WEN design problem, where single-shaft-turbine-compressor (SSTC) units, instead of (direct) work exchangers introduced in this work, were used for mechanical energy recovery. In their work, a superstructure for WEN configuration was proposed and a mixed-integer nonlinear programming (MINLP) model was described for identifying an optimal solution in terms of minimum total annualized cost. Their design problem is selected for our case study, aiming at identifying the maximum amount of recoverable mechanical energy. Table 3.4 lists the data of the synthesis problem. The minimum acceptable pressure difference between any pair of high-pressure and low-pressure streams (i.e., ΔP_{min}) is 70 kPa. It is assumed that each stream is an ideal gas, and the work transfer units are operated under adiabatic conditions. It is also assumed that the process operational efficiency is 100%.

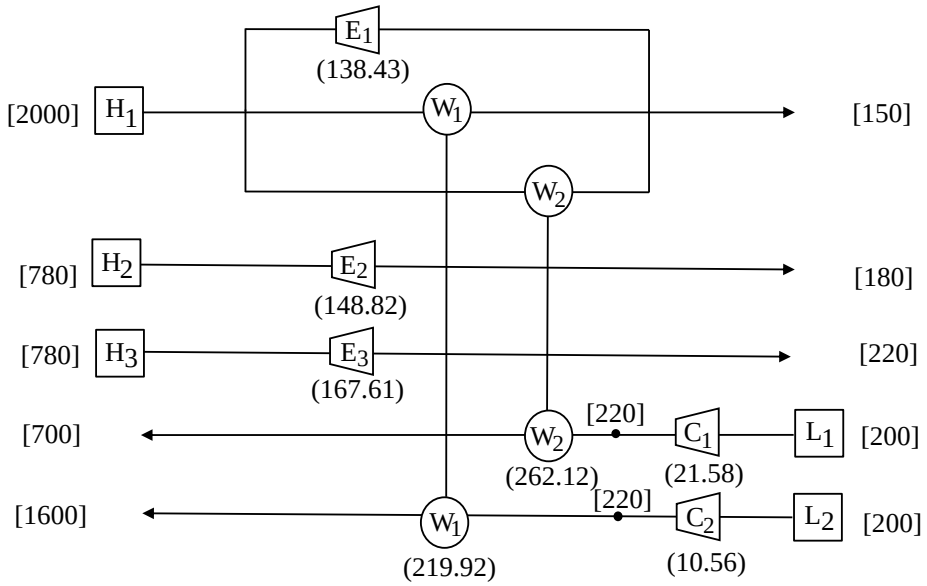

(a)

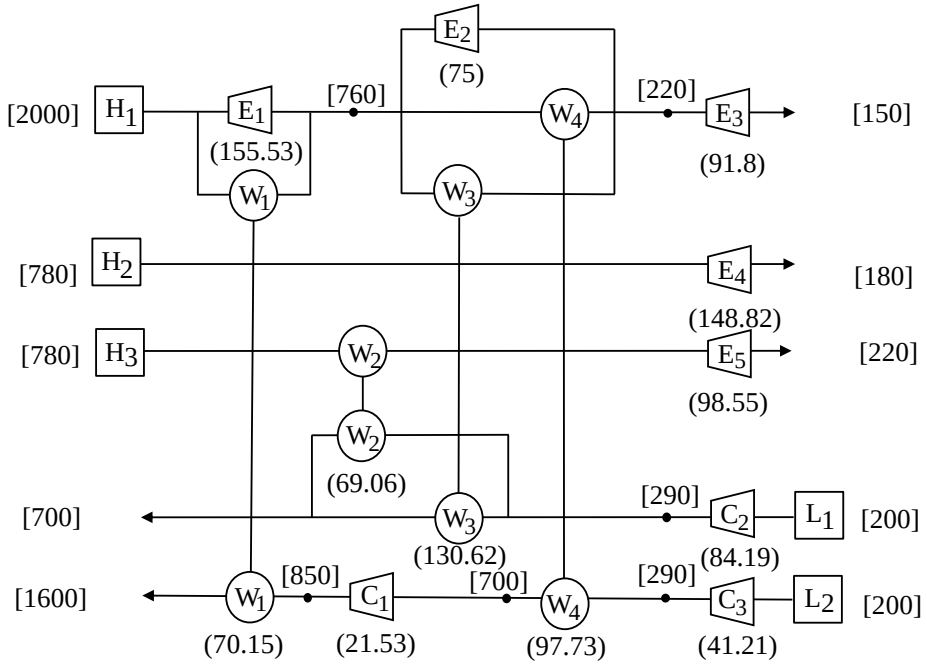

(b)

Legend [ ] : Pressure (kPa) W Work exchanger

( ) : Work load (kW) C Compressor E Expander

Figure 3.3. Work exchange networks designed by different methods for Case 1: (a) the solution by the proposed model-based method to achieve the maximum energy recovery, and (b) the solution derived by Liu *et al.* (2014).

Table 3.4. Process stream data for Case 2

Stream No.	Supply pressure (P^s, kPa)	Target pressure (P^t, kPa)	Flowrate (kg/s)	Source temperature (T^s, K)	Target temperature (T^t, K)	Heat capacity (C_P, kJ/kg.k)
H_1	850	100	3	600	430	1.432
H_2	960	160	5	580	300	0.982
H_3	800	300	2	960	300	1.046
L_1	100	510	3	300	700	1.432
L_2	100	850	3	300	600	1.432

Following the procedure in Figs. 3.1 and 3.2, we can derive the element values of matrices $\overline{\boldsymbol{\Gamma}}$ and $\overline{\boldsymbol{P}}$ that are listed below.

$$\overline{\boldsymbol{\Gamma}} = \begin{pmatrix} [170,\ 510] & [170,\ 780] \\ [230,\ 510] & [230,\ 850] \\ [370,\ 510] & [370,\ 730] \end{pmatrix}, \tag{3.55}$$

and

$$\overline{\boldsymbol{P}} = \begin{pmatrix} [170, 230] & [170, 230] \\ [230, 510] & [230, 850] \\ [0, 0] & [0, 0] \end{pmatrix}. \tag{3.56}$$

As shown, the element values in the last row of matrix $\overline{\boldsymbol{P}}$ are all zero. This means that high-pressure stream H_3 will not transfer energy to any low-pressure stream.

Following the same procedure, we can derive matrix $\boldsymbol{W}_\beta$, which contains the information about the mechanical energy transferrable between any pair of high-pressure stream and low-pressure stream. This matrix is derived as:

$$\boldsymbol{W}_\beta = \begin{pmatrix} 237.26 & 231.90 \\ 803.22 & 1{,}448.22 \\ 0 & 0 \end{pmatrix} \tag{3.57}$$

The mechanical energy that should be removed from each high-pressure stream can be evaluated using Eqs. 3.12 and 3.13: $W_{H_1} = 1{,}044.50$ kW, $W_{H_2} = 1{,}308.80$ kW, and $W_{H_3} = 417.80$ kW. Having these data, together with the data in matrix $\boldsymbol{W}_{\beta}$, we can derive vector $\boldsymbol{W}_{\gamma}$ using Eqs. 3.10 and 3.11 as follows:

$$\boldsymbol{W}_{\gamma} = \begin{pmatrix} W_{\gamma_1} \\ W_{\gamma_2} \\ W_{\gamma_3} \end{pmatrix} = \begin{pmatrix} 575.33 \\ -942.64 \\ 417.80 \end{pmatrix}. \tag{3.58}$$

Different from Case 1, this vector contains one negative number. This means stream H_2 does not have enough energy to be transferred to streams L_1 and L_2. This amount (942.64 kW) can be only obtained from an external compression power source (see Eq. 3.15), i.e.,

$$W_{C_1}^{U} = 942.64 \text{ kW}. \tag{3.59}$$

This is, however, not the total demand of external compression power. This other portion is $W_{C_2}^{U}$, which can be calculated using Eqs. 3.16-3.18 as follows:

$$\begin{aligned} W_{C_2}^{U} &= W_{L}^{tot} - W_{H\to L}^{tot} = (3{,}406.10) - (237.26 + 231.90 + 803.22 + 1{,}488.22) \\ &= 685.49 \text{ kW}. \end{aligned} \tag{3.60}$$

Therefore,

$$W_{C}^{U} = W_{C_1}^{U} + W_{C_2}^{U} = 1{,}628.13 \text{ kW}. \tag{3.61}$$

As to the minimum requirement of the external expansion power, it can be readily obtained using Eq. 3.14; the result is:

$$W_{E}^{U} = W_{\gamma_1} + W_{\gamma_3} = 575.33 + 417.80 = 993.13 \text{ kW}. \tag{3.62}$$

Based on the results obtained above, we can calculate the maximum amount of recoverable mechanical energy using either Eq. 3.20 or 3.22, i.e.,

$$W_R^{tot} = W_H^{tot} - W_E^U = (1,044.50 + 1,308.80 + 417.80) - 993.13 = 1,777.97 \text{ kW}, \quad (3.63)$$

or

$$W_R^{tot} = W_L^{tot} - W_C^U = (1,386.60 + 2,019.50) - 1,628.13 = 1,777.97 \text{ kW}. \quad (3.64)$$

As shown in Table 3.5, the total amount of work exchanged is 1,777.97 kW, accounting for 52.20% of the total energy demanded by the two low-pressure streams, and 64.16% of that provided by all high-pressure streams. This is a very significant contribution to energy reccovery.

Table 3.5. Energy recovery analysis for Case 2

External utility type	External energy requirement (kW)		Energy recovery by WEN (%)
	Without WEN	Using WEN	
Compression	3,406.10	1,628.13	52.20
Expansion	2,771.10	993.13	64.16

To demonstrate the achievability of the predicted maximum energy recovery in design, we have synthesized a WEN, which is plotted in Fig. 3.4(a). Since network synthesis is beyond the scope of this chapter, we do not describe the synthesis methodology here. As shown in Fig. 3.4(a), the energy target of recovering 1,777.97 kW is achieved using four work exchangers. This network also contains three compressors and two expanders. Note that since the pressurization/depressurization operation occurs under adiabatic conditions, the temperatures of the process streams leaving work exchangers, compressors, and expanders will change. Therefore, there is a need to consider recovery of thermal energy through integrating a heat exchanger network (HEN). In Fig. 3.4(a), three hot streams (marked as HS1 – HS3) and two cold streams (marked as CS1 and CS2) are identified, which define a HEN design problem. A synthesized HEN

is shown in Fig. 3.4(b). This network can recover 36.7% of thermal energy from hot streams (645.95 kW out of 1,759.1 kW).

In Razib *et al.* (2012), a WEN is proposed using single-shaft-turbine-compressor (SSTC) units, which is different from the work exchanger introduced in this work. Since their synthesis target was to minimize the total annualized cost, a trade-off between the capital cost and operating cost was made. Therefore, a complete comparison between our solution and their solution is not approriate. However, a partial comparison is possible, which is summarized in Table 3.6. As shown, our solution can recover more mechanical energy. Besides, our solution compares well with their solution, in terms of the number of work transfer units (direct work exchangers in our solution versus SSTCs in their work, compressors and expanders) as well as the number of heaters and coolers.

Table 3.6. Performance comparison of WENs by different methods for Case 2

Type of device used in WEN	Mech. energy recovered (kW)	High-pressure recovery (%)	Low-pressure recovery (%)	No. of exchan-ger units	No. of heaters and coolers	No. of external compre-ssors	No. of external turbines
Direct work exchanger	1,778	64.16	52.20	4	5	3	2
SSTC, in Razib *et al.* (2012)	1,573	56.77	46.19	7	11	2	3

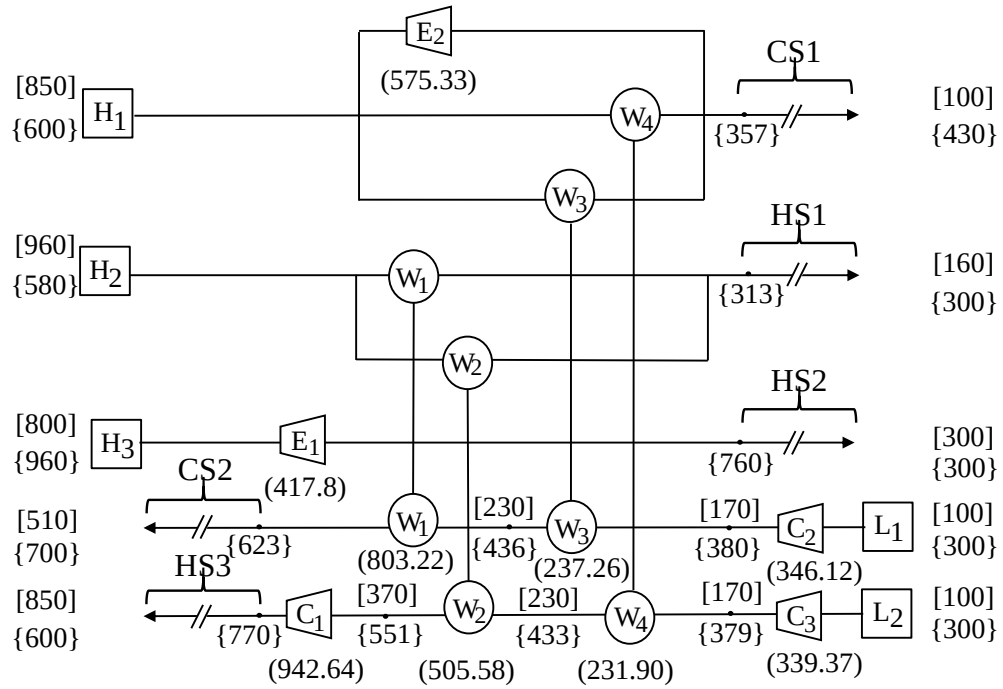

(a)

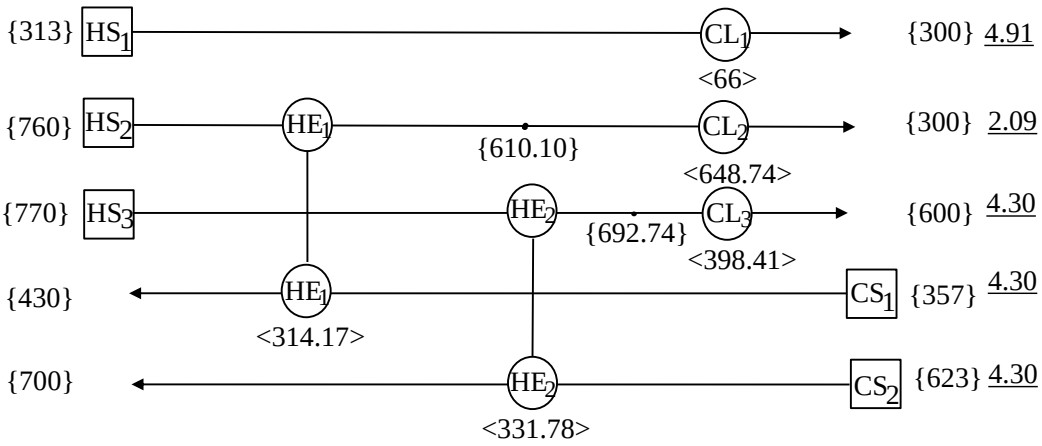

(b)

Legend

[ ] Pressure (kPa) { } Temperature (K) ( ) Work load (kW)

MC_P (kW/K) < > Heat load (kW) E Expander

W Work exchanger C Compressor —//— Heat transfer unit(s) to be placed

HE Heat exchanger CL Cooler

Figure 3.4. Flowsheet of heat-integrated work exchange network for Case 2: (a) work exchanger network, and (b) heat exchanger network.

3.3.3 Discussion

As stated, the case studies are presented to demonstrate that the maximum amount of recoverable mechanical energy predicted by the introduced model-based methodology is achievable during the process flowsheet development phase. It is shown that the WENs derived in the case studies can recover more mechanical energy than those known designs in the open literature. In addition, the work transfer units used in each derived network are fewer than those in the known ones. Thus, energy target setting before WEN synthesis is highly desirable. The introduced model-based energy prediction methodology should be a valuable tool for process designers.

Although the derived WENs in the case studies are better solutions than known ones, the solution optimality cannot be ensured here. There may be other configurations that can also achieve the energy recovery goal at the lowest total annualized cost. Optimal process flowsheet development requires a sophisticated synthesis methodology, which is beyond the scope of this chapter.

3.4 Summary

Mechanical energy recovery is a very important issue in energy efficiency improvement in the chemical process industry. However, this has drawn attention only in recent years. Apparently, significant effort on methodological and applied research is needed. Since the operational mode of the introduced (direct) work exchanger is very different from traditional heat transfer units, Pinch Analysis, which is a mature methodology for heat exchanger network (HEN) synthesis, is not directly applicable for work integration. Thus, a class of entirely new methodologies for work exchanger network (WEN) synthesis is needed.

To facilitate WEN synthesis, we have introduced a thermodynamic modeling and analysis methodology for predicting the recoverable mechanical energy prior to process flowsheet development. The methodology is rigorous and general for a synthesis problem of any size, and it can be used for work exchange operations under isothermal, isentropic, or polytropic conditions. Case studies have shown that the energy targets are set precisely, and they are achievable in the process flowsheet development stage. The comparison with the solutions in the open literature has demonstrated the efficacy of the introduced methodology.

Note that when a WEN is operated under adiabatic conditions, process stream temperatures through different work transfer units will be changed within the system. In such a case, heat integration technology should be used to design a HEN in order to ensure the efficiency of thermal energy recovery as well. Since energy efficiency is of utmost importance in the chemical process industry, it is conceivable that significant progress on the research for simultaneous recovery of mechanical and thermal energy will be made in the near future.

CHAPTER 4 SYNTHESIS OF COST EFFECTIVE HEAT INTEGRATED WORK EXCHANGE NETWORK

A mathematical modeling and analysis method was introduced in Chapter 3 to predict the maximum amount of mechanical energy that can be feasibly recovered using direct work exchangers prior to WEN configuration development (Amini-Rankouhi and Huang, 2017). As the next step towards completion of WEN synthesis, a comprehensive methodology is required. Also, due to temperature and pressure correlation in gas phase streams, recovery of thermal energy through heat integration will significantly impact the amount of energy recovery and total annualized cost. In this chapter, we will introduce a thermodynamic model-based synthesis approach to develop a heat-integrated work exchanger network (HIWEN), in which direct work exchangers may work under different operating conditions. Case studies will demonstrate that the resulting HIWENs can recover the maximum amount of mechanical and thermal energy at the lowest cost.

4.1 Work Exchanger Network Synthesis Methodology

In the following, we will introduce a work exchanger network synthesis methodology which will allow us to develop the flowsheet after the prediction stage. The flowsheet can be combined with heat exchanger networks that are integrated before or after the WEN synthesis. The location of HEN network is assigned based on the design with the lower operating cost. In the end, the design can be modified using an adjustment instruction.

Flowsheet development procedure. For any specific case study with given information, after determination of the maximum recoverable energy through the prediction methodology, variables N_H, N_L and matrices $\overline{\boldsymbol{P}}$, $\boldsymbol{W}_H$, $\boldsymbol{W}_L$, $\boldsymbol{W}_\beta$, and $\boldsymbol{W}_\gamma$ will be used as inputs for the synthesis stage. Figures 4.1 and 4.2 show the procedure in detail for final flowsheet development.

Placement of work exchangers using matrices W_W and $\overline{P}_M$. As discussed in Chapter 3, Matrix W_β represents the amount of mechanical energy that can be feasibly transferred from each individual high-pressure stream to each individual low-pressure stream. However, the amount of energy each high-pressure stream can provide could be higher or lower based on the vector W_γ. Therefore, to generate W_W which is the matrix of work exchanger workloads between i-th high-pressure stream and j-th low-pressure stream, matrix W_β and vector W_L would be the best options to find the most appropriate location for work exchangers. Any positive term from vector W_γ shows that the i-th high-pressure stream can provide sufficient mechanical energy to the low-pressure streams it is assigned to through the preparation of matrices $\overline{P}$ and W_β. Based on the flowchart shown in Fig. 4.1, while W_{γ_i} has a positive value or its absolute value is less than $W_{\beta_{H_i,L_j}}$, a work exchanger should be placed with workload equal to $W_{\beta_{H_i,L_j}}$. While W_{γ_i} has a negative value and its absolute value is higher than $W_{\beta_{H_i,L_j}}$, a work exchanger should be placed with workload equal to $W_{\beta_{H_i,L_j}} - \left|W_{\gamma_i}\right|$ unless $W_{\beta_{H_i,L_j}}$ is the largest number in the j-th column. Therefore, we can introduce matrix W_W to accommodate work exchangers with highest workloads in the following structure:

$$W_W = \begin{pmatrix} W_{W_{H_1,L_1}} & W_{W_{H_1,L_2}} & \cdots & W_{W_{H_1,L_{N_L}}} \\ W_{W_{H_2,L_1}} & W_{W_{H_2,L_2}} & \cdots & W_{W_{H_2,L_{N_L}}} \\ \vdots & \vdots & \ddots & \vdots \\ W_{W_{H_{N_H},L_1}} & W_{W_{H_{N_H},L_2}} & \cdots & W_{W_{H_{N_H},L_{N_L}}} \end{pmatrix}, \tag{4.1}$$

Generation of matrix $\overline{\boldsymbol{P}}_{\boldsymbol{M}}$. Each term in matrix $\overline{\boldsymbol{P}}_{\boldsymbol{M}}$ defines the range of each low-pressure stream which will receive energy from each high-pressure stream in the range of $\left[P_{H_i}^{t}, P_{H_i}^{s}\right]$. Therefore, after construction of matrix $\overline{\boldsymbol{P}}_{\boldsymbol{M}}$, for each term, one work exchanger will be placed between $\left[P_{H_i}^{t}, P_{H_i}^{s}\right]$ and $\left[P_{M_{H_i,L_j}}^{a}, P_{M_{H_i,L_j}}^{b}\right]$ with energy to be exchanged in amount of $W_{W_{H_i,L_j}}$. Note that based on this methodology, each high-pressure stream may transfer energy in the range of $\left[P_{H_i}^{t}, P_{H_i}^{s}\right]$ to more than one low-pressure stream which means that there will be splitting in high-pressure streams under this condition. Matrix $\overline{\boldsymbol{P}}_{\boldsymbol{M}}$ which contains $N_H \times N_L$ intervals will be structured as follows:

$$\overline{\boldsymbol{P}}_{\boldsymbol{M}} = \begin{pmatrix} \overline{P}_{M_{H_1,L_1}} & \overline{P}_{M_{H_1,L_2}} & \cdots & \overline{P}_{M_{H_1,L_{N_L}}} \\ \overline{P}_{M_{H_2,L_1}} & \overline{P}_{M_{H_2,L_2}} & \cdots & \overline{P}_{M_{H_2,L_{N_L}}} \\ \vdots & \vdots & \ddots & \vdots \\ \overline{P}_{M_{H_{N_H},L_1}} & \overline{P}_{M_{H_{N_H},L_2}} & \cdots & \overline{P}_{M_{H_{N_H},L_{N_L}}} \end{pmatrix}, \tag{4.2}$$

where

$$\overline{P}_{M_{H_i,L_j}} = \left[P_{M_{H_i,L_j}}^{a}, P_{M_{H_i,L_j}}^{b}\right]. \tag{4.3}$$

To determine element $\overline{P}_{M_{H_i,L_j}}$, the upper-bound of the interval will be assumed equal to the upper-bound of the interval $\overline{P}_{H_i,L_j}$, and the lower-bound will be calculated based on the workload of the assigned work exchanger. Then,

$$P_{M_{H_i,L_j}}^{b} = P_{H_i,L_j}^{b}, \tag{4.4}$$

and

$$P^{a}_{M_{H_i,L_j}} = \begin{cases} P^{b}_{M_{H_i,L_j}} \exp\left(-\dfrac{W_{W_{H_i,L_j}}}{zRT^{s}_{L_j}\left(\dfrac{V_{L_j}\rho_{L_j}}{M_{w_{L_j}}}\right)} \right); & \text{Isothermal condition} \\ \left(P^{b}_{M_{H,L}} \right)^{\left(\frac{k_L}{k_L-1}\right)} - \dfrac{W_{W_{H_i,L_j}} \left(P^{s}_{L}\right)^{\frac{k_L-1}{k_L}}}{\left(\dfrac{k_L}{k_L-1}\right) zRT^{s}_{L}\left(\dfrac{V_L\rho_L}{M_{w_L}}\right)} \Bigg)^{\left(\frac{k_L}{k_L-1}\right)}; & \text{Isentropic condition (adiabatic)} \\ \left(P^{b}_{M_{H,L}} \right)^{\left(\frac{m_L}{m_L-1}\right)} - \dfrac{W_{W_{H_i,L_j}} \left(P^{s}_{L}\right)^{\frac{m_L-1}{m_L}}}{\left(\dfrac{m_L}{m_L-1}\right) zRT^{s}_{L}\left(\dfrac{V_L\rho_L}{M_{w_L}}\right)} \Bigg)^{\left(\frac{m_L}{m_L-1}\right)}; & \text{Polytropic condition (adiabatic)} \end{cases} \quad (4.5)$$

Note that for cases which a heat exchanger network will be located before the work exchange network, the formulation shown in Eq. 4.5 will be slightly changed. The formulation will be discussed later.

Placement of compressors using vectors W_{C_1} and W_{C_2}. Vector W_{C_1} represents the compressors that are required when the high-pressure streams are not able to provide enough energy for each specific low-pressure stream even under thermodynamically feasibility conditions. At this stage, one or more compressors with a total workload of $W_{C_{1j}}$ will be placed in the j-th low-pressure stream for the regions that still require pressurization. Thus, vector W_{C_1} will be structured as follows:

$$\boldsymbol{W}_{C_1} = \begin{pmatrix} W_{C_{1_1}} \\ W_{C_{1_2}} \\ \\ W_{C_{1_{N_L}}} \end{pmatrix}, \tag{4.6}$$

where

$$W_{C_{1_j}} = \sum_{i=1}^{N_H} \left(W_{\beta_{H_i, L_j}} - W_{W_{H_i, L_j}} \right). \tag{4.7}$$

Each term in the j-th row of vector $\boldsymbol{W}_{C_2}$ represents placement of one or two compressors in the j-th low-pressure stream, which cannot receive energy from any high-pressure stream because of thermodynamic feasibility conditions ($P_H^{in} - P_L^{out} \geq \Delta P_{\min}$ and $P_L^{in} - P_H^{out} \geq \Delta P_{\min}$) which was assigned from the initial step of prediction stage in the construction of matrices $\overline{\boldsymbol{\Gamma}}$ and $\overline{\boldsymbol{P}}$. Comparing the pressure interval of the j-th column in matrix $\overline{\boldsymbol{P}}$ with the supply and target pressures of the j-th low-pressure stream (i.e., $\left\lfloor P_{L_j}^s, P_{L_j}^t \right\rfloor$), the compressors can be placed in the beginning/end of the j-th low-pressure stream with a total workload of $W_{C_{2_j}}$.

$$\boldsymbol{W}_{C_2} = \begin{pmatrix} W_{C_{2_1}} \\ W_{C_{2_2}} \\ \\ W_{C_{2_{N_L}}} \end{pmatrix}, \tag{4.8}$$

where

$$W_{C_{2_j}} = W_{L_j} - \sum_{i=1}^{N_H} W_{\beta_{H_i, L_j}} . \tag{4.9}$$

Placement of expanders using vector W_E. Any positive value in the vector W_γ represents the amount of energy that the i-th high-pressure stream cannot provide to any low-pressure stream and an external expander should be placed. Therefore, the vector W_E will be constructed based on the values from vector W_γ. Each non-zero value in vector W_E defines placement of one expander in the range of $\left[P_{H_i}^t, P_{H_i}^s\right]$ in the amount of W_{E_i} in the i-th high-pressure stream. For high-pressure streams which are also transferring energy to a low-pressure stream through work exchange and still requires an expander, there will be stream splitting.

$$\boldsymbol{W_E} = \begin{pmatrix} W_{E_1} \\ W_{E_2} \\ \\ W_{E_{N_L}} \end{pmatrix}, \tag{4.10}$$

where

$$W_{E_i} = \begin{cases} 0; & W_{\gamma_i} \le 0 \\ W_{\gamma_i}; & W_{\gamma_i} > 0 \end{cases}. \tag{4.11}$$

The four final outputs of the flowcharts shown in Figs. 4.1 and 4.2 which are matrices and vectors will provide the information for the placement of the unit operations such as work exchangers, external compressors, and external expanders. However, for an energy efficient and cost effective design, integration of heat into the work exchanger network design and also capital and operating cost estimation should be analyzed.

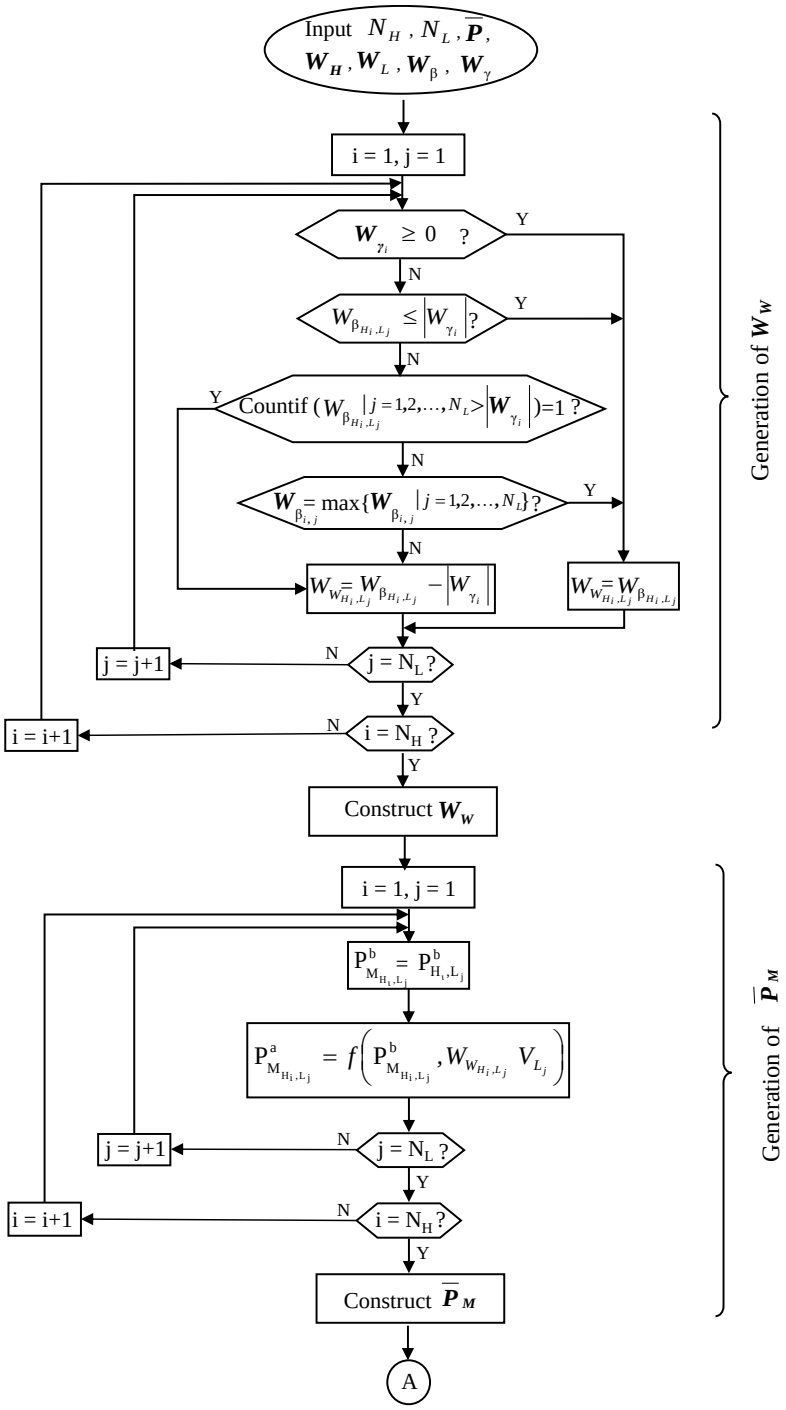

Figure 4.1. Generation of W_W and $\overline{P}_M$.

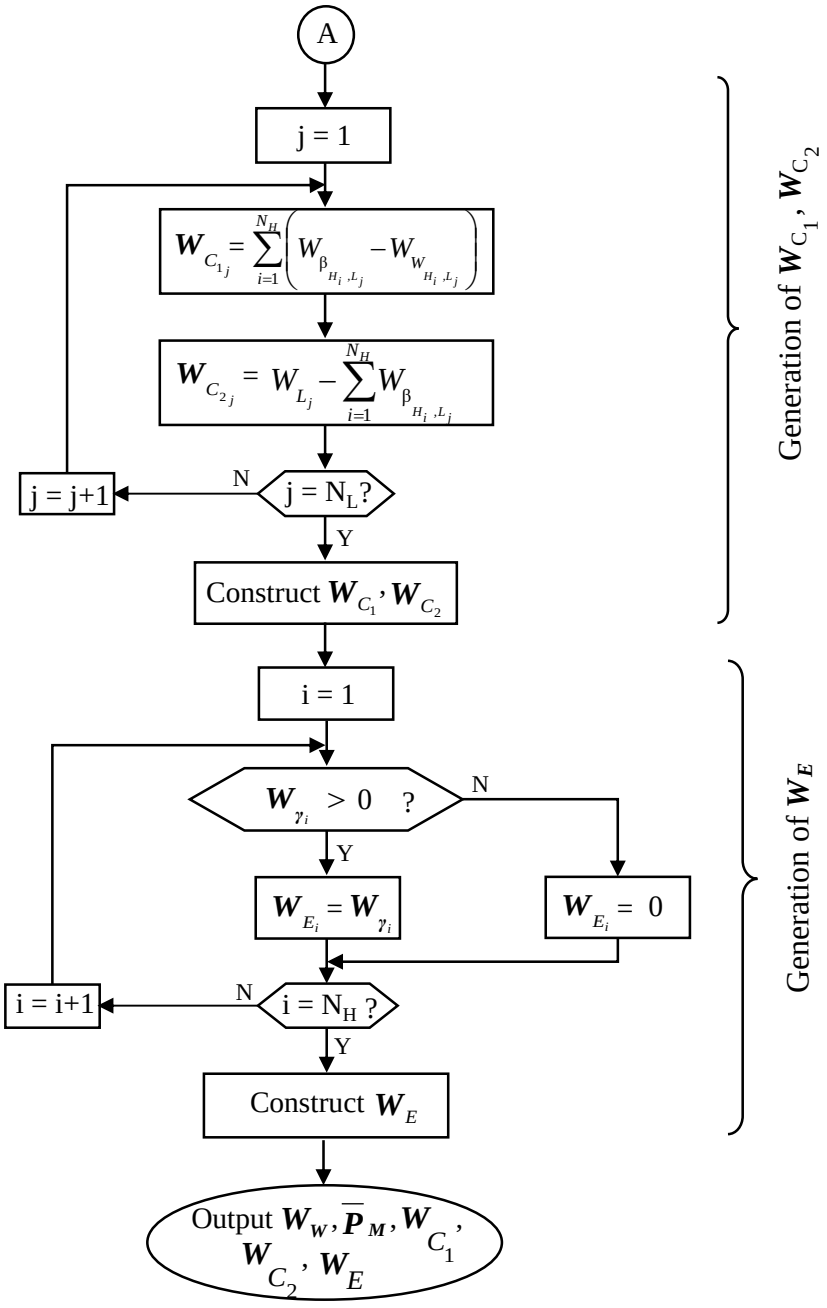

Figure 4.2. Generation of W_{C_1} , W_{C_2} ,and W_E .

4.2 Heat Integrated Work Exchange Network Design

Temperature change after each stage of pressurization and depressurization cannot be neglected in real industrial cases. In the study by Deng *et al.* (2010), it was shown that applying gas phase streams in work exchangers requires significant attention in comparison to liquid streams

especially due to temperature dependence. This is the reason, in processes under the adiabatic condition where the outlet temperature after each stage of pressurization or depressurization is not the desired temperature and needs to be heated or cooled based on the streams specification, heat integration should be taken into consideration in addition to work integration. With a derived WEN flowsheet, the process streams with different temperature profiles will be identified, and a corresponding thermal energy recovery system will be synthesized.

For design problems with one or more streams with given target temperature. When dealing with streams in the gas phase, temperature plays a key role in the amount of energy that is required for compression or provided through expansion. Depending on the design problem, a target temperature may or may not be specified. For the cases where the outlet temperature of the pressurization/depressurization stage is different from the target temperature, heating or cooling is required. In such cases, the heat exchanger network (HEN) can be developed to recover thermal energy to minimize the external heating and cooling utilities. To prevent complexity of the solution development, HEN can be placed before or after the WEN. Figure 4.3 shows a flowchart on how to develop HEN before/after WEN and decide the location based on the lowest operational cost. In this stage, the prediction methodology presented in chapter 3 will be used to estimate the amount of mechanical energy that will be recovered, and external compression and expansion utilities. Thermal energy recovery and external heating and cooling will be estimated using the temperature interval and cascade diagram of pinch analysis (Linnhoff and Flower, 1978). Note that the shaft work formulation in the prediction methodology will differ based on the HEN location.

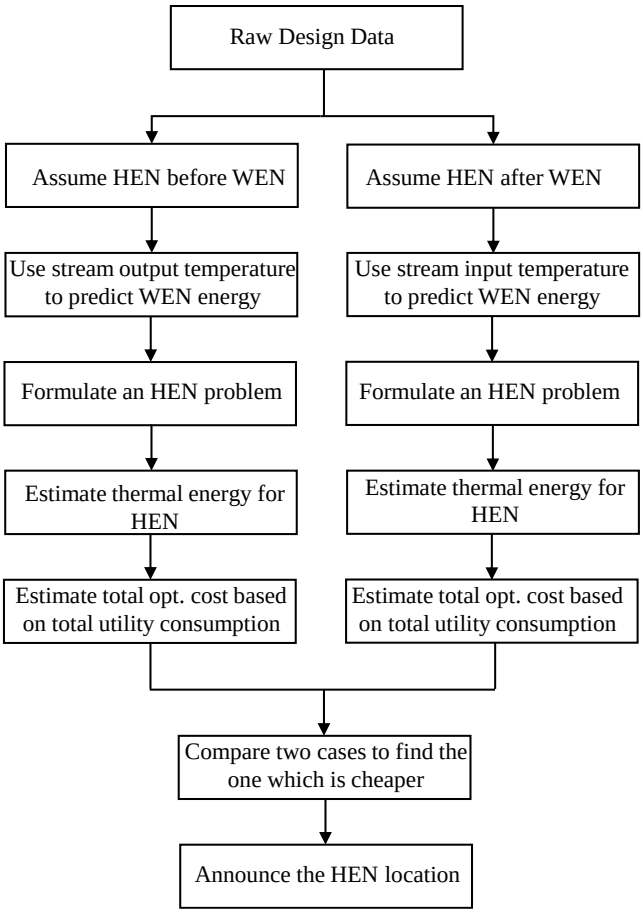

Figure 4.3. Flowchart for HEN location decision making.

(a) When a heat exchanger network will be assumed before the work exchanger network, the target temperature of high-pressure and low-pressure streams will be assumed constant and inlet temperatures of the streams to the WEN system will be calculated based on the target temperature provided by the problem design. As an example, T_i shown in Fig. 4.4(a) can be calculated as follows for each individual high-pressure and low-pressure stream under polytropic (adiabatic frictional) conditions for ideal gas streams:

$$T_i^H = \frac{T_H^t}{\left(\frac{P_H^t}{P_H^s}\right)^{\frac{m_H - 1}{m_H}}}, \tag{4.12}$$

and

$$T_i^L = \frac{T_L^t}{\left(\frac{P_L^t}{P_L^s}\right)^{\frac{m_L-1}{m_L}}}. \tag{4.13}$$

Therefore, for shaft work calculation used in the prediction and synthesis stages, target temperatures given for each individual stream should be replaced by supply temperatures. In Table 4.1, changes that will be made in the formulation of the prediction and synthesis stages for polytropic condition (frictional adiabatic) have been summarized.

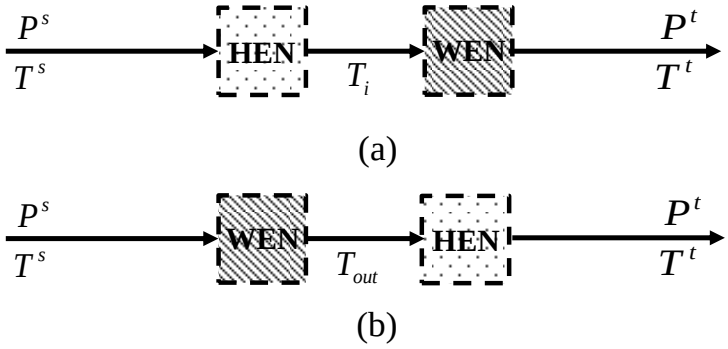

Figure 4.4. (a) HEN located before WEN design, and (b) HEN located after WEN design.

After estimation of T_i and calculating new W_E^U, W_C^U, and W_{tot}^R values for the WEN design where the HEN is located before WEN, hot and cold streams will be derived and using pinch analysis, the total amount of thermal energy that can be recovered in addition to total external hot and cold utilities will be calculated. In the next stage, operating cost ($OPEX$) using Eq. 4.14 will be calculated.

$$OPEX = C_{elec}\left(\sum_{j=1}^{N_L}\left(W_{C_{1_j}} + W_{C_{2_j}}\right)\right) + C_{steam}\left(\sum_{i=1}^{N_{LT}} Q_m\right) + C_{CW}\left(\sum_{i=1}^{N_{HT}} Q_n\right) \tag{4.14}$$

where C_{elec} is the cost of electricity (\$/kWh), C_{steam} is the cost of steam used as a heating utility (\$/kWh), C_{CW} is the cost of cooling water used as a cooling utility, Q_m and Q_n represent the heat

duty of the heating and cooling utilities, respectively. N_{LT} is the total number of streams required for heating and N_{HT} is the total number of streams required for cooling.

(b) When a heat exchanger network will be assumed after the work exchanger network, the supply temperature of high-pressure and low-pressure streams will be assumed constant and outlet temperature of the streams leaving the WEN system will be calculated based on the supply temperature provided by the problem design as shown in Fig 4.4(b). Each stream temperature that will go through stages of pressurization or depressurization will increase or decrease, respectively. Equations 4.15 and 4.16 show a calculation example under polytropic (adiabatic frictional) conditions for ideal gas streams:

$$T_{out}^{H} = T_{H}^{s}\left(\frac{P_{H}^{t}}{P_{H}^{s}}\right)^{\frac{m_H - 1}{m_H}}, \tag{4.15}$$

and

$$T_{out}^{L} = T_{L}^{s}\left(\frac{P_{L}^{t}}{P_{L}^{s}}\right)^{\frac{m_L - 1}{m_L}}. \tag{4.16}$$

While the target temperature is specified for a case study, heating or cooling may be required to reach the target temperature from T_{out}^{H} and T_{out}^{L}. Heat exchanger networks will be integrated to recover the thermal energy of the heating and cooling utilities. The amount of mechanical energy that can be recovered and external utilities (W_E^U, W_C^U, and W_{tot}^R) will be calculated using prediction methodology. Hot and cold streams will be derived to conduct the pinch analysis and the operating cost will be calculated using Eq. 4.14.

Comparing the final operating cost from the methods (a) and (b), the HEN will be located based on the design with the lowest operating cost.

Table 4.1. Directory of formulas to be used in prediction and synthesis stages for HEN located before/after WEN design

		HEN before	HEN after
Prediction stage	W_β	$\left(\frac{m_L}{m_L-1}\right)zRT_L^t\left(\frac{P_{H,L}^b}{P_L^t}\right)^{\frac{m_L-1}{m_L}}\left(\frac{V_L\rho_L}{M_{w_L}}\right)\left(1-\left(\frac{P_{H,L}^a}{P_{H,L}^b}\right)^{\frac{m_L-1}{m_L}}\right)$ (T4.1-1)	$\left(\frac{m_L}{m_L-1}\right)zRT_L^s\left(\frac{P_{H,L}^a}{P_L^s}\right)^{\frac{m_L-1}{m_L}}\left(\frac{V_L\rho_L}{M_{w_L}}\right)\left(\left(\frac{P_{H,L}^b}{P_{H,L}^a}\right)^{\frac{m_L-1}{m_L}}-1\right)$ (T4.1-2)
	W_H	$\frac{m_H}{m_H-1}zRT_H^t\left(\frac{V_H\rho_H}{M_{w_H}}\right)\left(\left(\frac{P_H^s}{P_H^t}\right)^{\frac{m_H-1}{m_H}}-1\right)$ (T4.1-3)	$\frac{m_H}{m_H-1}zRT_H^s\left(\frac{V_H\rho_H}{M_{w_H}}\right)\left(1-\left(\frac{P_H^s}{P_H^t}\right)^{\frac{m_H-1}{m_H}}\right)$ (T4.1-4)
	W_L	$\left(\frac{m_L}{m_L-1}\right)zRT_L^t\left(\frac{V_L\rho_L}{M_{w_L}}\right)\left(1-\left(\frac{P_L^s}{P_L^t}\right)^{\frac{m_L-1}{m_L}}\right)$ (T4.1-5)	$\left(\frac{m_L}{m_L-1}\right)zRT_L^s\left(\frac{V_L\rho_L}{M_{w_L}}\right)\left(\left(\frac{P_L^t}{P_L^s}\right)^{\frac{m_L-1}{m_L}}-1\right)$ (T4.1-6)
Synthesis Stage	$P_{M_{H,L}}^a$	$P_{M_{H,L}}^b\left(1-\frac{W_{W_{H,L}}\left(P_L^b\right)^{\frac{m_L-1}{m_L}}}{\left(\frac{m_L}{m_L-1}\right)zRT_L^t\left(\frac{V_L\rho_L}{M_{w_L}}\right)\left(P_{M_{H,L}}^t\right)^{\frac{m_L-1}{m_L}}}\right)^{\left(\frac{m_L}{m_L-1}\right)}$ (T4.1-7)	$\left(\left(P_{M_{H,L}}^b\right)^{\left(\frac{m_L}{m_L-1}\right)}-\frac{W_{W_{H,L}}\left(P_L^s\right)^{\frac{m_L-1}{m_L}}}{\left(\frac{m_L}{m_L-1}\right)zRT_L^s\left(\frac{V_L\rho_L}{M_{w_L}}\right)}\right)^{\left(\frac{m_L}{m_L-1}\right)}$ (T4.1-8)

For design problems where target temperature has not been defined for any stream, the amount of recoverable mechanical energy will be calculated using prediction methodology. The outlet temperatures after pressurization/depressurization stages will be computed and the work exchanger network will be developed using the synthesis framework. The heat exchanger network may not be required as long as the target temperature is not specified for the process streams.

4.2.1 WEN Design Modification using Heat Integration

Correlation between temperature and pressure will provide the opportunity for further modification using heat integration, even after the final HIWEN flowsheet has been developed. Comparing the utility cost of external compressors (electricity) and heating or cooling utilities (e.g., steam or cooling water), it is concluded that a lower number of external compressors will be more profitable. In Zhuang *et al.* (2017) study, they have considered integrating heaters and coolers for minimizing the utility consumption which shows improvement in energy recovery. This helped us to understand that by modifying the inlet/outlet temperature of streams going through external expanders, we will be able to change the amount of energy provided through expansion which may result in an additional match between that specific expander and an existing external compressor. The temperature modification would be feasible by having an additional heater or cooler. Therefore, by using additional heating/cooling utilities, we can decrease the amount energy required for external compressors. It has been realized that this modification will be cost-effective for most case studies. However, the final total annualized cost (TAC) including the total capital and operating cost for each design should be always computed and the final design decision should be based on the flowsheet with the lowest total annualized cost. In case, heat-integration modification results in higher TAC, we will not take it into the consideration.

In the following, the step-by step procedure to conduct the heat integration into the final flowsheet to improve the energy efficiency of the whole system is summarized.

Step I. Locate the compressors defined by the vector $\boldsymbol{W}_{C_1}$, start with the one (element) which has the highest workload.

Step II. Locate the expanders defined by the vector $\boldsymbol{W}_{E}$, start with the one (element) which provides the highest amount of mechanical energy.

Step III. Calculate the inlet temperatures require for high-pressure streams assigned with the expander from step II. The temperature will be calculated based on the energy that the specified compressor from Step I requires. For the designs in which heat exchanger network is introduced before the work exchanger network, outlet temperature will be modified. Thus, designed HEN and WEN from previous stages will not be interrupted in terms of assumptions and calculations.

Step IV. Match the expander and compressor from steps I and II and replace them with a work exchanger. The workload will be the same as the compressor workload.

Step V. Add heaters or coolers before/after the work exchanger in the high-pressure stream to heat or cool the stream to reach the new temperature defined by step III.

Step VI. Return to step I.

4.3 Basic Cost Analysis

The energy cost in a HIWEN can be readily estimated. The capital cost of work transfer units, especially WE's, is determined by the number of units used, equipment structure, materials used, work transfer capacity, etc. Cheng and Fan (1968) studied the design of a flow work exchanger for a desalination process, where the equipment structure and a basic equipment cost estimation were illustrated. We conducted a preliminary study on equipment design for gas-gas work exchange.

Similar to the cost estimation formula for heat transfer units, we propose the following formula: $C_B = \alpha S^{\beta}$, where S is the volume of a displacement vessel (cylinder including piston), and α and β are the parameters to be determined through experiment. As a case study, for one work exchanger unit, the cost data collected for the main component parts of the unit including the displacement vessel, and valves for different sizes and tolerances can be used to determine the parameters. Figure 4.5 gives the cost estimation of a WE based on the volume of the displacement

vessel made of stainless steel, working in three different conditions with maximum pressure tolerance of the vessels and valves.

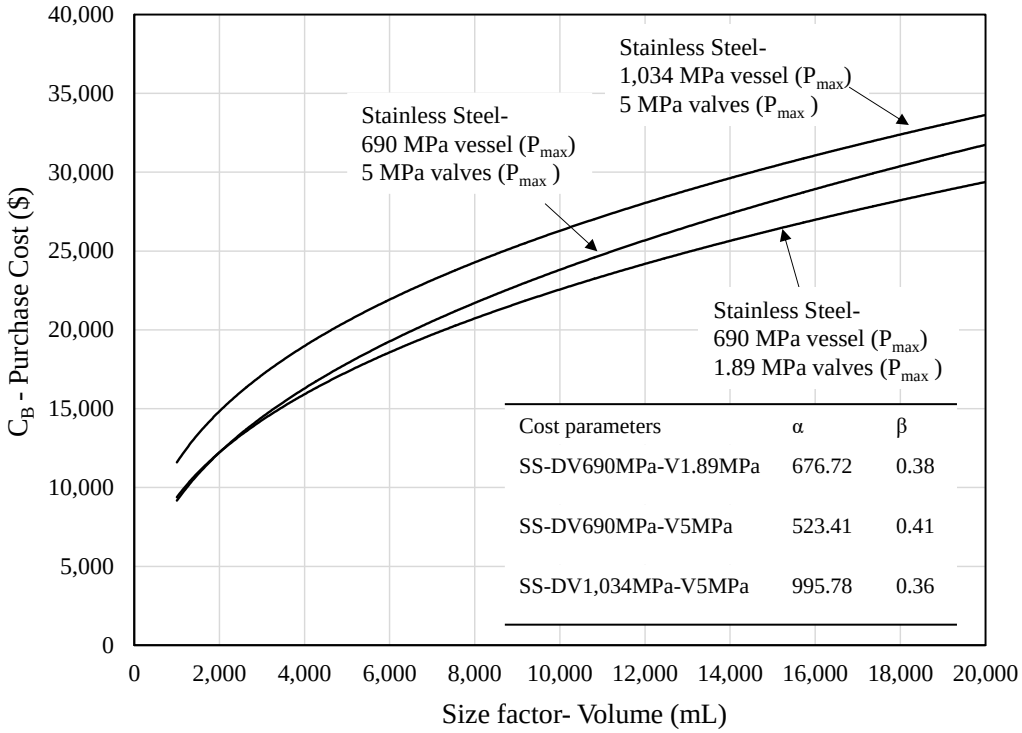

Figure 4.5. Cost estimation for one work exchanger unit.

Note that an accurate comparison of the capital cost of a compressor or expander with a WE is mainly determined by equipment structure and capacity, materials used for the unit, process stream types, especially for gas-gas WE's, and operating condition. On the other hand, work exchangers dealing with gas phase streams have not been commercialized yet. In Chapter 5, we will comprehensively discuss the challenges and opportunities regarding this type of device through simulation of the unit. At this stage, the preliminary cost estimation could be used as a logical basis for the capital cost estimation in WEN synthesis. However, more reliable cost estimation methods should be developed later when the unit is at the stage of manufacturing.

4.4 Case Studies

In this section, two case study problems from open literature are studied to demonstrate the effectiveness of the presented methodologies. For each case study, we will go through the flowchart from Fig. 4.3 to announce the best location for heat exchanger network design prior to the synthesis stage. The synthesis methodology will be implemented to develop the final flowsheet. In the last stage, the heat integration modification will be also applied for any further improvement in energy efficiency of the system. In both case studies, each gas stream has been assumed as an ideal gas with constant heat capacities. Compressors, expanders, and work exchangers are operated under the adiabatic/isentropic condition, reversible and with 100% efficiency. Pressure drop and heat losses are negligible in heat exchangers.

Case 1. A design problem from Razib *et al.* (2012) study is considered to design a cost effective heat integrated work exchanger network using (direct) work exchangers. This example has been also analyzed in Chapter 3 for predicting the maximum recoverable mechanical energy. This will help us to fasten the derivation as the matrices for the prediction stage. Razib *et al.* (2012) introduced a superstructure for WEN configuration using single-shaft-turbine-compressor (SSTC) units and conducted a mixed-integer nonlinear programming (MINLP) model identifying an optimal solution in terms of minimum total annualized cost. In Table 4.2, data for this synthesis problem is summarized.

Table 4.2. Process stream data for Case 1

Stream No.	Supply pressure (P^s, kPa)	Target pressure (P^t, kPa)	Flowrate (kg/s)	Source temperature (T^s, K)	Target temperature (T^t, K)	Heat capacity (C_P, kJ/kg.k)
H_1	850	100	3	600	430	1.432
H_2	960	160	5	580	300	0.982
H_3	800	300	2	960	300	1.046
L_1	100	510	3	300	700	1.432
L_2	100	850	3	300	600	1.432

Step a. Assume HEN before WEN. Considering the heat exchanger network before work exchanger design means that streams will go through a process of heating or cooling before entering the work exchanging stage. The first step is to use the specified outlet temperatures and calculate the temperature (T_i^H and T_i^L) that each stream will reach after exiting the HEN. Knowing the inlet temperature of each stream, stream data will be defined for the HEN problem. In the following, using Eqs. 4.12 and 4.13, the outlet temperature of HEN design for streams HP_1 and LP_1 is shown:

$$T_i^{H_1} = \frac{T_{H_1}^t}{\left(\frac{P_{H_1}^t}{P_{H_1}^s}\right)^{\frac{R}{C_P}}} = \frac{430}{\left(\frac{100}{850}\right)^{\frac{0.35}{1.43}}} = 722.96\,\text{K} \tag{4.17}$$

and

$$T_i^{L_1} = \frac{T_{L_1}^t}{\left(\frac{P_{L_1}^t}{P_{L_1}^s}\right)^{\frac{R}{C_P}}} = \frac{700}{\left(\frac{510}{100}\right)^{\frac{0.64}{1.43}}} = 337.21\text{K} \tag{4.18}$$

where C_p is the heat capacity, and R is the specific gas constant given by Razib *et al.* (2012).

With the same structure, all the temperatures are specified and the HEN design problem is defined as shown in Fig. 4.6a. As discussed and shown in Fig. 4.3, after calculating the T_i^H and T_i^L for all the streams, the maximum amount of mechanical energy that can be recovered for the problem design should be predicted using the methodology presented in Chapter 3. The three high-pressure streams will provide 2,676 kW mechanical energy through depressurization where two low-pressure streams require 3,132.02 kW energy for pressurization. Using the prediction methodology, 1,700.04 kW of mechanical energy of high-pressure streams can be transferred to low-pressure streams which accounts for 63.53% of total energy of high-pressure streams and 54.28% of the energy low-pressure streams required for pressurization. The next stage is to predict the maximum amount of thermal energy that can be recovered using the pinch analysis. Similar to the prediction stage, the detailed calculations for pinch analysis (i.e., temperature interval and cascade diagram) are not shown here. For this design problem as shown in Fig 4.6a, there are three hot streams (H_2, H_3, and L_1) with 1,619 kW energy and two cold streams (H_1 and L_2) which require 688 kW energy to be heated. The results from pinch analysis show that the total amount of energy that the cold streams require can be provided by the hot streams which accounts for 42% of the energy of hot streams and 100% of the energy of cold streams. The operating cost for the

current design considering costs of utilities such as electricity, steam and cooling water is calculated using Eq. 4.14.

Step b. Assume HEN after WEN. For this step, the design problem will be defined as shown in Fig. 4.6b where output temperatures have been calculated using Eqs. 4.15 and 4.16. The prediction stage will be conducted based on the formula for having HEN after the WEN design where three high-pressure streams will provide 2,771 kW mechanical energy through depressurization and two low-pressure streams require 3,406 kW energy for pressurization. Using the prediction methodology, 1,778 kW of mechanical energy from the high-pressure streams can be transferred to low-pressure streams which accounts for 64.16% of the total energy of the high-pressure streams and 52.20% of the energy of the low-pressure streams required for pressurization. The next stage is to predict the maximum amount of thermal energy that can be recovered using the pinch analysis. Similar to prediction stage, the detailed calculations for pinch analysis (i.e., temperature interval and cascade diagram) are not shown here. For this design problem as shown in Fig 4.6b, there are three hot streams (H_2, H_3, and L_2) with 1,759 kW energy and two cold streams (H_1 and L_1) which require 646 kW energy to be heated. The results from pinch analysis show that the total amount of energy that the cold streams require can be provided by the hot streams which accounts for 36.72% of the energy of the hot streams and 100% of the energy of the cold streams.

The results from both methods are shown in Table 4.3. Comparing the operating cost of the two designs shows that the heat exchanger network before the work exchanger design would be more cost-effective in terms of operating cost. For this reason, we will locate the heat exchanger network first (Figs. 4.4a and 4.6a) to heat and cool down the high-pressure and low-pressure streams and then design a work exchanger network to reach the target pressures and temperatures defined for this case study based on Table 4.2. After the decision on the location of HEN is made,

the work exchanger network will be synthesized using the synthesis methodology discussed using the formulation with target temperature (Figs. 4.1-4.2, Table 4.1). When the WEN synthesis is completed, the heat exchanger network will be developed based on the maximum thermal energy recovery results derived and shown in Table 4.3. In Fig. 4.6, bracket represents the stream pressure in kPa and parenthesis defines the stream temperature in Kelvin.

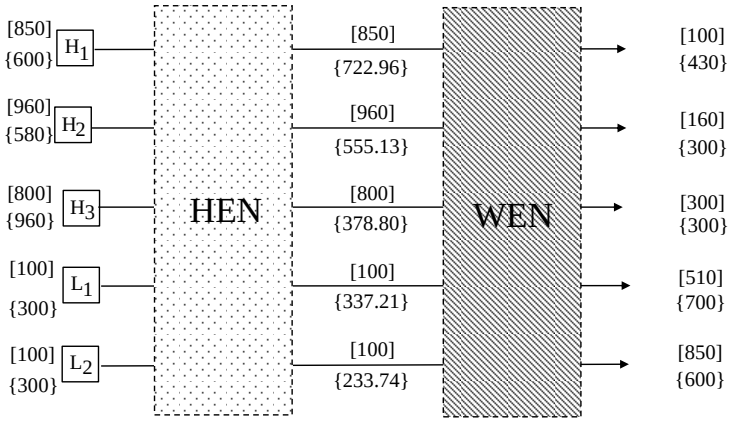

(a)

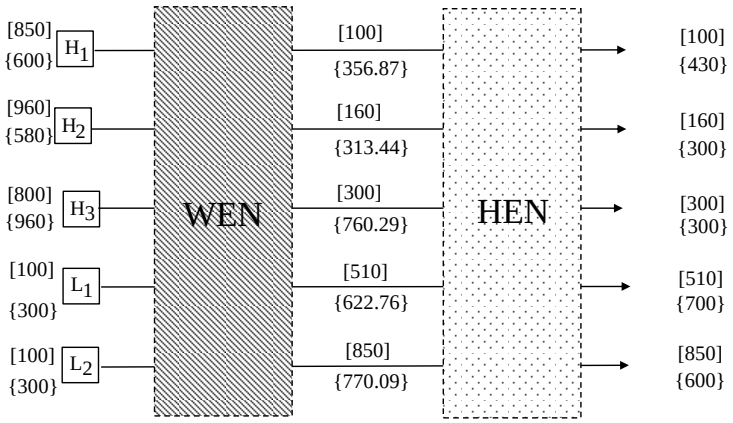

(b)

Figure 4.6. (a) HEN located before WEN design for Case 1, and (b) HEN located after WEN design for Case 1.

Table 4.3. Energy recovery and operation cost comparison based on HEN location for Case 1

Statistic	Placement of HEN	
	Before WEN	After WEN
External compressors energy (kW)	1,431.98	1,628.13
External expanders energy (kW)	976.04	993.13
Mech. energy recovery by WEs (kW)	1,700.04	1,777.97
External heaters energy (kW)	-	-
External coolers energy (kW)	934.54	1,113.14
Thermal energy recovery by HEs (kW)	688.07	645.95
OPEX (k$/year)	1,382	1,572
C_{elec}=0.12 $/kWh; C_{steam}=0.035 $/kWh; C_{CW}=0.001 kWh; Operating time=8000 h/year		

For design problem with three high-pressure streams and two low-pressure streams, given information from Table 4.2, and the design strategy of having the HEN before the WEN design, the following matrices are calculated using the prediction methodology from Chapter 3 as inputs to the flowcharts shown in Figs 4.1 and 4.2.

$$\overline{\boldsymbol{P}} = \begin{pmatrix} [170, 230] & [170, 230] \\ [230, 510] & [230, 850] \\ [0, 0] & [0, 0] \end{pmatrix}. \tag{4.19}$$

The vector of mechanical energy will be provided by each individual high-pressure stream:

$$\boldsymbol{W}_{\boldsymbol{H}} = \begin{pmatrix} 1{,}258.55 \\ 1{,}252.67 \\ 164.86 \end{pmatrix} \tag{4.20}$$

The vector of mechanical energy will be required by each individual low-pressure stream:

$$\boldsymbol{W}_{\boldsymbol{L}} = \begin{pmatrix} 1{,}558.56 \\ 1{,}573.46 \end{pmatrix} \tag{4.21}$$

Matrix $\boldsymbol{W}_{\beta}$, which contains the information about the mechanical energy transferrable between any pair of high-pressure and low-pressure streams:

$$\boldsymbol{W}_{\beta} = \begin{pmatrix} 266.69 & 180.68 \\ 902.83 & 1,128.36 \\ 0 & 0 \end{pmatrix} \tag{4.22}$$

and

$$\boldsymbol{W}_{\gamma} = \begin{pmatrix} 811.18 \\ -778.52 \\ 164.86 \end{pmatrix}. \tag{4.23}$$

Considering N_H=3, N_L=2, Eqs. 4.19-4.23, and Fig. 4.1, $\boldsymbol{W}_W$ is a 3×2 matrix as follows:

$$\boldsymbol{W}_W = \begin{pmatrix} W_{W_{H_1,L_1}} & W_{W_{H_1,L_2}} \\ W_{W_{H_2,L_1}} & W_{W_{H_2,L_2}} \\ W_{W_{H_3,L_1}} & W_{W_{H_3,L_2}} \end{pmatrix}, \tag{4.24}$$

where the six elements will be derived as follows:

Evaluation of $W_{W_{H_1,L_1}}$. Since W_{γ_1} (811.18 kW) is a positive value, we have:

$$W_{W_{H_1,L_1}} = W_{\beta_{H_1,L_1}} = 266.69\,\text{kW}. \tag{4.25}$$

Evaluation of $W_{W_{H_1,L_2}}$. Since W_{γ_1} (811.18 kW) is a positive value, we have:

$$W_{W_{H_1,L_2}} = W_{\beta_{H_1,L_2}} = 180.68\,\text{kW}. \tag{4.26}$$

Evaluation of $W_{W_{H_2,L_1}}$. Since W_{γ_2} (-778.52 kW) is a negative value, where its absolute value is less than $W_{\beta_{H_2,L_1}}$ (902.83 kW), both $W_{\beta_{H_2,L_1}}$ and $W_{\beta_{H_2,L_2}}$ (902.83 kW and 1,128.36 kW) are higher than the absolute value of W_{γ_2} (-778.52 kW), and $W_{\beta_{H_2,L_1}}$ (902.83 kW) will not be counted as the highest value among $W_{\beta_{H_2,L_1}}$ and $W_{\beta_{H_2,L_2}}$ (902.83 kW and 1,128.36 kW), we have:

$$W_{W_{H_2,L_1}} = W_{\beta_{H_2,L_1}} = 902.83\,\text{kW}. \tag{4.27}$$

Evaluation of $W_{W_{H_2,L_2}}$. Since W_{γ_2} (-778.52 kW) is a negative value, where its absolute value is less than $W_{\beta_{H_2,L_2}}$ (1,128.36 kW), both $W_{\beta_{H_2,L_1}}$ and $W_{\beta_{H_2,L_2}}$ (902.83 kW and 1,128.36 kW) are higher than the absolute value of W_{γ_2} (-778.52 kW), and $W_{\beta_{H_2,L_2}}$ (1,128.36 kW) will be counted as the highest value among $W_{\beta_{H_2,L_1}}$ and $W_{\beta_{H_2,L_2}}$ (902.83 kW and 1,128.36 kW), we have:

$$W_{W_{H_2,L_2}} = W_{\beta_{H_2,L2}} - \left|W_{\gamma_2}\right| = 1{,}128.36 - 778.52 = 349.84 \text{ kW}. \tag{4.28}$$

Evaluation of $W_{W_{H_3,L_1}}$. Since W_{γ_3} (164.86 kW) is a positive value, we have:

$$W_{W_{H_3,L_1}} = W_{\beta_{H_3,L_1}} = 0 \text{ kW}. \tag{4.29}$$

Evaluation of $W_{W_{H_3,L_2}}$. Since W_{γ_3} (164.86 kW) is a positive value, we have:

$$W_{W_{H_3,L_2}} = W_{\beta_{H_3,L_2}} = 0 \text{ kW}. \tag{4.30}$$

Therefore, a complete matrix $\boldsymbol{W}_W$ will be constructed using Eqs 4.25-4.30 as follows:

$$\boldsymbol{W}_W = \begin{pmatrix} 266.69 & 180.68 \\ 902.83 & 349.86 \\ 0 & 0 \end{pmatrix}. \tag{4.31}$$

Equation 4.31 shows the workload of each work exchanger unit between each individual high-pressure and low-pressure stream where using splitting H_1 and H_2 will transfer mechanical energy to L_1 and L_2 through four work exchangers. Now, $\overline{\boldsymbol{P}}_{\boldsymbol{M}}$ which is a 3×2 matrix will be constructed to identify the pressure interval in each individual low-pressure stream that the work exchangers will be placed.

$$\bar{\boldsymbol{P}}_{\boldsymbol{M}} = \begin{pmatrix} \bar{P}_{M_{H_1,L_1}} & \bar{P}_{M_{H_1,L_2}} \\ \bar{P}_{M_{H_2,L_1}} & \bar{P}_{M_{H_2,L_2}} \\ \bar{P}_{M_{H_3,L_1}} & \bar{P}_{M_{H_3,L_2}} \end{pmatrix}, \tag{4.32}$$

Derivation of two elements, $\bar{P}_{M_{H_1,L_1}}$ and $\bar{P}_{M_{H_2,L_2}}$ will be shown in the following. Calculation of the other four elements can be performed in the same way.

a) Calculation of $\bar{P}_{M_{H_1,L_1}}$. This interval is derived from $\bar{\boldsymbol{P}}_{H_1,L_1}$. According to Eq. 4.4, the upper-bound of both intervals will be the same and the lower-bound will be calculated using Eq. T4.1-7 from Table 4.1. Note that based on the case study data provided, equation T4.1-7 is modified to Eq. 4.34.

$$P^b_{M_{H_1,L_1}} = P^b_{H_1,L_1} = 230\,\text{kPa}, \tag{4.33}$$

and

$$P^a_{M_{H_1,L_1}} = P^b_{M_{H_1,L_1}} \left(1 - \frac{W_{W_{H_1,L_1}} \left(P^b_{M_{H_1,L_1}} \right)^{\frac{R}{C_{P_{L_1}}}}}{F_{L_1} C_{P_{L_1}} T^t_{L_1} \left(P^t_{L_1} \right)^{\frac{R}{C_{P_{L_1}}}}} \right)^{\left(\frac{C_{P_{L_1}}}{R} \right)} = 170\ \text{kPa} \tag{4.34}$$

Thus,

$$\bar{P}_{M_{H_1,L_1}} = [170, 230] \tag{4.35}$$

b) Calculation of $\bar{P}_{M_{H_2,L_2}}$. This interval is derived from $\bar{\boldsymbol{P}}_{H_2,L_2}$. According to Eq. 4.4, the upper-bound of both intervals will be the same and the lower-bound will be calculated using Eq. T4.1-7 from Table 4.1. Note that based on the case study data provided, equation T4.1-7 is modified to Eq. 4.37.

$$P^b_{M_{H_2,L_2}} = P^b_{H_2,L_2} = 850\,\text{kPa}, \tag{4.36}$$

and

$$P^{a}_{M_{H_2,L_2}} = P^{b}_{M_{H_2,L_2}} \left(1 - \frac{W_{W_{H_2,L_2}} \left(P^{b}_{M_{H_2,L_2}} \right)^{\frac{R}{C_{P_{L_2}}}}}{F_{L_2} C_{P_{L_2}} T^{t}_{L_2} \left(P^{t}_{L_2} \right)^{\frac{R}{C_{P_{L_2}}}}} \right)^{\left(\frac{C_{P_{L_2}}}{R} \right)} \tag{4.37}$$

$$= 610.40 \text{ kPa}$$

Thus,

$$\overline{P}_{M_{H_1,L_1}} = [610.40, 850] \tag{4.38}$$

c) Construction of a complete matrix $\overline{\boldsymbol{P}}_{\boldsymbol{M}}$. Using the same approach, we have calculated the interval of the four other elements in matrix $\overline{\boldsymbol{P}}_{\boldsymbol{M}}$ which are assembled as follows:

$$\overline{\boldsymbol{P}}_{\boldsymbol{M}} = \begin{pmatrix} [170,230] & [170,230] \\ [230,510] & [610.40,850] \\ [0,0] & [0,0] \end{pmatrix}. \tag{4.39}$$

According to Eq. 4.39, H_1 requires splitting which will transfer 266.69 kW through a work exchanger in $[100,\ 850]$ pressure interval to L_1 in the pressure interval of $[170,\ 230]$ and 180.68 kW within the same pressure interval to L_2 in the pressure interval of $[170,\ 230]$. H_2 also requires splitting and will transfer 902.83 kW through a work exchanger in $[100,\ 850]$ pressure interval to L_1 in the pressure interval of $[230,\ 510]$ and 349.84 kW within the same pressure interval to L_2 in the pressure interval of $[610.40,\ 850]$. At this stage, H_3 will not transfer any mechanical energy to any low-pressure stream.

Using Eqs. 4.6 and 4.7, vector $\boldsymbol{W}_{C_1}$ will be constructed as follows:

$$\boldsymbol{W}_{C_1} = \begin{pmatrix} W_{C_{1_1}} \\ W_{C_{1_2}} \end{pmatrix} = \begin{pmatrix} 1{,}169.52 - 1{,}169.52 \\ 1{,}309.04 - 530.52 \end{pmatrix} = \begin{pmatrix} 0 \\ 778.52 \end{pmatrix}. \tag{4.40}$$

Based on Eq. 4.40, one compressor will be placed in L_2. The compressor location can be defined as pressure interval of $[230,\ 610.40]$ by comparing the pressure intervals from the second column of matrices $\overline{\boldsymbol{P}}_{\boldsymbol{M}}$ and $\overline{\boldsymbol{P}}$. Matrix $\boldsymbol{W}_{C_2}$ will be derived using Eqs. 4.8 and 4.9 as shown below:

$$\boldsymbol{W}_{C_2} = \begin{pmatrix} W_{C_{2_1}} \\ W_{C_{2_1}} \end{pmatrix} = \begin{pmatrix} 1{,}558.57 - 1{,}169.52 \\ 1{,}573.46 - 1{,}309.04 \end{pmatrix} = \begin{pmatrix} 389.04 \\ 264.42 \end{pmatrix}. \tag{4.41}$$

Comparing the pressure intervals in matrix $\overline{\boldsymbol{P}}$ with the supply and target pressure of each low-pressure stream from Table 4.2, two compressors will be placed. One of the compressors will be placed in L_1 within the pressure interval of $[170,\ 230]$ with the workload of 389.04 kW and the other one in L_2 with the workload of 264.42 kW in the pressure interval of $[170,\ 230]$. In the end, vector $\boldsymbol{W}_{\boldsymbol{E}}$ will be derived using Eqs. 4.10 and 4.11.

$$\boldsymbol{W}_{\boldsymbol{E}} = \begin{pmatrix} W_{E_1} \\ W_{E_2} \\ W_{E_3} \end{pmatrix} = \begin{pmatrix} 811.18 \\ 0 \\ 164.86 \end{pmatrix}. \tag{4.42}$$

Thus, two expanders will be placed. The first one will be in H_1 through the splitting in the pressure interval of $[100,\ 850]$ with a workload of 811.18 kW, and the second one is in H_3 within

the $[300,\ 800]$ pressure interval with a workload of 164.86 kW. Figure 4.7a shows the flowsheet developed through the WEN synthesis methodology. In Fig. 4.7a, there are three hot streams (marked as HS1 – HS3) and two cold streams (marked as CS1 and CS2), which define a HEN design problem. A synthesized HEN is shown in Fig. 4.7b. This network can recover 42.4% of thermal energy from hot streams (688.07 kW out of 1,619.14 kW).

After the development of the work and heat exchanger network using the presented methodology, the design can be modified by the instructions provided in the WEN design modification using heat integration. According to Step I, the vector $\boldsymbol{W}_{C_1}$ contains only one compressor (C_1) which is placed in the $[230, 610]$ pressure interval with the workload of 778.52 kW. This compressor can be matched with expander E_1 by modifying the outlet temperature of the expander using heat integration based on Step II (this is the type of design where the HEN considered before the WEN). The adjusted outlet temperature for E_1 will be 412 K which will cause the expander E_1 to transfer the exact amount of energy the compressor C_1 requires. Therefore, after replacing expander E_1 and compressor C_1 with a work exchanger (W_5), a heater will be placed in the high-pressure stream so it will be heated to the target temperature (430 K). Using this adjustment, the total mechanical energy recovery improved 31%, and external compression utility consumption and expansion utility requirements decreased 54% and 17%, respectively.

In conclusion, to reach the target temperature and pressure, three high-pressure streams and two low pressure streams will go through a heat exchanger network (Fig. 4.7b) first and then a work exchanger network (Fig. 4.8) in which the maximum amount of thermal and mechanical energy will be recovered using this cost-effective design. The results are shown in Table 4.4.

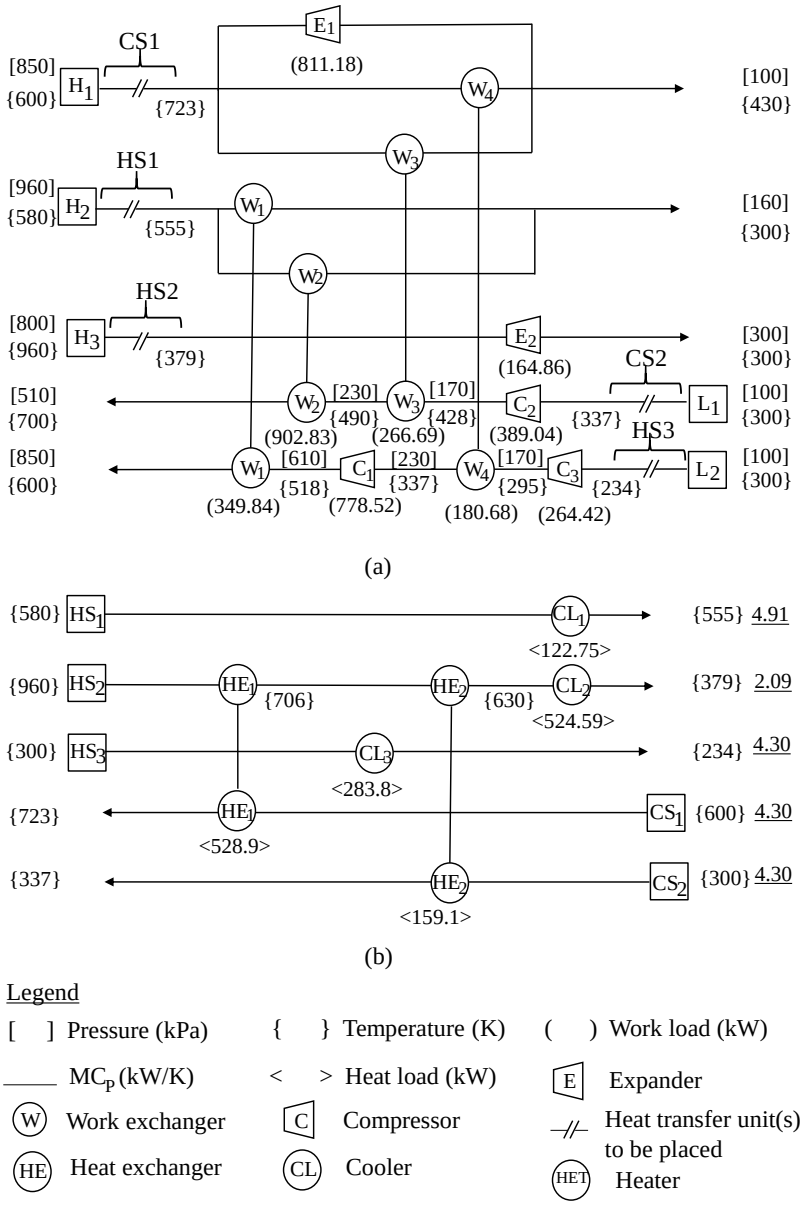

Figure 4.7. Flowsheet of heat-integrated work exchange network for Case 1 :(a) work exchanger network, (b) heat exchanger network.

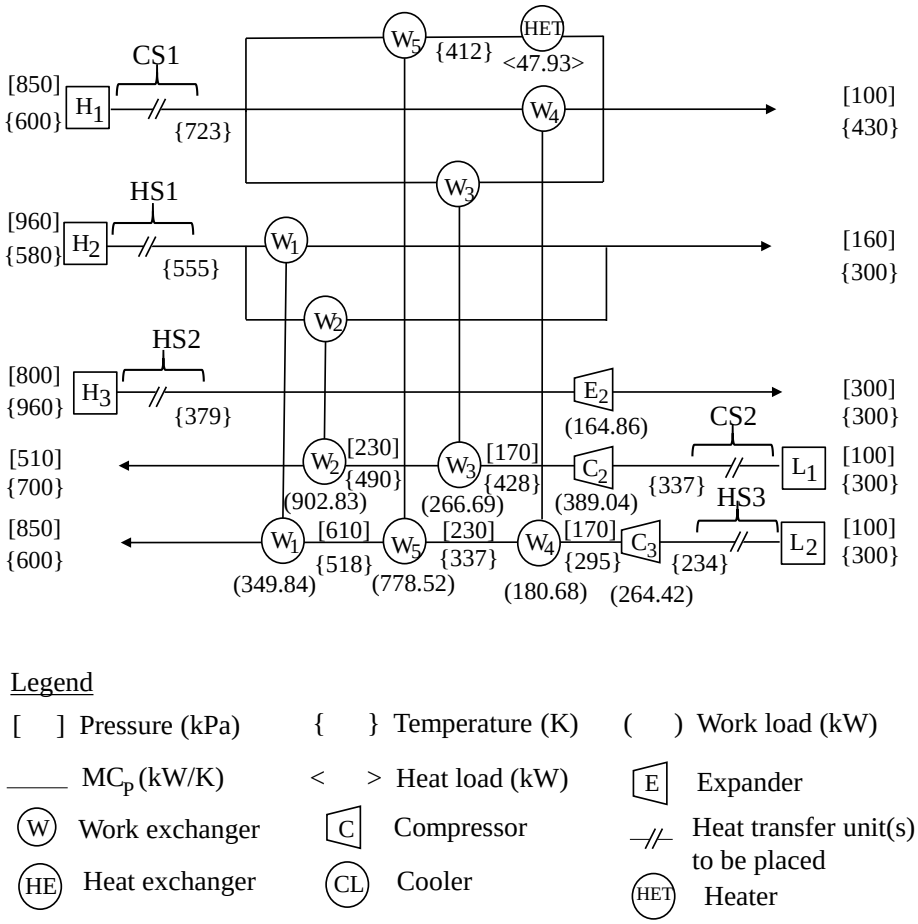

Figure 4.8. Flowsheet of modified heat-integrated work exchange network for Case 1.

Table 4.4. Energy recovery analysis for Case 1

Design	Mech. energy exchange (kW)	Thermal energy exchange (kW)	External compression utility (kW)	External expansion utility (kW)	External heating utility (kW)	External cooling utility (kW)
Without HEWEN	-	-	3,406.00	2,771.10	645.98	1,759.62
With HEWEN	1,700.01	688.10	1,431.98	976.04	-	931.14
Modified HEWN	2,478.53	688.10	653.46	164.86	47.93	931.14

Case 2. This design problem has been studied by Onishi *et al.* (2014) and Huang and Karimi (2016). In both studies, a superstructure for work-heat exchanger network configuration

using single-shaft-turbine-compressor (SSTC) units was introduced and a mixed-integer nonlinear programming (MINLP) model was conducted for identifying an optimal solution in terms of the minimum total annualized cost. In Table 4.5, data for this synthesis problem is summarized.

Table 4.5. Process stream data for Case 2

Stream No.	Supply pressure (P^s, kPa)	Target pressure (P^t, kPa)	Flowrate (kg/s)	Source temperature (T^s, K)	Target temperature (T^t, K)	Heat capacity (C_P, kJ/kg.k)
H_1	900	100	15	350	350	2.454
H_2	850	150	15	350	350	0.982
H_3	700	200	15	400	400	1.432
L_1	100	700	18	390	390	1.432
L_2	100	900	15	420	420	2.454

Step a. Assume HEN before WEN. Considering the heat exchanger network before the work exchanger design means that streams will go through a process of heating or cooling before entering the work exchanging stage. The first step is to use the specified outlet temperatures and calculate the temperature (T_i^H and T_i^L) each stream will reach after exiting the HEN. Knowing the inlet temperature of each stream, stream data will be defined for the HEN problem. In the following, using Eqs. 4.12 and 4.13, the outlet temperature after the HEN design is shown for streams HP_1 and LP_1.

$$T_i^{H_1} = \frac{T_{H_1}^t}{\left(\frac{P_{H_1}^t}{P_{H_1}^s}\right)^{\frac{K-1}{k}}} = \frac{350}{\left(\frac{100}{900}\right)^{\frac{0.4}{1.4}}} = 655.70\,\text{K} \tag{4.43}$$

and

$$T_i^{L_1} = \frac{T_{L_1}^t}{\left(\frac{P_{L_1}^t}{P_{L_1}^s}\right)^{\frac{k-1}{k}}} = \frac{390}{\left(\frac{700}{100}\right)^{\frac{0.4}{1.4}}} = 223.67\,\mathrm{K} \tag{4.44}$$

where k is the heat capacity ratio (adiabatic exponent).

With the same structure, all the temperatures are specified and the HEN design problem is defined as shown in Fig. 4.9a. As discussed and shown in Fig. 4.3, after calculating the T_i^H and T_i^L for the streams, the maximum amount of mechanical energy that can be recovered for the problem design should be predicted using the methodology presented in Chapter 3. The three high-pressure streams will provide 18,257.91 kW mechanical energy through depressurization where two low-pressure streams require 11,495.23 kW energy for pressurization. Using the prediction methodology 8,846.94 kW of mechanical energy of the high-pressure streams can be transferred to the low-pressure streams which accounts for 48.46% of the total energy of the high-pressure streams and 76.96% of the energy of the low-pressure streams required for pressurization. The next stage is to predict the maximum amount of thermal energy that can be recovered using the pinch analysis. Similar to the prediction stage, the detailed calculations for pinch analysis (i.e., temperature interval and cascade diagram) are not shown here. For this design problem as shown in Fig. 4.9a, there are three cold streams (H_1, H_2, and H_3) which require 18,257.91 kW energy to be heated and two hot streams (L_1 and L_2) with 11,495.23 kW energy. The results from pinch analysis show that about 2,908.2 kW energy that cold streams require can be provided by hot streams which accounts for 25% of the energy of the hot streams and 16% of the energy of the cold streams.

Operating cost for the current design considering the cost of utilities such as electricity, steam and cooling water is calculated using Eq. 4.14.

Step b. Assume HEN after WEN. For this step, the design problem will be defined as shown in Fig. 4.9b where output temperatures have been calculated using Eqs. 4.15 and 4.16. The prediction stage will be conducted based on the formula for having the HEN after the WEN design where three high-pressure streams will provide 10,606.49 kW of mechanical energy through depressurization and two low-pressure streams require 20,979.15 kW of the energy for pressurization. Using the prediction methodology 6,006.59 kW of mechanical energy of the high-pressure streams can be transferred to the low-pressure streams which accounts for 56.63% of the total energy of the high-pressure streams and 28.63% of the energy of the low-pressure streams required for pressurization. The next stage is to predict the maximum amount of thermal energy that can be recovered using the pinch analysis. Similar to the prediction stage, the detailed calculations for pinch analysis (i.e., temperature interval and cascade diagram) are not shown here. For this design problem as shown in Fig 4.9b, there are three cold streams (H_1, H_2, and H_3) which require 10,606.54 kW energy to be heated and two hot streams (L_1 and L_2) with 20,979.3 kW energy. The results from pinch analysis show that the total amount of energy that cold streams require can be provided by hot streams which accounts for 50.56% of the energy of the hot streams and 100% of the energy of the cold streams.

The results from both methods are summarized in Table 4.6. Comparing the operating cost of the two designs shows that the heat exchanger network before the work exchanger design would be more cost-effective in terms of operating cost. For this reason, we will locate the heat exchanger network first (Fig. 4.4a and 4.9a) to heat and cool down the high-pressure and low-pressure streams and then design a work exchanger network to reach the target pressure and temperature defined

for this case study based on Table 4.5. After the decision on the location of the HEN is made, the work exchanger network will be synthesized using the synthesis methodology (Figs. 4.1-4.2) and the formulation considering the target temperature (Table 4.1). The heat exchanger network will be also developed based on the maximum thermal energy recovery results shown in Table 4.6.

Table 4.6. Energy recovery and operation cost comparison based on HEN location for Case 2

Statistic	Placement of HEN	
	Before WEN	After WEN
External compressors energy (kW)	2,648.29	14,972.56
External expanders energy (kW)	9,410.97	4,599.90
Mech. energy recovery by WEs (kW)	8,846.94	6,006.59
External heaters energy (kW)	15,349.71	-
External coolers energy (kW)	8,587.03	10,372.76
Thermal energy recovery by HEs (kW)	2,908.20	10,606.54
OPEX (k$/year)	6,909	14,457
C_{elec}=0.12 $/kWh; C_{steam}=0.035 $/kWh; C_{CW}=0.001 kWh; Operating time=8000 h/year		

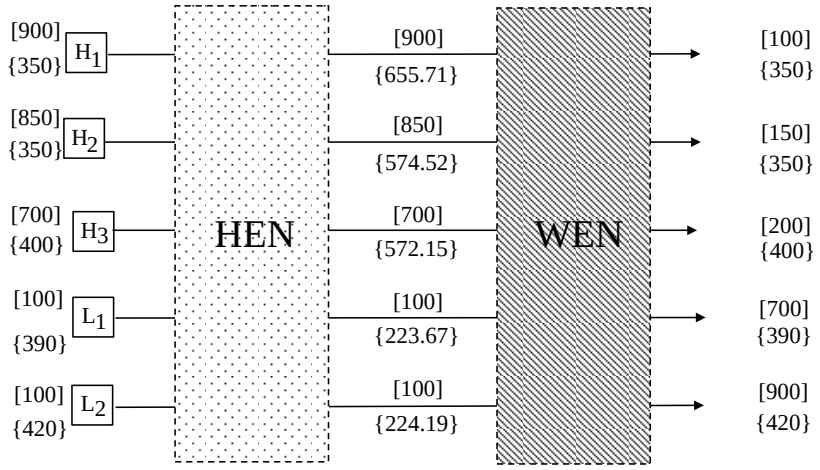

(a)

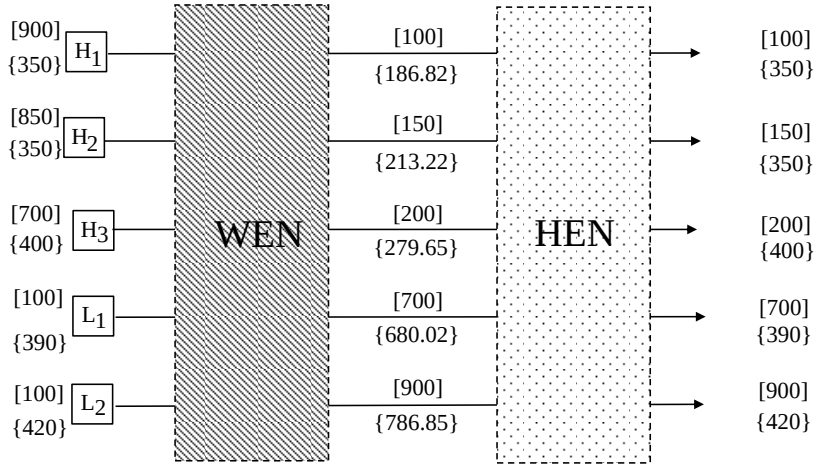

(b)

Figure 4.9. (a) HEN located before WEN design for Case 2, and (b) HEN located after WEN design for Case 2.

For design problem with three high-pressure streams and two low-pressure streams, given information from Table 4.5 and the design strategy of having the HEN before the WEN design, the following matrices are calculated using the prediction methodology as inputs to the flowcharts shown in Figs 4.1 and 4.2.

$$\overline{P} = \begin{pmatrix} [170,700] & [170,830] \\ [0,0] & [0,0] \\ [0,0] & [0,0] \end{pmatrix}. \tag{4.45}$$

The vector of mechanical energy will be provided by each individual high-pressure stream:

$$W_H = \begin{pmatrix} 11{,}253.02 \\ 3{,}307.17 \\ 3{,}697.73 \end{pmatrix}. \tag{4.46}$$

The vector of mechanical energy will be required by each individual low-pressure stream:

$$W_L = \begin{pmatrix} 4{,}287.32 \\ 7{,}207.91 \end{pmatrix}. \tag{4.47}$$

Matrix $\boldsymbol{W}_\beta$, which contains the information about the mechanical energy transferrable between any pair of high-pressure and low-pressure streams.

$$\boldsymbol{W}_\beta = \begin{pmatrix} 3{,}343.51 & 5{,}503.43 \\ 0 & 0 \\ 0 & 0 \end{pmatrix}, \tag{4.48}$$

and

$$\mathbf{W}_\gamma = \begin{pmatrix} 2{,}406.08 \\ 3{,}307.17 \\ 3{,}697.73 \end{pmatrix}. \tag{4.49}$$

Considering N_H=3, N_L=2, Eqs. 4.45-4.49, and Fig. 4.1, $\boldsymbol{W}_W$ is a 3×2 matrix as follows:

$$\boldsymbol{W}_W = \begin{pmatrix} W_{W_{H_1,L_1}} & W_{W_{H_1,L_2}} \\ W_{W_{H_2,L_1}} & W_{W_{H_2,L_2}} \\ W_{W_{H_3,L_1}} & W_{W_{H_3,L_2}} \end{pmatrix}, \tag{4.50}$$

The derivation of all the six elements is shown below:

Evaluation of $W_{W_{H_1,L_1}}$. Since W_{γ_1} (2,406.08 kW) is a positive value, we have:

$$W_{W_{H_1,L_1}} = W_{\beta_{H_1,L_1}} = 3{,}343.51\,\text{kW}. \tag{4.51}$$

Evaluation of $W_{W_{H_1,L_2}}$. Since W_{γ_1} (2,406.08 kW) is a positive value, we have:

$$W_{W_{H_1,L_2}} = W_{\beta_{H_1,L_2}} = 5{,}503.43\,\text{kW}. \tag{4.52}$$

Evaluation of $W_{W_{H_2,L_1}}$. Since W_{γ_2} (3,307.17 kW) is a positive value, we have:

$$W_{W_{H_2,L_1}} = W_{\beta_{H_2,L_1}} = 0\,\text{kW}. \tag{4.53}$$

Evaluation of $W_{W_{H_2,L_2}}$. Since W_{γ_2} (3,307.17 kW) is a positive value, we have:

$$W_{W_{H_2,L_2}} = W_{\beta_{H_2,L2}} = 0\,\text{kW}. \tag{4.54}$$

Evaluation of $W_{W_{H_3,L_1}}$. Since W_{γ_3} (3,697.73 kW) is a positive value, we have:

$$W_{W_{H_3,L_1}} = W_{\beta_{H_3,L_1}} = 0\,\text{kW}. \tag{4.55}$$

Evaluation of $W_{W_{H_3,L_2}}$. Since W_{γ_3} (3,697.73 kW) is a positive value, we have:

$$W_{W_{H_3,L_2}} = W_{\beta_{H_3,L_2}} = 0\,\text{kW}. \tag{4.56}$$

Therefore, the complete matrix $\boldsymbol{W}_W$ will be constructed using Eqs. 4.51-4.56 as follows:

$$\boldsymbol{W}_W = \begin{pmatrix} 3{,}343.51 & 5{,}503.43 \\ 0 & 0 \\ 0 & 0 \end{pmatrix}. \tag{4.57}$$

Equation 4.57 shows the workload of each work exchanger unit between each individual high-pressure and low-pressure stream. Using splitting, H_1 will transfer mechanical energy to L_1 and L_2 through two work exchangers. $\overline{\boldsymbol{P}}_{\boldsymbol{M}}$ which is a 3×2 matrix will be constructed to identify the pressure interval in each individual low-pressure stream that the work exchangers will be placed in.

$$\overline{\boldsymbol{P}}_{\boldsymbol{M}} = \begin{pmatrix} \overline{P}_{M_{H_1,L_1}} & \overline{P}_{M_{H_1,L_2}} \\ \overline{P}_{M_{H_2,L_1}} & \overline{P}_{M_{H_2,L_2}} \\ \overline{P}_{M_{H_3,L_1}} & \overline{P}_{M_{H_3,L_2}} \end{pmatrix}, \tag{4.58}$$

Derivation of the two elements, $\overline{P}_{M_{H_1,L_1}}$ and $\overline{P}_{M_{H_2,L_2}}$ will be shown in the following. Calculation of the other four elements can be performed in the same way.

a) Calculation of $\overline{P}_{M_{H_1,L_1}}$. This interval is derived from $\overline{\boldsymbol{P}}_{H_1,L_1}$. According to Eq. 4.4, the upper-bound of both intervals will be the same and the lower-bound will be calculated using Eq. T4.1-7 from Table 4.1. Note that based on the case study data provided, equation T4.1-7 is modified to Eq. 4.60.

$$P^b_{M_{H_1,L_1}} = P^b_{H_1,L_1} = 700\,\text{kPa}, \tag{4.59}$$

and

$$P^a_{M_{H_1,L_1}} = P^b_{M_{H_1,L_1}} \left(1 - \frac{W_{W_{H_1,L_1}} \left(P^b_{M_{H_1,L_1}} \right)^{\frac{k-1}{k}}}{F_{L_1} C_{P_{L_1}} T^t_{L_1} \left(P^t_{L_1} \right)^{\frac{k-1}{k}}} \right)^{\left(\frac{k}{k-1}\right)} \tag{4.60}$$

$$= 170\ \text{kPa}$$

Thus,

$$\overline{P}_{M_{H_1,L_1}} = [170, 700] \tag{4.61}$$

b) Calculation of $\overline{P}_{M_{H_2,L_2}}$. This interval is derived from $\overline{\boldsymbol{P}}_{H_2,L_2}$. According to Eq. 4.4, the upper-bound of both intervals will be the same and the lower-bound will be calculated using Eq. T4.1-7 from Table 4.1. Note that based on the case study data provided, equation T4.1-7 is modified to Eq. 4.63.

$$P^b_{M_{H_2,L_2}} = P^b_{H_2,L_2} = 830\,\text{kPa}, \tag{4.62}$$

and

$$P^{a}_{M_{H_2,L_2}} = P^{b}_{M_{H_2,L_2}} \left(1 - \frac{W_{W_{H_2,L_2}} \left(P^{b}_{M_{H_2,L_2}} \right)^{\frac{k-1}{k}}}{F_{L_2} C_{P_{L_2}} T^{t}_{L_2} \left(P^{t}_{L_2} \right)^{\frac{k-1}{k}}} \right)^{\left(\frac{k}{k-1}\right)} \tag{4.63}$$
$$= 170 \text{ kPa}$$

Thus,

$$\overline{P}_{M_{H_1,L_1}} = [170,830] \tag{4.64}$$

c) Construction of a complete matrix $\overline{\boldsymbol{P}}_{\boldsymbol{M}}$. Using the same approach, we have calculated the values of the four other elements in matrix $\overline{\boldsymbol{P}}_{\boldsymbol{M}}$. All these values are assembled as follows:

$$\overline{\boldsymbol{P}}_{\boldsymbol{M}} = \begin{pmatrix} [170,700] & [170,830] \\ [0,0] & [0,0] \\ [0,0] & [0,0] \end{pmatrix}. \tag{4.65}$$

According to Eq. 4.65, H_1 requires splitting which will transfer 3,343.51 kW through a work exchanger in the $[100,900]$ pressure interval to L_1 in the pressure interval of $[170,700]$ and 5,503.43 kW within the same pressure interval to L_2 in the pressure interval of $[170,830]$. H_2 and H_3 will not transfer any mechanical energy to any low-pressure stream.

Using Eqs. 4.6 and 4.7, vector $\boldsymbol{W}_{\boldsymbol{C_1}}$ will be constructed as follows:

$$\boldsymbol{W}_{\boldsymbol{C_1}} = \begin{pmatrix} W_{C_{1_1}} \\ W_{C_{1_2}} \end{pmatrix} = \begin{pmatrix} 3{,}343.51 - 3{,}343.51 \\ 5{,}503.43 - 5{,}503.43 \end{pmatrix}. \tag{4.66}$$
$$= \begin{pmatrix} 0 \\ 0 \end{pmatrix}$$

Matrix $\boldsymbol{W}_{\boldsymbol{C_2}}$ will be derived using Eqs. 4.8 and 4.9 as shown below:

$$\boldsymbol{W}_{C_2} = \begin{pmatrix} W_{C_{2_1}} \\ W_{C_{2_1}} \end{pmatrix} = \begin{pmatrix} 4{,}287.32 - 3{,}343.51 \\ 7{,}207.91 - 5{,}503.43 \end{pmatrix} = \begin{pmatrix} 943.81 \\ 1{,}704.48 \end{pmatrix}. \quad (4.67)$$

According to Eqs. 4.66 and 4.67, there will be only two compressors which will be placed by comparing the pressure intervals in matrix $\overline{\boldsymbol{P}}$ with the supply and target pressures of each low-pressure stream from Table 4.5. The comparison will end up with placing three compressors, the first one in L_1 within the pressure interval of $[100,170]$ with the workload of 943.81 kW, the second and third ones in L_2 with the total energy of 1,443.87 kW in the pressure intervals of $[100,170]$ and $[830,900]$ with workloads of 1,350.93 kW and 353.55 kW, respectively. In the end, vector $\boldsymbol{W}_{\boldsymbol{E}}$ will be derived using Eqs. 4.10 and 4.11.

$$\boldsymbol{W}_{\boldsymbol{E}} = \begin{pmatrix} W_{E_1} \\ W_{E_2} \\ W_{E_3} \end{pmatrix} = \begin{pmatrix} 2{,}406.08 \\ 3{,}307.17 \\ 3{,}697.73 \end{pmatrix}. \quad (4.68)$$

Thus, three expanders will be placed. The first one will be in H_1 through the splitting in the pressure interval of $[100,900]$ with the workload of 2,406.08 kW, the second one is in H_2 within the $[150,850]$ pressure interval with the workload of 3,307.17 kW, and the third one is in H_3 within the $[200,700]$ pressure interval with the workload of 3,697.73 kW. Figure 4.10a shows the flowsheet developed using the WEN synthesis methodology. In Fig. 4.10(a), there are three hot streams (marked as HS1 – HS3) and two cold streams (marked as CS1 and CS2), which define a HEN design problem. A synthesized HEN is shown in Fig. 4.10(b). This network can recover 25% of the thermal energy from the hot streams (8,587.03 kW out of 11,495.23 kW).

After the development of the work and heat exchanger networks using the presented methodologies, the design will be analyzed for any possibility of additional modification by heat integration. According to Eq. 4.66, there will not be any compressor placed using vector $\boldsymbol{W}_{C_1}$. Thus, there will not be any low-pressure stream in the thermodynamic feasibility pressure interval to be able to receive energy from the high-pressure streams by adjusting the temperature.

For this case study, we have conducted a cost analysis to estimate the Total Annualized Cost (TAC) including Capital Cost (CAPEX) and Operating Cost (OPEX). For a reasonable comparison of the final results with Huang and Karimi (2016) and Onishi *et al.* (2014), we have used the exact same assumptions for the cost calculation such as formulation, equipment cost coefficient and fixed cost, and utility cost. As mentioned earlier, those studies have used SSTC units for the mechanical energy recovery. Therefore, for the capital cost estimation of work exchangers in our design, we have used the base cost formula discussed in Section 4.3 and Fig. 4.5. The capital cost of external expanders ($CAPEX_E$) is computed using Eq. 4.69.

$$CAPEX_E = FC_E^U + FC_E\left(F\right) \tag{4.69}$$

where FC_E^U is the external expander fixed cost and is assumed to be 200 k$/year, FC_E is the cost coefficient and is equal to 1 k$/year, and F is the flowrate of stream flows through the expander. The capital cost of external compressors ($CAPEX_C$) is computed using Eq. 4.70.

$$CAPEX_C = FC_C^U + FC_C\left(F\right) \tag{4.70}$$

where FC_C^U is the external compressor fixed cost and is assumed to be 250 k$/year, FC_C is the cost coefficient and is equal to 1 k$/year, and F is the flowrate of stream flows through the

compressor. The capital costs of heat exchangers, heaters, and coolers ($CAPEX_{HE}$) are computed using Eq. 4.71.

$$CAPEX_{HE} = FC_H + C(A)^{\delta} \tag{4.71}$$

where FC_H is the heat exchanger fixed cost and is assumed to be 3 k$/year, C is the cost coefficient and is equal to 0.03 k$/year, A is the heat exchanger area, and δ is the exponent for area cost of the HE and is equal to 1. The capital cost of the work exchanger ($CAPEX_{WE}$) will be computed as follows:

$$CAPEX_{WE} = \alpha S^{\beta} \tag{4.72}$$

where S is the volume of one vessel and cost parameters assuming stainless steel, the pressure tolerance of 1,034 MPa for a vessel and 5 MPa for valves, are 995.78 and 0.36 for α and β, respectively.

For operating cost estimation, Eq. 4.14 and the assumptions for the utility cost from Table 4.6 are used. The cost estimation of all the units for case 2 shown in Fig. 4.10 is summarized in Table 4.7. The Total Annualized Cost (TAC) for this case study using the heat-integrated work exchange synthesis design using work exchangers will be $9,666,994. In Table 4.8, the results for the cost-effective design of the heat exchanger network (Fig. 4.10b) combined with a work exchanger network (Fig. 4.10a) that can recover a significant amount of thermal and mechanical energy are summarized and compared with the Onishi *et al.* (2014) and Huang and Karimi (2016) work.

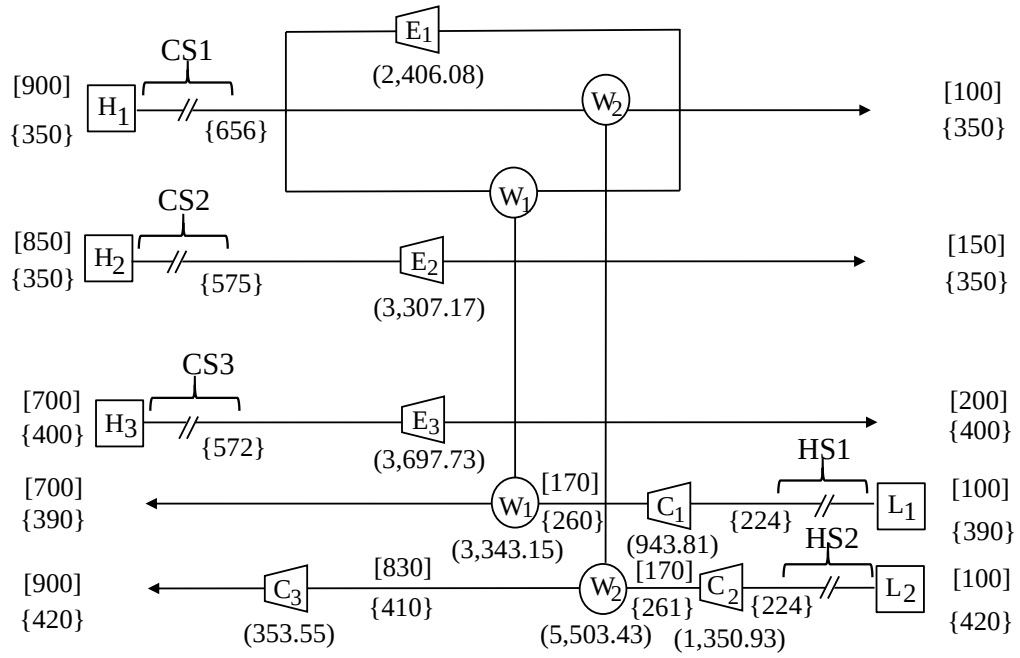

(a)

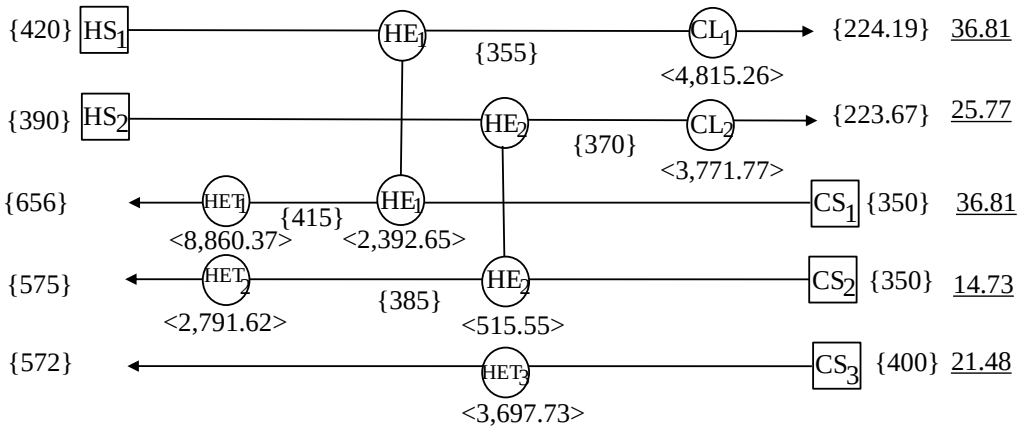

(b)

Legend

[ ] Pressure (kPa) { } Temperature (K) ( ) Work load (kW)

MC_p (kW/K) < > Heat load (kW) E Expander

W Work exchanger C Compressor Heat transfer unit(s) to be placed

HE Heat exchanger CL Cooler HET Heater

Figure 4.10. Flowsheet of heat-integrated work exchange network for Case 2: (a) work exchanger network, and (b) heat exchanger network.

Table 4.7. CAPEX and OPEX of units in Case 2

Equipment	Size Factor	CAPEX ($/year)	OPEX($/year)
HE1	A=9,570 m^2	290,118	-
HE2	A=952 m^2	31,554	-
HET1	A=734 m^2	118,226	2,480,904
HET2	A=182 m^2	76,816	781,654
HET3	A=245 m^2	25,021	1,035,364
CL1	A=3,841 m^2	8,469	38,522
CL2	A=2,461 m^2	10,351	30,174
C1	F= 25.77 kW/k	275,776	906,058
C2	F= 36.81 kW/k	286,810	339,408
C3	F= 36.81 kW/k	286,810	1,296,893
E1	F= 7.87 kW/k	207,871	-
E2	F= 14.73 kW/k	214,730	-
E3	F= 21.48 kW/k	221,480	-
W1	S= 20 L (10 vessels used)	351,993	-
W2	S= 20 L (10 vessels used)	351,993	-
Total		2,758,018	6,908,976

To size the heat exchangers, heaters and cooler, the formulation to compute the area and overall heat transfer coefficient is given by the Huang and Karimi (2016) study and can be found in their publication. Using the formulation presented, the details for the area calculation will be straightforward so they will not be discussed here. The size factor for compressors and expanders is the multiplication of flowrate and heat capacity given for each stream using Table 4.5 and Fig. 4.10a. To size the work exchangers, the volume of each vessel is required. However, to estimate the volume, the cycle time of the energy recovery in the device and volumetric flowrate of the stream flows through the unit are required. Cycle time of work exchangers dealing with gas phases will be addressed in Chapter 5. However, due to several challenges in estimation of cycle time, at this stage, we will make assumptions based on the worst case scenario. In addition, the volumetric flowrate for the streams is not provided and streams components are not available. Therefore, the mass flowrate given cannot be converted to a volumetric flowrate. It is expected that the streams

have a high volumetric flowrate based on the given mass flowrate and considering the low dense gases flowing through. Therefore, we have considered each vessel of the work exchanger with volume of 20 L which is among the largest displacement vessels were found in commercial scale; and assumed 10 vessels in each unit. Therefore, the cost that will be calculated from Eq. 4.72 for a vessel of 20 L will be multiplied by 10.

Table 4.8. Performance comparison of HIWENs by different methods for Case 2

Design	This Work	Onishi *et al.* (2014)	Huang and Karimi (2016)
Mech. energy exchange (kW)	8,847	10,474	11,579
Thermal energy exchange (kW)	2,908	8,794	15,920
Compression utility (kW)	2,648	8,840	7,734
Expansion utility (kW)	9,411	-	-
Heating utility (kW)	15,349	1,680	5,276
Cooling utility (kW)	8,587	10,520	13,010
No. of WEs	2	3 SSTC Compressors+3 SSTC Turbines	3 SSTC Compressors+3 SSTC Turbines
No. of HEs	2	8	6
No. of HET and CL	5	5	9
No. of compressors	3	2	1
No. of expanders/valves	3	1	-
CAPEX (k$/yr)	2,758	-	1,180
OPEX (k$/yr)	6,909	-	9,006
TAC (k$/yr)	9,667	10,502	10,187

In general, our design is less complicated with lower compression, heating, and cooling utility consumption. Note that due to pressure and temperature correlations, the assumptions made regarding the heat integration will impact the total amount of energy high-pressure streams can provide during the depressurization, and low-pressure streams required for pressurization. Therefore, total mechanical energy recovery will not be necessarily the best parameter for comparison at this stage. The capital cost for our design is higher than the Huang and Karimi (2016) superstructure design which can be explained as the result of more compressors and expanders, in addition to the cost of work exchangers which is still in the stage of preliminary

estimation. The total capital cost of SSTC compressors and SSTC turbines in the Huang and Karimi (2016) study is 431,382 $/year but for the work exchangers in our design is 703,986 $/year. As mentioned earlier, the unit sizing and cost estimation for the work exchanger has been performed under several assumptions considering the worst case scenario. Therefore, we are expecting the cost to decrease as more details are available regarding the design of work exchangers. The operating cost in our design is significantly lower than Huang and Karimi (2016) design as a result of lower utility consumption. The total Annualized Cost (TAC) of our design is about 5% lower than that for the Huang and Karimi (2016) superstructure. Even though we have not performed an optimization study for TAC minimization, our final solution is more cost effective than the previous studies. In addition, the solution is much simpler, and easier to conduct. This shows the efficacy of the presented heat integrated work exchange network synthesis methodology.

4.5 Summary

In this chapter, we proposed a heat-integrated work exchanger network synthesis methodology to develop a cost-effective network for mechancial and thermal energy recovery. It is preferred to determine the location of the HEN prior to completion of the final WEN network. However, in some studies, the HEN has been always located before the WEN design when low-pressure streams are considered as hot and high-pressure streams as cold streams. The goal is to increase the amount of energy provided by expansion and decrease the amount of energy required for compression. We believe that to be able to have a general methodology for heat and work exchanger network synthesis, the location of heat integration should be announced based on the option with the least operating cost which represents the design with lowest energy-intensive

utility. As shown in case studies, using the presented methodology we are able to derive less complicated designs with better performance in terms of utility consumption and operating cost.

Capital cost estimation was conducted for the first time in a design in which direct work exchangers are integrated. The cost estimation for the work exchanger can be considered as an early investigation in the economic analysis of the direct type of mechanical energy recovery devices known as work exchangers. However, it still requires further studies while the device is being modified to be used in chemical processes dealing with gas phase streams.

The heat-integrated work exchange network synthesis methodology can be also developed in the future for the design of more realistic flowsheets in terms of assumptions made through the flowsheet construction, temperatures computed using the heat-integration technique before or after the WEN, unit operation size and capacity, and the possibile phase change through the compression/expansion. Development of a framework for a simultaneous recovery of thermal and mechancial energy without initial assumptions of one network before or after the other, can be defined as a future study.

CHAPTER 5 MODELING AND SIMULATION OF A PISTON-TYPE WORK EXCHANGER FOR MECHANICAL ENERGY RECOVERY

The significance of energy efficiency improvement in chemical processes has led to increasing research opportunities for innovative process integration technologies. Recovery of mechanical energy through work exchanger network synthesis is a type of process integration that has been recently drawn a lot of attention. Direct (one-step) Work Exchangers (WEs) can be considered as a type of process unit for mechanical energy recovery in chemical plants. The type of device was first introduced for reverse osmosis (Cheng *et al.*, 1967; Cheng and Cheng, 1970). Dual Work Exchange Energy Recovery Device (DWEER) is a piston-type WE that has been widely used for seawater reverse osmosis (RO) desalination, which is one of the most efficient energy recovery systems developed to date. However, this type of unit cannot be directly used for the pressurization/depressurization of process streams in the gas phase in chemical plants.

5.1 Objectives and Significance

The work exchanger dealing with gas phase streams will have a different behavior. The safety issues regarding leakage and mixing losses will increase when dealing with gas streams. These will also impact the efficiency of the system, the maintenance cost, and the operating cost. DWEERs are always running with the same materials (i.e., brine and seawater) which are non-hazardous and non-flammable. On the other hand, the work exchangers for mechanical energy recovery through WEN will be operated using different types of materials and under various operating conditions such as temperature, pressure, and physical properties. Therefore, deep investigation through work exchanger component parts, future unit modification to ensure the safety, a possible improvement on unit efficiency, and compatiblity of the unit with different types of material would be required.

To show the feasibility of using a direct work exchanger as a device for mechanical energy recovery, we need to have better insight on the device performance. Computational modeling and simulation of the device could be the first stage prior to manufacturing of the unit in the pilot and industrial scales. To start the modeling of the work exchangers, the first step is to collect sufficient information about the device. A detailed description has been provided by Cheng and Fan (1968) regarding the size, structure, and work exchanger operation. In Chapter 2, the description of pressurization and depressurization steps provided by Cheng *et al*. (1967) has been discussed.

Based on the description provided for the desalination application, the device contains two displacement vessels, check valves, control valves, and three additional pumps. The pumps will be used for maintaining the inlet pressure of the low-pressure stream higher than the outlet pressure of the high-pressure stream, maintaining the inlet pressure of the high-pressure stream higher than the outlet pressure of the low-pressure stream, and pressurizing the excess part of the feed. To manufacture the unit, commercially available component parts were used with some modifications. Figure 5.1 shows a schematic of one piston-type work exchanger provided by Cheng and Fan (1968).

The unit contains two 2 gallon floating piston-type accumulators as the two displacement vessels (O_1 and O_2), four hydraulic check valves (v_1, v_2, v_3, and v_4), and two 2-way control valves or one 4-way hydraulic valve as the valves for v_5, v_6, v_7, and v_8. The details for other component parts such as pumps, flowmeters, the programming timer, and pipe fittings have not been discussed here since they will not impact the simulation and modeling setup at this stage. However, those parts should be studied at the time of manufacturing of the unit for gas phase streams.

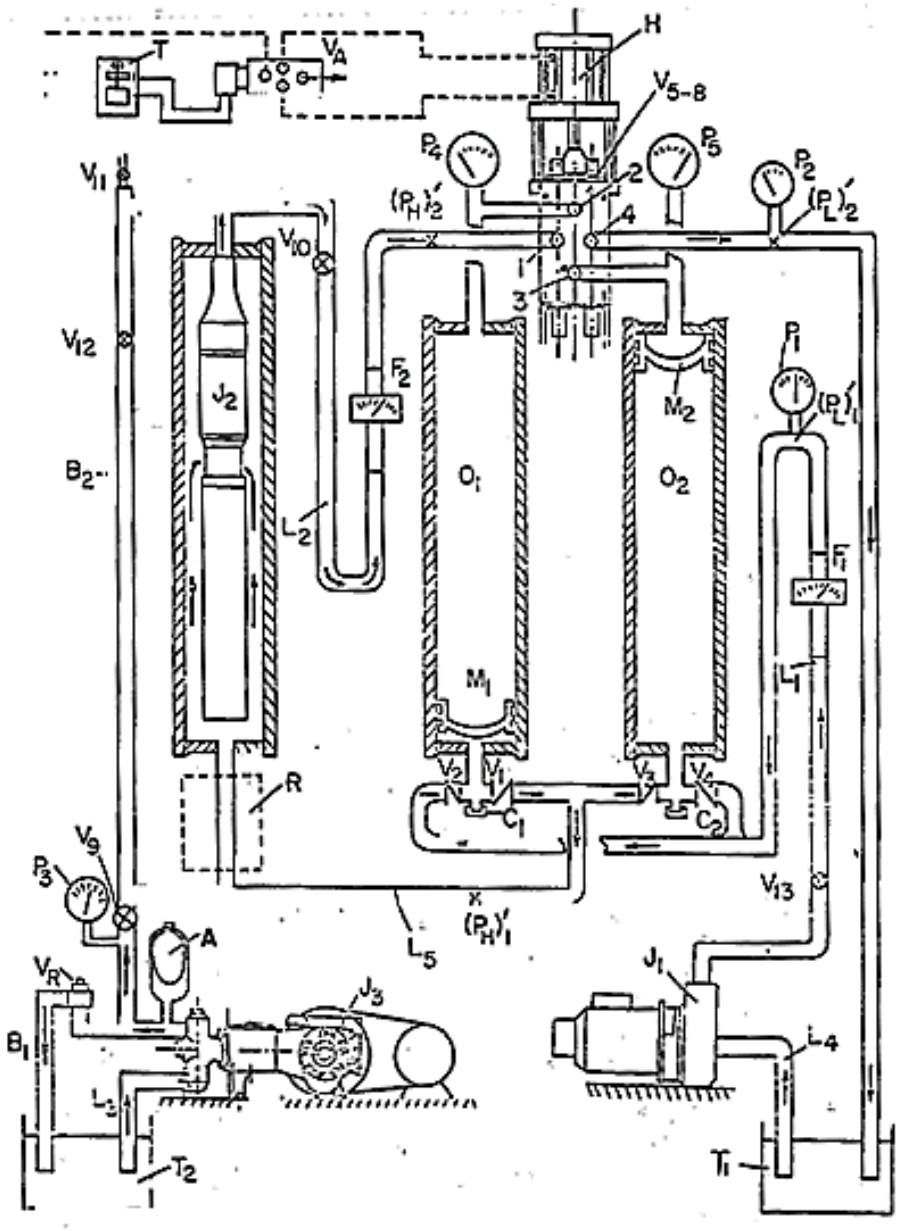

Figure 5.1. Schematic illustration of a piston-type work exchanger (Cheng and Fan, 1968).

The component parts were connected by 3/4", schedule-160 steel pipes in assembling the unit. The unit was operable up to 102 atm (1,500 psig) and delivered 2.45 m^3/hr (9 gpm). Water was used as the working fluid, and the cycle time for 2.45 m^3/hr (9 gpm) capacity was adjusted to 20 seconds. The maximum displacement of the piston per stroke was 6.81 L (1.8 gallons) but at each half cycle, 5.6 L (1.5 gallons) entered the vessel. To solve the problem of non-steady flow

because of the valve shifting, they installed an accumulator. It was mentioned that each of the flowrates multiplied by half of the time cycle time should not exceed the volume filled by the piston in a stroke, and the inlet rate for each side should be adjusted to the same value. Also, it was discussed that the capacity of the unit can be increased to 5.45 m3/hr (20 gpm) by changing pipe fittings, valves, and pipe size to 1".

Dual Work Exchanger Energy Recovery (DWEER) which is being manufactured at the industrial scale by Flowserve consists of two pressure vessels, four check valves, and one patented LinX control valve. The single unit can process up to 75 bar and 350 m^3/hr or 1.4 mgd and to achieve higher volume, the manufacturer suggested placing multiple units in parallel. This device is being used in Reverse Osmosis (RO) plants around the world such as in Spain, Australia, Dubai, and Singapore. Recovering up to 98% of the energy in the brine stream, operational flexibility, robust design, high availability, low maintenance costs, and low mixing and leakage rates have been mentioned as some of the main features (Flowserve, 2018).

In the following, the piston-type work exchanger has been simulated using customizing operation models in Aspen Plus and computational fluid dynamic modeling with Ansys Fluent. The main objective is to analyze the performance of the unit which is being used in desalination processes when dealing with the gas phase and different type of materials.

5.2 Modeling and Simulation of Work Exchanger Systems Using Aspen Plus

Simulation of unit operation is a tool to evaluate the process configuration and help to understand the parameters which impact the process specifications. The piston-type work exchanger is a new unit operation which can be used in process systems for mechanical energy recovery and is not available as a built-in unit operation similar to heat exchangers in any process

simulation software. However, Aspen Plus as one of the promising process simulators in the chemical industry allows users to add customized modules using Aspen Custom Modeler.

Aspen Custom Modeler in combination with Microsoft Excel and Visual Basic can be used to simulate a unit operation and include the customized unit into the Aspen Plus model library. This will enable users to model the particular unit operation, build the model library and export it into Aspen Plus for the process simulation. In the following, the simulation procedure is discussed.

5.2.1 Construction of work exchanger module with Aspen Plus

In a piston-type work exchanger, the high-pressure and low-pressure streams will be each on one side of the piston without having any contact. Due to opening and closing of the valves and movement of the piston, the pressure of each stream will change. The temperature may also differ under non-isothermal conditions. The module includes two inlet feeds and two outlet streams, one of each for the high-pressure stream and the low-pressure stream.

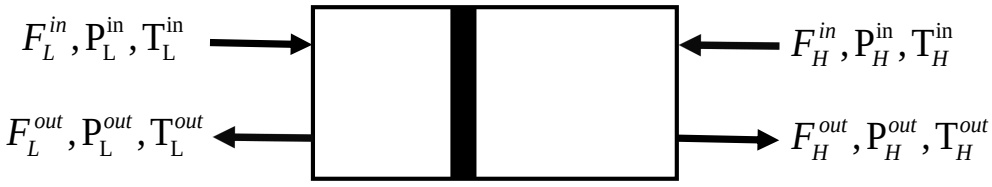

Figure 5.2. Schematic representation of a work exchanger module.

Figure 5.2 which shows the work exchanger module is a general representation of the unit which means that multiple vessels and valves for inlet and outlet streams will be included in the presented module. However, similar to other unit operations in Aspen Plus, the model formulation impacts how the outlet stream specification will be calculated using the given inlet stream information and additional parameters. In the work exchanger module, the high-pressure stream will be depressurized (expanded) and the low-pressure stream will be pressurized (compressed). Therefore, the following equations will be used in the simulation model for the unit operated with streams assumed to behave as ideal gas.

There will not be any reaction, and mixing or leakage through the process. Then, Eqs. 5.1-5.4 represent the model mass balance. The mass balance for the compartment containing the high-pressure stream will be as follows:

$$F_H^{in} = F_H^{out}, \tag{5.1}$$

and

$$F_H^{in} C_H^{in} = F_H^{out} C_H^{out}. \tag{5.2}$$

For the compartment containing the low-pressure stream:

$$F_L^{in} = F_L^{out}, \tag{5.3}$$

and

$$F_L^{in} C_L^{in} = F_L^{out} C_L^{out}. \tag{5.4}$$

where F represents the mass flowrate and C composition.

Based on the system degree of freedom, the outlet pressure of the high-pressure or low-pressure stream should be given. Therefore, the outlet pressure of the high-pressure stream will be defined through one of the three conditions shown in Eq. 5.5.

$$P_H^{out} = \begin{cases} P_H^{out}; & \text{User identified } P_H^{out} \\ \dfrac{P_H^{in}}{\exp\left(\dfrac{W}{n_H^{in} RT}\right)}; & \text{User identified } P_L^{out} \left(\text{Isothermal Condition}\right) \\ P_H^{in} \times \left(1 - \dfrac{W}{F_H^{in} C_p T_H^{in}}\right)^{\frac{m}{m-1}}; & \text{User identified } P_L^{out} \left(\text{Adiabatic Condition}\right) \end{cases}. \tag{5.5}$$

In a similar way, the outlet pressure of the low-pressure stream will be defined using Eq. 5.6.

$$P_L^{out} = \begin{cases} P_L^{out}; & \text{User identified } P_L^{out} \\ P_L^{in} \times e^{\left(\frac{W}{n_L^{in} RT}\right)}; & \text{User identified } P_H^{out} \left(\text{Isothermal Condition}\right). \\ P_L^{in} \times \left(\frac{W}{F_L^{in} C_p T_L^{in}} + 1\right)^{\frac{m}{m-1}}; & \text{User identified } P_H^{out} \left(\text{Adiabatic Condition}\right) \end{cases} \quad (5.6)$$

where W represents the mechanical energy exchanged between the high-pressure and low-pressure streams through the process. Table 2.1 can be used as the formula directory. n represents the molar rate. C_p is the heat capacity, R is the gas constant, and m is the adiabatic (polytropic) exponent. The outlet temperature for either the high-pressure or low-pressure stream will be calculated using Eq. 5.7.

$$T^{out} = \begin{cases} T^{in}; & \text{Isothermal Condition} \\ T^{in} \left(\frac{P^{out}}{P^{in}}\right)^{\left(\frac{m-1}{m}\right)}; & \text{Adiabatic Condition} \end{cases}. \quad (5.7)$$

5.2.2 Simulation Procedures

According to the modeling described in the previous section, the simulation has been completed. As mentioned earlier, in Aspen Plus users can create customized modules by modifying the available FORTRAN interface subroutine and the Excel model (Aspen Technology Inc., 2013). The simulation steps have been summarized in the following.

Setting up the model in Aspen Plus. After creating an Aspen Plus blank simulation, from User models, User2 icon PLUG will be selected as the model with two inlets and two outlet streams.

Setting up the Excel model. An Excel template available in the Aspen Plus user library will be customized based on our unit operation model. The Excel file contains several sheets for modifying the model integer and real parameters, input information and required formula for calculation of the model output streams. The gas constant and mechanical energy exchanged between high-pressure and low-pressure streams (W) will be considered as the real parameter. There will not be any integer parameter for this model. To solve the model, additional inputs are required according to the degree of freedom of the system. For this model, one of the outlet pressures is the additional information that needs to be provided by the user. Using the outlet pressure, W will be calculated by the system as discussed in section 5.2.1. The screenshots of the Excel model are highlighted in Fig. 5.3.

Revising the user subroutine. The unit operation model subroutine should be customized to pass the input data such as feed streams from the Aspen Plus to Excel and pass the calculated output data from the Excel to Aspen Plus. Similar to the Excel model, a template code for the User 2 model is available in the Aspen Plus library to be modified for our model. The User 2 user subroutine which has been analyzed and shown in *Aspen Plus User Models* and *Getting Started Customizing Unit Operation Models* (2012, 2013) will not be discussed in detail here as the changes are minor. Appendix C contains the customized User 2 unit operation model subroutine for Excel models from Aspen Plus *Getting Started Customizing Unit Operation Models* (2013) for the work exchanger model.

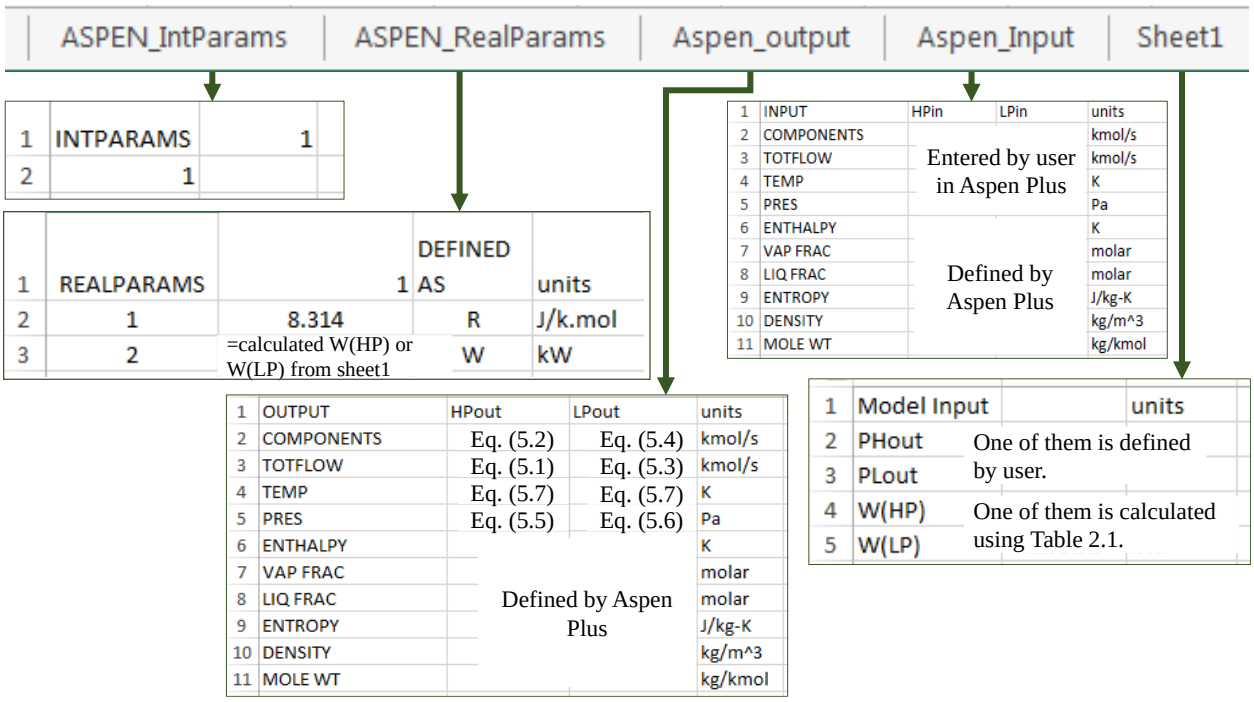

Figure 5.3. Summary of the Excel model set up.

The next steps include compiling and linking the subroutine to Aspen Plus, creating a shared library for the model, customizing the Aspen Plus model library, and editing the custom model schematic based on the work exchanger (Aspen Technology Inc., 2013). These steps will be similar for all models so we will not discuss them here.

5.2.3 Simulation Results

The simulation has been run using Aspen Plus V8.4, Visual Studio 2015, and Microsoft Excel 2013 in a computer operating with Microsoft Windows 7. At this stage, as long as the work exchanger model library is available in the Aspen Plus working folder, we will be able to add the work exchanger unit from the unit operations palette.

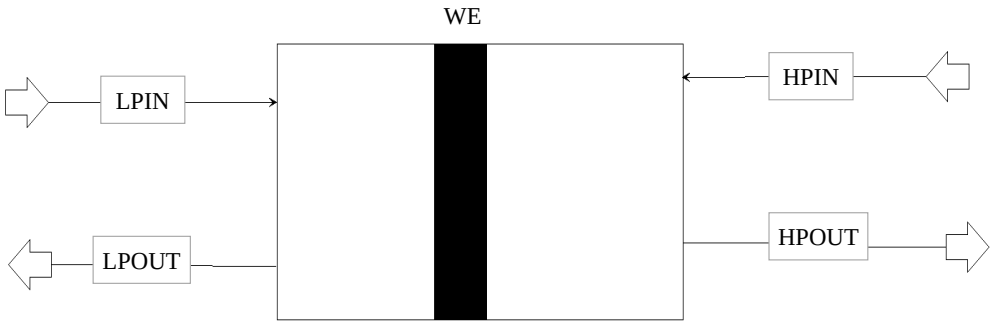

Figure 5.4. Work exchanger unit in the Aspen Plus environment.

Case 1. For a case study of a high-pressure stream that enters the work exchanger at 2,000 kPa and 525 k with a molar flowrate of 23.19 mol/s with ammonia as the only component, and a low-pressure stream that enters the unit at 220 kPa and 330 k with a molar flowrate of 82.54 mol/s and ammonia as the component, the objective is to depressurize the high-pressure stream to 150 kPa. The case study is under the isothermal condition, with the ideal gas assumption and considering 100% efficiency of the unit. The property method is Peng-Robinson. Figure 5.5 shows the inlet information for the streams and the specified outlet for the high-pressure stream in Aspen Plus.

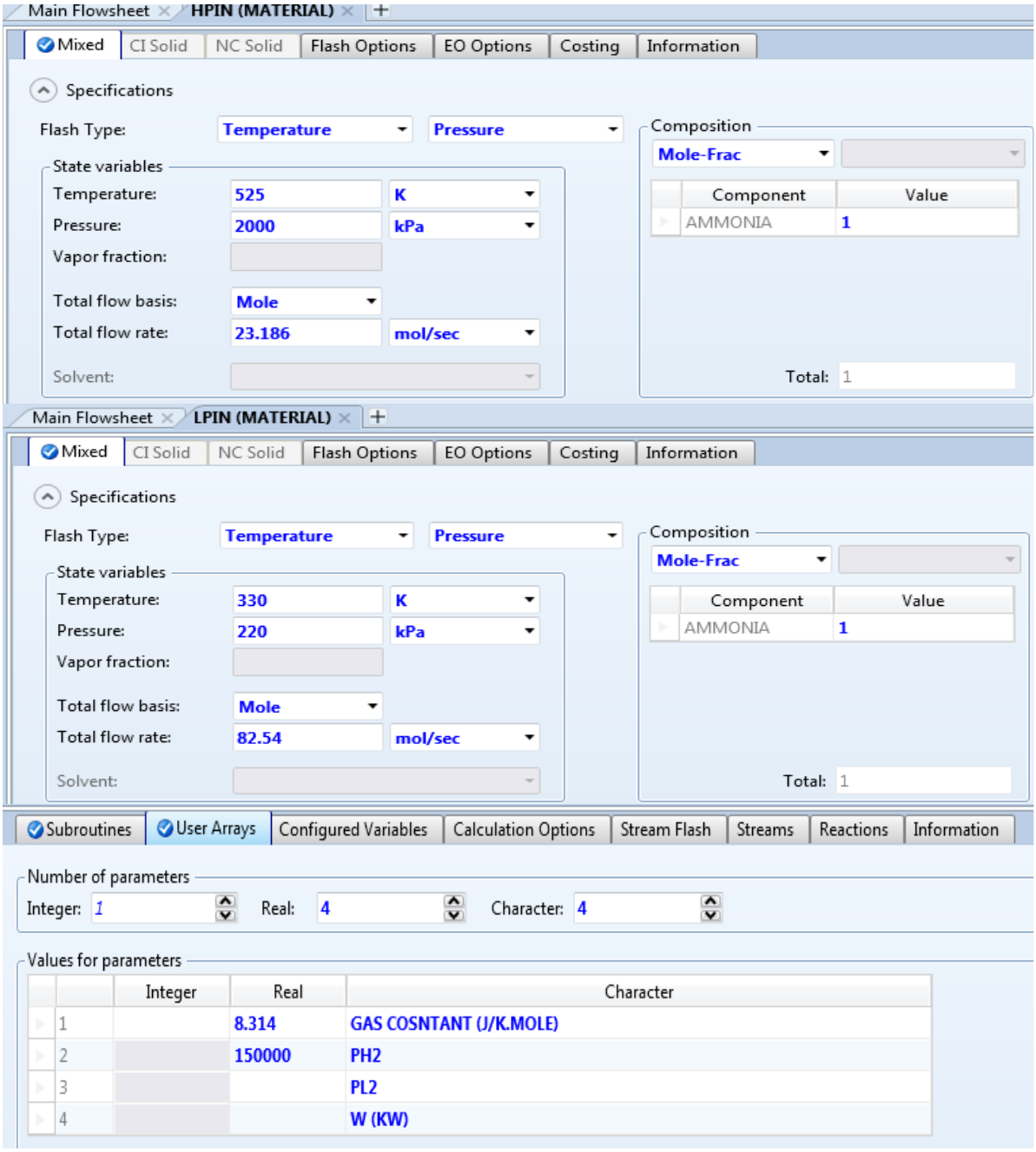

Figure 5.5. Inlet data required to run the simulation.

The simulation will be run and the outlet stream specification will be calculated by passing the inlet data from Aspen Plus to Excel for calculation through the FORTRAN user subroutine and the results will be passed back to Aspen Plus. Figure 5.6 shows the outlet stream's data and the amount of work that will be exchanged through the work exchanger.

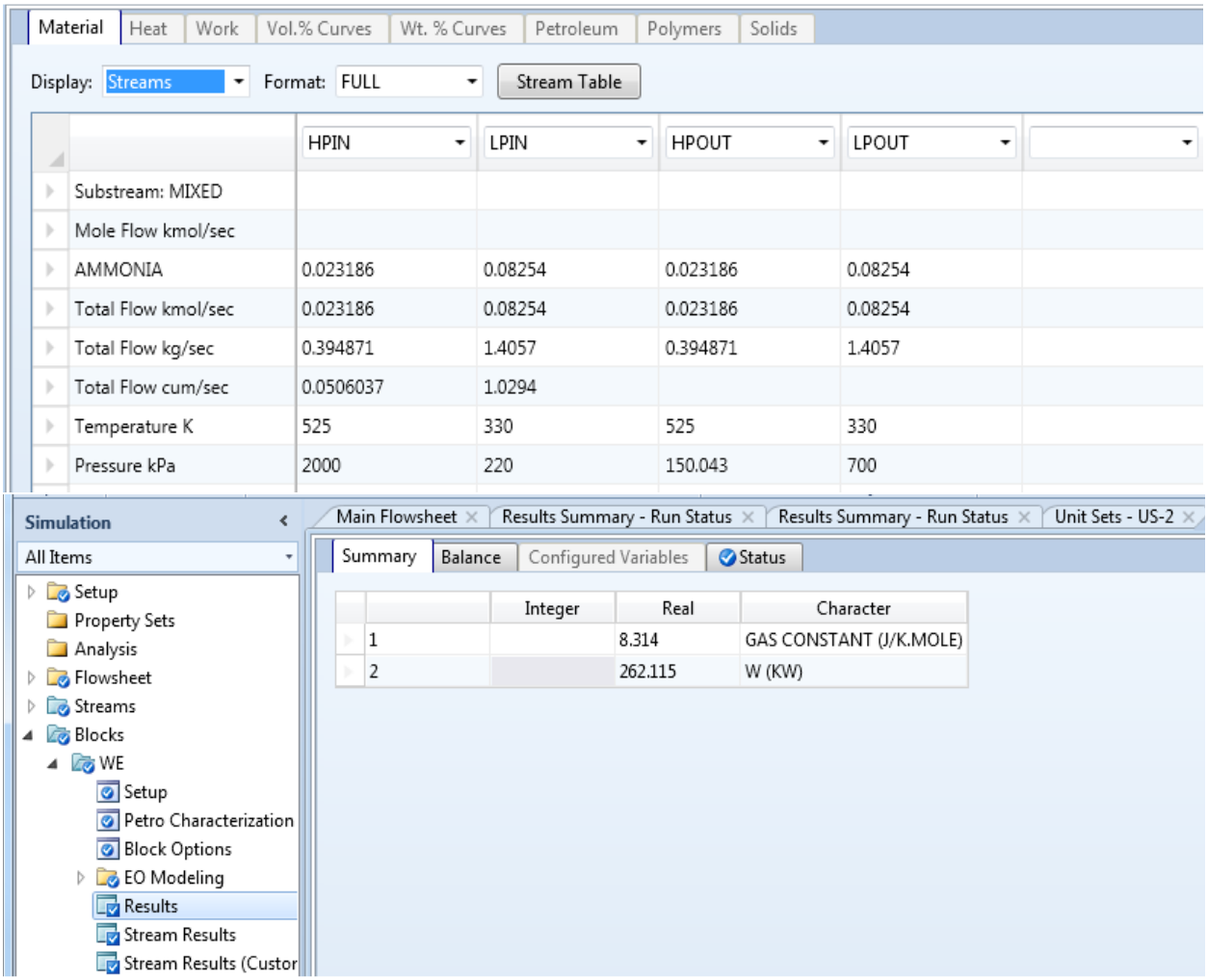

Figure 5.6. Final streams and unit capacity results for Case 1.

Case 2. To show the feasibility of simulating the customized work exchanger model with other unit operations, we have simulated the case study 1 from Chapter 3 (Liu *et al*., 2014). The same assumptions have been made through the simulation except there will be temperature change for the streams passing through the external compressors and expanders since these unit operations can be only simulated in Aspen Plus under non-isothermal conditions. Figure 5.7 represents the work exchange network designed in Chapter 3 (Figure 3.3a). We refer to section 3.2.2 for details on network design derivation.

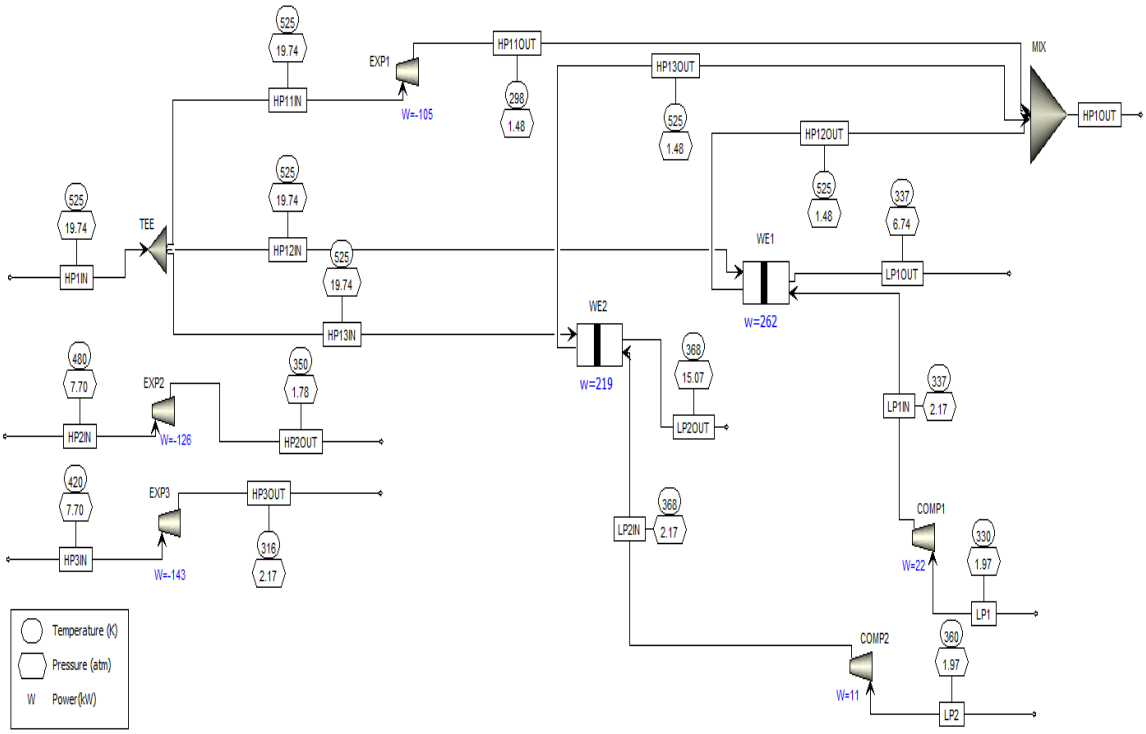

Figure 5.7. Simulated work exchanger network in Aspen Plus for Case 2.

The simulation of the work exchanger through Aspen Plus has been completed successfully. However, the simulation is under the steady-state condition and most importantly, will not reflect the dynamic performance of valves and piston. This motivated us to continue our investigation in the following section.

5.3 CFD-based Modeling and Simulation of Piston-type Direct Work Exchanger

Computational Fluid Dynamics (CFD) modeling of units helps to have a better understanding of the device performance. In this section, we present our investigation of the feasibility and design of a piston-type WE that works for processing gas-phase streams. Our main approach is to use a Computational Fluid Dynamics (CFD) technique to construct a WE model.

5.3.1 Challenges and Opportunities

There has not been any study to model or simulate the piston-type work exchanger. However, there are a lot of studies on modeling of units where their performance can inspire the modeling of the piston-type work exchanger. Conventional internal combustion (IC) engines have been studied and optimized through experiment and CFD modeling for years. Piston-type work exchangers can be compared with IC engines in terms of the cylinder chamber which contains a piston, and opening and closing of the valves through each stroke. However, in conventional IC engines, the piston movement will be controlled by the crank mechanism and the valves opening and closing will be controlled and modeled based on the crank angle (Heywood, 1988, Reitz and Rutland, 1995, ANSYS Inc., 2017). Free piston engines are another type of engine which has been investigated as an alternative to conventional engines. In a free piston engine, the piston motion will not be restricted by the position of rotating the crankshaft and will be defined by the interaction of gas and load forces. Variable stroke length, active control of piston positon, reduction in friction loss, and the compression ratio impact are some of the main device characteristics. Based on the structure of the piston cylinders and load forces, these engines are divided into four categories; as an example, a schematic of dual free piston engine is shown in Fig. 5.8 (Mikalsen and Roskilly, 2007).

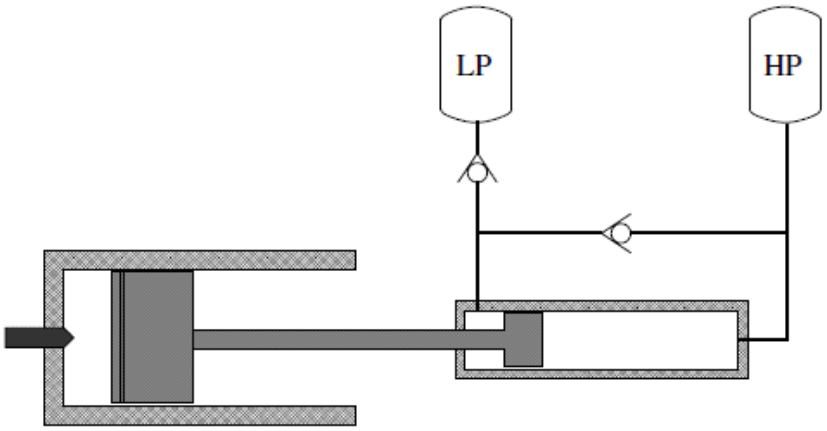

Figure 5.8. Single piston hydraulic free-piston engine (Mikalsen and Roskilly, 2009).

Mikalsen and Roskilly (2009) presented a novel approach for modeling of a spark ignited free-piston engine and introduced a solution-dependent mesh motion using the open source CFD software OpenFoam. Some operation variables such as piston position, ignition timing, compression ratio, fuel efficiency, and also the combustion process were studied (Mikalsen and Roskilly, 2008, Mikalsen and Roskilly, 2009). Mao *et al.* (2011) worked on CFD modeling of the scavenging process of a free-piston linear alternator using a time-based numerical simulation program built with Matlab and the dynamic mesh tool AVL_FIRE. They used different operating options to find the best combination for high scavenging.

Rotary energy recovery device or rotary pressure exchanger which is another type of energy recovery device used in seawater reverse osmosis has been modeled using CFD. In this device which contains a rotor, several circular ducts, a sleeve, and two end covers, the energy will be exchanged between high-pressure and low-pressure streams by the rotation of the rotor. Yihui *et al.* (2011) developed a 3D model to study the mixing rate and its relation to parameters such as rotor speed and inlet flow velocity, and leakage with pressure and clearance volume. In two other studies, Xu *et al.* (2016) optimized the rotor speed and improved the frictional state of the rotor through CFD modeling and validated the results of the experiment. Lack of studies on CFD

modeling of the piston-type work exchangers dealing with a liquid phase as the working fluid can be defined as a result of simple design and satisfactory performance of the device in desalination processes; thus, any investigation into different parameters which impact its performance would not sound necessary. However, proposing this device to be used in different chemical processes and dealing with gas phase stream, makes the design more complicated.

Our main objective is to investigate the feasibility of using a piston-type work exchanger for different types of chemical processes, therefore, there could be situations where there will be a gas phase stream as the working fluid on both sides of the piston, or a gas phase on one side and liquid phase stream on the other. The possibility of the working fluid phase change as a result of pressure and temperature change during the pressurization or depressurization should be considered as well. Dealing with different types of materials with various compositions that could be flammable is another issue that needs to be addressed. Challenges regarding the displacement nature of the unit, accurate control of piston motion, the existence of fluid leakage paths, the possibility of mixing of fluids, and the coexistence of working fluid and lubricant are some other main obstacles that should be dealt with. Dividing the displacement vessel into two piston cylinders similar to the free-piston engine structure could be one solution to fix the problem of mixing and leakage. However, this makes the structure of the WE unit different and it may impact the working procedures. Also, the control of piston motion will be still an issue as for free-piston engines. Design of devices which only deal with gas or liquid phase streams, preventing flammable components from being pressurized or depressurized through WE, and characterizing the WE device for only a specific operating condition can be also considered as some alternative solutions. However, these will limit the application of the device in chemical processes and may not be beneficial.

From the simulation point of view, we will also deal with some challenges. How to design the opening and closing of the valves, especially the control valves as described in Fig. 5.1, how to model the piston movement and most importantly how to model the piston moving back and forth, and identifying two different working fluids on each side of the piston are some examples. In the following, our preliminary investigations into CFD modeling of a piston-type WE including one displacement vessel are discussed.

5.3.2 Piston-Type Work Exchanger Configuration

Cheng *et al.* (1967) presented the design for a piston-type work exchanger for energy recovery in desalination processes. The design includes two displacement vessels, four check valves, and two control valves. In our simulation, we have focused on the performance of one displacement vessel with the goal of investigating the movement of the piston, valve positions and full cycle time for pressurization and depressurization steps. The design includes an approximately 3 Liter (one gallon) piston cylinder for which the piston is 10% of the total volume of the cylinder. To be able to appropriately model the valves using CFD software and to avoid a complicated model, we have assumed that all the valves through which high-pressure and low-pressure streams flow in and out, are check valves. Therefore, there will be four check valves (v_1, v_2, v_3, and v_4) which will be moved to the open or closed position due to the pressure difference between two sides of the valve.

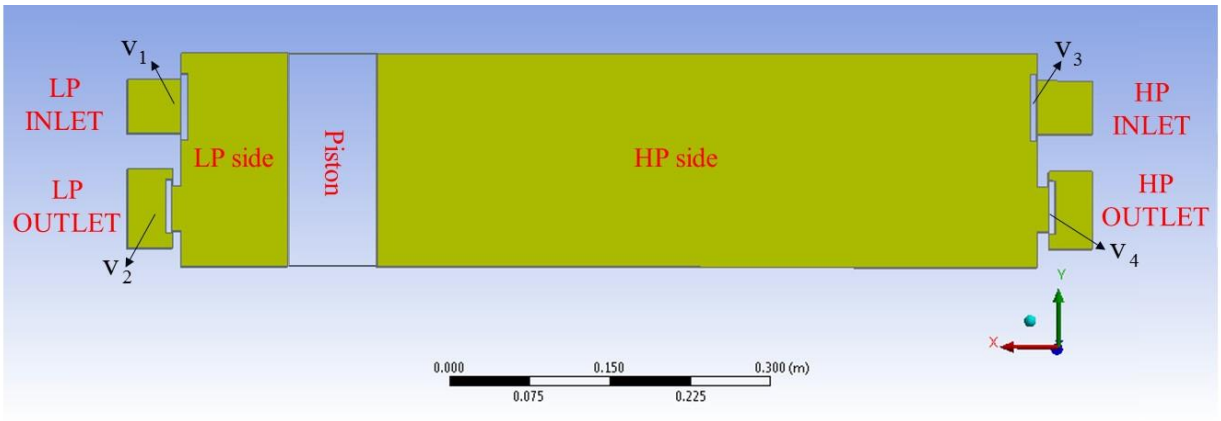

Figure 5.9. Piston-type work exchanger geometry model.

While the piston is at the left side of the cylinder and the HP side is filled with high-pressure stream at P_H^s, the HP outlet valve (v_4) will be opened and the high-pressure stream will flow out of the cylinder, and this will cause the pressure on the HP side to decrease. When the pressure of the HP side reaches a pressure lower than the inlet pressure of the low-pressure stream, the low-pressure stream will flow through valve v_1 into the LP side of the cylinder and due to the pressure difference between two sides of the piston, the piston moves from left to right. Similar to top and bottom dead centers in engines, the piston will not completely move to the end of the cylinder at each stroke and there will be 0.1 m distance between the piston position and the end of the cylinder. During the next stroke, while the LP side is filled with the low-pressure stream at P_L^s, the HP inlet valve (v_3) will be opened and high-pressure stream will flow into the HP side of the cylinder, and again the piston will start moving due to pressure difference between the two sides of the piston which will cause the low-pressure stream to be pressurized. The compressed low-pressure stream will flow out through valve v_2.

5.3.3 Modeling Piston Dynamics

Piston motion is one of the main challenges in the CFD modeling stage. In Fig. 5.10, the balance of forces on the piston is shown. The piston moves because of the pressure difference

between the high-pressure and low-pressure streams on the two sides and will stop while it reaches the equilibrium. However, to design the cylinder, the clearance volume should be also considered. This means that the piston can be only displaced to a certain location of the cylinder.

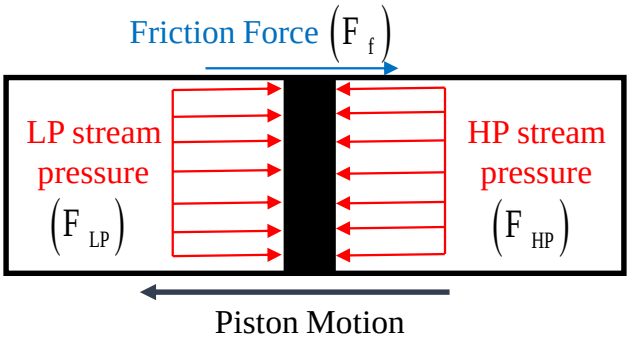

Figure 5.10. The balance of forces on the piston.

For a piston with given mass (m_p), based on Newton's second law, we will have:

$$m_p \cdot \frac{d}{dt} v = F_p - F_f \tag{5.7}$$

where v is the velocity of the piston motion, and t is the time interval. F_p is a force that results from the fluid pressure difference on two sides of the piston as shown in Eq. 5.8.

$$F_p = p \cdot A \tag{5.8}$$

where p results from the aerodynamic force due to gas pressure including high-pressure and low-pressure working fluids on the surface of the piston (A). According to Lyubarskyy and Bartel (2016), the friction force can be formulated similarly to the friction force between the piston ring and cylinder in a diesel engine.

$$F_f = F_{f_h} + F_{f_c} \tag{5.9}$$

where F_{f_h} consists of the hydrodynamic friction force calculated from the shear stress ($F_{f_h} = \tau_w \cdot A$), and F_{f_c} is the boundary friction force on the solid body contacts which is the result of asperity average contact pressure ($\bar{p}_c$) on the contact surface (A_c) and is equal to $F_{f_c} = f_c \cdot \bar{p}_c \cdot A_c$. f_c is the boundary friction coefficient. As the final step, the velocity over time can be written as Eq. 5.10:

$$\frac{dv}{dt} = \frac{v_{new} - v_{old}}{t_{step}} \tag{5.10}$$

Then,

$$v_{new} = \frac{d_{p_{new}} - d_{p_{old}}}{t_{step}} \tag{5.11}$$

where d_p is the position of the piston at each step. This allows us to estimate the location of the piston after each time interval as shown in Eq. 5.12.

$$d_{p_{new}} = \frac{F_P + F_f}{m_p} \times \left(t_{step}\right)^2 + v_{old} \times t_{step} + d_{p_{old}} \tag{5.12}$$

5.3.4 Simulation System Setup

The simulation is performed using the commercial CFD software Fluent 18.2. The geometry is generated by preprocessor ANSYS Workbench Design Modeler 18.2. The cylinder volume is 3.2 L for which the piston comprises 10% of the total volume. The model geometry is shown in Fig. 5.9. A fine hexahedral mesh is generated with 1,822 total elements in the preprocessor ANSYS Workbench Meshing 18.2. A transient pressure-based solver is chosen to solve the governing equations. Gravitational acceleration has not been considered in the simulation. The PISO pressure-velocity coupling algorithm, PRESTO! pressure, second order upwind momentum discretization scheme for momentum and energy, and first order upwind

discretization scheme for turbulent kinetic energy and dissipation rate are chosen in the modeling (Ansys Inc. Fluent User's Guide, 2017). The basic model equations can be written as follows. The continuity equation for incompressible fluid is formulated as:

$$\frac{\partial \rho}{\partial t} + \nabla.\left(\rho \vec{v}\right) = 0 \tag{5.13}$$

where $\vec{v}$ is the velocity vector and ρ is the density.

The momentum equation is described as:

$$\frac{\partial}{\partial t}\left(\rho \vec{v}\right) + \nabla.\left(\rho \vec{v}\vec{v}\right) = -\nabla p + \nabla.\left(\bar{\bar{\tau}}\right) \tag{5.14}$$

where p is the static pressure, and $\bar{\bar{\tau}}$ is the stress tensor which can be expressed as:

$$\bar{\bar{\tau}} = \mu\left[\nabla \vec{v} + \nabla \vec{v}^{\mathrm{T}}\right] \tag{5.15}$$

where μ is the molecular viscosity. The flow calculation is modeled using the standard k-ε turbulence model. This model is common for industrial flow simulation due to its accuracy and robustness. The transport equations for the turbulence kinetic energy (κ), and the rate of dissipation (ε) are formulated in Eqs. 5.16 and 5.17.

$$\frac{\partial}{\partial t}\left(\rho\kappa\right) + \frac{\partial}{\partial x_i}\left(\rho\kappa u_i\right) = \frac{\partial}{\partial x_i}\left[\left(\mu + \frac{\mu_t}{\sigma_\kappa}\right)\frac{\partial \kappa}{\partial x_i}\right] + G_\kappa - \rho\varepsilon - Y_M \tag{5.16}$$

where u_i is the time mean velocity, G_κ is the generation of turbulence kinetic energy due to the mean velocity gradients, and Y_M is the contribution of the fluctuating dilatation in compressible turbulence to the overall dissipation rate and should be taken into consideration when the ideal gas law is considered. σ_κ is the model constant and has the default value of $\sigma_\kappa = 1.0$ (Ansys Inc. Fluent Theory Guide, 2017).

$$\frac{\partial}{\partial t}(\rho\varepsilon)+\frac{\partial}{\partial x_i}(\rho\varepsilon u_i)=\frac{\partial}{\partial x_i}\left[\left(\mu+\frac{\mu_t}{\sigma_\varepsilon}\right)\frac{\partial\varepsilon}{\partial x_i}\right]+C_{1\varepsilon}\frac{\varepsilon}{\kappa}(G_\kappa)-C_{2\varepsilon}\rho\frac{\varepsilon^2}{\kappa} \tag{5.17}$$

where σ_ε, $C_{1\varepsilon}$, and $C_{2\varepsilon}$ are also model constants with default values of $\sigma_\varepsilon=1.3$, $C_{1\varepsilon}=1.44$, and $C_{2\varepsilon}=1.92$ (Ansys Inc. Fluent Theory Guide, 2017). The μ_t from Eqs. 5.16 and 5.17 is the turbulent viscosity which can be calculated as:

$$\mu_t=\rho C_\mu\frac{\kappa^2}{\varepsilon} \tag{5.18}$$

where constant C_μ is equal to 0.09.

The boundary conditions are all pressure-based for both high-pressure and low-pressure inlets and outlets. Air in the ideal gas condition has been used as the working fluid of the HP and LP sides. To model the valve and piston motion, dynamic mesh has been enabled with smoothing mesh methods. The valves and piston are defined as rigid bodies and modeled with the 6DOF solver. This solver uses external forces and moments such as aerodynamic and gravitational forces and moments on the rigid body objects to calculate the angular or translational motion of the center of gravity of the object. In this modeling, the normal force due to the pressure of the working fluid (gas) on the rigid body is the aerodynamic force and will cause translational motion of the objects including the valves and piston. In piston-type work exchanger, the piston only moves along one axis; thus, its motion is formulated using one DOF translation in the *x* axis based on the model geometry. The governing equation for piston translation motion has been discussed in section 5.3.3 through Eqs. 5.7- 5.12. However, for the initial modeling the effect of friction force is disregarded and only the aerodynamic force due to gas pressure including the high-pressure and low-pressure working fluids on the surface of the piston (A) will define the motion of the piston.

The position of the piston will be also restricted by assigning constraints on the piston position. Therefore, the piston will be stopped at 0.1 m distance to the right/left end of the piston.

At this stage of the modeling, we have assumed that there will be no energy loss through the energy exchanger (work exchange) between the high-pressure and low-pressure fluids. This means that while the fluid on one side of the piston pushes the piston and does work on it, the same amount of work will be done on the fluid on the other side by the piston. According to this assumption and considering the adiabatic condition for expansion and compression, we can write the following equation to present the pressure and volume relationship.

$$PV^{m} = \text{constant} \tag{5.19}$$

where m is the adiabatic ratio. Therefore, the work done by the fluid on the piston or the work the piston does on the fluid, will be calculated as follows:

$$\begin{aligned} W &= F \cdot l \\ &= P \cdot A \cdot l = \int_{V_1}^{V_2} P dV \end{aligned} \tag{5.20}$$

where F represents the force on the piston, P is the pressure of the fluid, A is the cross sectional area of the piston, and l defines the distance the piston moves inside the cylinder. Therefore, $A \cdot l$ will be equal to the swept volume of the piston. Using Eq. 5.19, the integration derived in Eq. 5.20 can be calculated considering the initial condition and final volume.

The motion for the check valves will be computed using the one DOF translation in the *x* axis while Hooke's Law with a spring constant of 2700 N/m will apply force to the valve's center of gravity. Figure 5.11 shows a schematic of an inlet check valve with one DOF translation taken from the Ansys Fluent Theory Guide (2017).

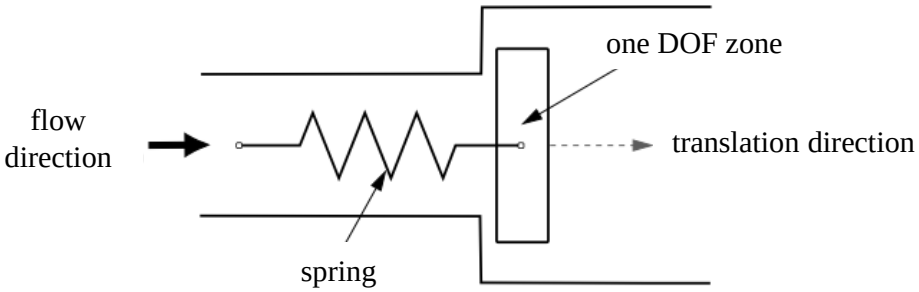

Figure 5.11. An inlet check valve with one DOF translation (Ansys Inc. Fluent Theory Guide, 2017).

5.3.5 Analysis of Direct Piston-type Work Exchanger Full Cycle

The simulation is completed using the modeling assumptions and simulation scheme discussed earlier. The main objective is to investigate the performance of a piston-type work exchanger including one piston cylinder through one full cycle. This will help us to have a better understanding of the system dynamics, cycle time, and depressurization and pressurization stages.

The full cycle of energy recovery through a work exchanger for a unit with one vessel (piston cylinder) which was described earlier (Fig. 2.2) includes four main stages. These stages have been simulated for a case study in which a high-pressure stream enters the unit at 900 kPa and 656 K and needs to be depressurized to 100 kPa, and a low-pressure stream enters the unit at 170 kPa and 260 K and should be pressurized to 700 kPa. As mentioned, ideal gas air has been assumed as the working fluid for both streams. The simulation is completed in two main steps which are stages I-II (high-pressure stream depressurization and low-pressure stream displacement), and stages III-IV (low-pressure stream pressurization and high-pressure stream displacement). Later, these two steps will be combined to analyze the full cycle of energy recovery during the two strokes.

Step 1- High-pressure stream depressurization and low-pressure stream displacement (Stages I-II). Initially, while the piston is at the left side of the cylinder, the HP

side is filled with the high-pressure stream at 900 kPa and 656 K (t=0 seconds). The valve v_4 will be activated in the simulation (opened) and the high-pressure stream will flow out. This will continue till the HP side pressure drops to a target outlet pressure lower than the low-pressure stream inlet pressure. At around 0.055 seconds, the pressure reaches about 100 kPa. At 0.057 seconds, the low-pressure stream flows into the LP side of the piston at 170 kPa and 260 K through valve v_1. The pressure difference between the two sides of the piston will cause the movement of the piston from the right to the left side while the high-pressure stream is still flowing out of the cylinder through valve v_4. The movement of the piston and displacement of the low-pressure stream counted as stage II takes about 0.05 seconds. Figure 5.12 summarizes the pressure contours for step 1 including stages I and II.

Step 2- Low-pressure stream pressurization and high-pressure stream displacement (Stages III-IV). While the piston is at the right side of the cylinder and the LP side is filled with low-pressure stream at 170 kPa, the valve v_3 will be activated in the simulation (opened) and the high-pressure stream will flow in at 900 kPa. Due to the pressure difference between the two sides of the piston, the piston will move from the right to the left and the LP side content will be compressed. At about 0.0057 seconds, the valve v_2 is activated (opened) and the pressurized low-pressure stream flows out through valve v_2. The movement of the piston and displacement of the high-pressure stream counted as stage IV takes about 0.009 seconds. Figure 5.13 summarizes the pressure contours for step 2 including stages III and IV. Note that, according to the calculation of the work that the piston does on the air in the LP side, if the piston moves from the end right to the end left side (considering clearance volume), the outlet pressure of the low-pressure stream will be higher than the target assigned. For this reason, the piston should be stopped at 0.152 m distance

from the end of the cylinder instead of 0.1 m so the low-pressure stream will not reach a higher pressure than the target pressure.

Full cycle. To analyze one complete cycle of energy recovery using the work exchanger, we have combined the simulation results of the two steps which include stages I-II and III-IV. Using this information, for our case study, the full cycle takes about 0.124 seconds. This time duration could be significantly different case by case as operating conditions play a key role in defining the cycle time. For instance, piston movement in stage IV takes only about 0.009 seconds which is lower compared to stage II in which the piston motion takes 0.05 seconds. In fact, the different pressure differences between the high-pressure and low-pressure streams of the two sides of the piston, 70 kPa for stage II and 730 kPa for stage IV, will result in different velocities for the piston movement. Note that in stage IV, the piston has been stopped before reaching the end of the cylinder to meet the target pressure of the low-pressure stream. However, continuing the simulation in stage IV until the piston reaches the same position as in stage II, the time only increases to 0.011 seconds which is still about one fifth of the time duration for piston motion in stage II. The impact of the operating conditions on piston movement and its speed of movement has been analyzed in section 5.3.6.

Figure 5.14 summarizes the pressure profile for both the high-pressure and low-pressure streams at the HP and LP sides. The piston position through the full cycle is shown in Fig. 5.15 and the check valve positions considering 0 for each valve being closed and 1 being open are plotted in Figs. 5.16-5-19.

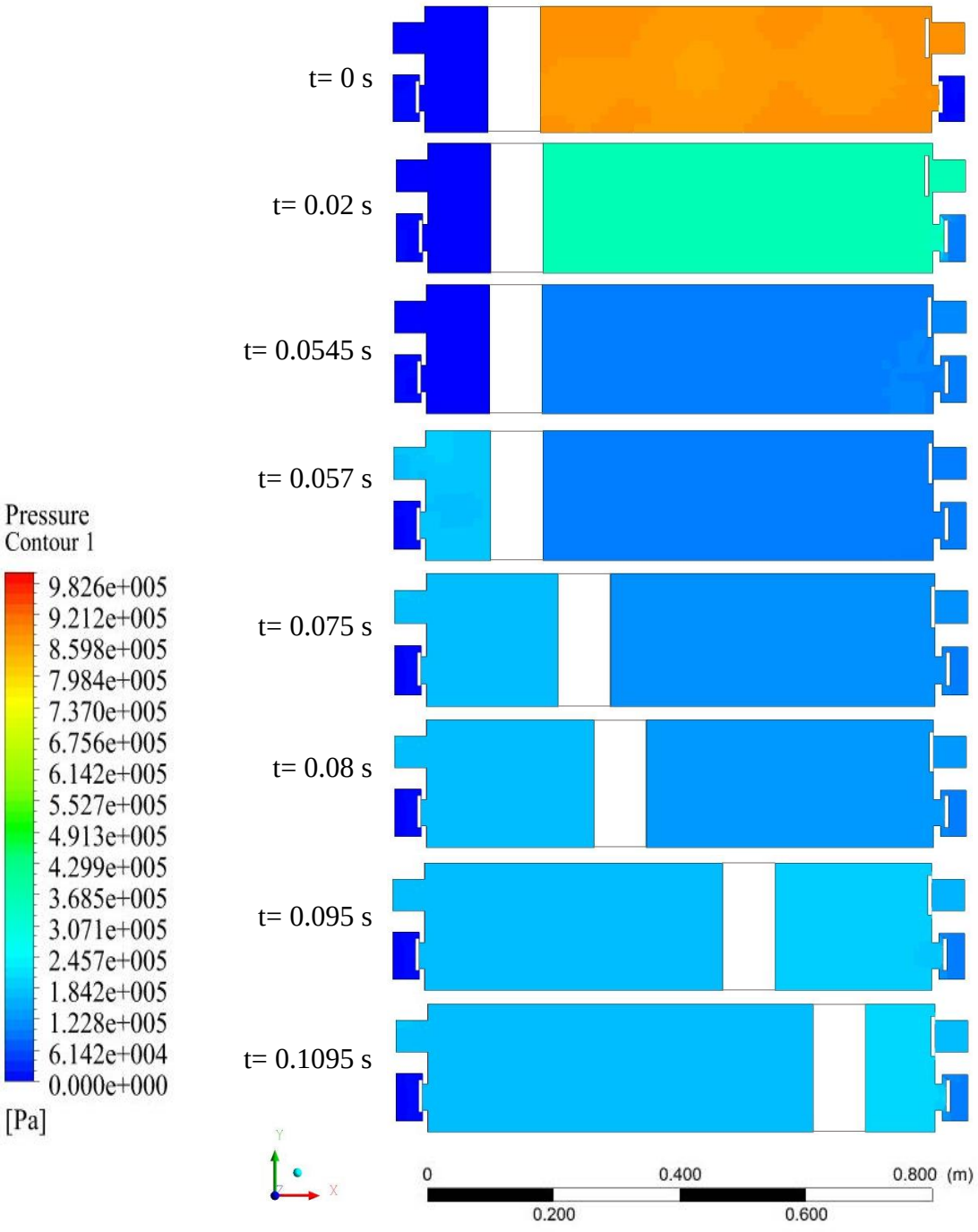

Figure 5.12. Contours of pressure variation during stages I-II.

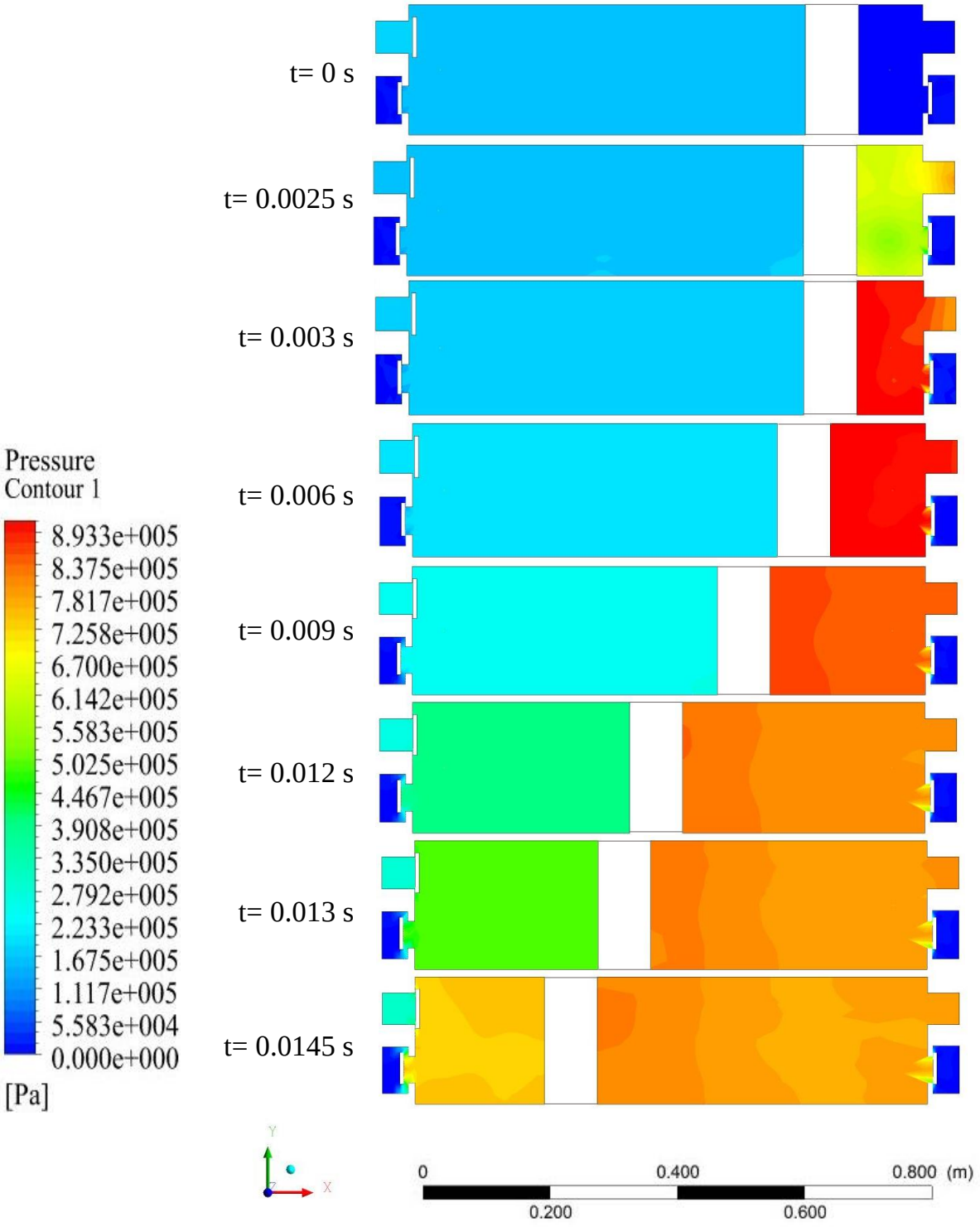

Figure 5.13. Contours of pressure variation during stages III-IV.

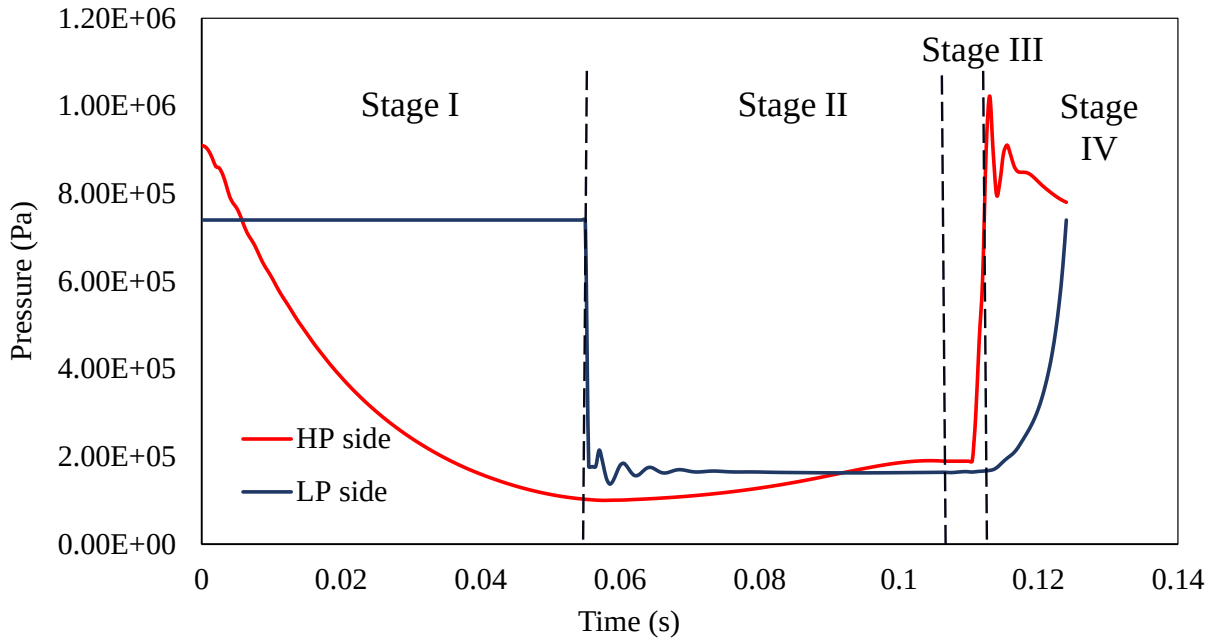

Figure 5.14. Pressure change profile for HP and LP streams in full cycle (Stages I-IV).

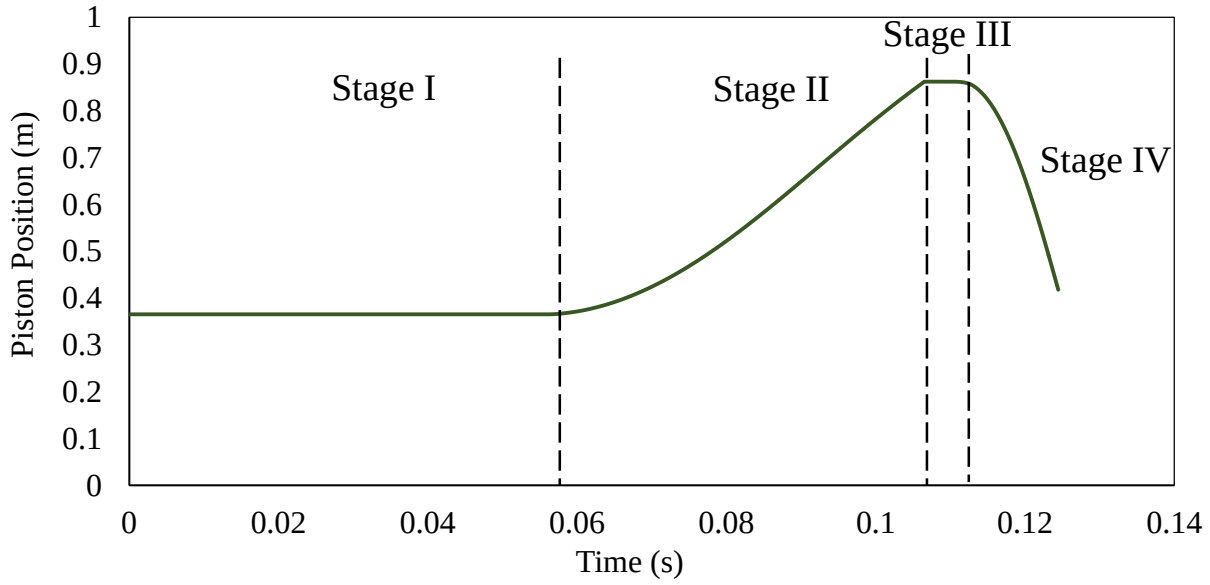

Figure 5.15. Piston position in a full cycle (Stages I-IV).

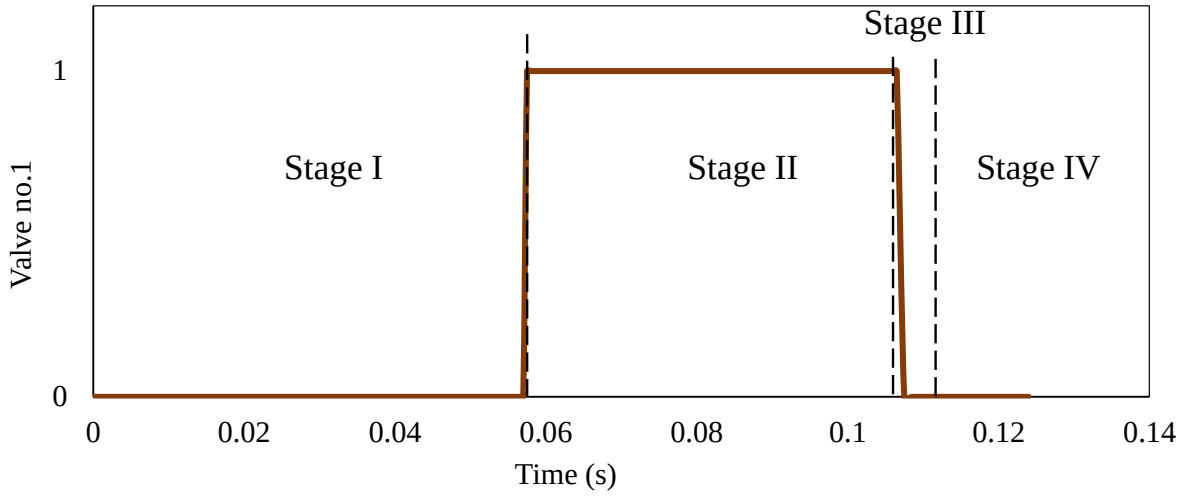

Figure 5.16. Valve no. 1 (inlet low-pressure stream) position during the full cycle (Stages I-IV).

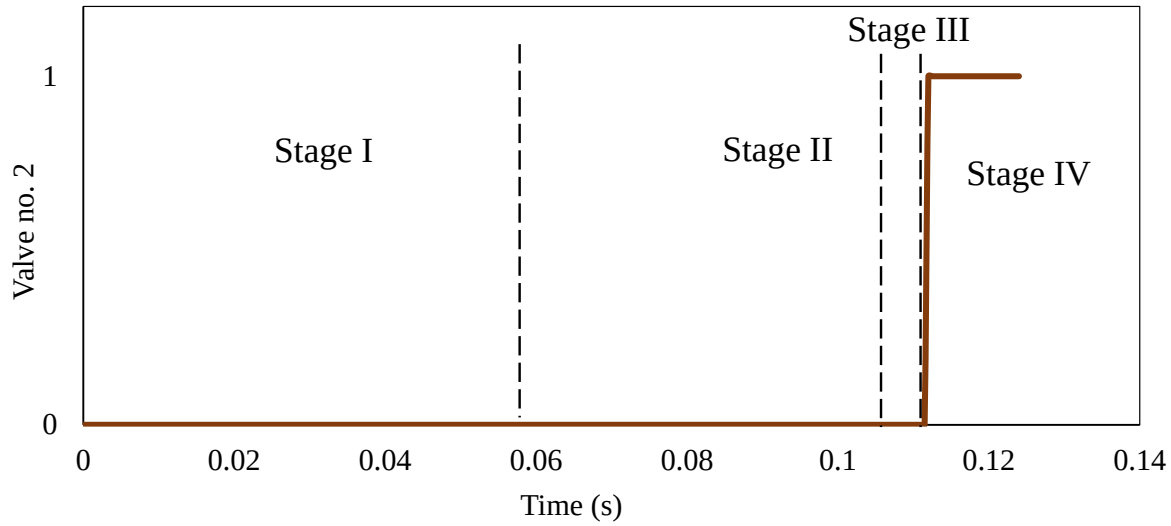

Figure 5.17. Valve no. 2 (outlet low-pressure stream) position during the full cycle (Stages I-IV).

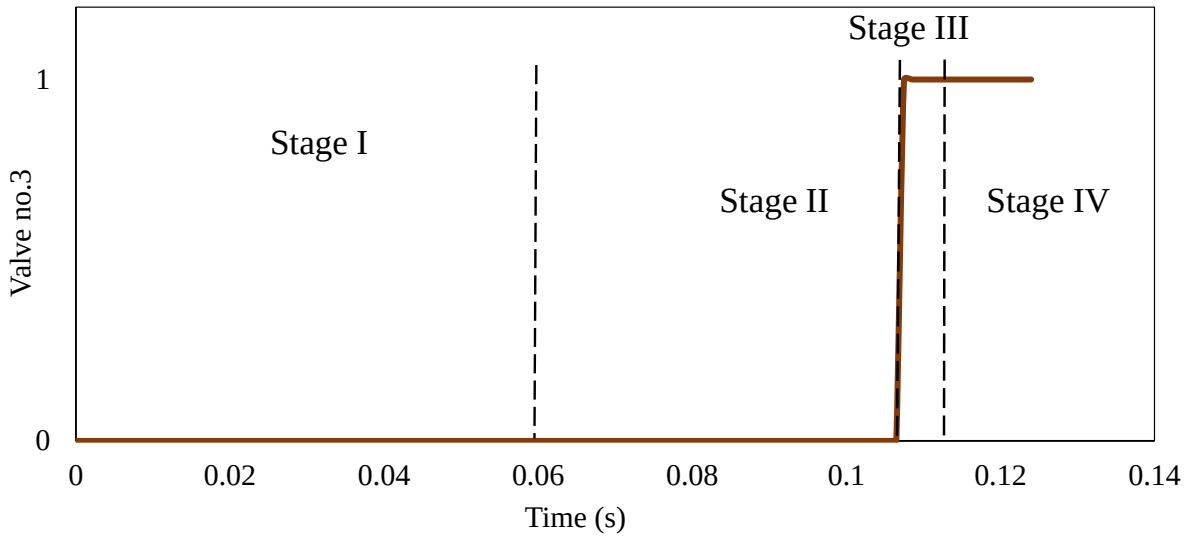

Figure 5.18. Valve no. 3 (inlet high-pressure stream) position during the full cycle (Stages I-IV).

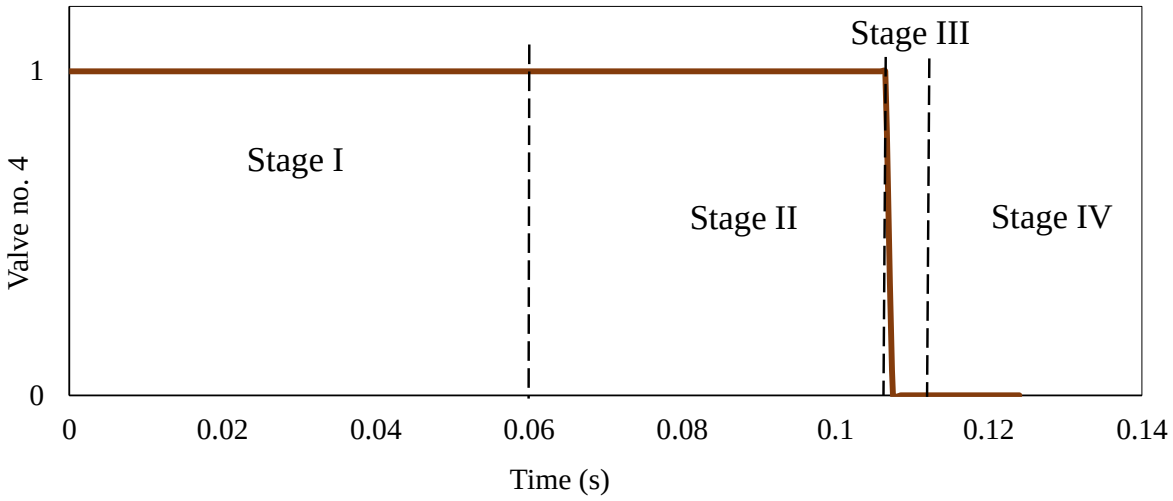

Figure 5.19. Valve no. 4 (outlet high-pressure stream) position during the full cycle (stages I-IV).

5.3.6 Piston Movement under Different Operating Conditions

To study the effect of operating conditions on the cycle time, we have mainly focused on the piston motion performance. The pressure and temperature can be defined as the main parameters which impact the amount of work that the piston does on the fluid, the target pressures, and how fast the piston moves from one side to the other. Piston motion can be considered as one of the most important challenges manufacturers may have while dealing with work exchangers operated by gas phase streams. In fact, the safety of the unit, dynamic performance of the unit, and its efficiency for feasible transfer of energy are all related to the motion of the piston.

CFX from Ansys Workbench allows us to analyze the performance of the rigid body under different operating conditions. For this reason, we have studied the piston motion under the same modeling formulation with Ansys Workbench CFX 18.2. For a minimum pressure difference of 70 kPa (the amount required for the piston movement according to the thermodynamic feasibility condition of mechanical energy transfer), we have conducted the simulation for different pressure differences of working fluids between the two sides of the piston. Figure 5.20 shows the amount of time it takes the piston to be moved from the right to the left side (considering clearance volume) while the pressure difference between the high-pressure and low pressure streams are different ratios of the minimum pressure difference such as 1ΔP, 2ΔP, 4ΔP, 8ΔP, and 28ΔP kPa. Dealing with different cycle times, un-steady flow in and out of the unit, and unsafe movement of the piston due to high pressure differences are some of the issues that we are able to address after completing this simulation.

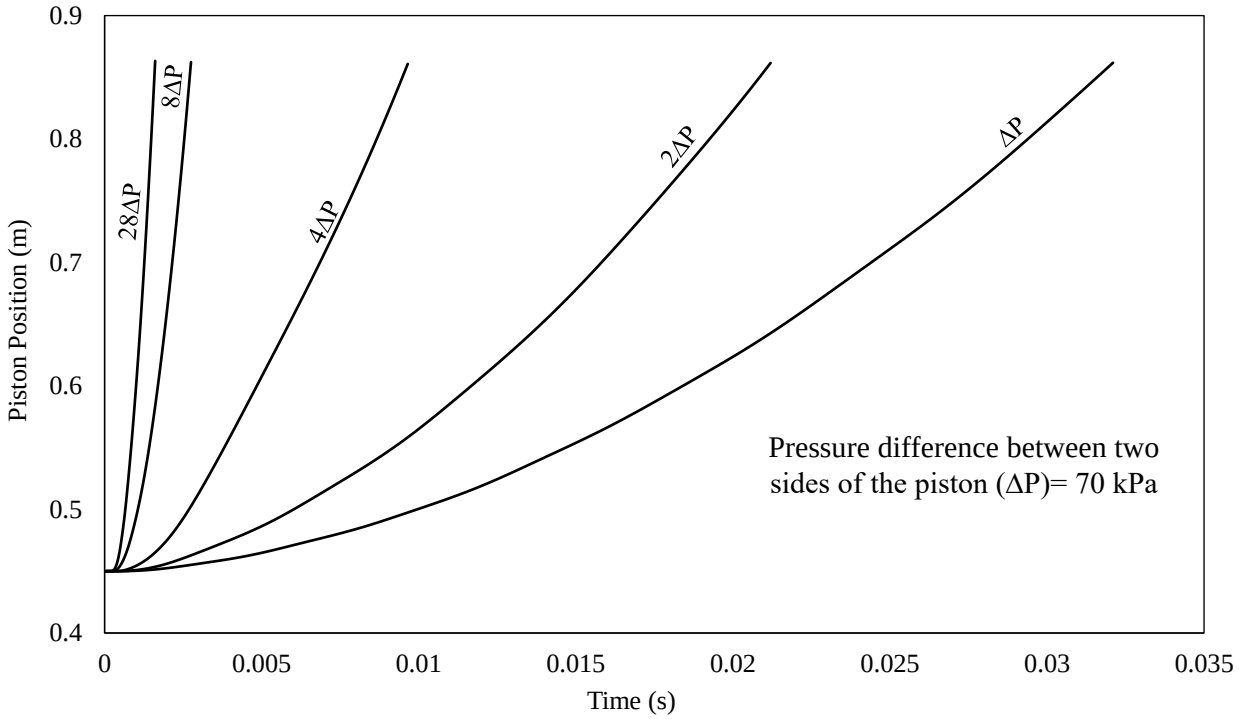

Figure 5.20. Piston position vs. time under different operating pressures.

Under the operating pressure of the high-pressure streams at 600 kPa and the low-pressure stream at 101 kPa, but different governing conditions in terms of dealing with isothermal compression, non-isothermal and equal temperature of the high-pressure and low-pressure streams, and non-isothermal but different operating temperatures, the compression cycle time will also differ significantly as shown in Fig. 5.21.

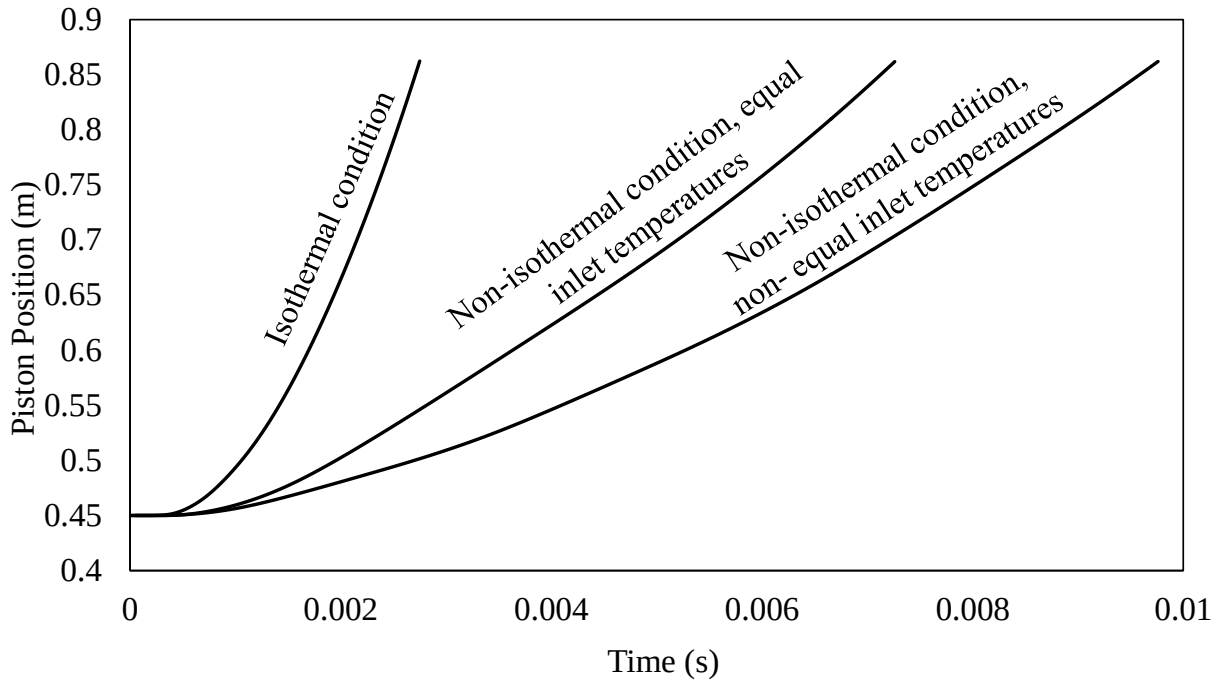

Figure 5.21. Piston position vs. time under different operating temperatures.

For different specified target low-pressure stream, the simulation was completed to study the relation of the speed of movement for the piston and the compression ratio. As shown in Fig. 5.22, there is a linear relationship between these two parameters. This will help to be able to control the speed of the piston to prevent fast and unsafe compression and also design and modify the operating conditions so the low-pressure stream will reach the target pressure (based on the compression ratio). The speed of movement can be controlled by the pressure of the high-pressure stream, and the cycle time.

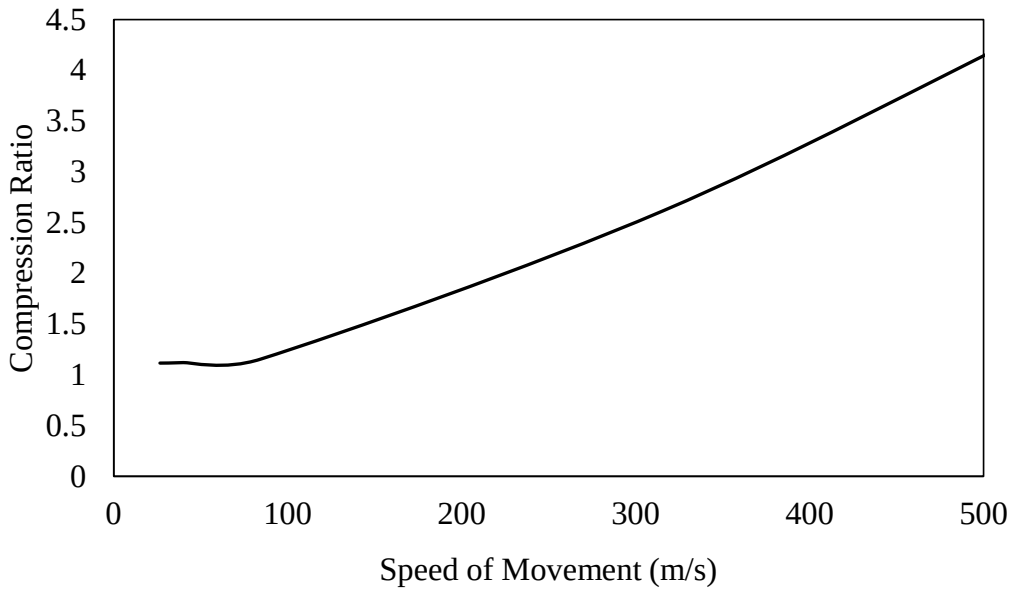

Figure 5.22. The compression ratio of the low-pressure stream for a maximum displacement of the piston.

5.4 Summary

In this chapter, the main objective was to discuss the feasibility of using a piston-type work exchanger for mechanical energy recovery and address the main challenges regarding this device when being used in chemical processes. Preliminary results have helped us to have better insight regarding these obstacles and to be able to develop a model close to reality. An Aspen Plus simulation of the unit by the custom modeler would be beneficial in terms of simulating the chemical processes which will be integrated with work exchangers for improvement of energy efficiency. However, to have a better estimation of the dynamic performance of the unit, Aspen Plus simulation would not be sufficient. Therefore, we continued our analysis with computational fluid dynamics modeling to precisely study the unit. Simulations show that the unit performance dealing with gas phase streams will be different compared to the cases from desalination processes. For instance, for the case study in which the complete cycle was simulated, the cycle time for the pressurization and depressurization of the high-pressure and low-pressure streams was defined as

low as 0.124 seconds which has a significant difference with the 10-15 seconds cycle time reported initially for the device in desalination processes. However, the simulation is still in the preliminary stages and it can be improved in many different aspects. Accurate design of the valves dealing with different fluid domains at each side of the piston, the possibility of fluids phase change through the process, friction loss due to movement of the piston, and controlling the piston motion are some of the main future challenges that need to be addressed.

CHAPTER 6 DATA-DRIVEN MODELING AND ANALYSIS OF ENERGY EFFICIENCY OF GEOGRAPHICALLY DISTRIBUTED MANUFACTURING

Thermal energy defined as process heating and mechanical energy defined as machine drive systems are categorized as the direct process energy systems in manufacturing sectors. They consume about 9,216 TBtu energy (48% of the total manufacturing energy consumption), out of which about 3,874 TBtu will be lost which is counted as 42% of the amount that has been consumed (U.S. DOE, 2018).

Over the past decades, energy efficiency in industries has been significantly and continuously improved. However, further efforts on energy efficiency improvement are needed, which requires to overcome a number of barriers, such as a lack of private-sector investment for technology deployment, a low turnover rate of energy system's capital-intensive infrastructure, and resource-supply challenges in technology deployment (NETL, 2009). Technically, manufacturing sectors in different geographical regions should responsively and systematically conduct more in-depth analysis of energy consumption, energy loss, and CO_2 emission. Energy Flow Analysis (EFA) is an effective tool for understanding energy consumption in industrial organizations (Chen and Chen, 2015), energy source distribution among manufacturing sectors (LLNL, 2018), and fuel types used by sectors (Decker *et al.*, 2000). The Input-Output Analysis (IOA) has been widely adopted as a tool to assess resource and environmental impact embodied in goods and service trade (Leontief, 1951, Chapman, 1974, Gay *et al.*, 1993). Energy consumption, land use, CO_2 emission, and material consumption are some examples of the indicators used in those studies. The IOA can be applied to the study of individual or multiple regions (Lenzen, 1998, Wiedmann *et al.*, 2007). Based on the IOA, the Ecological Network Analysis (ENA) was also introduced to study energy/material flows in ecosystems (Hannon, 1973). From a different perspective, the Data Envelope Analysis (DEA), a mathematical

programming method, has been employed to assess energy efficiency of a wide range of sectors, such as manufacturing sectors (Charnes *et al*., 1978, Ray, 2004). In the Mukherjee (2008) study, energy conservation, cost minimization, and capacity output were chosen as the objectives, and the performance of manufacturing sectors was analyzed for different time periods. Needless to say, data availability and data quality are key to industrial applications.

The U.S. Department of Energy (DOE) has published and continuously updated reports about the U.S. energy consumption/loss and CO_2 emission for manufacturing sectors (U.S. DOE, 2009, 2012, 2018). The reports contain the Energy Information Administration (EIA) data of primary energy use at the national level (U.S. EIA, 2010, 2014), and the information about onsite energy generation, direct energy use in process and non-process systems, and offsite energy use. The accessible information is for all manufacturing sectors (coded as NIACS 31-33), where the top 15 energy intensive manufacturing sectors are detailed, which consume 95% of the total energy used (U.S. DOE, 2018). However, the methodology described in the reports is not directly for energy efficiency analysis in geographical regions, such as individual states or counties.

U.S. Census Bureau (USCS), on the other hand, provides a huge amount of data about the locations of manufacturing sectors and subsectors (listed in NIACS 31-33) as well as the dollar value of shipment of manufactured products; these represent key economic information about manufacturing activities. However, the data collected by the USCS does not include any information about energy efficiency in manufacturing sectors. Interestingly, the American Council for an Energy-Efficient Economy (ACEEE) studied the energy efficiency performance of all the states in the U.S. and ranked them (ACEEE, 2018). This information is valuable for individual states to understand the challenges they are facing.

The aim of this chapter is to investigate energy efficiency in manufacturing sectors in different geographical regions, such as states and counties. In the following sections, we will first introduce a general data-driven modeling and analysis method to study energy consumption, energy loss, and CO_2 emission in manufacturing regions. The publically accessible data from the DOE, USCS, and ACEEE will be utilized to study energy consumption, energy loss, and CO_2 emission in different states and, as an example, the state of Michigan is chosen for more detailed study.

6.1 Data-driven Energy Analysis Methodology

National data presentation. As stated, the DOE reports contain three types of national data: energy consumption, energy loss, and CO_2 emission in manufacturing sectors. Figure 6.1 is an example showing the energy and carbon footprint for the chemical manufacturing sector in the U.S. in 2012 (U.S. DOE, 2012). To facilitate energy efficiency analysis in manufacturing sections, we introduce a few matrices, which are described below.

Energy consumption. Let $\boldsymbol{EC}(M \times N)$ be an energy consumption matrix that contains the information about M types of energy systems defined by the DOE (e.g., process heating, process cooling, and onsite transportation) in N types of manufacturing sectors (e.g., chemical, alumina and aluminum, and fabricated metals). The matrix has the following structure:

$$\boldsymbol{EC} = \begin{bmatrix} EC_{1,1} & EC_{1,2} & \cdots & EC_{1,N} \\ EC_{2,1} & EC_{2,2} & \cdots & EC_{2,N} \\ \vdots & \vdots & \ddots & \vdots \\ EC_{M,1} & EC_{M,2} & \cdots & EC_{M,N} \end{bmatrix}, \tag{6.1}$$

where $EC_{i,j}$ is the amount of energy consumed by the i-th energy system in the j-th manufacturing sector. The element data in matrix $\boldsymbol{EC}$ can be directly obtained from the DOE reports (U.S. DOE, 2009, 2012, 2018).

The types of energy systems may differ, depending on user's interest. It is possible that not every type of energy system is included in matrix ***EC*** due to data availability issue. Therefore, in some cases, the summation of the element values in a column of matrix ***EC*** does not represent the total amount of energy consumed in a specific manufacturing sector. For this reason, variable γ_j is introduced to represent the total energy consumption in each manufacturing sector in the reports describing the nation's energy consumption. Using this information, we can derive a percentage-based energy consumption matrix, named $\boldsymbol{EC_P}$, as follows:

$$\boldsymbol{EC_P} = \begin{bmatrix} EC_{P_{1,1}} & EC_{P_{1,2}} & \cdots & EC_{P_{1,N}} \\ EC_{P_{2,1}} & EC_{P_{2,2}} & \cdots & EC_{P_{2,N}} \\ \vdots & \vdots & \ddots & \vdots \\ EC_{P_{M,1}} & EC_{P_{M,2}} & \cdots & EC_{P_{M,N}} \end{bmatrix}, \tag{6.2}$$

where element $EC_{P_{i,j}}$ is the percentage of the energy consumed by the *i*-th energy system in the *j*-th manufacturing sector, i.e.,

$$EC_{P_{i,j}} = \frac{EC_{i,j}}{\gamma_j} \tag{6.3}$$

Note that each element in matrix $\boldsymbol{EC}_P$ represents how energy consumption is distributed among the energy systems in a manufacturing sector. The percentages are the average in the nation and can be reasonably considered constant in different geographical regions.

Energy loss estimation. Let $\boldsymbol{EL}$ $(M \times N)$ be a matrix that contains the energy loss information about *M* types of energy systems in *N* types of manufacturing sectors. The matrix has the following structure:

$$\boldsymbol{EL} = \begin{bmatrix} EL_{1,1} & EL_{1,2} & \cdots & EL_{1,N} \\ EL_{2,1} & EL_{2,2} & \cdots & EL_{2,N} \\ \vdots & \vdots & \ddots & \vdots \\ EL_{M,1} & EL_{M,2} & \cdots & EL_{M,N} \end{bmatrix}, \tag{6.4}$$

where element $EL_{i,j}$ is the amount of energy loss in the *i*-th energy system of the *j*-th manufacturing sector.

Note that the ratio of $EL_{i,j}$ and $EC_{i,j}$ is the energy loss percentage of the *i*-th energy system in the *j*-th manufacturing sector. The following matrix is named the energy loss percentage matrix:

$$\boldsymbol{EL_P} = \begin{bmatrix} EL_{P_{1,1}} & EL_{P_{1,2}} & \cdots & EL_{P_{1,N}} \\ EL_{P_{2,1}} & EL_{P_{2,2}} & \cdots & EL_{P_{2,N}} \\ \vdots & \vdots & \ddots & \vdots \\ EL_{P_{M,1}} & EL_{P_{M,2}} & \cdots & EL_{P_{M,N}} \end{bmatrix}, \tag{6.5}$$

where

$$EL_{P_{i,j}} = \frac{EL_{i,j}}{EC_{i,j}}. \tag{6.6}$$

<u>*Carbon dioxide (CO_2) emission*</u>. Energy related CO_2 emission data can be organized in a vector, named $\boldsymbol{CE}$ $(N \times 1)$ as follows:

$$\boldsymbol{CE} = \begin{bmatrix} CE_1 & CE_2 & \cdots & CE_N \end{bmatrix}^T, \tag{6.7}$$

where CE_j is the amount of CO_2 emission from the *j*-th manufacturing sector in the nation.

State-level energy analysis. To derive state-level energy efficiency, the DOE's national energy and carbon footprint maps and additional information are needed. As stated, the USCS' database contains rich information about the business performance of various manufacturing sectors in different regions of the country. The data types include the number of manufacturing establishments, the total value of product shipments, the total capital expenditure, the total cost of

materials, the value added, and the total number of employees. It is known that energy intensity is quantified by the energy consumption per economic factor. The total value of shipments and services received (SSR) is defined as the dollar value of products sold by the manufacturing establishments and is based on net selling values, f.o.b. (free on board) plant, after excluding discounts and allowances (USCS Manufacturers Shipments, Inventories, and Orders, 2018). According to the Industrial Demand Module (IDM) of the National Energy Modeling System (NEMS), it demonstrates largely industrial economic activities, and energy consumption is a main factor of it (U.S. EIA Industrial Demand Module, 2018). The total value of SSR is also used in the Manufacturing Energy Consumption Survey (MECs) energy statistics (U.S. EIA MECS Industry Analysis, 2018). Therefore, in this work, the total value of SSR is adopted as a measurement of manufacturing economic activities when estimating energy consumption in different geographical regions.

State-level energy consumption estimation. Let's introduce a vector, named $\boldsymbol{B}$, to include the energy consumption data for all types of manufacturing sectors in a state.

$$\boldsymbol{B} = \begin{bmatrix} B_1 & B_2 & \cdots & B_N \end{bmatrix}^T, \tag{6.8}$$

where B_j is the energy consumption of the j-th manufacturing sector in the state. This type of data is unavailable in the DOE reports. However, it can be estimated using the information from the USCS as follows:

$$B_j = \gamma_j \times \frac{\theta_j}{\varphi_j}, \tag{6.9}$$

where γ_j is the total energy consumption in the j-th manufacturing sector in the U.S., θ_j and φ_j are, respectively, the total value of SSR of the j-th manufacturing sector in one state and that in the nation.

Note that the total energy consumption by all *N* types of manufacturing sectors of a state can be simply calculated as follows:

$$B^{tot} = \sum_{j=1}^{N} B_j \tag{6.10}$$

In matrix $\boldsymbol{EC}_P$ shown in Eq 2, element $EC_{p_{i,j}}$ is the percentage of the energy consumed by the *i*-th energy system in the *j*-th manufacturing sector. Since B_j is the total energy consumed by the *j*-th manufacturing sector in the state, the energy consumption in each type of energy systems in a manufacturing sector in a state, designated as $EC^s_{i,j}$, can be estimated as:

$$EC^s_{i,j} = EC_{p_{i,j}} \times B_j \tag{6.11}$$

Thus, for a state having N types of manufacturing sectors, matrix $\boldsymbol{EC}^s$ is defined as follows,

$$\boldsymbol{EC}^s = \begin{bmatrix} EC^s_{1,1} & EC^s_{1,2} & \cdots & EC^s_{1,N} \\ EC^s_{2,1} & EC^s_{2,2} & \cdots & EC^s_{2,N} \\ \vdots & \vdots & \ddots & \vdots \\ EC^s_{M,1} & EC^s_{M,2} & \cdots & EC^s_{M,N} \end{bmatrix}, \tag{6.12}$$

State-level energy loss estimation. Matrix $\boldsymbol{EL}_P$ in Eq 5 contains only national average energy loss information. To estimate the state-level energy loss in manufacturing sectors in states, each state's energy efficiency ranking identified by the American Council of an Energy Efficient Economy (ACEEE, 2018) can be used. The ranking is simply a number between 1 and 51 for 50 states plus a federal district (Washington, D.C.), with 1 the best, and 51 the worst in terms of energy efficiency. Thus, 26 is the middle number in the ranking. This ranking information allows us to differentiate energy loss in different states. Here, we introduce a parameter for energy loss percentage correction as follows:

$$\alpha_{i,j} = 1 - \frac{(26 - R_s)}{100}, \tag{6.13}$$

where R_s is the ranking number of that state. The value of $\alpha_{i,j}$ is between 75% and 125%. Thus, a state's ranking number (R_s) less than 26 means better energy efficiency and less energy loss than at least 26 states. Now let's define a matrix, named $\boldsymbol{EL}^s$, to quantify energy loss in different energy systems of those manufacturing sectors in a state as follows:

$$\boldsymbol{EL}^s = \begin{bmatrix} EL^s_{1,1} & EL^s_{1,2} & \cdots & EL^s_{1,N} \\ EL^s_{2,1} & EL^s_{2,2} & \cdots & EL^s_{2,N} \\ \vdots & \vdots & \ddots & \vdots \\ EL^s_{M,1} & EL^s_{M,2} & \cdots & EL^s_{M,N} \end{bmatrix}, \tag{6.14}$$

where

$$EL^s_{i,j} = \alpha_{i,j} \times EL_{p_{i,j}} \times EC^s_{i,j}. \tag{6.15}$$

As shown, the energy loss percentage for a state is calculated through converting the national energy loss percentage ($EL_{p_{i,j}}$) using parameter $\alpha_{i,j}$. This is possibly a best feasible way for adjustment based on the information available. Note that if a state's ranking number (R_s) is larger than 26, the adjusted energy loss percentage ($\alpha_{i,j} \times EL_{p_{i,j}}$) may be greater than 100%; in such a case (although very unlikely), the value of $EL^s_{i,j}$ should be set to $EC^s_{i,j}$.

Using the information contained in $\boldsymbol{EL}^s$, we can readily calculate the total amount of energy loss of a specific manufacturing sector (EL^s_j, j = 1, 2, …, N) and that of all manufacturing sectors in a state, $EL^{s,tot}$, i.e.,

$$EL^s_j = \sum_{i=1}^{M} EL^s_{i,j}. \tag{6.16}$$

and

$$EL^{s,tot} = \sum_{j=1}^{N} EL_j^s \,. \tag{6.17}$$

State-level CO_2 emission estimation. The CO_2 emission of individual manufacturing sector in a state (CE_i^s) can be estimated as follows:

$$CE_j^s = CE_j \times \frac{\theta_j}{\varphi_j} \tag{6.18}$$

where CE_j is the CO_2 emission of the *j*-th manufacturing sector in the nation; θ_j and φ_j are, respectively, the total value of SSR of the *j*-th manufacturing sector in one state and that in the nation.

For a state having N manufacturing sectors, the CO_2 estimation is included in vector $\boldsymbol{CE}^s$:

$$\boldsymbol{CE}^s = \begin{bmatrix} CE_1^s & CE_2^s & \cdots & CE_N^s \end{bmatrix}^T, \tag{6.19}$$

The sum of the element values in the above vector gives the estimation of the total energy-related CO_2 emission of all N manufacturing sectors in the state, i.e.,

$$CE^{s,tot} = \sum_{j=1}^{N} CE_j^s \,. \tag{6.20}$$

County-level energy analysis. Estimation of energy consumption, energy loss and CO_2 emission at the county level can be performed using the state-level information.

County-level energy consumption estimation. Let's introduce a matrix, named $\boldsymbol{EC}^c$ that contains the energy consumption data in *N* types of manufacturing sectors in H counties of the selected state:

$$\boldsymbol{EC}^c = \begin{bmatrix} EC^c_{1,1} & EC^c_{1,2} & \cdots & EC^c_{1,N} \\ EC^c_{2,1} & EC^c_{2,2} & \cdots & EC^c_{2,N} \\ \vdots & \vdots & \ddots & \vdots \\ EC^c_{H,1} & EC^c_{H,2} & \cdots & EC^c_{H,N} \end{bmatrix}, \tag{6.21}$$

Where the element $EC^c_{i,j}$ is the energy consumption in the *j*-th manufacturing sector in the *i*-th county. This element can be estimated as:

$$EC^c_{i,j} = B_j \times \frac{\omega_{i,j}}{\theta_j}, \tag{6.22}$$

where B_j is the energy consumption of the *j*-th manufacturing sector in the state; θ_j and $\omega_{i,j}$ are, respectively, the total value of SSR of *j*-th type of manufacturing sector in the state and that in the *i*-th county, which can be obtained from the USCS database.

Using the information contained in matrix $\boldsymbol{EC}^c$, we can estimate each county's total energy consumption of the manufacturing sectors as follows:

$$EC^c_i = \sum_{j=1}^{N} EC^c_{i,j}. \tag{6.23}$$

Note that the total energy consumption of the *N* manufacturing sectors in all *H* counties should be equal to the total energy consumption of the state.

County-based energy loss estimation. The county-level energy loss in manufacturing sectors can be estimated based the state-level energy loss data. Let's define $EL^c_{i,j}$ as the energy loss of the j-th type of manufacturing sector in the i-th county of the selected state. Its value can be estimated as:

$$EL^c_{i,j} = EL^s_j \times \frac{\omega_{i,j}}{\theta_j}, \tag{6.24}$$

where EL^s_j is the energy loss of the j-th manufacturing sector in the state (see Eq. 6.16).

The results obtained using Eq. 6.24, we can construct matrix $\boldsymbol{EL}^c$ to include the energy loss of the manufacturing sectors in all individual counties in the state:

$$\boldsymbol{EL}^c = \begin{bmatrix} EL_{1,1}^c & EL_{1,2}^c & \cdots & EL_{1,N}^c \\ EL_{2,1}^c & EL_{2,2}^c & \cdots & EL_{2,N}^c \\ \vdots & \vdots & \ddots & \vdots \\ EL_{H,1}^c & EL_{H,2}^c & \cdots & EL_{H,N}^c \end{bmatrix}, \tag{6.25}$$

Note that the energy loss in all manufacturing sectors of a county, designated as EL_i^c, is the sum of the element values in the i-th row of matrix $\boldsymbol{EL}^c$, i.e.,

$$EL_i^c = \sum_{j=1}^{N} EL_{i,j}^c \,. \tag{6.26}$$

County-level CO_2 emission estimation. The CO_2 emission of a sector in a county under the selected state can be defined as:

$$CE_{i,j}^c = CE_j^s \times \frac{\omega_{i,j}}{\theta_j} \,. \tag{6.27}$$

where θ_j and $\omega_{i,j}$ are, respectively the total value of SSR of the *j*-th type of manufacturing sector in the state and that in the *i*-th county.

Thus, the CO_2 emission information of all H counties in a state can be included in matrix $\boldsymbol{CE}^c$ as follows:

$$\boldsymbol{CE}^c = \begin{bmatrix} CE_{1,1}^c & CE_{1,2}^c & \cdots & CE_{1,N}^c \\ CE_{2,1}^c & CE_{2,2}^c & \cdots & CE_{2,N}^c \\ \vdots & \vdots & \ddots & \vdots \\ CE_{H,1}^c & CE_{H,2}^c & \cdots & CE_{H,N}^c \end{bmatrix}, \tag{6.28}$$

Note that the total CO_2 emission of manufacturing sectors in an individual county is the sum of the element value of the corresponding row in matrix $\boldsymbol{CE}^c$, i.e.,

$$CE_i^c = \sum_{j=1}^{N} CE_{i,j}^c \ . \tag{6.29}$$

6.2 Case Study

Energy efficiency improvement in manufacturing sectors is a key approach for energy sustainability. This requires a comprehensive energy efficiency analysis on energy consumption, energy loss, and carbon emission. In this section, the developed methodology is used to examine energy-intensive manufacturing sectors and generate detailed information of energy consumption, energy loss, and CO2 emission at the national, state, and county levels.

Energy-intensive manufacturing sectors. According to the DOE report (2018), there are 15 manufacturing sectors consuming about 95% of the total energy among all the manufacturing sectors. These include (1) the alumina and aluminum sector, (2) the cement sector, (3) the chemical sector, (4) the computers, electronics and electrical equipment sector, (5) the fabricated metals sector, (6) the food and beverage sector, (7) the forest product sector, (8) the foundry sector, (9) the glass sector, (10) the iron and steel sector, (11) the machinery sector, (12) the petroleum refining sector, (13) the plastics and rubber product sector, (14) the textile sector, and (15) the transportation equipment sector. Each sector has a number of subsectors, according to North American Industry Classification System (NAICS).

Data source. DOE releases the national energy and carbon footprint data regularly through its website based on the updated EIA Manufacturing Energy Consumption Survey (MECS) (2010, 2014). The latest accessible data is for 2014. However, the latest information about the total values of shipment and service received (SSR) data for each manufacturing sector in the nation and individual states and counties reported in the economic activity survey by the U.S. Census Bureau is for 2012. Therefore, to ensure data consistency in evaluation, we will use the DOE's energy and carbon footprint data also for 2012 in the case study. Note that the available data

reflects the adjusted energy use statistics from MECS, in collaboration with industrial experts, under a number of assumptions. The reported footprint analysis provides detailed information about how in those sectors, the primary energy (including fuel, electricity, and steam supplied from offsite sources) was consumed (1) for offsite and onsite energy generation and (2) by onsite energy use in process and non-process systems.

Figure 6.1 is an example adopted from the DOE report (2012), which provides quantitative energy distribution data (energy consumption, energy loss, and CO2 emission) in the chemical manufacturing sector in the nation. As shown, the process energy use is for process heating, process cooling and refrigeration, other process use, electro-chemical use, machine drive and machine driven system use (such as those by pumps, fans, compressed air, material handling and processing, and other systems), while the non-process energy use is for facility HVAC, lighting, other facility support, onsite transportation, and other non-process purposes (U.S. DOE, 2018).

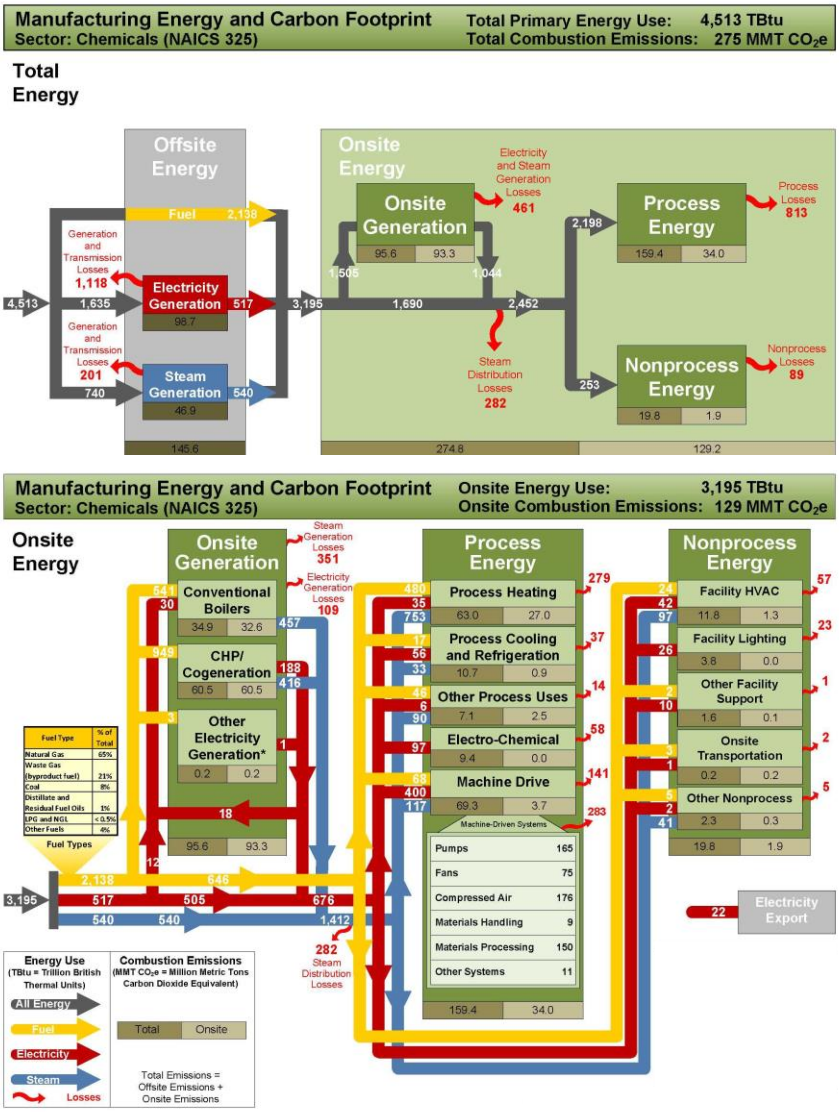

Figure 6.1. Chemical sector manufacturing energy and carbon footprint (U.S. DOE, 2012).

Results and discussions. The case study aims at deriving answers to the following questions: how much did these sectors consume energy in different types of systems, how much energy was lost in the energy systems of these sectors, and what is the amount of energy-related CO2 emitted in these sectors?

It is known that in 2012, the total annual energy consumption in the manufacturing industries in the U.S. reached 21,972 TBtu (including 11,327 TBtu for process use and 1,647 TBtu

for non-process use; the rest for offsite and onsite generation). Among this very high energy consumption, a total of 14,452 TBtu were lost, which counts for 65.7% of total energy consumption. These include process energy loss of 4,807 TBtu (i.e., 42.4% of process energy consumption) and non-process energy loss of 647 TBtu (i.e., 39.3% of non-process energy consumption). The reported total combustion emission reached 1,261 MMT CO_2e (U.S. DOE, 2012).

National energy data presentation. The DOE's national energy consumption and loss information is used to construct matrices ***EC*** and ***EL*** defined by Eqs. 6.1 and 6.4, respectively. These two matrices are used to derive, respectively, matrices $\boldsymbol{EC}_P$ and $\boldsymbol{EL}_P$ defined by Eqs. 6.2 and 6.5; the element values are shown in Tables 6.1 and 6.2. In this work, the detailed energy analysis is focused on the direct energy use in the manufacturing sectors, which includes process and non-process energy. Similar to energy consumption, the CO_2 emission data for each sector in the nation given in the DOE report (2012) is structured using Eq. 6.7.

Table 6.1. Manufacturing-sector-based energy consumption percentage in the U.S. in 2012

System Type	Alumina and Aluminum	Cement	Chemical	Electronics and computer	Fabricated Metals	Food and Beverage	Forest Products	Foundries
Process system								
Process heating	16.75	66.03	28.10	9.68	28.39	28.65	30.96	37.72
Process cooling	0.50	0.00	2.35	2.47	0.85	5.43	1.12	0.36
Other process uses	0.66	0.85	3.15	2.09	1.41	2.84	1.97	0.71
Electro-chemical	19.90	0.00	2.15	0.38	0.42	0.00	0.14	0.71
Machine drive & machine driven systems	3.65	8.28	12.96	6.83	10.17	8.69	14.72	6.41
Non-process system								
Facility HVAC	1.49	1.70	3.61	13.85	9.18	5.48	4.27	7.12
Facility lighting	0.50	0.42	0.58	3.04	1.98	1.14	0.65	1.07
Other facility support	0.33	0.21	0.27	1.52	0.71	0.83	0.20	0.71
Onsite transportation	0.17	0.42	0.09	0.57	0.42	0.26	0.65	0.36
Other non-processes	0.17	0.21	1.06	0.76	0.14	0.88	1.40	0.00

System Type	Glass	Iron and Steel	Machinery	Petroleum Refining	Plastics	Textiles	Transportation Equipment
Process system							
Process heating	54.72	48.82	8.33	66.16	13.85	20.97	12.94
Process cooling	0.43	0.07	0.68	0.68	2.19	2.54	1.88
Other process uses	1.29	1.89	1.58	3.02	1.37	1.91	4.87
Electro-chemical	0.00	0.61	0.00	0.00	0.00	0.00	0.22
Machine drive & machine driven systems	6.22	7.56	12.61	8.49	13.17	11.65	8.74
Non-process system							
Facility HVAC	5.36	4.52	14.41	1.16	7.68	8.26	16.48
Facility lighting	0.86	0.54	3.60	0.11	2.19	1.91	3.21
Other facility support	0.00	0.14	1.13	0.11	0.96	0.42	1.22
Onsite transportation	0.00	0.20	0.45	0.03	0.41	0.21	0.55
Other non-processes	0.21	0.14	0.68	0.34	0.14	0.21	0.22

Table 6.2. Manufacturing-sector-based energy loss percentage in the U.S. in 2012

System Type	Alumina and Aluminum	Cement	Chemical	Electronics and computer	Fabricated Metals	Food and Beverage	Forest Products	Foundries
Process system								
Process heating	50.50	39.87	22.00	37.25	37.81	67.15	63.97	50.94
Process cooling	33.33	0.00	34.91	38.46	33.33	35.24	35.00	0.00
Other process uses	0.00	0.00	9.86	9.09	10.00	10.91	10.00	0.00
Electro-chemical	60.00	0.00	59.79	50.00	66.67	0.00	60.00	50.00
Machine drive & machine driven systems	45.45	76.92	72.48	61.11	62.50	65.48	58.21	50.00
Non-process system								
Facility HVAC	33.33	25.00	34.97	34.25	35.38	34.91	34.87	35.00
Facility lighting	100.00	100.00	88.46	87.50	85.71	90.91	91.30	100.00
Other facility support	0.00	0.00	8.33	12.50	20.00	12.50	14.29	0.00
Onsite transportation	100.00	50.00	50.00	66.67	66.67	60.00	60.87	100.00
Other non-processes	0.00	0.00	10.42	0.00	0.00	11.76	10.00	0.00

System Type	Glass	Iron and Steel	Machinery	Petroleum Refining	Plastics	Textiles	Transportation Equipment
Process system							
Process heating	56.08	51.04	37.84	17.99	21.78	67.68	37.61
Process cooling	50.00	100.00	33.33	37.50	37.50	33.33	35.29
Other process uses	16.67	10.71	14.29	10.28	10.00	11.11	9.09
Electro-chemical	0.00	66.67	0.00	0.00	0.00	0.00	50.00
Machine drive & machine driven systems	62.07	48.21	62.50	66.45	62.50	63.64	62.03
Non-process system							
Facility HVAC	36.00	35.82	35.94	34.15	35.71	35.90	34.90
Facility lighting	100.00	87.50	87.50	100.00	87.50	88.89	89.66
Other facility support	0.00	0.00	20.00	0.00	14.29	0.00	9.09
Onsite transportation	0.00	66.67	50.00	100.00	66.67	100.00	60.00
Other non-processes	0.00	0.00	0.00	8.33	0.00	0.00	0.00

State-level energy analysis. The detailed state-level energy consumption data can be estimated using Eqs. 6.8-6.12 and the information in Table 6.1. In estimation, all 15 top energy-intensive manufacturing sectors are counted, and for each sector, five types of energy systems for process use and five types of energy systems for non-process energy use in each sector are evaluated. Note that according to the DOE's report, the top 15 manufacturing sectors consumes 95% of total energy use in the nation. Thus, to calculate the total manufacturing energy consumption of each state using Eq. 6.10, the result is multiplied by a coefficient of 1.0526 to consider all the manufacturing sectors. In this case study, the state of Michigan (MI) is selected as an example.

Energy consumption estimation. Table 6.3 provides the following types of estimated values of all 15 manufacturing sectors: (1) the value of variable γ_i - the total energy consumption in each manufacturing sector in the nation (U.S. DOE, 2012); (2) the value of variable φ_i - the total value of SSR of each manufacturing sector in the U.S. (USCS, Table EC1200A1), (3) the value of variable θ_i - the total value of SSR of each manufacturing sector in the state (USCS, Table EC1231A1), and (4) the value of B_i - the energy consumption of each manufacturing sector in a state. Note that the energy consumptions of the cement and the petroleum refining sectors are not available, because the total value of SSR of these two sectors is not reported by the U.S. Census Bureau database (USCS, Table EC1231A1).

The detailed energy consumption in each type of energy system (such as process heating, process cooling, etc.) can be also calculated using Eqs. 6.11–6.12. The estimation results are shown in Table 6.4. For the same reason, the energy consumptions in the cement and the petroleum refining sectors are not shown. On the other hand, in MI, the number of manufacturing

establishments and the production capacity of each are all relatively small (only 9 cement establishments and 3 petroleum refining establishments) (USCS, Table EC1231SA1). As a result of the following calculation, the total manufacturing energy consumption in the state of MI in 2012 would be 611.31 TBtu.

Using the same approach for the energy consumption estimation for MI, the energy consumption map for 50 states and one federal district is shown in Fig. 6.2, and the total manufacturing energy consumption would be 20,049 TBtu, which shows 8% difference as compared with the data from the averaged total annual energy consumption in the manufacturing industries in the U.S., where no specific information in each type of energy system of each manufacturing sector of each state is available (U.S. DOE, 2012). This comparison supports the estimations under the assumptions by the introduced methodology.

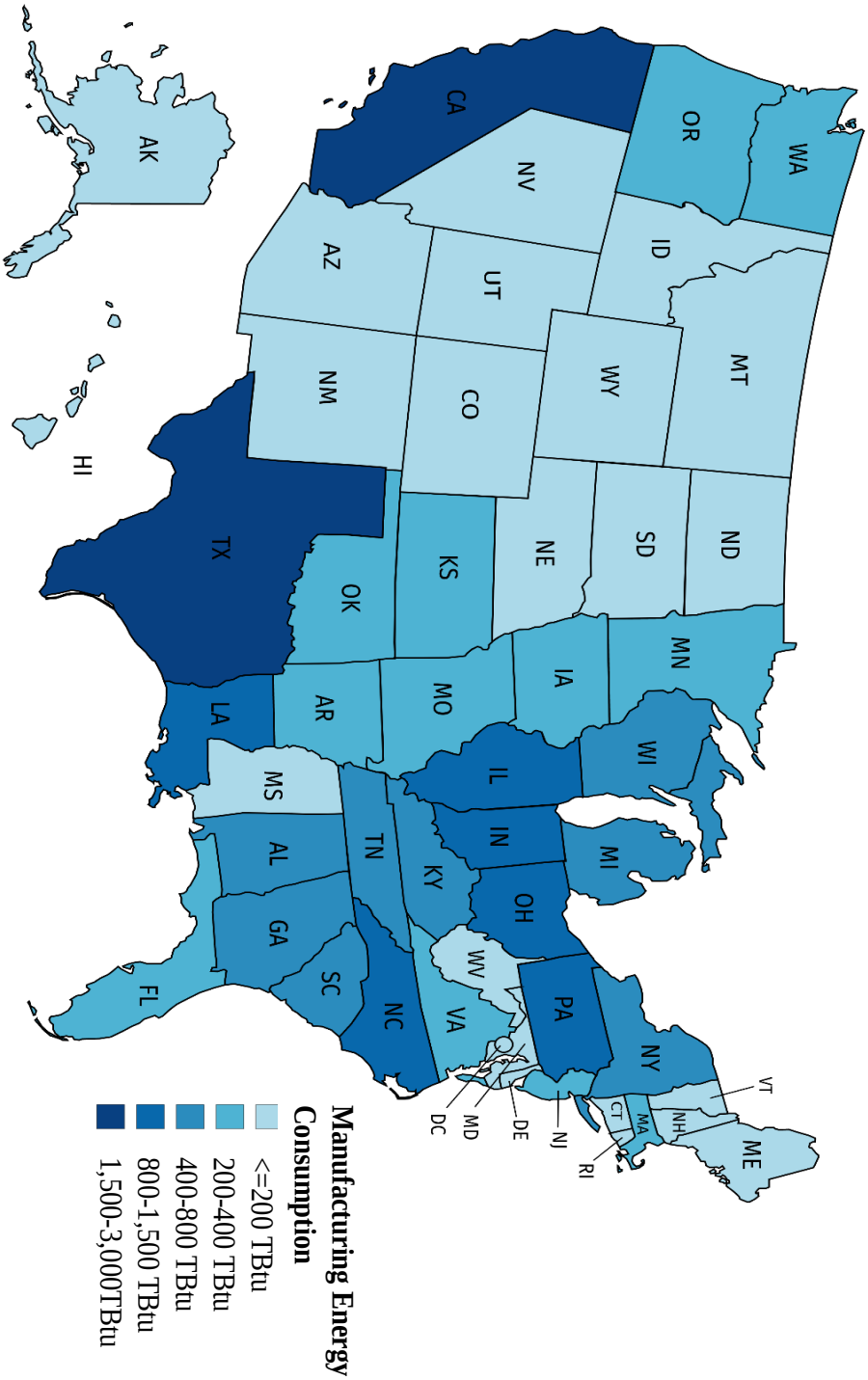

Figure 6.2. Manufacturing energy consumption map.

Table 6.3. Manufacturing-sector-based energy consumption and total value of shipment in the U.S. and State of MI in 2012

Variable	Alumina and Aluminum	Cement	Chemical	Electronics and computer
γ (TBtu)	603	471	4,513	527
φ ($1,000)	37,652,496	5,894,830	785,299,730	437,205,393
θ ($1,000)	1,176,722	N/A	16,352,747	7,966,689
B (TBtu)	18.85	N/A	93.98	9.6
Variable	Fabricated Metals	Food and Beverage	Forest Products	Foundries
γ (TBtu)	708	1,934	3,559	281
φ ($1,000)	339,926,995	881,507,355	258,733,912	31,894,334
θ ($1,000)	16,655,933.00	6,490,399	7,386,782	2,863,907
B (TBtu)	34.69	14.24	101.61	25.23
Variable	Glass	Iron and Steel	Machinery	Petroleum Refining
γ (TBtu)	466	1,481.00	444	3,546
φ ($1,000)	28,080,825	138,505,940	402,177,024	801,904,517
θ ($1,000)	1,806,216	6,490,399	20,440,978	N/A
B (TBtu)	29.97	69.4	22.57	N/A
Variable	Plastics	Textiles	Transportation Equipment	
γ (TBtu)	729	472	904	
φ ($1,000)	218,571,414	69,567,122	785,685,996	
θ ($1,000)	11,233,740	499,694	104,074,154	
B (TBtu)	37.47	3.39	119.75	

Table 6.4. Manufacturing-sector-based energy consumption in State of MI in 2012

System Type	Alumina and Aluminum	Cement	Chemical	Electronics and computer	Fabricated Metals	Food and Beverage	Forest Products	Foundries
Process system (TBtu)								
Process heating	3.16	N/A	26.40	0.93	9.85	4.08	31.46	9.52
Process cooling	0.09	N/A	2.21	0.24	0.29	0.77	1.14	0.09
Other process uses	0.13	N/A	2.96	0.20	0.49	0.40	2.00	0.18
Electro-chemical	3.75	N/A	2.02	0.04	0.15	0.00	0.14	0.18
Machine drive & machine driven systems	0.69	N/A	12.18	0.66	3.53	1.24	14.96	1.62
Non-process system								
Facility HVAC	0.28	N/A	3.39	1.33	3.18	0.78	4.34	1.80
Facility lighting	0.09	N/A	0.54	0.29	0.69	0.16	0.66	0.27
Other facility support	0.06	N/A	0.25	0.15	0.24	0.12	0.20	0.18
Onsite transportation	0.03	N/A	0.08	0.05	0.15	0.04	0.66	0.09
Other non-processes	0.03	N/A	1.00	0.07	0.05	0.13	1.43	0.00

System Type	Glass	Iron and Steel	Machinery	Petroleum Refining	Plastics	Textiles	Transportation Equipment
Process system (TBtu)							
Process heating	16.40	33.88	1.88	N/A	5.19	0.71	15.50
Process cooling	0.13	0.05	0.15	N/A	0.82	0.09	2.25
Other process uses	0.39	1.31	0.36	N/A	0.51	0.06	5.83
Electro-chemical	0.00	0.42	0.00	N/A	0.00	0.00	0.26
Machine drive & machine driven systems	1.87	5.25	2.85	N/A	4.93	0.40	10.46
Non-process system							
Facility HVAC	1.61	3.14	3.25	N/A	2.88	0.28	19.74
Facility lighting	0.26	0.37	0.81	N/A	0.82	0.06	3.84
Other facility support	0.00	0.09	0.25	N/A	0.36	0.01	1.46
Onsite transportation	0.00	0.14	0.10	N/A	0.15	0.01	0.66
Other non-processes	0.06	0.09	0.15	N/A	0.05	0.01	0.26

Energy loss estimation. Energy loss calculation is completed using Table 6.2 data and Eqs. 6.13-6.17. According to ACEEE (2012), MI's ranking on energy efficiency is 12 in the nation. This ranking number is the value of R_s in Eq. 6.13. Table 6.5 shows the manufacturing-sector-based energy loss percentage in MI in 2012, while Table 6.6 lists the detailed process and non-process energy loss in different manufacturing sectors in MI, which is calculated using the data in Tables 6.2, 6.4, and 6.5 and Eqs. 6.14-6.15. Comparison of the corresponding values in Table 6.2 (for the U.S.) and Table 6.5 (for MI) shows MI's energy loss in each manufacturing sector is clearly less than the national average. The total amount of direct energy loss in MI's manufacturing sector ($EL^{s,tot}$) is 132.06 TBtu, which includes the process energy loss of 108.42 TBtu (i.e., 17.7% of the total energy consumption or 41.3% of the process energy consumption), and the non-process energy loss of 23.64 TBtu (i.e., 3.9% of the total energy consumption or 35.3% of the non-process energy consumption).

CO_2 emission estimation. The energy footprint analysis is completed by the analysis of energy-related CO_2 emission of manufacturing sectors at the state level. Using Eqs. 6.7 and 6.18-6.20, the total energy-related CO_2 emission for each sector in MI is estimated, and the same approach is used for estimation in other states. The estimation results are plotted in Fig. 6.3. The summarized estimation shows that in 2012, the total manufacturing combustion (energy-related CO_2) emission of all 51 states was 1,134 MMT CO_2e, which shows 10% difference as compared to the value from the national reported, which does not contain any state-based manufacturing sector specific information on CO_2 emission (U.S. DOE, 2012). Thus, the estimation by the introduced methodology is quite satisfactory.

Table 6.5. Manufacturing-sector-based energy loss percentage in MI in 2012

System Type	Alumina and Aluminum	Cement	Chemical	Electronics and computer	Fabricated Metals	Food and Beverage	Forest Products	Foundries
Process system								
Process heating	43.43	34.29	18.92	32.04	32.52	57.75	55.02	43.81
Process cooling	28.67	0.00	30.02	33.08	28.67	30.30	30.10	0.00
Other process uses	0.00	0.00	8.48	7.82	8.60	9.38	8.60	0.00
Electro-chemical	51.60	0.00	51.42	43.00	57.33	0.00	51.60	43.00
Machine drive & machine driven systems	39.09	66.15	62.33	52.56	53.75	56.31	50.06	43.00
Non-process system								
Facility HVAC	28.67	21.50	30.07	29.45	30.43	30.02	29.99	30.10
Facility lighting	86.00	86.00	76.08	75.25	73.71	78.18	78.52	86.00
Other facility support	0.00	0.00	7.17	10.75	17.20	10.75	12.29	0.00
Onsite transportation	86.00	43.00	43.00	57.33	57.33	51.60	52.35	86.00
Other non-processes	0.00	0.00	8.96	0.00	0.00	10.12	8.60	0.00

System Type	Glass	Iron and Steel	Machinery	Petroleum Refining	Plastics	Textiles	Transportation Equipment
Process system							
Process heating	48.23	43.89	32.54	15.47	18.73	58.20	32.34
Process cooling	43.00	86.00	28.67	32.25	32.25	28.67	30.35
Other process uses	14.33	9.21	12.29	8.84	8.60	9.56	7.82
Electro-chemical	0.00	57.33	0.00	0.00	0.00	0.00	43.00
Machine drive & machine driven systems	53.38	41.46	53.75	57.14	53.75	54.73	53.34
Non-process system							
Facility HVAC	30.9	30.81	30.91	29.37	30.71	30.87	30.01
Facility lighting	86.00	75.25	75.25	86.00	75.25	76.44	77.10
Other facility support	0.00	0.00	17.20	0.00	12.29	0.00	7.82
Onsite transportation	0.00	57.33	43.00	86.00	57.33	86.00	51.60
Other non-processes	0.00	0.00	0.00	7.17	0.00	0.00	0.00

Table 6.6. Manufacturing-sector-based energy loss in MI in 2012

System Type	Alumina and Aluminum	Cement	Chemical	Electronics and computer	Fabricated Metals	Food and Beverage	Forest Products	Foundries
Process system (TBtu)								
Process heating	1.37	N/A	5.00	0.30	3.20	2.36	17.31	4.17
Process cooling	0.03	N/A	0.66	0.08	0.08	0.23	0.34	0.00
Other process uses	0.00	N/A	0.25	0.02	0.04	0.04	0.17	0.00
Electro-chemical	1.94	N/A	1.04	0.02	0.08	0.00	0.07	0.08
Machine drive & machine driven systems	0.27	N/A	7.59	0.34	1.90	0.70	7.49	0.70
Non-process system (TBtu)								
Facility HVAC	0.08	N/A	1.02	0.39	0.97	0.23	1.30	0.54
Facility lighting	0.08	N/A	0.41	0.22	0.51	0.13	0.52	0.23
Other facility support	0.00	N/A	0.02	0.02	0.04	0.01	0.02	0.00
Onsite transportation	0.03	N/A	0.04	0.03	0.08	0.02	0.34	0.08
Other non-processes	0.00	N/A	0.09	0.00	0.00	0.01	0.12	0.00

System Type	Glass	Iron and Steel	Machinery	Petroleum Refining	Plastics	Textiles	Transportation Equipment
Process system (TBtu)							
Process heating	7.91	14.87	0.61	N/A	0.97	0.41	5.01
Process cooling	0.06	0.04	0.04	N/A	0.27	0.02	0.68
Other process uses	0.06	0.12	0.04	N/A	0.04	0.01	0.46
Electro-chemical	0.00	0.24	0.00	N/A	0.00	0.00	0.11
Machine drive & machine driven systems	1.00	2.18	1.53	N/A	2.65	0.22	5.58
Non-process system (TBtu)							
Facility HVAC	0.50	0.97	1.01	N/A	0.88	0.09	5.92
Facility lighting	0.22	0.28	0.61	N/A	0.62	0.05	2.96
Other facility support	0.00	0.00	0.04	N/A	0.04	0.00	0.11
Onsite transportation	0.00	0.08	0.04	N/A	0.09	0.01	0.34
Other non-processes	0.00	0.00	0.00	N/A	0.00	0.00	0.00

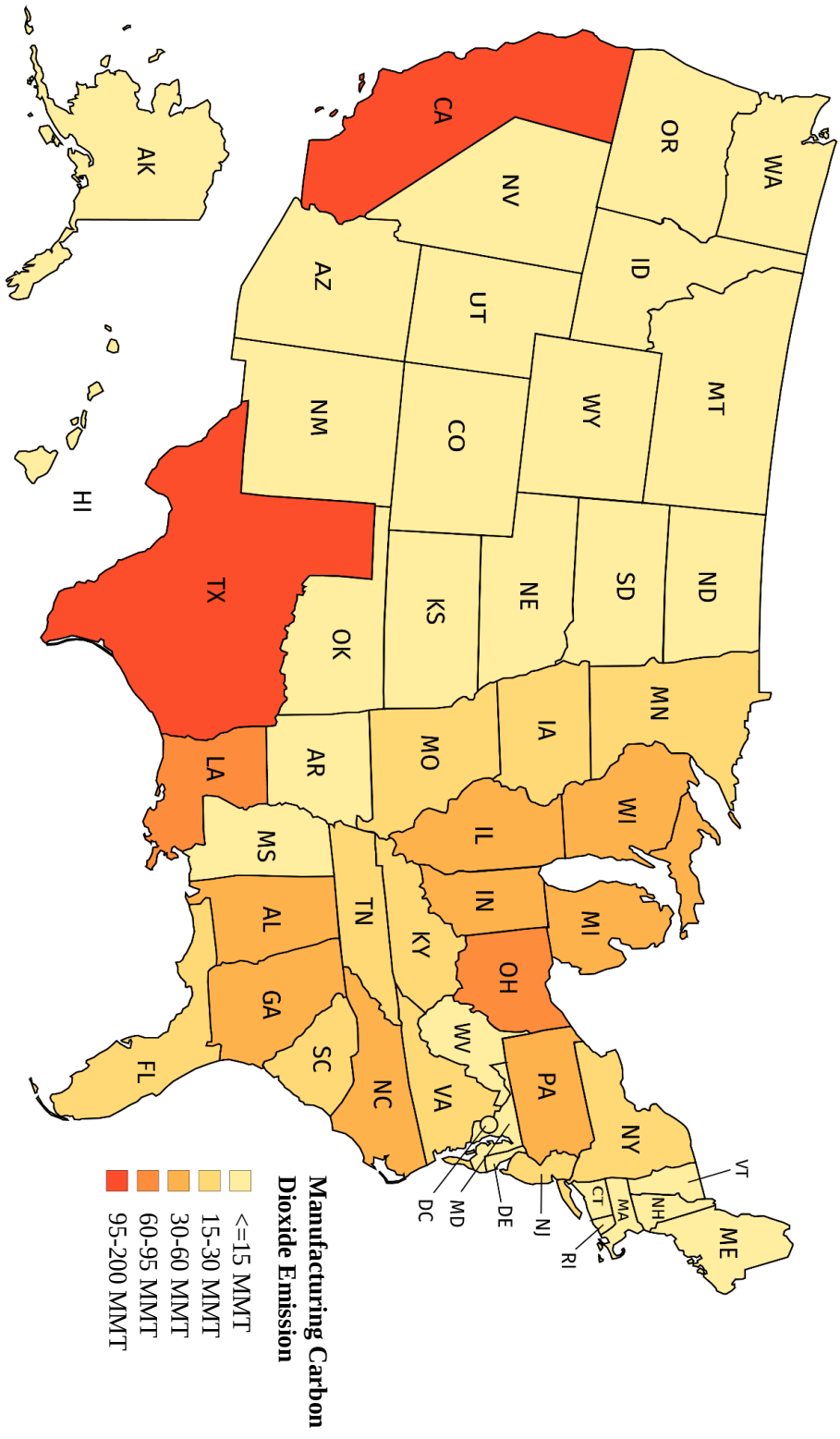

Figure 6.3. Manufacturing carbon dioxide emission map.

County-level energy analysis. Sector-based energy consumption at the county level can be estimated using Eqs. 6.21-6.22, and the total energy consumption of all manufacturing sectors in a county using Eq. 6.23 (see Fig. 6.4). In this case study, as we have selected the state of Michigan (MI) at the state level estimation, the counties of MI are used in our calculation. The state has 83 counties. The sector-based direct energy loss of each county is calculated using Eqs. 6.24-6.26. In Michigan, the three most energy-intensive counties are Wayne County, Oakland County, and Macomb County, and the numbers of manufacturing establishments in these counties are 1,483, 1,669, and 1,593, respectively (USCS, Table EC1231SA1). Table 6.7 shows the total values of SSR of the eight main manufacturing sectors in these counties (USCS, Table EC1231A1), while Table 6.8 gives the estimated energy consumption and direct energy loss of each of the eight manufacturing sectors in these counties. The CO_2 emission estimations for the state as well as the eight manufacturing sectors of the three countries are shown in Table 6.9. The total manufacturing energy consumption, energy loss, and energy-related CO_2 emission of the three counties are shown in Fig. 6.5. Note that the same approach was used to generate estimations of energy consumption and energy loss in seven other manufacturing sectors; the estimation result is omitted here.

Table 6.7. Total value of shipment for manufacturing sectors in three energy intensive counties in MI

Region	Chemical	Electronics and Computer	Fabricated Metals	Food and Beverage
	Total Value of shipment- ω ($1000)	Total Value of shipment- ω ($1000)	Total Value of shipment- ω ($1000)	Total Value of shipment- ω ($1000)
Wayne	1,907,458	1,099,542	2,077,699	859,989
Oakland	1,219,885	1,045,018	2,138,317	N/A
Macomb	760,934	277,267	2,398,485	92,176
Region	Forest Products	Machinery	Plastics	Transportation Equipment
	Total Value of shipment- ω ($1000)	Total Value of shipment- ω ($1000)	Total Value of shipment- ω ($1000)	Total Value of shipment- ω ($1000)
Wayne	441,938	3,282,221	861,696	34,981,849
Oakland	89,144	3,992,381	846,207	6,693,498
Macomb	56,699	2,630,031	996,818	18,696,841

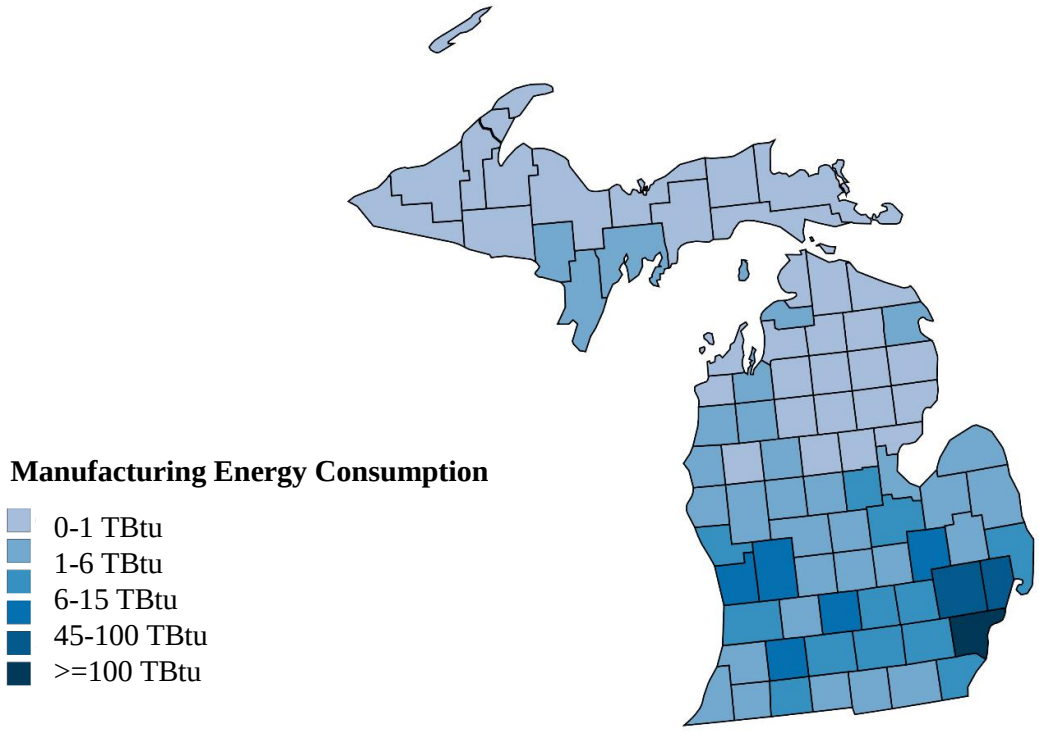

Figure 6.4. Manufacturing energy consumption in counties of Michigan.

Table 6.8. Manufacturing-sector-based energy consumption and direct loss in three energy intensive counties in MI

Region	Chemical		Electronics and Computer	
	EC_C (TBtu)	EL_C (TBtu)	EC_C (TBtu)	EL_C (TBtu)
Wayne	10.96	1.88	1.33	0.19
Oakland	7.01	1.2	1.26	0.19
Macomb	4.37	0.75	0.33	0.05
Region	Fabricated Metals		Food and Beverage	
	EC_C (TBtu)	EL_C (TBtu)	EC_C (TBtu)	EL_C (TBtu)
Wayne	4.33	0.86	1.89	0.49
Oakland	4.45	0.89	N/A	N/A
Macomb	5	1	0.2	0.05
Region	Forest Products		Machinery	
	EC_C (TBtu)	EL_C (TBtu)	EC_C (TBtu)	EL_C (TBtu)
Wayne	6.08	1.66	3.62	0.63
Oakland	1.23	0.33	4.41	0.77
Macomb	0.78	0.21	2.9	0.51
Region	Plastics		Transportation Equipment	
	EC_C (TBtu)	EL_C (TBtu)	EC_C (TBtu)	EL_C (TBtu)
Wayne	2.87	0.43	40.25	7.12
Oakland	2.82	0.42	7.7	1.36
Macomb	3.32	0.49	21.51	3.81

Table 6.9. Carbon dioxide emission of MI and three counties with respect to manufacturing sectors

Sector/Region	Michigan (MMT)	Wayne (MMT)	Oakland (MMT)	Macomb (MMT)
Chemical	5.73	0.67	0.43	0.27
Electronics and Computer	0.56	0.08	0.07	0.02
Fabricated Metals	2.01	0.25	0.26	0.29
Food and Beverage	0.86	0.11	0	0.01
Forest Products	4	0.24	0.05	0.03
Machinery	1.32	0.21	0.26	0.17
Plastics	2.26	0.17	0.17	0.2
Transportation Equipment	7.02	2.36	0.45	1.26
Total	32.67	7.74	2.52	3.69

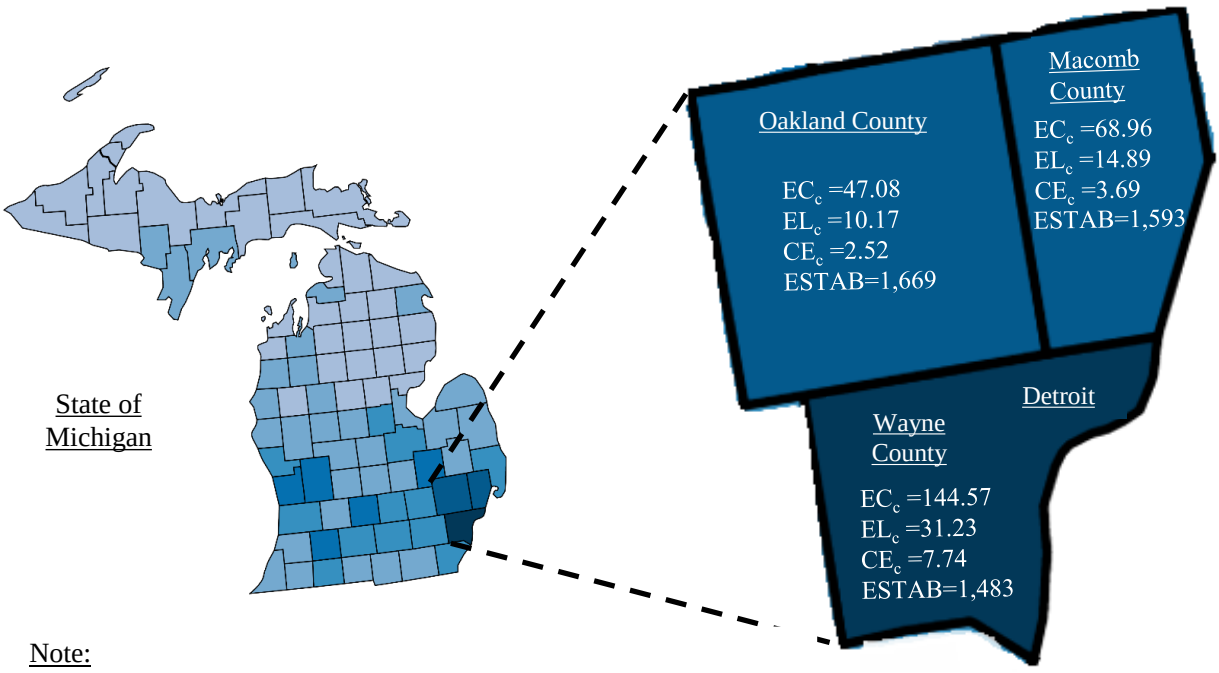

Note:
EC_c =Manufacturing Energy Consumption (TBtu)
EL_c =Manufacturing Energy Loss-Direct use(TBtu)
CE_c =Manufacturing Energy-Related CO_2 Emission (MMT)
ESTAB= No. of Manufacturing Establishments (year 2012)

Figure 6.5. Energy consumption, energy loss, and carbon dioxide emission of three energy intensive counties in MI.

6.3 Summary

Energy efficiency in the manufacturing industry is continuously one of the most critical factor in energy sustainability and thus the nation's economic, environmental, and social sustainability. A variety of energy and related CO_2 emission information and data are openly accessible, which were generated with possibly different purposes, under different assumptions, focusing on different time periods, and by different organizations. Integrated use of the accessible information could generate very valuable information on energy and CO_2 footprint in the geographical regions of interest.

In this chapter, we have introduced a simple, general energy efficiency and CO_2 emission analysis method for energy use performance estimation in manufacturing industries in different

geographical regions. The case study has demonstrated methodological efficacy, as we are able to identify the performance of different manufacturing sectors in terms of the amount of energy used and lost in various energy-consuming systems, and CO_2 emission of individual state and thus county in the U.S. The study has been also applied to the state of Michigan and its counties, which has provided a better insight for the possible improvement directions.

CHAPTER 7 CONCLUSIONS AND FUTURE WORK

In this chapter, the dissertation objectives and the contributions are summarized in the first section. Recommendations for the possible extension of this research and future work is discussed in the second part.

7.1 Conclusions

Improvement of energy efficiency in process systems has been always a key concern in the chemical process industry. However, the recovery of mechanical energy, as compared to thermal energy recovery, has not received sufficient attention. This renders a research need on work integration through designing WEN for chemical plants.

This research has focused on the recovery of mechanical energy using work exchangers that were introduced by Cheng *et al*. (1967). A general review of the current research progress is provided, together with a basic thermodynamic analysis on work exchange, the challenges and opportunities. This facilitates the introduction of a mathematical modeling and analysis method which aims at predicting the maximum amount of mechanical energy that can be feasibly recovered using work exchangers.

The thermodynamic modeling and analysis method is a general tool to predict the maximum amount of mechanical energy recoverable by a WEN prior to network synthesis for any design problem. The methodology referred to as prediction stage can be easily modified based on the operation condition, phase, and also when combined with a heat or mass exchange network. The modification does not change the structure of the methodology and only the shaft work formulation will differ.

Using the mathematical framework provided in the prediction stage, the work exchange network synthesis can be completed by the set of matrices and vectors which identify the placement of work exchangers, utility compressors and expanders if needed. Similar to the

prediction stage, the formulation is general and can be extended to different operating conditions, assumptions, and energy calculations. Note that the temperature will change through the pressurization and depressurization processes when dealing with gas phase streams. Through the process of compression, temperature increases, which means that heat will be added to the system, and temperature decreases through the expansion, which means that heat will be consumed. In addition, the energy required for compression decreases while the stream that goes through pressurization has a lower temperature, and the energy provided through expansion increases while the stream has a higher temperature. Therefore, due to the pressure and temperature correlation in pressurization and depressurization, heat integration would play a key role in cases under non-isothermal conditions. In fact, heat integration would be required for these cases not only for thermal energy recovery but also for improving the amount of mechanical energy that can be recovered. In Chapter 4, the integration of a heat exchanger network (HEN) into the work exchanger network synthesis is discussed and it has been shown that the location of the HEN will impact the amount of thermal and mechanical energy recovery. In the presented framework, the final location of the HEN is assigned based on the lowest operating cost which reflects the design with lower utility consumption. The methodological efficacy is illustrated by case studies, where both mechanical and thermal energy efficiencies as well as an economic feasibility analysis are provided.

In this study, a direct work exchanger has been considered as the mechanical energy recovery device for the development of work exchange network synthesis. This unit was introduced for reverse osmosis processes and has been used in the desalination industry due to its distinctive performance. However, the device has not been considered for mechanical energy recovery in other industries such as the chemical and petrochemical industries. Different

characteristics of the chemical processes require investigation into the operational flexibility of the unit, and challenges related to the unit safety. In Chapters 2-4, we discussed the piston-type direct work exchanger's fundamentals, and introduced a thermodynamic analysis approach to design a work exchange network synthesis using the direct work exchangers in chemical processes. While the feasibility of using these units has been shown by significant improvements in mechanical energy recovery of process systems, how these units can be implemented in real industrial processes is still under investigation. Due to lack of computational and experimental studies on piston-type direct work exchangers operated by gas phase streams, we have conducted research on modeling of the unit using simulation software. The customized model has been generated by Aspen Plus simulation software which helps us to add the work exchanger to the Aspen Plus unit operations library and be able to simulate the synthesized work exchange network using direct work exchangers, compressors, and expanders. This will ensure the design feasibility and optimum operating conditions. The model formulation can be easily modified in the future as the piston-type work exchanger develops. Computational Fluid Dynamics (CFD) modeling has been studied for better understating of the operational behavior of the unit. We have been able to plot the four operation stages of pressurization and depressurization in terms of piston motion, high-pressure and low-pressure streams pressure profiles, and valve positions. In addition, the performance of a unit under various operating conditions such as pressure and temperature is investigated. This is a significant accomplishment towards modification of the piston-type work exchangers dealing with gas phase streams.

Energy efficiency in manufacturing systems becomes increasingly critical in energy sustainability due to a trend toward the depletion of non-renewable resources and the challenges owing to carbon dioxide (CO_2) emission. For better evaluation of energy consumption in

manufacturing industries, various energy consumption-related databases have been created by a number of research studies and government agencies. However, a general methodology to study the energy efficiency of manufacturing sectors in various geographical scales is not available. In Chapter 6, we proposed a general data-driven methodology for energy efficiency and CO_2 emission analysis of manufacturing sectors in different geographical scopes. The analysis method can be used as a baseline to identify the performance of different manufacturing sectors in terms of the amount of energy that will be used or lost for various systems, and the combustion emission of each state across the U.S. and its counties. The study has been also applied to the state of Michigan as a case study and its counties to have a better insight on improvement directions and to support the future of the energy advancement in industries. Future analysis will look to further combine the methodology with decision making modules for energy efficiency improvement in different geographical areas.

7.2 Future Work

The dissertation establishes a solid knowledge foundation for the research related to mechanical energy recovery through a work exchange network synthesis approach. This section discusses the possible extension of this research for future development.

Optimization-based heat integrated work exchange network synthesis. The superstructure-based framework has been considered in heat exchanger network synthesis by the chemical industries to find the local optimum design and for more complicated problems. A superstructure-based simultaneous heat and work exchange network has been also studied using SSTC compressors and turbines counted as the indirect work exchangers. This framework can be also extended for designs in which direct work exchangers are implemented. The direct work exchangers show a unique performance for mechanical energy recovery, and their feasibility for

work exchange network design has been demonstrated by the thermodynamic modeling approach. Even though the energy targeting methodology and sequential flowsheet development generate a WEN with the maximum energy recovery, the optimality of the design is not guaranteed. Thus, development of superstructure methods to solve the heat and work exchange network synthesis problems simultaneously and to find the optimum design is suggested. The objective function can be taken as a minimization of the total annualized cost. In the following, the initial mathematical formulation of a MINLP model regarding WEN synthesis is shown. However, comprehensive study is still required to complete the mathematical formulation.

Decision variables can be stated as:

$P_{i,k}$, $P_{j,k}$ = pressure of each HP and LP stream after each match

W_{ijk}= workload of each work exchanger between HP and LP streams at stage k

$W_{HPu,j}$= workload of HP external utility

$W_{LPu,\,i}$ = workload of LP external utility

$$z_{ijk} = \begin{cases} 1 \text{ if there is a work exchanger between stream i and j in stage k} \\ 0 \text{ if there is not a work exchanger between stream i and j in stage k} \end{cases}$$

$$z_{Hu,j} = \begin{cases} 1 \text{ if there is a HP utility for stream j} \\ 0 \text{ if there is not a HP utility for stream j} \end{cases}$$

$$z_{Lu,i} = \begin{cases} 1 \text{ if there is a LP utility for stream i} \\ 0 \text{ if there is not a LP utility for stream i} \end{cases}$$

The objective function can be written as:

Minimize

$$C_{TAC} = \sum_{i=1}^{I}\sum_{j=1}^{J}\sum_{k=1}^{K} CF_{ij}\, z_{ijk} + \sum_{i=1}^{I} CF_{i,LPu}\, z_{Lu,i} + \sum_{j=1}^{J} CF_{j,HPu} z_{Hu,j} + \sum_{i=1}^{I}\sum_{j=1}^{J}\sum_{k=1}^{K} C_{ij}\left(S_{ij}\right) + \sum_{i=1}^{I} C_{i,LPu}\left(S_{i,LPu}\right) + \sum_{j=1}^{J} C_{j,HPu}\left(S_{j,HPu}\right) + \sum_{i=1}^{I} CLu\left(W_{LPu,i}\right) + \sum_{j=1}^{J} CHu\left(W_{HPu,j}\right) \tag{7.1}$$

Subject to:

$$S_{ij} = f_1(W_{ij}) \tag{7.2}$$

$$W_{ij} = f_2\left(V_i, V_j, P_{ik}, P_{jk}\right) \tag{7.3}$$

$$S_{i,LPu} = f_3(W_{LPu,i}) \tag{7.4}$$

$$W_{LPu,i} = f_4(V_i, P_{ik}, P_i^s, P_i^t) \tag{7.5}$$

$$S_{j,HPu} = f_5(W_{HPu,j}) \tag{7.6}$$

$$W_{HPu,j} = f_6(V_j, P_{jk}, P_j^s, P_j^t) \tag{7.7}$$

where

I: number of HP process streams

J: number of LP process streams

K: index for stage, and pressure location

LPu: low-pressure utility

HPu: high-pressure utility

P^s, P^t: source and target pressure

ΔP_{min}: minimum approach pressure difference

V_i, V_j: volumetric flowrates

CLu: per unit cost of LP utility

Chu: per unit cost of HP utility

CF_{ij}, $CF_{i,\,LPu}$, $CF_{j,\,HPu}$: fixed charges for exchangers

C_{ij}, $C_{i,\,LPu}$, $C_{j,\,HPu}$: cost coefficient

S_{ij}, $S_{i,\,LPu}$, $S_{j,\,HPu}$: size factors of exchangers

The feasibility constraints, work balance at each stage, should be added later to complete the mathematical formulation to solve the problem using appropriate optimization software. It is suggested that the optimization be completed under isothermal conditions first to investigate the work exchanger formulation feasibility, and then the non-isothermal conditions should be considered for development of the heat integrated WEN synthesis superstructure. In addition, phase behavior correlation of each high-pressure and low-pressure stream should be considered.

Development of appropriate user interface for work exchange network synthesis. In Chapters 3 and 4, a mathematical formulation was presented which will predict the maximum amount of mechanical energy that can be recovered and will provide the information regarding the placement of work exchangers, external compressors, and external expanders through a set of matrices and vectors. The formulation for the prediction stage has been developed in MATLAB which will help users to easily calculate the amount of energy that can be recovered for a case study of any size. However, it is recommended to develop a graphical user interface for the coded methodology using the appropriate compiler. This will help users, especially industry, to investigate work exchange network synthesis in processes in which mechanical energy is being wasted and quickly define the feasibility and profitability of the technology.

CFD modeling verification by experiment. In Chapter 5, a preliminary investigation into the operational behavior of piston-type work exchangers operated by gas phase streams was presented. However, there are still different unit configurations that should be studied. The main areas that the modeling should be extended can be summarized as: possible phase change through

the pressurization and depressurization of working fluids, dealing with different fluid domains at each side of the piston, and non-reversible behavior of the compression and expansion due to friction loss between the piston ring and the cylinder wall which will impact the shaft work formulation. Working alongside IC engine experts will help to integrate the modeling for possible manufacturing of the unit at the laboratory and pilot scale. This will help to address challenges related to energy recovery of the device from the unit-based to network-based scale and will be a beginning for commercializing the piston-type work exchangers operated by gas phase streams in the chemical and petrochemical industry.

Minimum pressure difference optimization. After conducting the CFD modeling, we found that how the pressure difference between two sides of the piston will impact the piston speed of movement and the operational cycle. Previously, Cheng *et al.* (1967) analyzed the flow work exchanger performance for reverse osmosis and concluded that the minimum pressure difference for the piston motion should between 35 kPa to 70 kPa. This range could be significantly different while dealing with different processes, working fluids with various compression ratios, and also with the size and the materials used to manufacture the unit component parts. Thus, the minimum pressure difference should be studied and optimized later using the results from the modeling and pilot study validation.

APPENDICES

Appendix A

Appendix A contains the step-by-step derivation of matrices $\overline{\boldsymbol{\Gamma}}$ and $\overline{\boldsymbol{P}}$ using the flowchart shown in Fig. 3.1 and Eqs. 3.3-3.7 for a case study from the Huang and Fan (1996) work.

Table A-1. Streams data for a case study from Huang and Fan (1996)

Stream No.	P^s (MPa)	P^t (MPa)	V (m^3/s)
H_1	5.72	2.21	0.099
H_2	3.10	0.26	0.076
L_1	1.72	3.10	0.083
L_2	0.10	2.21	0.050
L_3	0.51	5.72	0.073

For this case study with two high-pressure streams and three low-pressure streams:

$N_H = 2;\ N_L = 3$

Construct matrix $\overline{\boldsymbol{\Gamma}}$

In this case study $\overline{\boldsymbol{\Gamma}}$ is a (2×3) matrix and $\Delta P_{\min}$ is assumed to be 0.07 MPa. Each element of $\overline{\boldsymbol{\Gamma}}$ is constructed using the flowchart shown in Figure 2.

$$\overline{\boldsymbol{\Gamma}} = \begin{pmatrix} \overline{\Gamma}_{H_1,L_1} & \overline{\Gamma}_{H_1,L_2} & \overline{\Gamma}_{H_1,L_3} \\ \overline{\Gamma}_{H_2,L_1} & \overline{\Gamma}_{H_2,L_2} & \overline{\Gamma}_{H_2,L_3} \end{pmatrix} \tag{A-1}$$

For $\overline{\Gamma}_{H_1,L_1} = \left[\Gamma^a_{H_1,L_1}, \Gamma^b_{H_1,L_1}\right]$:

Calculation of $\Gamma^a_{H_1,L_1}$

$$P^s_{L_1} < P^t_{H_1} + 0.07 \tag{A-2}$$

$$1.72 < 2.21 + 0.07 \ \Rightarrow \text{Yes} \tag{A-3}$$

and

$$P^s_{L_1} < P^t_{H_1} + 0.07 < P^t_{L_1} \tag{A-4}$$

$$1.72 < 2.21 + 0.07 < 3.10 \Rightarrow \text{Yes} \tag{A-5}$$

Then,

$$\begin{aligned} \Gamma^{a}_{H_1,L_1} &= P^{t}_{H_1} + 0.07 \\ &= 2.28 \text{ MPa} \end{aligned} \tag{A-6}$$

Calculation of $\Gamma^{b}_{H_1,L_1}$

$$P^{s}_{H_1} < P^{t}_{L_1} + 0.07 \tag{A-7}$$

where

$$5.72 < 3.10 + 0.07 \Rightarrow \text{NO} \tag{A-8}$$

Then,

$$\begin{aligned} \Gamma^{b}_{H_1,L_1} &= P^{t}_{L_1} \\ &= 3.10 \text{ MPa} \end{aligned} \tag{A-9}$$

Then,

$$\overline{\Gamma}_{H_1,L_1} = [2.28, 3.10] \tag{A-10}$$

For $\overline{\Gamma}_{H_2,L_1} = [\Gamma^{a}_{H_2,L_1}, \Gamma^{b}_{H_2,L_1}]$:

Calculation of $\Gamma^{a}_{H_2,L_1}$

$$P^{s}_{L_1} < P^{t}_{H_2} + 0.07 \tag{A-11}$$

$$1.72 < 0.26 + 0.07 \Rightarrow \text{No} \tag{A-12}$$

Then,

$$\begin{aligned} \Gamma^{a}_{H_2,L_1} &= P^{s}_{L_1} \\ &= 1.72 \text{ MPa} \end{aligned} \tag{A-13}$$

Calculation of $\Gamma^{b}_{H_2,L_1}$

$$P^{s}_{H_2} < P^{t}_{L_1} + 0.07 \tag{A-14}$$

where

$$3.10 < 3.10 + 0.07 \Rightarrow \text{Yes} \tag{A-15}$$

and

$$P_{L_1}^s < P_{H_2}^s - 0.07 < P_{L_1}^t \tag{A-16}$$

$$1.72 < 3.10 - 0.07 < 3.10 \Rightarrow \text{Yes} \tag{A-17}$$

Then,

$$\begin{aligned} \Gamma_{H_2,L_1}^b &= P_{H_2}^s - 0.07 \\ &= 3.03 \text{ MPa} \end{aligned} \tag{A-18}$$

Then,

$$\overline{\Gamma}_{H_2,L_1} = [1.72, 3.03] \tag{A-19}$$

For $\overline{\Gamma}_{H_1,L_2} = \left[\Gamma_{H_1,L_2}^a, \Gamma_{H_1,L_2}^b\right]$

Calculation of Γ_{H_1,L_2}^a

$$P_{L_2}^s < P_{H_1}^t + 0.07 \tag{A-20}$$

$$0.10 < 2.21 + 0.07 \Rightarrow \text{Yes} \tag{A-21}$$

and

$$P_{L_2}^s < P_{H_1}^t + 0.07 < P_{L_2}^t \tag{A-22}$$

$$0.10 < 2.21 + 0.07 < 2.21 \Rightarrow \text{No} \tag{A-23}$$

Then,

$$\Gamma_{H_1,L_2}^a = 0 \tag{A-24}$$

Calculation of Γ_{H_1,L_2}^b

$$P_{H_1}^s < P_{L_2}^t + 0.07 \tag{A-25}$$

where

$$5.72 < 2.21 + 0.07 \Rightarrow \text{No} \tag{A-26}$$

Then,

$$\Gamma^{b}_{H_1,L_2} = 0 \tag{A-27}$$

and

$$\overline{\Gamma}_{H_1,L_2} = [0,0] \tag{A-28}$$

Going through the same procedure, matrix $\overline{\boldsymbol{\Gamma}}$ will be constructed.

$$\overline{\boldsymbol{\Gamma}} = \begin{pmatrix} [2.28,3.10] & [0,0] & [2.28,5.65] \\ [1.72,3.03] & [0.33,2.21] & [0.51,3.03] \end{pmatrix} \tag{A-29}$$

Construct matrix $\overline{\boldsymbol{P}}$

$$\overline{\boldsymbol{P}} = \begin{pmatrix} \overline{P}_{H_1,L_1} & \overline{P}_{H_1,L_2} & \overline{P}_{H_1,L_3} \\ \overline{P}_{H_2,L_1} & \overline{P}_{H_2,L_2} & \overline{P}_{H_2,L_3} \end{pmatrix}, \tag{A-30}$$

and $k \le |1|$ but $k \neq 0$ and $0 < (i+k) \le 2$.

For $\overline{P}_{H_1,L_1} = \left[P^{a}_{H_1,L_1}, P^{b}_{H_1,L_1}\right]$:

where $j=1; i=1; k=1 \Rightarrow 0 < (1+1) \le 2$ OK

$$\overline{P}^{1}_{H_1,L_1} = \begin{cases} \overline{\Gamma}_{H_1,L_1}; & \text{if } V_{H_1} > V_{H_2} \\ \overline{\Gamma}_{H_1,L_1} \cap \overline{\overline{\Gamma}_{H_1,L_1} \cap \overline{R}_{(H_1,L_1)\to(H_2,L_1)}}; & \text{otherwise} \end{cases} \tag{A-31}$$

and

$$V_{H_1} = 0.099 \ m^3/s; V_{H_2} = 0.0763 \ m^3/s \tag{A-32}$$

Then,

$$\begin{aligned}\overline{P}^{1}_{H_1,L_1} &= \overline{\Gamma}_{H_1,L_1} \\ &= [2.28, 3.10]\end{aligned} \tag{A-33}$$

where $j=1; i=1; k=-1$ => $0<(1+-1)\leq 2$ will not be met.

Then,

$$\overline{P}^{-1}_{H_1,L_1} \text{ does not exist} \tag{A-34}$$

and

$$\begin{aligned}\overline{P}_{H_1,L_1} &= \cap\left(\overline{P}^{1}_{H_1,L_1}, \overline{P}^{-1}_{H_1,L_1}\right) \\ &= [2.28, 3.10]\end{aligned} \tag{A-35}$$

For $\overline{P}_{H_2,L_1} = \left[P^{a}_{H_2,L_1}, P^{b}_{H_2,L_1}\right]$:

where $j=1; i=2; k=1$ => $0<(2+1)\leq 2$ will not be met.

Then,

$$\overline{P}^{1}_{H_2,L_1} \text{does not exist} \tag{A-36}$$

where $j=1; i=2; k=-1$ => $0<(2-1)\leq 2$ OK

$$\overline{P}^{-1}_{H_2,L_1} = \begin{cases} \overline{\Gamma}_{H_2,L_1}; & \text{if } V_{H_2} > V_{H_1} \\ \overline{\Gamma}_{H_2,L_1} \cap \overline{\overline{\Gamma}_{H_2,L_1} \cap \overline{R}_{(H_2,L_1)\to(H_1,L_1)}}; & \text{otherwise} \end{cases}; \tag{A-37}$$

and

$$V_{H_2} = 0.0763 \ m^3/s; V_{H_1} = 0.0990 \ m^3/s \tag{A-38}$$

Then,

$$\overline{P}^{-1}_{H_2,L_1} = \overline{\Gamma}_{H_2,L_1} \cap \overline{\overline{\Gamma}_{H_2,L_1} \cap \overline{R}_{(H_2,L_1)\to(H_1,L_1)}} \tag{A-39}$$

where

$$\begin{aligned}\overline{R}_{(H_2,L_1)\to(H_1,L_1)} &= \left[\left(\Gamma^a_{H_2,L_1} \vee \Gamma^a_{H_1,L_1}\right), \left(\Gamma^b_{H_2,L_1} \wedge \Gamma^b_{H_1,L_1}\right)\right] \\ &= \left[(1.72 \vee 2.28), (3.03 \wedge 3.10)\right] \\ &= \left[2.28, 3.03\right]\end{aligned} \tag{A-40}$$

Then,

$$\begin{aligned}\overline{P}^{-1}_{H_2,L_1} &= \left[1.72,3.03\right] \cap \overline{\left[1.72,3.03\right]} \cap \left[2.28, 3.03\right] \\ &= \left[1.72,2.28\right]\end{aligned} \tag{A-41}$$

and

$$\begin{aligned}\overline{P}_{H_2,L_1} &= \cap\left(\overline{P}^{1}_{H_2,L_1}, \overline{P}^{-1}_{H_2,L_1}\right) \\ &= \left[1.72,2.28\right]\end{aligned} \tag{A-42}$$

Going through the same procedure, matrix $\overline{\boldsymbol{P}}$ will be constructed.

$$\overline{\boldsymbol{P}} = \begin{pmatrix} [2.28,3.10] & [0,0] & [2.28,5.65] \\ [1.72,2.28] & [0.33,2.21] & [0.51,2.28] \end{pmatrix} \tag{A-43}$$

Appendix B

Appendix B contains the MATLAB code written for calculation of the prediction methodology discussed in Chapter 3. As a sample, the code for calculating maximum energy recovery using the prediction methodology is shown for case 2 from Chapter 4 (Table 4.5).

```
function [Result,WR,WR2,Whpu,Wlpu,Pa,Pb,dM,WM,Wm,dQ,WQ,WG]=
casestudy41(I,J,WHTOTAL,WLTOTAL,Phs,Pht,Pls,Plt,dpmin,rs,etta,ml,mh,Ths,Tht,T
ls,Tlt)
I=3;
J=2;
%WHTOTAL=2771.1;
%WLTOTAL=3406.1;
Phs=[900;850;700];
Ths=[350;350;400];
Pht=[100;150;200];
Tht=[350;350;400];
Pls=[100;100];
Tls=[390;420];
Plt=[700;900];
Tlt=[390;420];
dpmin=70;
rs=1.4;
etta=1;
```

```
ml=[25.78;36.81];
mh=[36.81;14.73;21.48];
%Rh=[0.347662;0.337287;0.248735];
%Rl=[0.641965;0.630812];
%Cph=[1.432;0.982;1.046];
%Cpl=[1.432;1.432];
dQ=zeros((I*(I-1)/2),J);
WG = zeros(1, I);
Wexp= zeros(1, I);
Wcomp= zeros(1, I);
N=zeros(1,(I*(I-1)/2));
N1=zeros(1,(I*(I-1)/2));
N2=zeros(1,(I*(I-1)/2));
%M matrix represent the italic p matrix
%Q matrix represent the italic O matrix
%G matrix represent the italic wo matrix
%Wleft matrix represent the italic WL matrix
for j=1:J
    for i=1:I
        if Phs(i)>=Plt(j)+dpmin
            Pa(i,j)=Plt(j)
        elseif Pls(j)<Phs(i)-dpmin & Phs(i)-dpmin<Plt(j)
            Pa(i,j)=Phs(i)-dpmin
        else
            Pa(i,j)=0
        end
        if Pls(j)>=Pht(i)+dpmin
            Pb(i,j)=Pls(j)
        elseif Pls(j)<Pht(i)+dpmin & Pht(i)+dpmin<Plt(j)
            Pb(i,j)=Pht(i)+dpmin
        else
            Pb(i,j)=0
        end
        if Pa(i,j)==0
            Pb(i,j)=0
        elseif Pb(i,j)==0
            Pa(i,j)=0
        else
        end
%alpha(j)=Rl(j)/Cpl(j);
%Betta(i)=Rh(i)/Cph(i);
dM(i,j)=[(((Pa(i,j)/Pb(i,j))^((rs-1)/rs))-1)*(1+(Pb(i,j)/Pls(j))^((rs-1)/rs)-
1)]
Vl(j)=ml(j)*Tls(j)

Vh(i)=mh(i)*Ths(i)
    end
end
WM=dM*diag(Vl)*etta;
d=ones(J,1)
Wm=WM*d
for i=1:I
    Wh(i)=Vh(i)*(1-(Pht(i)/Phs(i))^((rs-1)/rs))
    Wt(i)=Wh(i)-Wm(i)
end
for j=1:J
    n=1
```

```
    for i=1:I
        for k=i+1:I
            if (Pb(i,j)==0 & Pa(i,j)==0)
                        N(1,n)=0
                        N1(1,n)=min(Vh(i),Vh(k))
            elseif (Pb(k,j)==0 & Pa(k,j)==0)
                        N(1,n)=0
                        N1(1,n)=min(Vh(i),Vh(k))
            else

N(1,n)=((max(intersect(Pb(i,j):0.01:Pa(i,j),Pb((k),j):0.01:Pa((k),j)))/min(in
tersect(Pb(i,j):0.01:Pa(i,j),Pb((k),j):0.01:Pa((k),j))))^((rs-1)/rs))-1
            N1(1,n)=min(Vh(i),Vh(k))

N2(1,n)=ml(j)*Tls(j)*(etta)*(1+(min(intersect(Pb(i,j):0.01:Pa(i,j),Pb((k),j):
0.01:Pa((k),j)))/Pls(j))^((rs-1)/rs)-1)
            end
            n=n+1;

        end
    end
    for s=1:n-1
        dQ(s,j)=N(1,s)
        E(s,j)=N1(1,s)
       VV(s,j)=N2(1,s)
    end
end
WQ=dQ.*VV
for j=1:J
    for s=1:(I*(I-1))/2
        if s+1>(I*(I-1))/2
            break
        elseif WQ(s,j)==WQ(s+1,j)
            WQ(s+1,j)=0
        else
        end
    end
end
for s=1:(I*(I-1))/2
    for j=1:J
        for i=1:I
            if E(s,j)==Vh(i)
                WG(i)= WG(i)+ WQ(s,j)
            else
                WG(i)=WG(i)+0
            end

        end
    end
end
for j=1:J
        for i=1:I
            WF(i)=Wt(i)+WG(i)

            WL(j)=Vl(j)*((Plt(j)/Pls(j))^((rs-1)/rs)-1)
            d1=ones(1,I);
```

```
            d2=ones(1,(I*(I-1)/2));
           % Wq=d2*WQ;
           % Wmm=d1*WM;
          %  Wleft(j)=Wq(j)-WL(j)-Wmm(j)
            if WF(i)>=0
                Wexp(i)=WF(i)
            else
                Wexp(i)=0
            end
            if WF(i)<=0
                Wcomp(i)=WF(i);
            else
                Wcomp(i)=0
            end
        end
end
d3=ones(I,1);
d4=ones(J,1);
d5=ones(1,I);
Wlpu=Wexp*d3
wleft=WL*d4-(d5*Wm-WG*d3)
Whpu=abs(Wcomp*d3)+abs(wleft)
WR=WL*d4-Whpu
WR2=Wh*d3-Wlpu
WHTOTAL=Wh*d3
WLTOTAL=WL*d4
Result=[WHTOTAL;WLTOTAL;WR;WR2;Whpu;Wlpu]
end
```

Appendix C

Appendix C includes the customized code listing-subroutine for the direct work exchanger modeled in Aspen Plus. Note that only the parts that are highlighted in red have been modified using the code provided by Aspen Plus for USER 2 unit operation (Aspen Tech, Getting Started Customizing Unit Operation Models, 2013).

The code is listed and edited as follows.

```
C
C     User2 Unit Operation Model Subroutine for Excel Models
C
C     This routine is used by default to communicate with User-Written
C     Excel Unit Operation models.  The feed streams, and user-defined
C     real and integer parameters are automatically copied to Excel.
C     The workbook calculations are invoked and the Aspen Plus
C     simulation is updated with the product streams, and user-defined
C     real and integer parameters that were calculated by the Excel
C     Workbook.

      SUBROUTINE WE2 (NMATI,  MSIN,   NINFI,   SINFI,  NMATO,
     2                SOUT,   NINFO,  SINFO,   IDSMI,  IDSII,
```

```
     3                  IDSMO,  IDSIO,  NTOT,    NSUBS,  IDXSUB,
     4                  ITYPE,  NINT,   INTV,    NREAL,  REALV,
     5                  IDS,    NPO,    NBOPST,  NIWORK, IWORK,
     6                  NWORK,  WORK,   NSIZE,   ESIZE,  INTSIZ,
     7                  LD   )
C
      IMPLICIT NONE
C
C     DECLARE VARIABLES USED IN DIMENSIONING
C
      INTEGER NMATI, NINFI, NMATO, NINFO, NTOT,
     +        NSUBS, NINT,  NPO,   NIWORK,NWORK,
     +        NSIZE
C
C     DECLARE ARGUMENTS
C
      INTEGER IDSMI(2,NMATI), IDSII(2,NINFI), IDSMO(2,NMATO),
     +        IDSIO(2,NINFO), IDXSUB(NSUBS),  ITYPE(NSUBS),
     +        INTV(NINT),      IDS(2,3),       NBOPST(6,NPO),
     +        IWORK(NIWORK),  INTSIZ(NSIZE),  NREAL, LD

      REAL*8  MSIN(NTOT,NMATI), SINFI(NINFI), SOUT(NTOT,NMATO),
     +        SINFO(NINFO),     WORK(NWORK),  ESIZE(NSIZE),
     +        REALV(NREAL)
C
C-------------------- Aspen Plus Common Definitions -------------------
C
#include "dms_errout.cmn"
#include "ppexec_user.cmn"
#include "dms_ncomp.cmn"
#include "dms_plex.cmn"
      REAL*8 B(1)
      EQUIVALENCE (B(1),IB(1))
C
C-------- Declare Aspen Plus utility functions that will be used ------
C
      INTEGER DMS_IRRCHK, DMS_IFCMNC
C
C--------------------- Local Variable Declarations --------------------
C
      INTEGER OFFSET,     NUM_COLS,   NUM_ROWS,   RETCODE,   LID,
     +        IBLANK(2),  KREAL(3),   KINT(3),    KINPUT(2), KOUTPUT(2),
     +        LDATA,      I,J,K,      LEN,        KDIAG,     IDX(10),
     +        LIDSC,      NCD,        C_OFF,      ERRNUMBER, NUM_LINES,
     +        SOURCE(16), HOL_STRLEN, SOR_LENGTH, SSID(2),   IPROG(2),
     +        DESC_LENGTH,KOUTSOL(3), EXCEL_NAME_LEN,
     +        EXCEL_NAME(64),         KINPSOL(3),
     +        DESCRIPTION(128)
      INTEGER LABELS(2,9), ROWNAMES(2,NCOMP_NCC+9)     !Moved LABELS and ROWNAMES
declarations.
      INTEGER REALROWS(2,NTOT+1)
      CHARACTER*8 RealLabels(2)    !Realparam row ID's.

      REAL*8  INSTREAM(NTOT*NMATI),OUTSTREAM(NTOT*NMATO)

C
C-------------------------- Data Section ----------------------------
C
```

```
      DATA KINPUT      /4HINPU, 4HT   /
      DATA KOUTPUT     /4HOUTP, 4HUT  /
      DATA KREAL       /4HREAL, 4HPARA, 4HMS  /
      DATA KINT        /4HINTP, 4HARAM, 4HS   /
      DATA KINPSOL     /4HINP_, 4H    , 4H    /
      DATA KOUTSOL     /4HOUT_, 4H    , 4H    /
      DATA IPROG       /4HUSRX, 4HLS  /
      DATA IBLANK      /4HIMIS, 4HS   /

      DATA LABELS      /4HTOTF, 4HLOW ,
     2                  4HTEMP, 4H    ,
     3                  4HPRES, 4H    ,
     4                  4HENTH, 4HALPY,
     5                  4HVAP , 4HFRAC,
     6                  4HLIQ , 4HFRAC,
     7                  4HENTR, 4HOPY ,
     8                  4HDENS, 4HITY ,
     9                  4HMOLE, 4H WT /
      DATA RealLabels  /'R' ,
     +                  'W'          /    ! Labels for Realparam table

C-----------------------------------------------------------------------
C- Establish Excel link and call StartIteration Workbook Hook Function
C
      CALL USRUTL_GETEXCEL(EXCEL_NAME, EXCEL_NAME_LEN)
       CALL StartIteration(RETCODE, EXCEL_NAME,64, IDS(1,1), 8)
       IF(RETCODE .NE. 0) GOTO 1000

C--------------- Build Aspen_Input Data Table -------------------------
C
C     The Excel Aspen_Input Sheet serves as the Aspen Plus interface for
C     the material feeds having liquid and vapor components.
C
C     The component flow rates and stream variables will be entered into
C     column 1 as the Excel row identifier.  A separate column will be
C     entered for each material feed stream.  The number of rows equals
C     the number of components plus the number of stream properties (9).
C
C       Place the 8 character component name (2 integer words) for all
C       conventional components (NCOMP_NCC) into the first column of
C       the Excel table (ROWNAMES).  The Aspen Plus function,
C       DMS_IFCMNC, returns the start of the component id storage
C       location.

          OFFSET = DMS_IFCMNC('IDSCC')
          DO J=1, NCOMP_NCC
            I = OFFSET + 2*(J-1) + 1
            ROWNAMES(1,J) = IB(I)
            ROWNAMES(2,J) = IB(I+1)
          END DO

C       Copy the Aspen Plus stream vector property names into the table.
C       There are 9 standard stream properties in a material vector.
C
          DO K=1, 9
            J = K + NCOMP_NCC
            ROWNAMES(1,J) = LABELS(1,K)
             ROWNAMES(2,J) = LABELS(2,K)
```

```
          END DO
          NUM_ROWS = NCOMP_NCC+9
C
C       Copy the material feed variables into the table.  Data for
C       each material stream will be placed in separate columns.
C       NMATI equals the number of material feeds.

          NUM_COLS = NMATI
          DO J=1, NUM_COLS
            OFFSET  = (J-1)*(NCOMP_NCC+9)
            DO I=1, NUM_ROWS
              INSTREAM(OFFSET+I) = MSIN(I,J)
            END DO
          END DO

C--------------- Send Aspen_Input table to Excel ----------------------

      LDATA = 8*NUM_ROWS*NUM_COLS
      CALL WriteTable(RETCODE , KINPUT, 8       , NUM_ROWS,
     +                ROWNAMES, 8     , NUM_COLS, IDSMI   ,
     +                8       , 2     , INSTREAM, LDATA   )
      IF (RETCODE .NE. 0) GO TO 1000

C
C------------ Send Aspen_IntParams table to Excel ---------------------
C
C     The Aspen_IntParams Excel sheet serves as the interface for the
C     User2 model integer parameters.
C
      LDATA = 8*NINT
      CALL WriteTable(RETCODE, KINT, 12 , NINT  ,
     +                IBLANK , 0   , 1  , IBLANK,
     +                0      , 1   , INTV,LDATA )
      IF (RETCODE .NE. 0) GO TO 1000

C
C-------------- Send Aspen_RealParams table to Excel ------------------
C
C     The Aspen_RealParams Excel sheet serves as the interface for the
C     User2 model real parameters.
C
      LDATA = 8*NREAL
      CALL WriteTable(RETCODE, KREAL, 12  , NREAL ,
     +                IBLANK , 0    , 1   , IBLANK,
     +                0      , 2    , REALV,LDATA )
      IF (RETCODE .NE. 0) GO TO 1000

C
C-------- Initialize the Aspen_Output Excel table ---------------------
C
C     The Aspen_Output Excel sheet serves as the interface for the
C     product streams having liquid and vapor components.  This
C     initialization step is optional.
      NUM_ROWS=NCOMP_NCC+9
      DO J=1, NMATO
        OFFSET  = (J-1)*(NCOMP_NCC+9)
        DO I=1, NUM_ROWS
          OUTSTREAM(OFFSET+I) = 0.D0
```

```
          END DO
        END DO

         NUM_COLS = NMATO
        LDATA = 8*NUM_ROWS*NUM_COLS
        CALL WriteTable(RETCODE , KOUTPUT, 8        , NUM_ROWS,
       +                ROWNAMES, 8      , NUM_COLS , IDSMO   ,
       +                8       , 2      , OUTSTREAM, LDATA   )
        IF (RETCODE .NE. 0) GO TO 1000

C
C------------- Solid Substream Section --------------------------------
C
C     When a simulation contains either conventional or nonconventional
C     solids, another Excel sheet will be created as the interface with
C     a separate sheet being created for each substream.  The name of
C     substream will be appended onto the sheet name.  For example, a
C     sheet called Aspen_INP_CISOLID will be created for the CISOLID
C     substream.  The component names and stream properties for this
C     stream will be prepared similarly to Aspen_Input. A separate
C     column will be used for each feed.  NSUBS will be greater than 1
C     if any solid substreams exist.

        IF (NSUBS .GT. 1) Then

C       Build the input tale for each solid substream
          DO K=2,NSUBS

            IF (ITYPE(K) .EQ. 3) THEN
C             Nonconventional solid
              LIDSC = DMS_IFCMNC('IDSNCC')
              NCD = NCOMP_NNCC
            ELSE
C             Conventional solid
              LIDSC = DMS_IFCMNC('IDSCC')
              NCD = NCOMP_NCC
            ENDIF

            DO J=1, NCD
              LID = LIDSC + 2*(J-1)
              ROWNAMES(1,J) = IB(LID+1)
              ROWNAMES(2,J) = IB(LID+2)
            END DO
C
C           Place stream property labels in column 1
            DO J=1, 9
              I=NCD+J
              ROWNAMES(1,I) = LABELS(1,J)
              ROWNAMES(2,I) = LABELS(2,J)
            END DO
            NUM_ROWS = NCD+9
C
C           Append the substream name onto the end of the input
C           and output Excel sheet name.
            CALL SHS_PID(LD, K, SSID)
            KINPSOL(2) = SSID(1)
             KINPSOL(3) = SSID(2)
            KOUTSOL(2) = SSID(1)
```

```
           KOUTSOL(3) = SSID(2)
C
C          Register the stream data
           NUM_COLS = NMATI
           DO J=1, NUM_COLS
             OFFSET  = (J-1)*(NCD+9)
             DO I=1, NCD+9
               INSTREAM(OFFSET+I) = MSIN(IDXSUB(K)+I-1,J)
             END DO
           END DO
C
C          Send interface table to Excel
           LDATA = 8*NUM_ROWS*NUM_COLS
           CALL WriteTable(RETCODE , KINPSOL, 12      , NUM_ROWS,
     +                     ROWNAMES, 8      , NUM_COLS, IDSMI   ,
     +                     8       , 2      , INSTREAM, LDATA   )
           IF (RETCODE .NE. 0) GO TO 1000
C
C          Initialize the Excel output interface for the substream
           NUM_COLS = NMATO
               DO J=1, NUM_COLS
             OFFSET  = (J-1)*(NCD+9)
             DO I=1, NCD+9
               OUTSTREAM(OFFSET+I) = 0.D0
             END DO
           END DO
C
C          Send interface table to Excel
C
           NUM_ROWS = NCD+9
           LDATA = 8*NUM_ROWS*NUM_COLS
           CALL WriteTable(RETCODE , KOUTSOL, 12       , NUM_ROWS,
     +                     ROWNAMES, 8      , NUM_COLS , IDSMO   ,
     +                     8       , 2      , OUTSTREAM, LDATA   )
           IF (RETCODE .NE. 0) GO TO 1000

         END DO

        End If
C
C------------ Invoke Excel Workbook Calculations ----------------------
C
       CALL CalculateData(RETCODE)
       IF (RETCODE .NE. 0) GOTO 1000

C---------- Obtain model results from Excel interface sheets ----------
C
C    -- Read back integer parameter table since some may represent results
C
           LDATA = 8*NINT
           CALL ReadTable(RETCODE, KINT, 12 ,  NINT ,
     +                    1      , 1   , INTV, LDATA)
           IF (RETCODE .NE. 0) GOTO 1000
C
C    -- Read back real parameter table
C
           LDATA = 8*NREAL
           CALL ReadTable(RETCODE, KREAL, 12  ,  NREAL,
```

```
     +                 1      , 2    , REALV, LDATA)
          IF (RETCODE .NE. 0) GOTO 1000
C
C    -- Read product stream information from Aspen_Output
C
          NUM_ROWS = NCOMP_NCC+3    !Change 9 to 3; One flow rate + tot flow, temp, pres.
          NUM_COLS = NMATO
          LDATA = 8*NUM_ROWS*NUM_COLS
          CALL ReadTable(RETCODE , KOUTPUT, 8        , NUM_ROWS,
     +                 NUM_COLS, 2      , OUTSTREAM, LDATA   )
          IF (RETCODE .NE. 0) GOTO 1000
C
C    -- Store product stream results in outlet stream vectors
C
          DO J = 1, NMATO
            OFFSET  = (J-1)*(NCOMP_NCC+3)  !Change 9 to 3.
            DO I = 1, NCOMP_NCC+3          !Change 9 to 3
              SOUT(I, J) = OUTSTREAM(OFFSET+I)
            END DO
          END DO
C-----------------------------------------------------------------------
C For solid substreams, obtain product info from Excel interface sheets
C
          IF (NSUBS .GT. 1) Then
C
C           Retrieve data for each substream
            DO K = 2,NSUBS
              IF (ITYPE(K) .EQ. 3) THEN
                NCD = NCOMP_NNCC
              ELSE
                NCD = NCOMP_NCC
              ENDIF

              CALL SHS_PID(LD, K, SSID)
              KOUTSOL(2) = SSID(1)
              KOUTSOL(3) = SSID(2)
C
C             Read Excel interface product sheet for substream
              NUM_ROWS = NCD+9
              NUM_COLS = NMATO
              LDATA = 8*NUM_ROWS*NUM_COLS

              CALL ReadTable(RETCODE , KOUTSOL, 12       , NUM_ROWS,
     +                       NUM_COLS, 2      , OUTSTREAM, LDATA   )
              IF(RETCODE .NE. 0) GO TO 1000
C
C             Store data into outlet stream vector
              DO J=1, NMATO
               OFFSET= (J-1)*(NCD+9)
                   DO I=1, NCD+9
                  SOUT(IDXSUB(K)+I-1, J) = OUTSTREAM(OFFSET+I)
               END DO
              END DO
            END DO

          End If
C
C--------------- End of Current Iteration -----------------------------
```

```
      CALL EndIteration(RETCODE)
      RETURN

C----------------------- Error Handling Section ----------------------
 1000 CONTINUE
C
C  ALL ERRORS COME HERE TO REPORT ERRORS
C
C  Call GetLastTableDataErr()
C
C  HOL_STRLEN SETS THE PADDING FOR ERROR HANDLING STRING RETURNED
C  FROM THE EXCEL INTERFACE.
C
         HOL_STRLEN = 64
         DESC_LENGTH= 512
         SOR_LENGTH = 64
C
      CALL GetLastTableDataErr(RETCODE,     ERRNUMBER,  DESCRIPTION,
     +                         DESC_LENGTH, HOL_STRLEN, SOURCE,
     +                         SOR_LENGTH)
C
C  REGISTER SEVERE SIMULATION ERROR FROM USER2 WITH ENGINE
C
          USER_ICONVG = -3
          IF (DMS_IRRCHK(IPROG, 1, 4, 4, USER_IUMISS,
     +                   0, 0, 2) .NE. 0) THEN
C
C  DETERMINE NUMBER OF LINES OF LENGTH HOL_STRLEN TO PRINT
C  MAX IS 10 SO WE CAN USE 8 FOR DESCRIPTION OF ERROR.
C
            NUM_LINES  = ( (DESC_LENGTH+HOL_STRLEN-1) /HOL_STRLEN)
            IF (NUM_LINES .GT. 8 ) NUM_LINES = 8
C
C  MOVE STRINGS TO ERROUT_IEROUT ARRAY OF STRINGS. WILL BE PRINTED
C  TO HISTRY FILE BY ERRPRT(). FIRST WRITE "MS Excel" THEN SOURCE
C  STRING RETURNED BY API AS ERROR HEADING.
C
            WRITE(ERROUT_IEROUT(1), 10)
            WRITE(ERROUT_IEROUT(2), 11)(SOURCE(I), I=1,(SOR_LENGTH+3)/4)
C
C  WRITE ERROR MESSAGE RETURNED FROM EXCEL API TO THE HISTORY FILE
C
            DO 111 J=1,NUM_LINES
              C_OFF = (J-1) * HOL_STRLEN/4
              WRITE(ERROUT_IEROUT(J+2), 11)
     +             ( DESCRIPTION(I+C_OFF), I=1,(HOL_STRLEN+3)/4 )
 111        CONTINUE
C
C  PRINT ERROR MESSAGES TO HISTORY FILE USING THE FIRST NUMLINES+2
C  LINES OF THE ERROUT_IEROUT ARRAY OF STRINGS.
C
            CALL DMS_ERRPRT(NUM_LINES+2)
          ENDIF
C
C  END ERROR REPORTING TO HISTORY FILE
C
 2000 CONTINUE
```

```
C
C  Call EndIteration()
C
C  EndIteration IS CALLED EVEN WHEN A SEVERE ERROR OCCURS ABOVE.
C
      CALL EndIteration(RETCODE)
C
 999  CONTINUE

C
C     FORMAT STATEMENTS
C
 10   FORMAT('      MS EXCEL Interface Reports:')
 11   FORMAT('      ',16A4)

       END
```

REFERENCES

American Council of an Energy Efficient Economy (ACEEE), the State Energy Efficiency Scorecard. 2018. Available at: http://aceee.org/state-policy/scorecard.

American Council of an Energy Efficient Economy (ACEEE), the State Energy Efficiency Scorecard. 2012. Available at: http://aceee.org/research-report/e12c.

Amini-Rankouhi A, Huang Y. Prediction of Maximum Recoverable Mechanical Energy via Work Integration: A Thermodynamic Modeling and Analysis Approach. *AIChE J*. 2017; 63:4814-4826.

Annual Energy Outlook (AEO). Energy information administration (EIA), USA. 2015; 12-13.

ANSYS, Inc. Fluent Theory Guide (R18.2). 2017.

ANSYS, Inc. Fluent User's Guide (R18.2). 2017.

ANSYS, Inc. Internal Combustion Engines in Workbench. 2017.

Aspelund A, A Novel Concept for Offshore Production of LNG. In: *Cryoprague 2006*. Prague, Czech Republic; 2006.

Aspelund A, Berstad DO, Gundersen T. An Extended Pinch Analysis and Design Procedure Utilizing Pressure Based Exergy for Subambient Cooling. *Appl. Therm. Eng*. 2007; 27(16): 2633-2649.

Aspen Technology, Inc. Getting Started Customizing Unit Operation Models. 2013.

Aspen Technology, Inc. User Models. 2012.

British Petroleum, BP Statistical Review of World Energy. June 2017. Available at: https://www.bp.com/content/dam/bp/en/corporate/pdf/energy-economics/statistical-review-2017/bp-statistical-review-of-world-energy-2017-full-report.pdf. Accessed February 10, 2018.

Chapman PF. 1. Energy Costs: A Review of Methods. *Energ. policy*. 1974; 2:91-103.

Charnes A, Cooper WW, Rhodes E. Measuring the Efficiency of Decision-Making Units. *Eur. J. oper. Res*. 1978; 2:429-444.

Chen H, Feng X. Graphical Approach for Targeting Work Exchange Networks. *World Acad. Sci. Eng. Technol.* 2012; 6(8):977-981.

Chen S, Chen B. Urban Energy Consumption: Different Insights from Energy Flow Analysis, Input–Output Analysis and Ecological Network Analysis. *Appl. Energy*. 2015; 138:.99-107.

Cheng CY, Cheng SW, Fan LT. Flow Work Exchanger. *AIChE J*. 1967;13:438-442.

Cheng CY, Cheng SW. Method and Apparatus for Pressurizing and Depressurizing Of Fluids. US patent 3,489,159. 1970.

Cheng CY, Fan LT. A Flow Work Exchanger for Desalination Processes, US Dept. of the Interior, Office of Saline Water. 1968.

Cui C, Li X, Sui H, Sun J. Optimization of Coal-Based Methanol Distillation Scheme using Process Superstructure Method to Maximize Energy Efficiency. *Energy*. 2017; 119: 110-120.

Decker EH, Elliott S, Smith FA, Blake DR, Rowland FS. Energy and Material Flow through the Urban Ecosystem. *Annu. Rev. Energy Environ.* 2000; 25:685-740

Deng JQ, Shi JQ, Zhang ZX, Feng X. Thermodynamic Analysis on Work Transfer Process of Two Gas Streams. *Ind. Eng. Chem. Res*. 2010; 49:12496-12502.

Energetics Inc. Manufacturing energy and carbon footprint. Prepared for the U.S. Department of Energy, Advanced Manufacturing Office. 2014.

Floudas CA, Ciric AR, Grossmann IE. Automatic Synthesis of Optimum Heat Exchanger Network Configurations. *AIChE J*. 1986; 32(2): 276–290.

Flowserve, Energy Recovery Device DWEER, Available at: https://www.flowserve.com/en/products/pumps/specialty-products/energy-recovery-device/energy-recovery-device-dweer, Accessed March 8, 2018.

Flowserve. Dual Work Exchanger Energy Recovery (DWEER), Available at: https://www.desalination.biz/59280/products/Dual-Work-Exchanger-Energy-Recovery-DWEER-by-Flowserve/4008 . Accessed January 25, 2017.

Fu C, Gundersen T. Heat and Work Integration: Fundamental Insights and Applications to Carbon Dioxide Capture Processes. *Energy Convers. Manag*. 2016; 121:36-48.

Fu C, Gundersen T. Integrating Compressors into Heat Exchanger Networks above Ambient Temperature. *AIChE J*. 2015; 61:3770–3785.

Gay PW, Proops JLR. Carbon Dioxide Production by the UK Economy: An Input-Output Assessment. *Appl. Energy*. 1993:44: 113-130.

Hannon B. The Structure of Ecosystems. *J. Theor. Biol.* 1973; 41: 535-546.

Heywood JB. *Internal Combustion Engine Fundamentals*, McGraw-Hill, New York. 1988.

Huang K, Karimi I. Work-Heat Exchanger Network Synthesis (WHENS). *Energy*. 2016; 113:1006-1017.

Huang YL, Fan LT. Analysis of a Work Exchanger Network. *Ind. Eng. Chem. Res*. 1996; 35:3528-3538.

International Energy Agency (IEA), World Energy Outlook, 2017.

Kyle BG. *Chemical and Process Thermodynamics*, *3rd Ed*. Englewood Cliffs, N.J.: Prentice Hall, 2003.

Lawrence Livermore National Laboratory (LLNL), Energy Flow. 2018. Available at: https://flowcharts.llnl.gov/archive.html, Accessed February 10, 2018.

Lenzen M. Primary Energy and Greenhouse Gases Embodied in Australian Final Consumption: an Input–Output Analysis. *Energ. policy*. 1998; 26: 495-506.

Leontief WW. Input-Output Economics. *Sci Am*, 1951; 185: 15-21.

Linnhoff B, Flower JR. Synthesis of Heat Exchanger Networks: I. Systematic Generation of Energy Optimal Networks. *AIChE J*. 1978; 24:633-642.

Linnhoff B, Flower JR. Synthesis of Heat Exchanger Networks: II. Evolutionary Generation of Networks with Various Criteria of Optimality. *AIChE J*. 1978; 24(4), 642-654.

Liu GL, Zhou H, Shen RJ, Feng X. A Graphical Method for Integrating Work Exchange Network. *Appl. Energy*. 2014; 114:588-599.

Lyubarskyy P, Bartel D. 2D CFD-Model of the Piston Assembly in a Diesel Engine for the Analysis of Piston Ring Dynamics, Mass Transport and Friction. *Tribol. Int*. 2016; 104; 352-368.

Mao J, Zuo Z, Li W, Feng H. Multi-Dimensional Scavenging Analysis of a Free-Piston Linear Alternator Based on Numerical Simulation. *Appl. Energy*. 2011; 88(4):1140-1152.

Mikalsen R, Roskilly AP. A Computational Study of Free-Piston Diesel Engine Combustion. *Appl. Energy*. 2009; 86(7-8):1136-1143.

Mikalsen R, Roskilly AP. A Review of Free-Piston Engine History and Applications. *Appl. Therm. Eng*. 2007; 27(14-15):2339-2352.

Mikalsen R, Roskilly AP. The Design and Simulation of a Two-Stroke Free-Piston Compression Ignition Engine for Electrical Power Generation. *Appl. Therm. Eng*. 2008; 28(5-6):589-600.

Mukherjee K. Energy Use Efficiency in US Manufacturing: A Nonparametric Analysis. *Energ. Econ*. 2008; 30: 76-96.

Nair SK, Nagesh Rao H, Karimi IA. Framework for Work-Heat Exchange Network Synthesis (WHENS). *AIChE J*. DOI 10.1002/aic.16129.

National Energy Technology Laboratory (NETL), Affordable, Low-Carbon Diesel Fuel from Domestic Coal and Biomass. January 14, 2009. Available at: https://www.netl.doe.gov/energy-analyses/pubs/CBTL%20Final%20Report.pdf.

Onishi VC, Ravagnani M, Caballero JA. Simultaneous Synthesis of Work Exchange Networks with Heat Integration. *Chem. Eng. Sci*. 2014; 112:87-107.

Onishi VC, Ravagnani MA, Jiménez L, Caballero JA. Multi-Objective Synthesis of Work and Heat Exchange Networks: Optimal Balance between Economic and Environmental Performance. *Energy Convers. Manag*. 2017; 140: 192-202.

Pique GG. Pressure Exchange Technology Makes Seawater Desalination Affordable, *Water and Wastewater International Magazine*. 2003.

Ray SC. *Data Envelopment Analysis: Theory and Techniques for Economics and Operations Research*. Cambridge University Press, 2004.

Razib MS, Hasan MMF, Karimi IA. Preliminary Synthesis of Work Exchange Networks. *Comput. Chem. Eng*. 2012; 37:262-277.

Reitz RD, Rutland CJ. Development and Testing of Diesel Engine CFD Models. *Prog. Energy Combust. Sci*. 1995; 21(2):173-196.

Shenoy UV. *Heat Exchanger Network Synthesis: Process Optimization by Energy and Resource Analysis*. Gulf Professional Publishing, 1995.

Simonds OH, Williams VC. Process for Liquefaction of Natural Gas and Transportation by Marine Vessel. US patent 3,400,547. 1968.

Strelzoff S. *Technology and Manufacture of Ammonia*. Krieger Publishing, 1987.

Townsend DW, Linnhoff B. Heat and Power Networks in Process Design. Part 1: Criteria for Placement of Heat Engines and Heat Pumps in Process Networks. *AIChE J*. 1983; 29:742-748.

U.S. Census Bureau, 2012 Economic Census of the United States (Table EC1200A1). Available at:https://factfinder.census.gov/faces/tableservices/jsf/pages/productview.xhtml?pid=ECN_2012_US_00A1&prodType=table. Accessed February 10, 2018.

U.S. Census Bureau, 2012 Economic Census of the United States (Table EC1231A1). Available at:https://factfinder.census.gov/faces/tableservices/jsf/pages/productview.xhtml?pid=ECN_2012_US_31A1&prodType=table. Accessed February 10, 2018.

U.S. Census Bureau, 2012 Economic Census of the United States (Table EC1231SA1). Available at:https://factfinder.census.gov/faces/tableservices/jsf/pages/productview.xhtml?pid=ECN_2012_US_31SA1&prodType=table. Accessed February 10, 2018.

U.S. Census Bureau, Manufacturers' Shipments, Inventories, & Orders. Available at: https://www.census.gov/manufacturing/m3/definitions/index.html. Accessed February 10, 2018.

U.S. Census Bureau, North American Industry Classification System. Available at: https://www.census.gov/eos/www/naics/. Accessed February 10, 2018.

U.S. Department of Energy, Energy Use, Loss and Opportunities Analysis: U.S. Manufacturing and Mining. 2009. Available at: https://energy.gov/sites/prod/files/2013/11/f4/energy_use_loss_opportunities_analysis.pdf.

U.S. Department of Energy, Office of Energy Efficiency and Renewable Energy, U.S. Manufacturing Energy Use and Greenhouse Gas Emissions Analysis. Available at: https://energy.gov/eere/amo/downloads/us-manufacturing-energy-use-and-greenhouse-gas-emissions-analysis. Accessed February 10, 2018.

U.S. Department of Energy, U.S. Manufacturing Energy Use and Greenhouse Gas Emissions Analysis. 2012. Available at: https://energy.gov/eere/amo/downloads/us-manufacturing-energy-use-and-greenhouse-gas-emissions-analysis. Accessed February 10, 2018.

U.S. Energy Information Administration, Industrial Demand Module - NEMS Documentation 2018. Available at: https://www.eia.gov/analysis/pdfpages/m064index.php. Accessed February 10, 2018.

U.S. Energy Information Administration, Manufacturing Energy Consumption Survey Data. 2010. Available at: https://www.eia.gov/consumption/manufacturing/data/2010/. Accessed February 10, 2018.

U.S. Energy Information Administration, Manufacturing Energy Consumption Survey Data. 2014. Available at: https://www.eia.gov/consumption/manufacturing/data/2014/. Accessed February 10, 2018.

U.S. Energy Information Administration, MECS Industry Analysis Briefs. Available at: https://www.eia.gov/consumption/manufacturing/briefs/. Accessed February 10, 2018.

U.S. Energy Information Administration, Monthly Energy Review, Tables 1.1, 2.1, 2.4, 3.3a, 12.1, and 12.4. Available at: https://www.eia.gov/totalenergy/data/monthly/. Accessed February 10, 2018.

Walas SM. *Chemical Process Equipment - Selection and Design*. Butterman-Heinemam Series, 1990.

Wiedmann T, Lenzen M. Turner K, Barrett J. Examining the Global Environmental Impact of Regional Consumption Activities-Part 2: Review of Input–Output Models for the Assessment of Environmental Impacts Embodied in Trade. *Ecol. Econs*. 2007; 61: 15-26.

Xu E, Wang Y, Wu J, Xu S, Wang Y, Wang S. Investigations on the Applicability of Hydrostatic Bearing Technology in a Rotary Energy Recovery Device through CFD Simulation and Validating Experiment. *Desalination*. 2016; 383:60-67.

Xu E, Wang Y, Zhou J, Xu S, Wang S. Theoretical Investigations on Rotor Speed of the Self-Driven Rotary Energy Recovery Device through CFD Simulation. *Desalination*. 2016; 398:189-197.

Yee TF, Grossmann IE. Simultaneous Optimization Models for Heat Integration - II. Heat Exchanger Network Synthesis. *Comput. Chem. Eng*. 1990; 14(10):1165-1184.

Yihui Z, Mingshu B, Yu L. *Rotary Pressure Exchanger for SWRO*. Expanding Issues in Desalination. InTech, 2011.

Zhuang Y, Liu L, Liu Q, Du J. Step-Wise Synthesis of Work Exchange Networks Involving Heat Integration Based on the Transshipment Model. *Chin. J. of Chem. Eng*. 2017; 25: 1052-1060.

Zhuang Y, Liu L, Zhang L, Du J. Direct Work Exchanger Network Synthesis of Isothermal Process Based on Improved Transshipment Model. *J. Taiwan Inst. Chem. Eng*. 2017; 81:295-304.

Zhuang Y, Liu L, Zhang L, Du J. Upgraded Graphical Method for the Synthesis of Direct Work Exchanger Networks. *Ind. Eng. Chem. Res.* 2017; 56: 14304-14315.

ABSTRACT

MAXIMUM RECOVERY OF MECHANICAL ENERGY THROUGH WORK INTEGRATION: A WORK EXCHANGE NETWORK SYNTHESIS APPROACH

by

AIDA AMINI RANKOUHI

August 2018

Advisor: Dr. Yinlun Huang

Major: Chemical Engineering

Degree: Doctor of Philosophy

Sustainable development has become a key concern in industries, largely due to natural resource depletion, global competition, and environmental pressure. Despite the efforts for sustainability improvement, still over a half of energy consumption is wasted in manufacturing sectors, where the chemical industry is responsible for an energy efficiency lower than it should be. Many attempts have been made to recover the thermal energy using heat integration techniques. Although process work is more expensive than process heat, no efficient solution has been studied to recover mechanical energy yet. In chemical plants, many process streams need to be pressurized or depressurized in different operational stages. Therefore, the energy of these streams can be recovered by a new class of exchange, which is called work exchange.

From the thermodynamics point of view, in heat integration, temperature is a state variable and the temperature difference is the driving force for heat transfer. In work integration, pressure is a state variable. A system reaches a mechanical equilibrium if at every point within a given system there is no change in pressure with time, and there is no movement of material. Work integration through direct work exchangers could contribute significantly to mechanical energy recovery through synthesizing work exchange networks (WENs), where work exchangers are

operated in a batch mode, while compressors and expanders as utility units are operated in a continuous mode; these render WENs a type of sophisticated hybrid network system.

This research focuses on a new type of process integration for effective work integration through WEN synthesis. The concept of work integration has been studied and a mathematical modeling and analysis method is introduced to predict the maximum amount of mechanical energy that can be feasibly recovered using direct work exchangers prior to WEN configuration development. A thermodynamic model-based synthesis approach is developed to design a cost-effective heat-integrated work exchanger network (HIWEN), in which direct work exchangers may work under different operating conditions. Note that direct work exchangers have been used widely for seawater reverse osmosis (RO) desalination, where liquid streams are pressurized or depressurized. This type of unit, however, cannot be directly used for mechanical energy recovery involving streams in gas phase in chemical process systems. Thus, investigation of direct work exchangers that can be operated for mechanical energy recovery involving gas streams has been performed. A CFD-based model is developed to conduct various simulations to study the design of such a device, and its operational behavior under different operating conditions. The findings from this dissertation can have great potential for improvement of energy efficiency in manufacturing sectors.

AUTOBIOGRAPHICAL STATEMENT

EDUCATION

- M.S., Chemical Engineering, Wayne State University, Detroit, MI, 05/2014
- B.S., Chemical Engineering, University of Tehran, Tehran, Iran, 12/2011
- Graduate Certificate, Sustainable Engineering, Wayne State University, Detroit, MI, 05/2017

AWARDS

- American Institute of Chemical Engineers (AIChE) Sustainable Engineering Forum (SEF) Best Student Paper Award, 2018.
- Frederick G. Weed Graduate Scholarship, Department of Chemical Engineering and Materials Science, Wayne State University, 2017.
- The Best Poster Presentation (Co-Awardee), the 5th International Congress on Sustainability Science & Engineering (ICOSSE'16), Suzhou, Jiangsu, China, October 24-27, 2016.
- The Best Oral Presentation Award, the 4th International Conference on Sustainable Chemical Product and Process Engineering (SCPPE'16), Nanjing, China, May 31-June 3, 2016.
- Outstanding Graduate Teaching Assistant, Department of Chemical Engineering and Materials Science, Wayne State University, 2016.
- U.S. National Science Foundation Student Travel Award, to attend the 4th International Conference on Sustainable Chemical Product and Process Engineering, Nanjing, China, May 31-June 3, 2016.
- Best Presentation in Session on Energy Sustainability, Challenges and Solutions, AIChE Annual National Meeting, Salt Lake City, UT, November 8-13, 2015.
- Student Presentation Award (1st Place), Graduate Research Symposium, Department of Chemical Engineering and Materials Science, Wayne State University, October 30, 2015.

PROFESSIONAL ACCOMPLISHMENTS

- President, ChE/MSE Graduate Students Organization, Wayne State University, Detroit, MI, 2016-2017.
- Co-Chair, Annual Graduate Research Symposium, Wayne State University, Detroit, MI, November 7, 2014.

PUBLICATIONS

- **Amini-Rankouhi, A.** and Y. Huang, "Prediction of Maximum Recoverable Mechanical Energy via Work Integration: A Thermodynamic Modeling and Analysis Approach," *AIChE Journal*, 2017, 63: 4814–4826, 2017.
- **Amini-Rankouhi, A.** and Y. Huang, "Mechanical Energy Recovery through Work Exchanger Network Integration: Challenges and Opportunities," accepted. *Proceedings of the 13th International Symposium on Process Systems Engineering – PSE 2018*.
- **Amini-Rankouhi, A**., Smith, S., Akgun, H., and Y. Huang, "Data-driven Modeling and Analysis of Energy Efficiency of Geographically Distributed Manufacturing," submitted, Smart and Sustainable Manufacturing Systems, 2018.
- **Amini-Rankouhi, A.** and Y. Huang, "Synthesis of Cost Effective Heat Integrated Work Exchange Network," to be submitted, *AIChE Journal*, 2018.